International Journal of Chemical Engineering

Catalytic Upgrading of Biorenewables to Value-Added Products

Lead Guest Editor: Hu Li
Guest Editors: Masaru Watanabe and Shunmugavel Saravanamurugan

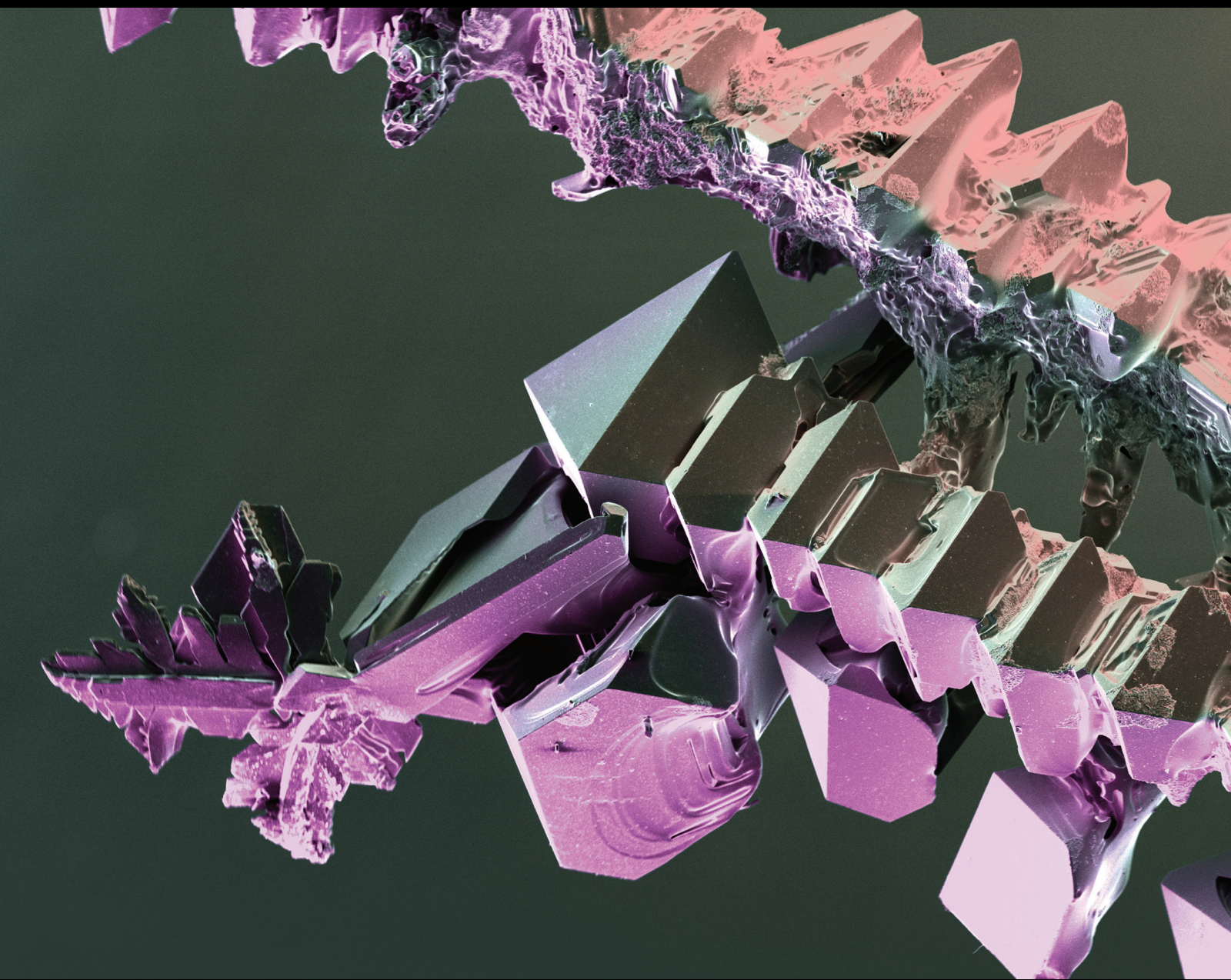

Catalytic Upgrading of Biorenewables to Value-Added Products

International Journal of Chemical Engineering

Catalytic Upgrading of Biorenewables to Value-Added Products

Lead Guest Editor: Hu Li
Guest Editors: Masaru Watanabe
and Shunmugavel Saravanamurugan

Editorial Board

Contents

Hindawi
International Journal of Chemical Engineering
Volume 2019, Article ID 4107613, 2 pages
https://doi.org/10.1155/2019/4107613

Editorial

Catalytic Upgrading of Biorenewables to Value-Added Products

Hu Li,[1] **Masaru Watanabe**,[2] **and Shunmugavel Saravanamurugan**[3]

[1]*State-Local Joint Engineering Lab for Comprehensive Utilization of Biomass, Center for R&D of Fine Chemicals, Guizhou University, Guiyang, Guizhou 550025, China*
[2]*Research Center of Supercritical Fluid Technology, Graduate School of Engineering, Tohoku University, 6-6-11, Aoba, Aramaki, Aoba-ku, Sendai 980-8579, Japan*
[3]*Laboratory of Bioproduct Chemistry, Center of Innovative and Applied Bioprocessing (CIAB), Mohali 140306, Punjab, India*

Correspondence should be addressed to Hu Li; hli13@gzu.edu.cn

Received 24 March 2019; Accepted 24 March 2019; Published 2 May 2019

Lignocellulosic biomass, as a promising candidate, is being developed to be the most abundant and carbon-neutral feedstock for manufacturing petroleum-based commodities through appropriate design of catalytic materials with controllable functionalities or establishment of fitting catalytic processes. This special issue intends to highlight current progress on the development and optimization of catalytic systems and processes for the selective transformation of biorenewables to value-added products. The papers selected are on the application of new and green technologies to upgrade biomass and waste resources, and those with topics on the preparation of functional catalytic materials and the use of correlated auxiliaries to boost reaction rate and selectivity in the production process are also considered. Hereby, we are pleased to share ten exciting papers on biomass valorization with the readers. We would like to appreciate all the authors for submitting their articles and all the reviewers for their excellent feedback.

In the paper entitled "Influence of Ethanol Organosolv Pulping Conditions on Physicochemical Lignin Properties of European Larch," M. Hochegger et al. characterize and assess the potential applicability of the organosolv lignin fraction from European larch sawdust, based on eight different samples prepared under various reaction conditions (reaction temperature: 420–460 K and sulfuric acid loading: 0.00–1.10%) with one milled wood lignin sample as reference. The antiradical potential, the chemical structure, and the molecular weight distribution of the isolated lignin exhibit a direct relationship with the examined reaction parameters.

In the paper entitled "Effect of Metal Chlorides on the Pyrolysis of Wheat Straw," Y. V. Lugovoy et al. present the influence of the addition of 10 wt.% $FeCl_3$, $CoCl_2$, $NiCl_2$, $ZnCl_2$, $SnCl_2$, or $CuCl_2$ on the wheat straw pyrolysis process. Among the investigated metal chlorides, $CuCl_2$ shows the highest influence on the pyrolysis process of wheat straw, which not only results in a decrease in the molecular weight distribution of volatile products but also leads to a decrease in the yield of gaseous pyrolysis products as well as an increase in the specific surface area of the solid pyrolysis residue.

In the paper entitled "Upgrading Bio-Oil Produced from Corn Cobs and *Cedrela odorata* via Catalytic Olefination and Esterification with 3,7-Dimethyloct-1-ene and Butanol," F. A. Dawodu et al. upgrade bio-oil produced from corn cobs and *Cedrela odorata* by simultaneous olefination and esterification using 3,7-dimethyl-1-octene and butanol as a reagent and co-solvent, respectively. The upgraded bio-oils reveal a significant reduction in water and oxygen contents and an increase in the high heating value and flammability.

In the paper entitled "One-Step Synthesis of CaO-ZnO Efficient Catalyst for Biodiesel Production," J. T. Arana et al. introduce one-step preparation of CaO-ZnO microparticles via mixing ZnO with $CaCO_3$ and subsequent calcination, which is disclosed to have the characteristic crystallographic cubic structure of CaO and the hexagonal phase of ZnO. A moderate biodiesel yield of 73% can be obtained from

soybean oil through transesterification over the heterogeneous CaO-ZnO catalyst at 60°C after 6 h.

In the paper entitled "Synthesis of a New Copper-Based Supramolecular Catalyst and Its Catalytic Performance for Biodiesel Production," F. Chang et al. prepare a new copper-based supramolecular catalyst from $CuSO_4{\cdot}5H_2O$ and β-cyclodextrin (β-CD) by simple chemical complex. After reacting at 120°C for 9 h, the Cu-β-CD catalyst affords a high biodiesel yield of 88.6% from transesterification of *Xanthium sibiricum* Patr oil. As compared with the sole species copper or β-CD, the improvement in the activity of the Cu-based catalyst can be attributed to the synergistic catalytic role of Cu^{2+} and β-CD.

In the paper entitled "Carbon-Based Catalyst from Pyrolysis of Waste Tire for Catalytic Ethanol Dehydration to Ethylene and Diethyl Ether," E. Chaichana et al. investigate the utilization of waste tire as a carbon source in the preparation of carbon-based catalysts for ethanol dehydration. The carbon catalyst prepared by treatment with HCl and calcination at 420°C displays superior ethanol conversion of 36.2% at 400°C with selectivity of 65.9 and 33.5% toward ethylene and diethyl ether, respectively, which can be ascribed to the relatively high surface acid density.

In the paper entitled "Ethanol Dehydration over WO_3/TiO_2 Catalysts using Titania Derived from Sol-Gel and Solvothermal Methods," A. Tresatayawed et al. study the catalytic activity of WO_3/TiO_2 in the dehydration of ethanol to value-added products including ethylene, diethyl ether, and acetaldehyde. The preparation methods (i.e., the sol-gel and solvothermal approach) are found to essentially alter the physicochemical properties of TiO_2 supports, where the pore structure, acidity, and WO_3 distribution of the catalysts directly affect the reactivity and product selectivity. The WO_3/TiO_2 catalyst prepared by the solvothermal method with high acidity exhibits the highest ethanol conversion (ca. 88%) at 400°C, while the presence of WO_3 offers a remarkable increase in diethyl ether selectivity (ca. 68%) at 250°C.

In the paper entitled "Catalytic Transfer of Fructose to 5-Hydroxymethylfurfural over Bimetal Oxide Catalysts," Q. Zhang et al. modify aluminum-molybdenum mixed oxide with stearic acid to be prominent solid acid catalysts for the direct conversion of sugars to 5-hydroxymethylfurfural (HMF). A high HMF of 49.8% is obtained from fructose by dehydration, with moderate HMF yields of 24.9% and 27.6% being attained from glucose and sucrose, respectively. The good activity and reusability of the catalyst can be resulted from its sufficient acidic site, mesoporous structure, high surface area, and good stability.

In the paper entitled "Upgrading of Carbohydrates to the Biofuel Candidate 5-Ethoxymethylfurfural (EMF)," X. Liu and R. Wang review the reaction performance of various catalysts (e.g., mineral salts, zeolites, heteropolyacid-based hybrids, sulfonic acid-functionalized materials, and ionic liquids) in the selective conversion of hexose sugars to EMF, providing potential strategies and directions for the design of novel catalytic materials and systems to further improve the yield and selectivity toward EMF.

In the paper entitled "Chemocatalytic Production of Lactates from Biomass-Derived Sugars," H. Zhang et al. comment on the state of the art for the synthesis of lactic acid and its esters from sugars and real biomass like rice straw catalyzed by homogeneous and heterogeneous acids and bases. Emphasis is placed on the advantages of heterogeneous catalytic systems, and suggestions on the improvement of their catalytic reactivity in the production of lactic acid are given thereof.

Conflicts of Interest

The editors declare that they have no conflicts of interest.

Hu Li
Masaru Watanabe
Shunmugavel Saravanamurugan

Hindawi
International Journal of Chemical Engineering
Volume 2019, Article ID 3890298, 6 pages
https://doi.org/10.1155/2019/3890298

Research Article

Catalytic Transfer of Fructose to 5-Hydroxymethylfurfural over Bimetal Oxide Catalysts

Qiuyun Zhang,[1] **Xiaofang Liu**,[2] **Tingting Yang**,[1] **Quanlin Pu**,[1] **Caiyan Yue**,[1] **Shuya Zhang**,[1] **and Yutao Zhang**[1]

[1]*School of Chemistry and Chemical Engineering, Anshun University, Anshun 561000, Guizhou, China*
[2]*Food and Pharmaceutical Engineering Institute, Guiyang University, Guiyang 550005, Guizhou, China*

Correspondence should be addressed to Qiuyun Zhang; sci_qyzhang@126.com and Yutao Zhang; zyt0516@126.com

Received 18 October 2018; Revised 1 February 2019; Accepted 4 March 2019; Published 1 April 2019

Guest Editor: Masaru Watanabe

Direct conversion of fructose into 5-hydroxymethylfurfural (HMF) is achieved by using modified aluminum-molybdenum mixed oxide (S-AlMo) as solid acid catalysts. The synthesized catalyst was characterized by powder XRD, nitrogen adsorption-desorption isotherm, NH_3-TPD, and SEM. As a result, the presence of strong acidity, mesostructures, and high surface area in the S-AlMo catalyst was confirmed by nitrogen adsorption-desorption isotherm and NH_3-TPD studies. A study by optimizing the reaction conditions such as catalyst dosage, reaction temperature, and time has been performed. Under the optimal reaction conditions, HMF was obtained in a high yield of 49.8% by the dehydration of fructose. Moreover, the generality of the catalyst is also demonstrated by glucose and sucrose with moderate yields to HMF (24.9% from glucose; 27.6% from sucrose) again under mild conditions. After the reaction, the S-AlMo catalyst can be easily recovered and reused four times without significant loss of its catalytic activity.

1. Introduction

With diminishing fossil fuel and degradation of the environment, catalytic routes to the production of fuels and chemicals from sustainable sources have aroused much concern over past decades [1–4]. An abundant renewable and carbon-neutral biomass resource is a promising alternative to petroleum for the production of fuels and chemicals [5]. In recent years, many chemicals have been successfully synthesized from biomass, and among the various platform molecules, 5-hydroxymethylfurfural (HMF) is considered a flexible chemical platform owing to their versatile functions and benign properties [6, 7], and it can be further oxidized into 5-ethoxymethylfurfural (EMF), 2,5-diformylfuran (DFF), and 2,5-furandicarboxylic acid (FDCA) [8–10]. Therefore, extensive investigations have been performed for the transformation of carbohydrates into HMF [11–13].

As a sustainable precursor for biofuel chemistry, HMF is obtained mainly by dehydration of monosaccharide, disaccharide, and polysaccharide, using homogeneous acids (such as H_2SO_4 and HCl) or heterogeneous acid as catalysts (Scheme 1). However, the major drawback of homogeneous acid suffered from problems of equipment corrosion, product separation, and difficult recycle and reuse. In turn, solid acid catalysts were found to be efficient, are easy to separate, and have reusability and lower catalyst loading; some of them that can be produced with methods that have a low environmental impact have received significant attention in recent years; and several types of solid acid catalysts include metal salts [14], acidic resins [15], solid organocatalyst [16], ionic liquids [17], sulfonated graphene quantum dots [18], and zeolites [19].

Metal oxides as heterogeneous acid catalyst typically possess Lewis and Brønsted acid sites that have shown a heterogeneous pathway for biodiesel production, dehydration, hydrolysis, isomerization, etc. Single metal oxide has appeared as a kind of catalyst for catalytic performance in acid-catalyzed reaction due to low-cost and their good

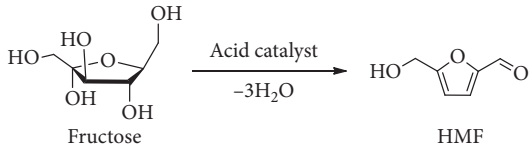

Scheme 1: Synthesis of HMF from fructose dehydration.

thermal stability. But, the single metal oxide is often associated with distinct disadvantages such as low catalytic activity, repeated poor usability, tough experimental conditions, which limit their applications. Recently, the original idea of preparing the mixed metal oxide solid catalysts were to enhance acid strength, increase the surface area, and strengthen the stability of these catalysts in comparison with single metal oxide for various organic reactions [20, 21]. However, in few studies, mixed metal oxides were used in dehydration of carbohydrates to HMF. Very recently, we have already reported that AlMo oxides are solid acids which exhibit unique acidic properties and good stability in the esterification reaction. Based on the above discussion, we report within this paper that modified aluminum-molybdenum mixed oxide in the presence of stearic acid is used as a solid catalyst for the synthesis of HMF from fructose. The catalyst was characterized using various analytical techniques such as powder XRD, NH_3-TPD, nitrogen adsorption-desorption isotherm, and SEM. The effect of reaction temperature, reaction time, and catalyst dosage on HMF yield along with catalyst reusability was investigated.

2. Experimental

2.1. Materials. Aluminum isopropoxide ($C_9H_{21}AlO_3$, 98%), $MoCl_5$ (99.6%), stearic acid (>99%), fructose, glucose, sucrose, and dimethylsulfoxide (DMSO) were purchased from Sinopharm Chemical Reagent Co., Ltd; HMF of reagent grade (99%) were purchased from Shanghai Aladdin Industrial Inc. All other chemicals were of analytical grade and used as received, unless otherwise noted.

2.2. Preparation of Aluminum-Molybdenum Mixed Oxides. Modified aluminum-molybdenum mixed oxides were prepared using stearic acid as a modifier by following the previous methods by our group [22, 23], and the catalyst was denoted as S-AlMo. For comparison, stearic acid-modified aluminum oxide was also prepared by the same method, and it was denoted as S-Al.

2.3. Characterization of Catalysts. The powder X-ray diffraction (XRD) patterns of the catalysts were obtained using a Rigaku D/max 2000 ultima plus diffractometer (monochromatic nickel filter, Cu Ka radiation). The acidity of the catalysts was measured by temperature-programmed desorption (TPD) of ammonia (AutoChem 2920, Micromeritics, USA). Nitrogen adsorption-desorption isotherm was determined with ASAP 2020M volumetric adsorption analyzer (Micromeritics, USA). SEM was performed using a field-emission scanning electron microscope (FESEM, XL-30, Philips) at 25 KV.

2.4. Catalytic Activity Measurement. Conversion of fructose was conducted in a batch glass tube heated in the oil bath with magnetic stirring condition. After catalysts and fructose were placed into the batch glass tube with the organic solvent DMSO, the reaction was started by heating the mixture to the given reaction temperature. As to the reaction media containing low boiling point or aqueous solvent, a sealed stainless steel autoclave was used under other same conditions. After the specified time, the resultant mixture was cooled to room temperature, and the solids were filtered off, then diluted with deionized water, and further analyzed by high-performance liquid chromatography (HPLC; Agilent 1100, USA) equipped with a LiChrospher C18 column and an UV detector (284 nm). The concentration of HMF was calculated based on the standard curve obtained with the standard substances. HMF yield was calculated according to the following equation:

$$\text{HMF yield}\,(\text{mol}\%) = \frac{\text{moles of HMF produced}}{\text{moles of starting fructose}} \times 100\%. \quad (1)$$

3. Results and Discussion

3.1. Characterization of S-AlMo. The structural properties and acidity of S-AlMo sample prepared were characterized by powder XRD, nitrogen adsorption-desorption, NH_3-TPD, and SEM (see Figure 1S). Powder XRD measurements showed that the S-AlMo sample has $Al_2(MoO_4)_3$ and crystalline MoO_3 peaks [24, 25] and was closely related to active sites for dehydration reaction. Nitrogen adsorption-desorption analysis showed that the sample gave type-IV isotherms with type H2 hysteresis loop in the high pressure region, characteristic of materials with mesostructure, indicating that stearic acid-modified aluminum-molybdenum mixed oxide catalyst could get the mesoporous structure, which was consistent with our previous work [13, 22, 23]. In addition, the Brunauer–Emmett–Teller (BET) surface area, pore volume, and average pore size were 49.82 $m^2 \cdot g^{-1}$, 0.17 $cm^3 \cdot g^{-1}$, and 14.19 nm, respectively. Compared with the S-Al sample, the Brunauer–Emmett–Teller (BET) surface area, pore volume, and average pore size were 21.73 $m^2 \cdot g^{-1}$, 0.03 $cm^3 \cdot g^{-1}$, and 5.68 nm, respectively. Moreover, there were two desorption profiles (100–200°C and around 750°C) over the temperature range of 50–800°C in the NH_3-TPD profiles, suggesting the catalyst contains weak and strong acid sites on its surface; meanwhile, the acid concentration of S-AlMo sample (0.87 mmol/g) was higher than that of S-Al sample (0.78 mmol/g). SEM also allows us to get insights into the morphological data of catalysts, and the images reveal that the aggregation of small particles in irregular shapes formed a grainy structure.

3.2. Effect of the Type of Catalysts on Fructose Dehydration to HMF. In this study, we initially explored the effects of the

type of catalysts on the dehydration of fructose to HMF in DMSO at 140°C for 60 min (Figure 1). As shown in Figure 1, it is apparent that various catalysts have diverse effects on HMF yields, and it can be observed that the HMF yield is lower without adding the catalyst. However, the S-AlMo catalyst gives the highest HMF yield of 49.8%, and the S-Al catalyst gives the low HMF yield of 35.4%. These results are in good agreement with the characterization of NH_3-TPD, where a higher number of acid concentrations led to a better catalytic performance in dehydration reaction. Therefore, the S-AlMo catalyst was applied as the most active solid acid for the synthesis of 5-HMF from fructose.

3.3. Effect of Different Solvents on Fructose to HMF Conversion. For determination of catalytic activity, the S-AlMo as the solid acid catalyst was carried out in different types of organic solvent. Four types of solvents (DMSO, DMA, DMF, and MIBK) were applied in the dehydration of fructose to HMF at 140°C for 60 min, and the results are summarized in Table 1. In DMSO solvent, the yield of HMF is 49.8% with fructose as raw material. In DMA, DMF, and MIBK solvents, the yields of HMF are 10.5%, 1.7%, and 0%, respectively (entries 1–3). This may be due to that DMSO could inhibit the occurrence of side reactions such as rehydration of HMF into levulinic acid and formic acid [26]. Above results show that the S-AlMo catalytic system could effectively transform fructose to HMF in the DMSO solvent. Hence, DMSO was selected as an organic solvent for the subsequent experiments in this work.

3.4. Effect of Reaction Time and Temperature on Fructose Dehydration to HMF. In order to get the highest HMF yield, the reaction conditions, such as reaction temperature and time, were optimized. The results are shown in Figure 2. In the case of fructose dehydration into HMF, the reaction temperature and time showed a critical role in the reaction with respect to the HMF yield. When the dehydration of fructose was conducted at 100°C, a low HMF yield of 8.7% was obtained after 120 min. Then, the reaction temperature was up to 120°C, HMF yield increased from 8.7% at 100°C to 46.9% at 120°C at the same of 120 min, and these results show that a relatively higher temperature promotes the formation of HMF. Further increasing the reaction temperature to 140°C, the maximum HMF yield (49.8%) of HMF is achieved after 60 min. Meanwhile, it was clear that the HMF yield had a slow decrease that further prolonged reaction time at 140°C, indicating that the product HMF was not very stable at a high temperature and a long time. It is possible due to the rehydration of HMF into levulinic acid (LA) or other byproducts [27–29]. Overall, a temperature of 140°C and time of 60 min were proper for fructose dehydration to HMF using the S-AlMo catalyst.

3.5. Effect of Catalyst Dosage on Fructose Dehydration to HMF. The effect of catalyst dosage on the fructose-to-HMF transformation was studied by varying the weight of the S-AlMo catalyst ranging from 5 to 40 mg (see Table 2). As shown in Table 2, an initial steep increase in the yield of HMF is observed when the dosage of the catalyst is increased up to 20 mg, and a maximum yield (49.8%) can achieve. Continuing to increase catalyst dosage, the yield of HMF smoothly decreases; this may be due to excess catalyst

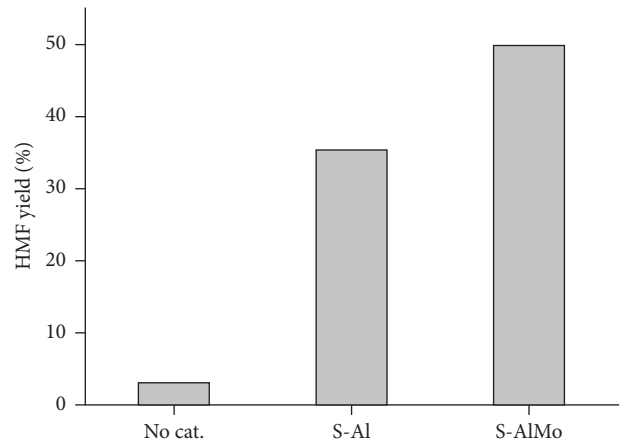

Figure 1: Effect of the type of catalysts on fructose dehydration to HMF. Conditions: fructose (50 mg), catalyst (20 mg), DMSO (1.0 g), $T = 140$°C, and $t = 60$ min.

Table 1: Effect of different types of solvents on the acid-catalyzed dehydration of fructose to HMF[a].

No.	Solvent	Temperature (°C)	Time (min)	HMF yield (%)
1	MIBK	140	60	Not detected
2	DMF	140	60	1.7
3	DMA	140	60	10.5
4	DMSO	140	60	49.8

[a]Conditions: fructose (50 mg), S-AlMo catalyst (20 mg), and solvent (1.0 g).

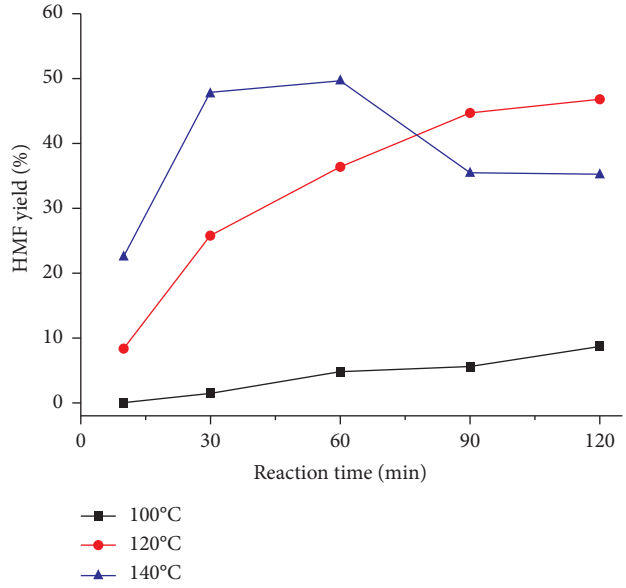

Figure 2: Effect of reaction time and temperature on fructose dehydration to HMF with S-AlMo catalyst. Reaction conditions: fructose (50 mg), S-AlMo catalyst (20 mg), and DMSO (1.0 g).

Table 2: Effect of catalyst weight on the acid-catalyzed dehydration of fructose to HMF[a].

No.	Catalyst weight (mg)	Temperature (°C)	Time (min)	HMF yield (%)
1	5	140	60	27.5
2	10	140	60	39.8
3	20	140	60	49.8
4	30	140	60	28.9
5	40	140	60	26.6

[a]Reaction conditions: fructose (50 mg) and DMSO (1.0 g).

dosages that not only provides large active sites in this reaction system, which would accelerate the synthesis of HMF, but also promotes more side reactions such as the formation of levulinic acid and humins [30, 31]. Thus, we have considered 20 mg as the optimized catalyst amount of S-AlMo for fructose dehydration to HMF at 140°C for 60 min reaction time in this work.

3.6. Effect of Water Amount in the System. The influence of water amount in DMSO on dehydration of fructose to HMF is also investigated. As displayed in Figure 3, surprisingly, the addition of water clearly led to a serious decrease of the HMF yield. When the deionized water was increased from 0 to 0.6 mL, the HMF yield decreased from 49.8% to 4.4%. It was possible that water impaired the poisoning of acid sites, causing the declined catalytic activity of S-AlMo and giving a low HMF yield. To some extent, these findings were in good agreement with the results reported by Qi et al. [32].

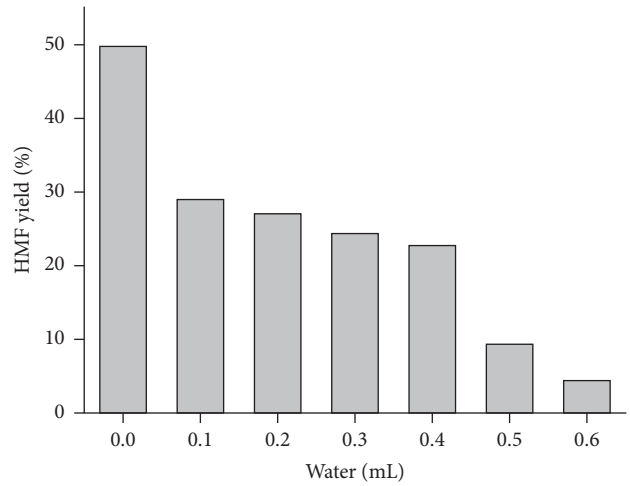

Figure 3: Effect of water added into system on the degradation of fructose. Reaction conditions: fructose = 50 mg, S-AlMo catalyst = 20 mg, DMSO = 1.0 g, $T = 140^{\circ}C$, and $t = 60$ min.

3.7. Synthesis of HMF from Sugars Catalyzed by S-AlMo Catalyst. Additionally, the developed method was also used to the synthesis of HMF with sugars as raw material, and the results are demonstrated in Table 3. The moderate HMF yield at 24.9% and 27.6% was obtained from glucose and sucrose in the DMSO system, respectively. The experiment results indicated that the S-AlMo catalyst with the presence of basic sites (eg., Al_2O_3 moieties) as well as acidic sites (eg., $Al_2(MoO_4)_3$ and MoO_3) was similar to the result reported by Li et al. [33].

Table 3: Synthesis of HMF from sugars in DMSO system with S-AlMo catalysts[a].

No.	Substrate	Temperature (°C)	Time (min)	HMF yield (%)
1	Fructose	140	60	49.8
2	Glucose	140	180	24.9
3	Sucrose	140	180	27.6

[a]Sugars (50 mg), S-AlMo catalyst (20 mg), and DMSO (1.0 g).

3.8. Catalyst Recycling Experiments. The reusability of the solid acid catalyst is very important to the low-cost and environmentally friendly biomass transformation. Thus, recycling of the S-AlMo catalyst was tested, and the dehydration of fructose into HMF was used as a model reaction. After the reaction, the catalyst was separated by filtration, washed, and dried prior to being reused in the next run. Then, the recovered S-AlMo catalyst was used to catalyze the dehydration of fructose to 5-HMF over four successive reactions under the same reaction conditions (Figure 4). As shown in Figure 4, no significant loss in the yield of HMF was observed over four cycles (49.8% in the first cycle versus 36.6% in the fourth cycle), and the slight loss of activity with respect to the first reaction cycle could be attributed to partial oligomeric products adhering to the surface of the catalyst [31, 34]. These results clearly indicated that the S-AlMo catalyst could be reused without

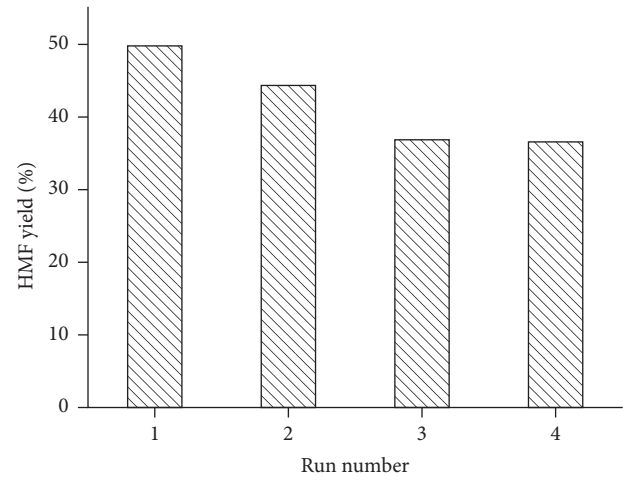

Figure 4: Recyclability study of S-AlMo catalyst for fructose dehydration reaction. Reaction conditions: fructose = 50 mg, S-AlMo catalyst = 20 mg, DMSO = 1.0 g, $T = 140^{\circ}C$, and $t = 60$ min.

significantly losing its catalytic activity. Therefore, the catalyst is capable under mild reaction condition.

4. Conclusions

In conclusion, stearic acid-modified aluminum-molybdenum mixed oxide is an efficient solid acid catalyst for direct conversion of fructose into HMF. The S-AlMo catalyst exhibited excellent textural properties (e.g., strong acidic sites, mesostructures, and large surface area) and better catalytic activity for dehydration reaction. HMF was obtained with a good yield of 49.8% by the dehydration from fructose, and the moderate HMF yield of 24.9% and 27.6% were also obtained from glucose and sucrose, respectively. Moreover, the catalyst can be recycled and reused for four cycles without significant loss in the HMF yield. Therefore, the S-AlMo catalyst would have promising potential for other acid-catalyzed chemical reactions.

Data Availability

The data used to support the findings of this study are available from the corresponding author upon request.

Conflicts of Interest

The authors declare that they have no conflicts of interest.

Authors' Contributions

Qiuyun Zhang and Xiaofang Liu contributed equally to this work.

Acknowledgments

This work was financially supported by the Technical Talent Support Program of Guizhou Education Department (no. KY [2018]069), the Guizhou Science and Technology Foundation (no. [2019]1009), the Joint Science and Technology Funds of the Youth Growth S&T Personnel Foundation of Guizhou Education Department (no. KY [2018]292), the Start-Up Funding Research Projects of Guiyang University Introduced Talents (no. GYU-ZRD [2018]-015), the Creative Research Groups Support Program of Guizhou Education Department (no. KY [2017]049), the Joint Science and Technology Funds of Guizhou S&T Department, Anshun City People's Government, and Anshun University (no. LH [2016]7278), and the Construction Projects of Innovation Platform from S&T Bureau in Anshun (no. [2016]-4).

Supplementary Materials

The structural properties and acidity of S-AlMo sample prepared were characterized by powder XRD, nitrogen adsorption-desorption, NH_3-TPD, and SEM (Figure 1S). Powder XRD measurements showed that the S-AlMo sample have $Al_2(MoO_4)_3$ and crystalline MoO_3 peaks [24, 25] and was closely related to active sites for dehydration reaction. Nitrogen adsorption-desorption analysis showed that the sample gave type-IV isotherms with type H2 hysteresis loop in the high pressure region, characteristic of materials with mesostructure, indicating that stearic acid-modified aluminum-molybdenum mixed oxide catalyst could get the mesoporous structure, which was consistent with our previous work [13, 22, 23]. In addition, the Brunauer–Emmett–Teller (BET) surface area, pore volume, and average pore size were 49.82 $m^2 \cdot g^{-1}$, 0.17 $cm^3 \cdot g^{-1}$, and 14.19 nm, respectively. Compared with the S-Al sample, the Brunauer–Emmett–Teller (BET) surface area, pore volume, and average pore size were 21.73 $m^2 \cdot g^{-1}$, 0.03 $cm^3 \cdot g^{-1}$, and 5.68 nm, respectively. Moreover, there were two desorption profiles (100–200°C and around 750°C) over the temperature range of 50–800°C in the NH3-TPD profiles, suggesting the catalyst contains weak and strong acid sites on its surface; meanwhile, the acid concentration of the S-AlMo sample (0.87 mmol/g) was higher than that of the S-Al sample (0.78 mmol/g). SEM also allows us to get insights into the morphological data of catalysts, and the images reveal that the aggregation of small particles in irregular shapes formed a grainy structure. (*Supplementary Materials*)

References

[1] H. Li, Z. Fang, R. L. Smith Jr., and S. Yang, "Efficient valorization of biomass to biofuels with bifunctional solid catalytic materials," *Progress in Energy and Combustion Science*, vol. 55, pp. 98–194, 2016.

[2] Rozina, S. Asif, M. Ahmad, M. Zafar, and N. Ali, "Prospects and potential of fatty acid methyl esters of some non-edible seed oils for use as biodiesel in Pakistan," *Renewable and Sustainable Energy Reviews*, vol. 74, pp. 687–702, 2017.

[3] Q. Y. Zhang, F. F. Wei, Q. Li, J. S. Huang, Y. M. Feng, and Y. T. Zhang, "Mesoporous $Ag_1(NH_4)_2PW_{12}O_{40}$ heteropolyacids as effective catalysts for the esterification of oleic acid to biodiesel," *RSC Advances*, vol. 7, no. 81, pp. 51090–51095, 2017.

[4] Q. Y. Zhang, X. F. Liu, T. T. Yang, C. Y. Yue, Q. L. Pu, and Y. T. Zhang, "Facile synthesis of polyoxometalates tethered to post Fe-BTC frameworks for esterification of free fatty acids to biodiesel," *RSC Advances*, vol. 9, pp. 8113–8120, 2019.

[5] H. Li, A. Riisager, S. Saravanamurugan et al., "Carbon-increasing catalytic strategies for upgrading biomass into energy-intensive fuels and chemicals," *ACS Catalysis*, vol. 8, no. 1, pp. 148–187, 2018.

[6] H. Li, T. Yang, and Z. Fang, "Biomass-derived mesoporous Hf-containing hybrid for efficient meerwein-ponndorf-verley reduction at low temperatures," *Applied Catalysis B: Environmental*, vol. 227, pp. 79–89, 2018.

[7] J. Wang, Z. Zhang, S. Jin, and X. Shen, "Efficient conversion of carbohydrates into 5-hydroxylmethylfurfan and 5-ethoxymethylfurfural over sufonic acid-functionalized mesoporous carbon catalyst," *Fuel*, vol. 192, pp. 102–107, 2017.

[8] A. Boisen, T. B. Christensen, W. Fu et al., "Process integration for the conversion of glucose to 2,5-furandicarboxylic acid," *Chemical Engineering Research and Design*, vol. 87, no. 9, pp. 1318–1327, 2009.

[9] J. C. Serrano-Ruiz, R. Luque, and A. Sepúlveda-Escribano, "Transformations of biomass-derived platform molecules: from high added-value chemicals to fuels via aqueous-phase processing," *Chemical Society Reviews*, vol. 40, no. 11, pp. 5266–5281, 2011.

[10] H. Li, K. S. Govind, R. Kotni, S. Shunmugavel, A. Riisager, and S. Yang, "Direct catalytic transformation of carbohydrates into 5-ethoxymethylfurfural with acid-base bifunctional hybrid nanospheres," *Energy Conversion and Management*, vol. 88, pp. 1245–1251, 2014.

[11] H. Li, S. Yang, and S. Yang, "Catalytic transformation of fructose and sucrose to HMF with proline-derived ionic liquids under mild conditions," *International Journal of Chemical Engineering*, vol. 2014, Article ID 978708, 7 pages, 2014.

[12] T. D. Swift, H. Nguyen, Z. Erdman, J. S. Kruger, V. Nikolakis, and D. G. Vlachos, "Tandem lewis acid/brønsted acid-catalyzed conversion of carbohydrates to 5-hydroxymethylfurfural using zeolite beta," *Journal of Catalysis*, vol. 333, pp. 149–161, 2016.

[13] Q. Y. Zhang, F. F. Wei, D. Luo, P. H. Ma, and Y. T. Zhang, "Mesoporous Ti-Mo mixed oxides catalyzed transformation of carbohydrates into 5-hydroxymethylfurfural," *China Petroleum Processing & Petrochemical Technology*, vol. 19, pp. 26–32, 2017.

[14] H. Li, Q. Zhang, X. Liu et al., "$InCl_3$-ionic liquid catalytic system for efficient and selective conversion of cellulose into 5-hydroxymethylfurfural," *RSC Advances*, vol. 3, no. 11, pp. 3648–3654, 2013.

[15] C. Antonetti, A. M. Raspolli Galletti, S. Fulignati, and D. Licursi, "Amberlyst A-70: a surprisingly active catalyst for the MW-assisted dehydration of fructose and inulin to HMF in water," *Catalysis Communications*, vol. 97, pp. 146–150, 2017.

[16] J. Dai, L. Zhu, D. Tang et al., "Sulfonated polyaniline as a solid organocatalyst for dehydration of fructose into 5-hydroxymethylfurfural," *Green Chemistry*, vol. 19, no. 8, pp. 1932–1939, 2017.

[17] H. Guo, X. Qi, Y. Hiraga, T. M. Aida, and R. L. Smith Jr., "Efficient conversion of fructose into 5-ethoxymethylfurfural with hydrogen sulfate ionic liquids as co-solvent and catalyst," *Chemical Engineering Journal*, vol. 314, pp. 508–514, 2017.

[18] K. Li, J. Chen, Y. Yan et al., "Quasi-homogeneous carbocatalysis for one-pot selective conversion of carbohydrates to 5-hydroxymethylfurfural using sulfonated graphene quantum dots," *Carbon*, vol. 136, pp. 224–233, 2018.

[19] A. Pande, P. Niphadkar, K. Pandare, and V. Bokade, "Acid modified H-USY zeolite for efficient catalytic transformation of fructose to 5-hydroxymethyl furfural (biofuel precursor) in methyl isobutyl ketone-water biphasic system," *Energy & Fuels*, vol. 32, no. 3, pp. 3783–3791, 2018.

[20] Q. Liu, F. Yang, H. Yin, and Y. Du, "Conversion of saccharides into levulinic acid and 5-hydroxymethylfurfural over WO_3-Ta_2O_5 catalysts," *RSC Advances*, vol. 6, no. 55, pp. 49760–49763, 2016.

[21] J. Guo, S. Zhu, Y. Cen, Z. Qin, J. Wang, and W. Fan, "Ordered mesoporous Nb-W oxides for the conversion of glucose to fructose, mannose and 5-hydroxymethylfurfural," *Applied Catalysis B: Environmental*, vol. 200, pp. 611–619, 2017.

[22] Q. Zhang, F. Wei, P. Ma, Y. Zhang, F. Wei, and H. Chen, "Mesoporous Al-Mo oxides as an effective and stable catalyst for the synthesis of biodiesel from the esterification of free-fatty acids in non-edible oils," *Waste and Biomass Valorization*, vol. 9, no. 6, pp. 911–918, 2018.

[23] Q. Zhang, H. Li, and S. Yang, "Facile and low-cost synthesis of mesoporous Ti-Mo bi-metal oxide catalysts for biodiesel production from esterification of free fatty acids in *Jatropha curcas* crude oil," *Journal of Oleo Science*, vol. 67, no. 5, pp. 579–588, 2018.

[24] W. T. A. Harrison, "Crystal structures of paraelastic aluminum molybdate and ferric molybdate, β-$Al_2(MoO_4)_3$ and β-$Fe_2(MoO_4)_3$," *Materials Research Bulletin*, vol. 30, no. 11, pp. 1325–1331, 1995.

[25] M. Kassem, "Phase relations in the Al_2O_3-MoO_3 and Al-MoO_3 systems, investigated by X-ray powder diffraction, FTIR, and DTA techniques," *Inorganic Materials*, vol. 42, no. 2, pp. 165–170, 2006.

[26] C. Lansalot-Matras and C. Moreau, "Dehydration of fructose into 5-hydroxymethylfurfural in the presence of ionic liquids," *Catalysis Communications*, vol. 4, no. 10, pp. 517–520, 2003.

[27] Y. Li, H. Liu, C. Song et al., "The dehydration of fructose to 5-hydroxymethylfurfural efficiently catalyzed by acidic ion-exchange resin in ionic liquid," *Bioresource Technology*, vol. 133, pp. 347–353, 2013.

[28] H. Gao, Y. Peng, J. Pan et al., "Synthesis and evaluation of macroporous polymerized solid acid derived from pickering HIPEs for catalyzing cellulose into 5-hydroxymethylfurfural in an ionic liquid," *RSC Advances*, vol. 4, no. 81, pp. 43029–43038, 2014.

[29] H. Shirai, S. Ikeda, and E. W. Qian, "One-pot production of 5-hydroxymethylfurfural from cellulose using solid acid catalysts," *Fuel Processing Technology*, vol. 159, pp. 280–286, 2017.

[30] S. Xiao, B. Liu, Y. Wang, Z. Fang, and Z. Zhang, "Efficient conversion of cellulose into biofuel precursor 5-hydroxymethylfurfural in dimethyl sulfoxide-ionic liquid mixtures," *Bioresource Technology*, vol. 151, pp. 361–366, 2014.

[31] D. Chen, F. Liang, D. Feng et al., "An efficient route from reproducible glucose to 5-hydroxymethylfurfural catalyzed by porous coordination polymer heterogeneous catalysts," *Chemical Engineering Journal*, vol. 300, pp. 177–184, 2016.

[32] X. Qi, M. Watanabe, T. M. Aida, and R. L. Smith Jr., "Efficient process for conversion of fructose to 5-hydroxymethylfurfural with ionic liquids," *Green Chemistry*, vol. 11, no. 9, pp. 1327–1331, 2009.

[33] H. Li, Q. Zhang, J. Liu et al., "Selective transformation of carbohydrates into HMF promoted by carboxylic acids modified ZrMo mixed oxides," *Biomass Conversion and Biorefinery*, vol. 4, no. 1, pp. 59–66, 2014.

[34] Z. Yang, W. Qi, R. Huang, J. Fang, R. Su, and Z. He, "Functionalized silica nanoparticles for conversion of fructose to 5-hydroxymethylfurfural," *Chemical Engineering Journal*, vol. 296, pp. 209–216, 2016.

Hindawi
International Journal of Chemical Engineering
Volume 2019, Article ID 9042425, 6 pages
https://doi.org/10.1155/2019/9042425

Research Article

Upgrading Bio-Oil Produced from Corn Cobs and *Cedrela odorata* via Catalytic Olefination and Esterification with 3,7-Dimethyloct-1-ene and Butanol

Folasegun A. Dawodu,[1] Olubunmi O. Ayodele,[2] John O. Akintola,[1] Oluwamayokun A. Obembe,[1] Ameerah O. Sanni,[1] and Bosede D. Agbejinmi[3]

[1]*Department of Chemistry (Industrial), University of Ibadan, Ibadan, Oyo State, Nigeria*
[2]*Department of Forest Products Development and Utilization, Forestry Research Institute of Nigeria, Ibadan, Oyo State, Nigeria*
[3]*Biotechnology Section, Bioscience, Department, Forestry Research Institute of Nigeria, Ibadan, Oyo State, Nigeria*

Correspondence should be addressed to Olubunmi O. Ayodele; bayodele2002@gmail.com

Received 5 November 2018; Revised 27 January 2019; Accepted 17 February 2019; Published 1 April 2019

Guest Editor: Shunmugavel Saravanamurugan

In this study, corn cobs (CC) and *Cedrela odorata* (CO) sawdust which are common waste materials in Nigeria were used as raw materials in the production of bio-oil through pyrolysis at 500°C, for 2 h. The biochar produced in the process was sulfonated with concentrated sulfuric acid under reflux at 150°C for 6 h and used as a solid acid catalyst for bio-oil upgrading. The bio-oil was upgraded by simultaneous olefination and esterification using 3,7-dimethyloct-1-ene and butanol which served as a reagent and cosolvent. FT-IR spectra of the activated biochar from CC and CO raw materials showed an absorbance in the range of 1032–1180 cm^{-1}, which is indicative of asymmetric S=O bonds, and the spectra also revealed a band between 3400 and 3700 cm^{-1}, which indicated presence of hydrogen-bonded hydroxyl groups and thus successful activation of the biochar. This observed IR absorbance was absent in the nonactivated biochar. Proximate analysis of upgraded bio-oils revealed a significant reduction in percentage water and oxygen contents, an increase in the high heating value (HHV) and flammability. The chemical composition of the bio-oils was determined using GC-MS, and it showed significant reduction in oxygenated compounds in the upgraded bio-oil as against their high composition in raw bio-oils.

1. Introduction

The world energy demand has increased rapidly in recent years as a result of the steady increase in global population and civilization. We consume vast amount of energy in our industries, high-rise buildings (offices and hotels), and even in our homes just to mention a few. In our everyday lifestyle, we require, consume, and even waste energy. The International Energy Outlook (IEO) backed this up with statistics showing an all-time rise in values of global energy consumption since 2010, despite an increase in global energy production over the years under review [1]. Using computational modeling and analysis, a projected increase in global energy consumption was predicted and alarming values were seen [1]. This requires further exploration into other sources of energy in order to tackle the current high energy demands required for human existence. Energy from renewable resources such as solar, biomass, geothermal, tidal wave, and wind is currently experiencing an increase in growth rate (about 2.6%/year), as reported by International Energy Outlook [1].

Searching for alternative source of energy to fossil fuel at this crucial time is imperative as it provides an escape route from the numerous problems such as global warming, geopolitical friction, and environmental pollution that have originated from the burning of fossil fuels. Wilk et al. [2] highlighted the importance of renewable energy as a means to attain long-term economic sustainability, environmental benefits, and a transformation of the manufacturing and transportation sectors. Subsequently, biomass has been

recognized to possess a promising impact for a projected renewable and sustainable energy future although it is still important to develop technologies which enable the conversion of lignocellulosic and municipal solid waste (MSW) biomass resources into environmentally friendly energy, from a thermodynamic efficiency and system technology standpoints [3]. To achieve a complete transformation of global energy consumption from fossil fuel dependency to renewable energy, a complete paradigm shift to a sustainable development is necessary. Due to the perceived competition of some biomass use with food, the "waste-to-energy" idea was born and energy was generated from waste; technologies have also allowed energy to be obtained from some waste of biomass [4].

Pyrolysis is one of the most frequently used method of bio-oil production from biomass because of its cheap machinery, high yield of product, short time involved in production, ease of machine operation, and flexible production procedure [5]. Three major products are obtained from biomass pyrolysis: liquids (bio-oil or tars), solid (biochar), and low-molecular weight gases (volatiles). The bio-oil produced from pyrolysis contains high water content, high acid value, and low energy density, are unstable overtime, has a foul smell, and are immiscible with conventional hydrocarbon fuel due to high polarity [6]. Mullen and coworkers produced bio-oil and biochar from corn cobs and stover using a pilot-scale fluidized bed reactor. Yields of 60% bio-oil (HHV~20 MJ/kg) and ~18.0% biochar were obtained from the feedstock at an operating temperature of 500°C [7]. Microwave-assisted fast pyrolysis of corn cobs and other agricultural residues were performed, and corn cobs produced the highest yield of bio-oil (42.1 wt.%) with HHV of 22.38 MJ/kg when compared to corn stover, sawdust, and rice straw [8]. A similar study by Biswas et al. [9] also revealed a similar trend when corn cob, wheat straw, rice straw, and rice husk were used under a slow pyrolysis setup. Surprisingly, no report of bio-oil derived from *Cedrela odorata* has been reported in literature. However, bio-oils produced from corn cob and other feedstock contains high moisture content, acid values, and oxygenated compounds, thus limiting their utilization as fuels.

Bio-oil can be subjected to further processes called "upgrading," leading to formation of hydrocarbon fuels having similar physical and chemical properties with conventional fuels [10, 11]. Some methods of upgrading bio-oil include catalytic cracking, high-pressure thermal treatment, catalytic esterification, hydrodeoxygenation, carboxylation, and oxygenation [12], but the esterification reaction represents the cheapest option of bio-oil upgrading.

Esterification is a chemical process to convert the carboxylic acids present in bio-oils to esters, acetals, and ethers by reacting them with alcohols in the presence of an acid or base catalyst [13]. Research has proven that esterification via alcohol addition will reduce the acidity of the bio-oil, thereby improving the quality and stability of bio-oil [14]. More quality fuels can be produced from bio-oil upgrading via simultaneous olefination and esterification reactions. Addition of olefins to the reaction system produces mainly esters and ethers through the reaction of olefin with carboxylic acids and aldehydes [15, 16]. In this approach, acid-catalyzed addition reactions of carboxylic acids, phenolic compounds, alcohols, and water across olefins all occur simultaneously with esterification producing a bio-oil with enhanced fuel properties [17]. The alcohol added in this reaction functions as a coreagent, reduces phase separation, and increases esterification and acetal formation [18]. Chatterjee and coworkers (2013) employed ethanol and 1-octene as solvents in bio-oil upgrading in the presence of a solid acid catalyst, resulting in a product with low water content and acid value and increased heating value. This is advantageous because hydroxyl group addition across the olefin requires a temperature between 50°C and 130°C [19, 20], which is usually below the temperature required in hydrodeoxygenation or catalytic cracking processes. Thus, catalyst coking and bio-oil polymerization can be avoided [12]. However, the use of the low-cost commodity reagent and solvent ethanol was not as effective as less polar alcohol, 1-butanol, at promoting olefin/bio-oil-phase compatibility [18].

We report a new approach for bio-oil upgrading using simultaneous olefination and esterification reactions, and the catalysts employed were derived from biochar produced after pyrolysis of corn cobs and *Cedrela odorata* sawdust. The biochar was subjected to sulfonation in the presence of concentrated sulfuric acid to produce a solid acid catalyst capable of the one-step upgrading reaction. Bio-oil obtained from corn cobs and *Cedrela odorata* sawdust biomass, having high moisture content and acid value, was subjected to one-pot olefination and esterification reactions using 3,7-dimethyloct-1-ene and 1-butanol as the reactant and cosolvent. The resultant product was characterized using Fourier transform infrared (FT-IR) spectrometer, gas chromatography-mass spectrometer (GC-MS), and proximate analysis to determine bioactive composition and fuel quality.

2. Materials and Methods

2.1. Materials. Sulfuric acid (98.0%), paraffin oil, 1-butanol (99.0%), phenolphthalein, methanol (99.0%), and KOH (90.0%) were obtained from the Department of Chemistry, University of Ibadan. 3,7-Dimethyloct-1-ene (97.0%) was purchased from (J.T. Baker chemicals).

Corn cobs (CO) were obtained from Bodija market, Ibadan, dried at 105°C, and then pulverized using industrial milling machine, while *Cedrela odorata* (CO) sawdust was collected at the sawmill section of Forestry Research Institute of Nigeria (FRIN) Jericho, Ibadan, and then oven-dried at 105°C to constant weight.

2.2. Pyrolysis of Biomass. The experimental setup consists of a double-lagged cylindrical stainless steel reactor equipped with an electrical source and automatic temperature controller. Slow pyrolysis was adopted in the experimental process, and the schematic diagram of the setup is presented in Figure 1. Known grams of CC and CO biomass were weighed and carefully fed into the pyrolysis reactor. The

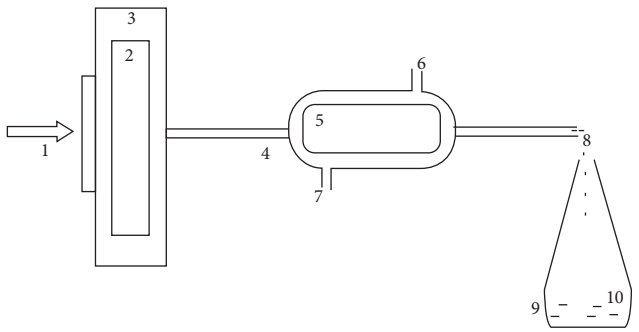

Figure 1: Schematic representation of the pyrolysis. 1, feedstock; 2, pyrolytic chamber; 3, furnace; 4, chamber rod; 5, condenser; 6, cold water inlet; 7, cold water outlet; 8, emitted gas; 9, conical flask; 10, pyrolytic oil.

pyrolyzer was operated at a controlled temperature of 500°C for 2 h at 1 atm. The pyrolyzer is equipped with a chamber rod connected to the condenser which cools the vapour, and the product is collected into an air-tight container, while the biochar by-products were collected at the bottom of the reactor.

2.3. Synthesis of Biochar-Based Solid Acid Catalyst. Biochar produced during pyrolysis of biomass was collected, sieved with a mesh size of 0.5 mm, and further dried at 105°C for 24 h. 20 g of biochar was sulfonated with 200 ml concentrated sulfuric acid in a 1 L round-bottom flask, and the resultant mixture was constantly stirred under reflux at 150°C for 6 h. The product obtained was cooled and then washed with warm distilled water to remove excess sulfuric ions until the pH of the filtrate was neutral (pH 7). Afterwards, the product was dried in the oven at 120°C for 8 h. Incorporation of SO_3H groups on the biochar was confirmed by FT-IR spectroscopy, and the internal structure (amorphous carbon) was determined by the X-ray diffraction technique.

2.4. Solid Acid-Catalyzed Upgrading of Bio-Oil. Catalytic upgrading of bio-oil was carried out in the presence of solid acid catalysts wherein the catalyst derived from CC biochar was utilized to upgrade bio-oil obtained from CC, while the CO biochar-based catalyst was applied in upgrading of bio-oil obtained from CO sawdust. Simultaneous olefination and esterification reactions were performed in a 250 ml round-bottom flask equipped with the temperature-controlled magnetic stirring system. A known weight of preheated bio-oil (5 g), 23.8 g of 3,7-dimethyloct-1-ene, 1 g of butanol (20 wt.% of bio-oil), and 1 g of sulfonated catalyst was added into the reaction chamber and heated to 140°C under reflux for 6 h. Mass balance calculations were used to estimate the yield of upgraded bio-oil, gaseous products, and char.

2.5. Product Characterization. The proximate analysis of moisture content, viscosity, density, acid value, pour point, flash point, oxygen content, and flammability was carried out in accordance with the ASTM D3175 standard procedure. Functional groups were determined with Fourier Transform Infrared Spectrometer (PerkinElmer BX) using KBr pellets.

Chemical composition of bio-oil was determined by GC-MS using Agilent 7890A series with an injector temperature of 270°C and silica capillary column coated with 5% phenyl methylpolysiloxane ($30\,\text{m} \times 0.32\,\text{mm} \times 0.25\,\mu$). Helium (≥99.9%) was used as the carrier gas. The initial oven temperature of 40°C (hold for 4 min) was used, and the temperature was then ramped at 5°C/min to 250°C and held for 5 min. The dilution solvent used was ethanol with a dilution ratio of 1 : 50.

3. Results and Discussion

3.1. Yield of Bio-Oil. The percentage yield of bio-oil which represents pyrolysis reaction efficiency is shown in Table 1. The pyrolysis products contain bio-oil, char, and non-condensable gases, and 35.1% bio-oil was obtained from CC while the yield of bio-oil from CO was 34.9%. Since we employed a slow pyrolysis process, the yield of char is usually higher compared to fast pyrolysis. As seen in Table 1, char yields for CC and CO were 34.5% and 34.6%, respectively. However, over 30% of the carbon material was lost as noncondensable gases; thus, the recoverable carbon of over 65% was achieved making the process sustainable, and the gases can be recovered using gas bags, thereby reducing carbon emissions into the environment.

3.2. Characterization of Sulfonated Biochar. Successful incorporation of SO_3H groups into CC and CO biochar was confirmed using FT-IR (Figures S1–S4), and the IR bands are shown in Tables 2 and 3. Band between 1032 and 1180 cm^{-1} indicates asymmetric S=O stretching, which is observed in the sulfonated biochar that indicates the presence of an acid (H_2SO_4), and also bands between 3400 and 3700 cm^{-1} indicate hydrogen-bonded hydroxyl groups.

The XRD patterns of the raw and acid-modified biochar are presented in Figure 2. The two broad peaks at $2\theta = 10$–32° and $2\theta = 46$–55° were due to the amorphous and graphitic carbon structures, respectively. The structural properties of the biochar did not change upon sulfonation, thus indicating that sulfuric acid did not distort the internal structure of CC and CO. The obtained XRD patterns are in tandem with what have been reported in literatures [21, 22].

3.3. Upgrading Process Using Sulfonated Biochar. Bio-oil upgrade is exceptionally a complex process because it is composed of a wide variety of oxygenated compounds and in some cases aliphatic or aromatic hydrocarbons and also with substantial amount of water. Sulfonated acid catalyst has been found to exhibit good activity and stability in preliminary catalytic upgrading of bio-oils by simultaneously reacting with alcohols and olefins [16]. The sulfonated catalyst also exhibits a higher water tolerance, thereby allowing complete upgrading as compared to other catalysts form.

Table 1: Products yield of pyrolysis of corn cobs and *Cedrela odorata* biomass.

Sample	Product yield (%)		
	Bio-oil	Char	Gas
Corn cobs	35.1	34.5	30.4
Cedrela odorata	34.9	34.6	30.1

Table 2: Analysis of FT-IR spectra of the raw and activated biochar from corn cob.

S/N	CC biochar	Sulfonated CC	Band assignment
1	461.53		C-H bending
2		606.99	C-O-H bending
3	872.72		C-H out-of-plane bending of benzene derivatives
4		1032.16, 1174.45	S=O symmetrical stretching
5	1437.61	1381.81	In-plane O-H bending and C-O stretch of dimers
6	1602.61	1606.29	C=O stretching vibration for -COOH groups
7	1695.10		C=O stretching
8	2356.22	2352.94	C-H bending
9	2857.14, 2925.16	2857.14, 2929.97	C-H stretching
10	3436.33	3425.73	O-H symmetrical stretching (H-bonded)
11	3770.30		O-H stretching vibration of hydroxyl functional groups

Table 3: Analysis of FT-IR spectra of the raw and activated biochar from *C. odorata*.

S/N	CO biochar	Sulfonated CO	Band assignment
1	458.74		C-H bending
2		617.00	C-O-H bending
3	873.09		C-H out-of-plane bending of benzene derivatives
4		1034.96, 1180.00	S=O symmetrical stretching
5	1441.69	1379.02	In-plane O-H bending and C-O stretch of dimers
6	1596.17	1592.38	C=O stretching vibration for -COOH groups
7	2352.94	2352.94	C-H bending
8	2857.14, 2924.36	2929.97	C-H stretching
9	3440.00	3419.00	O-H stretching vibration of hydroxyl functional groups

The physicochemical properties of bio-oil derived from CC and CO are shown in Table 4. There was no obvious change in appearance of bio-oils before and after upgrading (Figure not shown), but there was a noticeable change from the irritating heavy smoke-like smell of the bio-oil to a sweet-like smell. This is due to the changes from the alkylation of phenolic compounds (phenolic, guiacol, and methyl phenols) and also formation of butyl acetate and esters during upgrading.

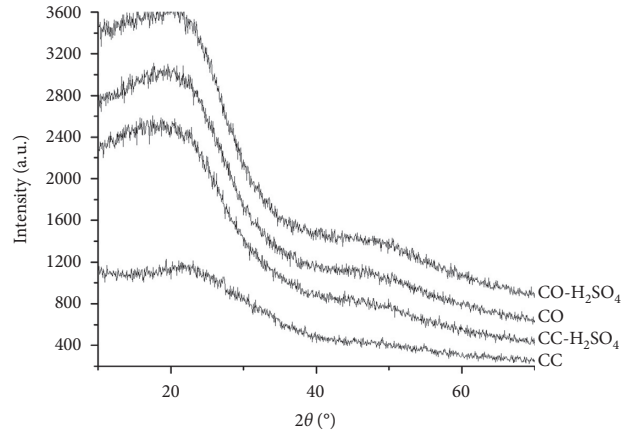

Figure 2: XRD patterns of the raw and acid-modified biochar.

Table 4: Properties of raw and upgraded bio-oil derived from CC and CO.

Parameters	CC bio-oil	CC upgraded bio-oil	CO bio-oil	CO upgraded bio-oil
pH	2.2	3.4	2.4	3.8
Viscosity (kg/m·s) (25°C)	0.1183	0.0586	0.1174	0.0538
Density (kg/m^3)	1.30	0.818	1.29	0.806
Acid value (mg KOH/g)	64.52	13.44	60.13	12.24
Flash point (°C)	250	97.5	250	80.5
HHV (MJ/kg)	11.20	32.80	10.10	30.90
Flammability	Low	High	Low	High
Pour point (°C)	−4	−12	−4	−18
Moisture content (%)	30.6	7.4	32.4	8.1
Oxygen content (%)	32.00	21.45	35.40	24.09
Odour	Irritating smell	Sweet smell	Irritating smell	Sweet smell

The water content of the upgraded bio-oil was reduced from 30.6% to 11.4% for CC and from 32.4% to 13.1% for CO. The decrease was due to acid-catalyzed addition of water across the olefin, leading to production of alcohol [16]. This process also removed some portion of water molecules formed during the esterification reaction and ether and acetal formation. This led to the increase in the high heating value of the bio-oil from 11.20 MJ/Kg to 32.80 MJ/Kg for CC and from 10.10 MJ/Kg to 30.90 MJ/Kg for CO. Water removal by acid-catalyzed olefin hydration is the key reason for the successful upgrading process. As water concentration drops, esterification and acetal formation equilibra shift towards ester and acetal products. In turn, the formed ester and acetal and the added alcohol help reduce the phase separation present between the hydrophilic bio-oil and hydrophobic olefin. All of this occurs while maintaining the heating value of raw bio-oil, alcohol, and olefin. Also the presence of residual 1-butanol and 3,7-dimethyloct-1-ene contributes to increase in the heating value of the bio-oil.

The oxygen content was lowered from 32 to 21.45% and from 35.40 to 24.09% for CC and CO, respectively. This reduction helped to increase the heating value and reduce the microphase separation in the bio-oil [23]. The upgraded bio-oil density was lowered from 1.30 to 0.818 kg/m^3 and from 1.29 to 0.806 kg/m^3 for CC and CO, respectively. The pH value of the bio-oil was reduced from 2.2 to 3.4 for CC and from 2.4 to 3.8 for CO. The reduction in the acidity shows that carboxylic acids present in the bio-oil has been converted to esters through the reaction of alcohols and olefin in the presence of the acid catalyst. This improves the quality and stability of the bio-oil [24]. The viscosity of the bio-oil was reduced compared to the upgraded one which shows the influence of the low viscosity of the olefin and the alcohol added. There was an increase in the flammability of the bio-oil which shows the effect of the olefin and alcohol.

3.4. Chemical Composition of Upgraded Bio-Oil. Crude bio-oil has a complex array of highly oxygenated components, which are nearly all oxygenated organic species which includes anhydrous sugars, carboxylic acids, phenols, aldehydes, ketones, mono- and poly-alcohols, ethers, esters, furans, hydroxyl aldehydes, and hydroxyl ketones, which is a major limitation factor [5, 25, 26].

Catalytic olefination and esterification reactions, where olefins and alcohol are added to bio-oil over the solid acid catalyst at low temperature, were employed in this study. The reaction produces mainly esters by the reaction of carboxylic acids, aldehydes, and ketones present in the bio-oil with olefins in the presence of alcohol as a solvent and coreagent. In this process, esterification, olefin hydration, phenol alkylation, etherification, and hydration reactions of olefin occur simultaneously, converting the acid compounds into esters, ethers, and alkylated phenols. The products are less hydrophilic, water is removed instead of being generated, the hydroxyl group was reduced, and oxygen content was reduced, giving a higher fuel value.

Table 5 shows the chemical composition of bio-oil derived from CC and CO biomass as determined by GC-MS analysis. Bio-oil obtained from CC contains mostly oxygenated compounds in form of phenol (37.33%), ester (3.80%), ketones and aldehydes (16.69%), acids (12.57%), alcohols (9.78%), and furans (7.09%), as compared to olefinated CC bio-oil, which contains less phenol (12.82%) and acids (11.03%), but there is an increase in ester formation (46.01%). Likewise, bio-oil obtained from CO also contains more oxygenated compounds: phenol (39.82%) and ketones and aldehydes (21.43%), while ester (2.105%) was considerably low. Upgrading caused an increase in ester (38.12%) and alcohols (11.90), while a decline was noticed in phenol (14.25%), ketones and aldehydes (8.35%), and acids (12.66%). Individual chemical components of the raw and upgraded bio-oils are presented in Tables S1–S4.

Presence of highly oxygenated compounds in the raw bio-oil contributed to its nonsuitability as automobile fuels. Therefore, reduction in the oxygenated compounds, acid content, and increase in esters show a high catalyst activity, leading to lower viscosity and hydrophilicity of the final product. These changes increase both stability and hydrocarbon blending ability of the upgraded bio-oil. These results showed that 3,7-dimethyloct-1-ene/butanol upgrading is feasible and produces less hydrophilic fuel molecules, which makes the olefinated bio-oil suitable for fossil fuel substitution.

Table 5: Chemical composition of raw and upgraded bio-oil from biomass.

Components	CC raw bio-oil (%)	CC upgraded bio-oil (%)	CO raw bio-oil (%)	CO upgraded bio-oil (%)
Acids	12.57	11.03	17.05	12.663
Esters	3.80	46.01	2.105	38.12
Phenols	37.33	12.82	39.82	14.253
Ketone and aldehyde	16.69	5.62	21.43	8.35
Alcohol	9.78	11.52	0	11.898
Furan	7.09	0.41	5.99	0
Octene	0.00	12.58	0	14.714
Others	5.76	0.00	4.165	0

4. Conclusion

Upgrading of pyrolyzed bio-oil obtained from corn cob and *Cedrela odorata* (sawdust) by catalytic olefination and esterification using 3,7-dimethyloct-1-ene in the presence of butanol with the solid sulfonated catalyst prepared from the biochar by-products was investigated to improve the properties of the crude bio-oils obtained and make it a suitable substitute for conventional fossil fuel. The change in the high heating value was moderate, in the presence of excess olefin which reduced the water content significantly. However, butanol helped to decrease acid content of starting raw bio-oil by formation of esters. Therefore, butanol remains a key component in catalytic olefination for bio-oil upgrading. The FT-IR analysis of the crude and catalyzed biochars shows the sulfonation and hydroxyl peak, indicating the suitability of the catalyzed biochars for the catalysis process. The GC-MS analysis results show that the crude bio-oil was dominated by oxygenated compounds, while the catalytic olefination and esterification bio-oil are dominated with desirable compounds such as esters and phenolics, thereby showing a lower percentage of undesirable acidic compounds. The proximate analysis results showed the acid-catalyzed olefination and esterification of the crude bio-oil in the presence of butanol were able to reduce the water content and acid value and thus increased the heating value and calorific value of the bio-oil. This study has further confirmed the assertion that catalytic olefination and esterification can significantly improve the fuel properties of bio-oil in the presence of some requisite such as alcohol and catalyst.

Data Availability

The data used to support the findings of this study are included within the article and also included within the supplementary information file(s). Furthermore, data of this study are available from the corresponding author upon request.

Conflicts of Interest

The authors declare that there are no conflicts of interest.

Acknowledgments

This work was supported through the grants provided by the Department of Chemistry, University of Ibadan. The authors of this work wish to acknowledge the efforts of Dr. I. A. Adegoke for his support in provision of the pyrolyzer and *Cedrela odorata* sawdust used in the production of bio-oil.

Supplementary Materials

Table S1: selected organic oxygen-containing components of raw bio-oil (corn cobs). Table S2: selected organic oxygen-containing components of upgraded bio-oil (corncobs). Table S3: selected organic oxygen-containing components of raw bio-oil (*Cedrela odorata*). Table S4: selected organic oxygen-containing components of upgraded bio-oil (*Cedrela odorata*). Figure S1: FT-IR spectra of raw corn cobs. Figure S2: FT-IR spectra of the corn cobs catalyst. Figure S3: FT-IR spectra of raw *Cedrela odorata*. Figure S4: FT-IR spectra of the *Cedrela odorata* catalyst. (*Supplementary Materials*)

References

[1] The International Energy Outlook, *An Assessment by the U.S. Energy Information Administration (EIA) of the Outlook for International Energy Markets through 2040*, 2016.

[2] R. R. Wilk, R. Bent, L. Orr, and R. Barker, "Culture and energy consumption," in *Energy Science, Policy and the Pursuit of Sustainability*, Island Press, Washington, DC, USA, 2002.

[3] G. W. Huber, S. Iborra, and A. Corma, "Synthesis of transportation fuels from biomass: chemistry, catalysts, and engineering," *Chemical Reviews*, vol. 106, no. 9, pp. 4044–4098, 2006.

[4] A. Demirbas, *Securing the Planet's Future Energy Needs*, Springer-Verlag London Limited, London, UK, 2009.

[5] D. Mohan, C. U. Pittman, and P. H. Steele, "Pyrolysis of wood/biomass for bio-oil: a critical review," *Energy and Fuels*, vol. 20, no. 3, pp. 848–889, 2006.

[6] J. P. Diebold, "A review of the chemical and physical mechanisms of the storage stability of fast pyrolysis bio-oils," in *Fast Pyrolysis of Biomass: A Handbook*, vol. 2, pp. 243–292, CPL Scientific Publishing, Newbury, UK, 2000.

[7] C. A. Mullen, A. A. Boateng, N. M. Goldberg, I. M. Lima, D. A. Laird, and K. B. Hicks, "Bio-oil and bio-char production from corn cobs and stover by fast pyrolysis," *Biomass and Bioenergy*, vol. 34, no. 1, pp. 67–74, 2010.

[8] C. Ravikumar, P. Senthil Kumar, S. K. Subhashni, P. V. Tejaswini, and V. Varshini, "Microwave assisted fast pyrolysis of corn cob, corn stover, saw dust and rice straw: experimental investigation on bio-oil yield and high heating values," *Sustainable Materials and Technologies*, vol. 11, pp. 19–27, 2017.

[9] B. Biswas, N. Pandey, Y. Bisht, R. Singh, J. Kumar, and T. Bhaskar, "Pyrolysis of agricultural biomass residues: comparative study of corn cob, wheat straw, rice straw and rice husk," *Bioresource Technology*, vol. 237, pp. 57–63, 2017.

[10] S. Czernik, R. French, C. Feik, and E. Chornet, "Hydrogen by catalytic steam reforming of liquid byproducts from biomass thermoconversion processes," *Industrial & Engineering Chemistry Research*, vol. 41, no. 17, pp. 4209–4215, 2002.

[11] M. Ikura, M. Slamak, and H. Sawatzky, "Pyrolysis liquid-in-diesel oil microemulsions," US Patent 5820640, 1998.

[12] S. Chatterjee, Z. Zhang, and C. U. Pittman Jr., "Acid-catalyzed olefination of bio-oil in the presence of ethanol," *Biofuels*, vol. 4, no. 3, pp. 285–294, 2013.

[13] R. N. Hilten, B. P. Bibens, J. R. Kastner, and K. C. Das, "In-line esterification of pyrolysis vapor with ethanol improves bio-oil quality," *Energy & Fuels*, vol. 24, no. 1, pp. 673–682, 2010.

[14] S. K. Tanneru, D. R. Parapati, and P. H. Steele, "Pretreatment of bio-oil followed by upgrading via esterification to boiler fuel," *Energy*, vol. 73, pp. 214–220, 2014.

[15] W. M. Xiong, M. Z. Deng, L. Deng, Y. Fu, and Q. X. Guoand, "Esterification of organic acid in bio-oil using acidic ionic liquid catalysts," *Energy & Fuels*, vol. 23, no. 4, pp. 2278–2283, 2009.

[16] Z. Zhang, S. Sui, F. Wang, Q. Wang, and C. Pittman Jr., "Catalytic conversion of bio-oil to oxygen-containing fuels by acid-catalyzed reaction with olefins and alcohols over silica sulfuric acid," *Energies*, vol. 6, no. 9, pp. 4531–4550, 2013.

[17] X. Yang, S. Chatterjee, Z. Zhang, X. Zhu, and C. U. Pittman Jr., "Reactions of phenol, water, acetic acid, methanol, and 2-hydroxymethylfuran with olefins as models for bio-oil upgrading," *Industrial & Engineering Chemistry Research*, vol. 49, no. 5, pp. 2003–2013, 2010.

[18] Z. Zhang, Q. Wang, P. Tripathi, and C. U. Pittman Jr., "Catalytic upgrading of bio-oil using 1-octene and 1-butanol over sulfonic acid resin catalysts," *Green Chemistry*, vol. 13, no. 4, pp. 940–949, 2011.

[19] A. Heidekum, M. A. Harmer, and W. F. Hoelderich, "Addition of carboxylic acids to cyclic olefins catalyzed by strong acidic ion-exchange resins," *Journal of Catalysis*, vol. 181, no. 2, pp. 217–222, 1999.

[20] J. Liu, S. Wang, and J. A. Guin, "Etherification of dimethylbutenes in excess methanol," *Fuel Processing Technology*, vol. 69, no. 3, pp. 205–219, 2001.

[21] F. A. Dawodu, O. O. Ayodele, J. Xin, and S. Zhang, "Application of solid acid catalyst derived from low value biomass for a cheaper biodiesel production," *Journal of Chemical Technology & Biotechnology*, vol. 89, no. 12, pp. 1898–1909, 2014.

[22] F. A. Dawo, O. Ayodele, J. Xin, S. Zhang, and D. Yan, "Effective conversion of non edible oil with high free fatty acid into biodiesel by sulphonated carbon catalyst," *Applied Energy*, vol. 114, pp. 819–826, 2014.

[23] A. V. Bridgwater, D. Meier, and D. Radlein, "An overview of fast pyrolysis of biomass," *Organic Geochemistry*, vol. 30, no. 12, pp. 1479–1493, 1999.

[24] C. G. Yang and C. He, "Gold(I)-Catalyzed intermolecular addition of phenols and carboxylic acids to olefins," *Journal of the American Chemical Society*, vol. 127, no. 19, pp. 6966-6967, 2005.

[25] A. V. Bridgwater, "Review of fast pyrolysis of biomass and product upgrading," *Biomass and Bioenergy*, vol. 38, pp. 68–94, 2012.

[26] L. Ingram, D. Mohan, M. Bricka et al., "Pyrolysis of wood and bark in an auger reactor: physical properties and chemical analysis of the produced bio-oils," *Energy & Fuels*, vol. 22, no. 1, pp. 614–625, 2008.

Hindawi
International Journal of Chemical Engineering
Volume 2019, Article ID 1806017, 7 pages
https://doi.org/10.1155/2019/1806017

Research Article

One-Step Synthesis of CaO-ZnO Efficient Catalyst for Biodiesel Production

Javier Toledo Arana,[1] Juan José Torres,[1] Diego F. Acevedo,[1] Cristian O. Illanes,[2] Nelio A. Ochoa,[2] and Cecilia L. Pagliero[1]

[1]*Instituto de Investigaciones en Tecnologías Energéticas y Materiales Avanzados (IITEMA), Planta Piloto de Ingeniería Química, Universidad Nacional de Río Cuarto, Facultad de Ingeniería, Dpto. de Tecnología Química, 5800 Río Cuarto, Argentina*
[2]*INFAP–CONICET-FONCYT, Universidad Nacional de San Luis, 5700 San Luis, Argentina*

Correspondence should be addressed to Cecilia L. Pagliero; cpagliero@ing.unrc.edu.ar

Received 20 November 2018; Revised 18 January 2019; Accepted 10 February 2019; Published 10 March 2019

Guest Editor: Shunmugavel Saravanamurugan

Biodiesel is the best candidate for fuel oil replacement, and to obtain it, heterogeneous catalysts offer large advantages: they can be separated from the product and reused. This work reviews a novel one-step synthesis of CaO-ZnO catalytic particles suitable for biodiesel production. The catalyst is synthesized using an original simple method that involves mixing of ZnO with $CaCO_3$ and subsequent calcination. The CaO-ZnO microparticles obtained present an average size of 2 μm. This material shows the characteristic crystallographic cubic structure of CaO and the hexagonal phase of ZnO. The temperature-programmed reduction experiment evidences an interaction between CaO and ZnO. Moreover, the infrared spectroscopy shows typical bands of these compounds. The catalyst shows high biodiesel yield, up to 73% in the first cycle and 64% in the second one. In this work, the synthesis of an efficient CaO-ZnO catalyst with a huge potential is revealed, which could be an economic alternative to produce biodiesel.

1. Introduction

Nowadays, searching for a renewable and alternative energy source is an important task due to the continuous increase in energy demand, the depletion of fossil fuel resources, the global warming, and the environmental pollution. The biodiesel (BD), fatty acid methyl esters (FAMEs), has been accepted worldwide as a renewable fuel alternative to the fossil diesel [1]. FAMEs are obtained by the transesterification of triglycerides (vegetable oils or animal fats) with methanol using catalysts [2]. FAMEs can be used as a substrate for the preparation of additives for diesel fuels and provide an environmentally friendly alternative to conventional diesel [2–4]. It is well known that the mechanism of the transesterification reaction to obtain biodiesel is the same for both alcohols: ethanol and methano. However, ethanol allows obtaining BD with better characteristics for the diesel engine: high cetane number and small cloud point [5–7]. Moreover, ethanol produces more environmentally friendly biodiesel than methanol because its combustion produces fewer amounts of CO, particles, and NOx. There are several kinds of catalysts (acid, basic, heterogeneous, and homogeneous) to produce biodiesel [8–13]. Basic homogeneous catalysts (sodium hydroxides or alkoxides) are frequently used for the transesterification of triglycerides in an industrial scale. However, these catalysts have serious disadvantages; for example, they are neither recyclable nor environmentally friendly and lead to formation of biodiesel and glycerol contaminated with sodium or potassium ions [14, 15] and they also produce soaps. Furthermore, these catalysts are deactivated when the feedstock presents a humidity level of more than 0.3 wt.% and/or the free fatty acid (FFA) level are higher than 0.5 wt.% [16]. Therefore, the use of homogeneous catalysts to produce biodiesel requires very pure raw materials. The nonedible oils, animal fat, cooking oils, or waste oils used as raw materials for the

biodiesel production are less expensive than edible oils and reduce the cost of biodiesel production [17–20]. However, these oils usually contain high amounts of FFAs (up to 12% by weight) and humidity (~3% by weight), and also a homogeneous base catalyst cannot be used for transesterification [21]. In order to achieve a solution to the abovementioned problems, the researchers have developed heterogeneous basic catalysts, which show several advantages over homogeneous ones. The main advantages are that they present a better catalytic performance and an easy separation from the reaction products. Moreover, they maintain its activity independently to the humidity content and the quantity of FFA in the feedstock, and they can also be recycled [4]. Additionally, the heterogeneous catalyst most frequently used for the transesterification reaction is calcium oxide, mainly due to its lack of toxicity and low cost [22–25]. The activity of pure CaO could be improved by preparing the oxide in the nanocrystalline form [26] or by potassium or lanthanum ion impregnation [22, 27, 28]. Hassan et al. found that a 2.0 M calcium precursor has high catalytic activity and it obtained 81% FAME yield within 3 h of the reaction [29]. Among the transition metal oxides, ZnO is another most studied catalyst [30–32]. In a recent work, a screening of the performance of ZnO and CaO catalysts showed that a conversion at 6 h for the transesterification reaction using soybean oil and methanol was 38% and 24%, respectively [33]. The performance of the ZnO/Li catalyst was tested using soybean oil esterified with methanol. Using this catalyst leads to a conversion efficiency of 96% in 3 h of reaction time [34]. Also, the preparation of CaO-ZnO has been reported by the coprecipitation method, varying the atomic ratio Ca/Zn [35]. The CaO-ZnO powder mixture has been used as a heterogeneous catalyst for the transesterification of soybean oil using methanol [36–38]. However, the proposed synthesis methods involve several steps to obtain the catalyst. In this work, a simple synthesis of CaO-ZnO catalysts, in only one step, is proved.

2. Materials and Methods

2.1. Preparation of Catalyst (CaO-ZnO). CaO-ZnO catalysts were prepared by adding 1 g of ZnO to 50 mL of a 2 M $CaCO_3$ aqueous solution. Such a ratio of Zn/Ca was chosen considering exploratory assays. A further increment of Zn concentration not showed a higher conversion in the transesterification reaction. As it was previously reported by Kumar and Ali [39], an increase of Zn content can affect the catalyst base strength. The prepared suspension was stirred for 3 hours. After that, this suspension was dried in an oven at 120°C for 24 hours. Afterwards, the obtained solid was calcined at 850°C in a muffle. The catalyst synthesis was performed from ambient temperature to 100°C with a heating rate of 4°C·min^{-1}; in a first plateau, the sample was kept at 100°C during 75 minutes and then the temperature was raised to 850°C at 3.5°C·min^{-1}. Once this temperature was reached, a second plateau was performed during 180 minutes. Finally, the temperature was reduced to 20°C with a cooling ramp of 3°C·min^{-1}.

The calcination temperature causes the decomposition of carbonate as it is shown in equation (1). This new material is synthesized in one step. Such *in situ* synthesis produces an intimate contact of the ZnO with the CaO during the calcination.

$$CaCO_3 \longrightarrow CaO + CO_2 \quad (1)$$

2.2. Catalyst Characterization. The catalyst was characterized using scanning electron microscopy (SEM), energy dispersive spectroscopy (EDS), X-ray diffraction analysis (XRD), Fourier transform infrared spectroscopy (FTIR), BET surface area, and thermal programmed reduction (TPR).

2.2.1. Scanning Electron Microscopy and Analysis of X-Ray Scattering. SEM micrographs were obtained by using a LEOGENESIS VP 1450 microscope. The samples were placed on aluminium pegs and sputtered with gold. The SEM equipment was operated under high vacuum, and the measurements were obtained using an accelerating voltage of 8 kV. Also, the elemental analyses were determined by energy dispersive spectroscopy (Genesis EDS probe).

2.2.2. Particle Size Distribution. The particle size distribution was determined employing a Sedigraph 5100 analyser. The device uses X-rays to detect the concentration of particles based on Stokes' law. The absorption of X-rays is directly proportional to the mass of the particles. The well-dispersed sample was placed for the cell analysis, where a beam of X-rays initially determines the amount of larger particles and then it registers particles of smaller sizes.

2.2.3. X-Ray Diffraction (XRD) and Thermal Programmed Reduction (TPR). The diffractogram of the catalyst was obtained on a Rigaku diffractometer operated at 30 kV and 20 mA, using Kα radiation ($\lambda = 0.15418$ nm) at a speed of 3°C min^{-1} between $2\theta = 20^\circ$ and 80°.

The TPR analysis was performed with a differential scanning calorimeter equipped with a cooling device (Netzsch DSC-204-F1-Phoenix). The catalyst (5 mg) was dried for 2 h at 650°C and reduced at 25 to 650°C (5°C·min^{-1}), with 5% H_2/N_2 mixture. The H_2 concentration in the effluent was monitored with a thermal conductivity detector. The TPR curves were obtained from 100°C to 590°C using N_2 liquid, at a scanning rate of 10°C·min^{-1}.

2.2.4. Fourier Transform Infrared Spectroscopy (FTIR). In order to verify the presence of characteristic absorption bands of CaO and ZnO, the FTIR spectra were collected by using a Nicolet Impact 410 spectrometer in transmission mode, from KBr pellets of solid samples; a total of 200 scans were averaged at a resolution of 4 cm^{-1}.

2.2.5. BET Surface Area. The surface area was measured with a Micromeritics Gemini V analyser by adsorption of

nitrogen at −196°C on 100 mg of a sample previously degassed at 250°C for 16 h under flowing N_2.

2.2.6. Biodiesel Synthesis. In order to synthesize BD, ethanol 99.4% v/v (EtOH) was provided by BIO4 S.A. (Río Cuarto, Argentina); the soybean oil was kindly provided by OLCA S.A.I.C. (General Cabrera, Argentina). The synthesis was performed in a two-necked round-bottom flask equipped with a reflux condenser and a magnetic stirrer. The heating of the reactive mixture was conducted by using a hot water bath (60°C) using a crystallizer with glycerol-water (90 : 10 v/v). Then 20 g of semirefined (degummed and neutral) soybean oil and the catalyst was placed into the flask at a ratio of 10% w/w and 30% w/w, respectively.

The oil and the catalyst were dispersed in EtOH 99.4% v/v. The quantity of EtOH was calculated to achieve an oil/alcohol molar ratio of 1 : 40. The temperature of the mixture was controlled at 60°C. The reactant system was kept under vigorous stirring (c.a. 800 rpm) for 6 hours. The catalyst was separated by centrifugation, and then the reaction mixture was transferred to a 250 mL decantation ampoule. At room temperature, phase separation was observed, an upper phase: ethyl ester (BD), and a bottom phase: glycerol. The latter was separated, quantified, and discarded, while the first phase (after ethanol evaporation in a rotary evaporator: 70°C, 20 torr, 1 h) was used for BD characterization. The yield of biodiesel (%EE) was calculated as presented in Eq. (2), being m_{oil} the mass of vegetable oil and m_{BD} the biodiesel mass:

$$\%\ \mathrm{EE} = \frac{m_{BD}}{m_{oil}} 100. \tag{2}$$

Free glycerol (FG) and total glycerol (TG) were determined by AOCS method Ca 14-56. Pro-analysis chloroform, glacial acetic acid 99.5% v/v, periodic acid, potassium iodide, potassium dichromate, potassium hydroxide, and hydrochloric acid were purchased from Cicarelli, while ethyl alcohol (EtOH) 95% v/v was obtained from Porta S.A., Argentina. All measurements were performed in duplicate with independent samples.

2.2.7. Catalyst Leaching Studies. The leaching of the reactive groups Ca(II) and Zn(II) was determined using atomic absorption spectroscopy (Varian 50AA spectrometer). Once the reaction was finished, the solid catalysts were separated by centrifugation (3000 rpm, 30 min). Then, the solution was mineralized by HNO_3 for 8 h. Ca(II) was determined at 422.7 nm with an N_2O/acetylene mixture, whereas Zn(II) was determined at 213.9 nm using an air/acetylene mixture.

2.2.8. Reusability. In order to study the reusability, the catalyst regeneration was performed by washing the used CaO-ZnO catalyst with ethyl alcohol and hexane, followed by calcination in a muffle furnace at 300°C for 3 hours to remove any remaining alcohol, oil, or biodiesel. Then, the BD production was carried out following the procedure depicted in Section 2.2.6.

3. Results and Discussion

3.1. Characterization of the Catalyst. The synthesis procedure employed to obtain the CaO and ZnO particles produces a relatively uniform size distribution as it is shown in Figure 1. The average of the particle size achieved is approximately 2 μm.

The SEM images (Figures 2(a) and 2(b)) of the catalyst show that the synthesized material presents particles of different sizes ranging from c.a. 1 μm to 20 μm. However, most of the particles present the size of c.a. 2 μm. The quantitative analysis results from EDS were used to determine the following composition: Ca 44.58%, Zn 20.81%, and O 34.62%. The image of the material indicates that the particles are formed by agglomeration of microparticles and nanoparticles generated during the calcination process (Figure 2). In addition, the external rugosity enhances the superficial area, allowing more available active sites for the catalytic process.

The measured specific surface area obtained was 10.3 $m^2 \cdot g^{-1}$, and this value is in agreement with another similar catalyst synthesized recently (7 to 11 $m^2 \cdot g^{-1}$) [29, 33].

The catalyst X-ray diffraction analysis is shown in Figure 3. The diffractogram reflects the characteristic peaks at c.a. 34.4°, 36.2°, 47.6°, 56.7°, and 62.7°, which correspond to a cubic crystallographic form of CaO (JCPDS 821 691), and peaks at c.a. 31°, 34°, 36°, 47°, 27°, 64°, 67°, 68°, and 69° (JCPDS 891 397), which match to the hexagonal phase of ZnO. These results confirm that the particles are formed by a combination of the two oxide phases CaO-ZnO.

In Figure 4, the TPR experiment of the mixture (CaO + ZnO) shows the typical peaks of the CaO (at c.a. 340°C) [40] and the ZnO (at c.a. 290°C and 500°C) [41]. On the other hand, the profile of the CaO-ZnO catalyst shows a peak at c.a. 330°C and a shoulder at 490°C, showing a TPR curve different than CaO + ZnO. Based on this result and considering the XRD diffractogram data, it is possible to ensure that the particles of the CaO-ZnO catalyst do not present the same physicochemical characteristics compared with the mixture of the two oxides CaO + ZnO.

The FTIR spectrum of the catalyst is shown in Figure 5. The spectrum shows a weak absorption band at 875 cm^{-1} that reveals the presence of carbonate [42]. It has been demonstrated that the contact of the CaO reactive surface area with air during calcination produces a considerable amount of CO_2 and H_2O. These compounds are adsorbed on the CaO surface in the form of free -OH and carbonate species (fundamental bands at 1465, 874, and 712 cm^{-1}) [42]. The characteristic band of the O-H stretching vibration of $Ca(OH)_2$ is located at 3643 cm^{-1}, and the bands at 2965 and 2880 cm^{-1} are attributed to the O-H groups from H_2O [43, 44]. Moreover, the band at 1080 cm^{-1} is attributed to the Zn-O-H bending vibration [36]. The absorption peaks recorded at 400–600 cm^{-1} could be considered to be of Zn-O stretching [45]. Since the infrared spectrum shows the characteristic band of ZnO and CaO, it is possible to ensure that catalysts are formed by both compounds.

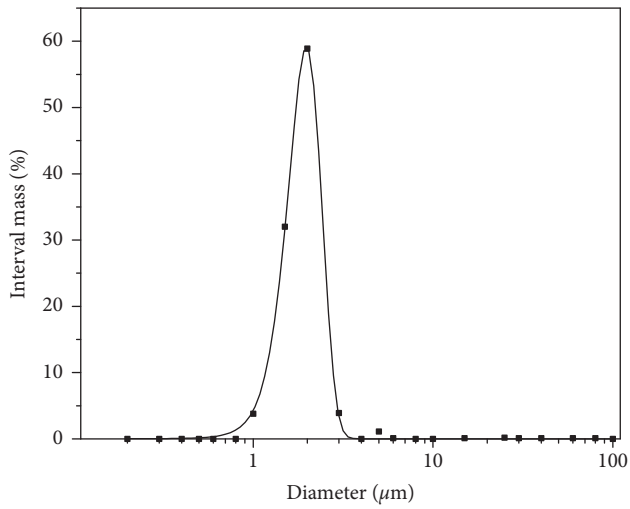

Figure 1: Particle size distribution of the CaO-ZnO catalyst.

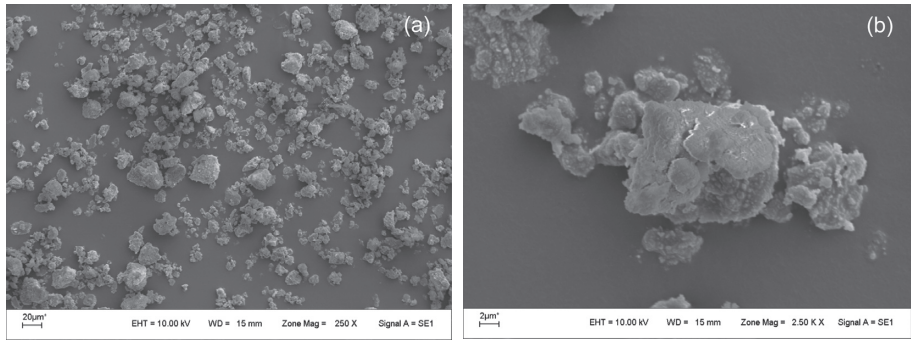

Figure 2: SEM images of the fresh catalyst.

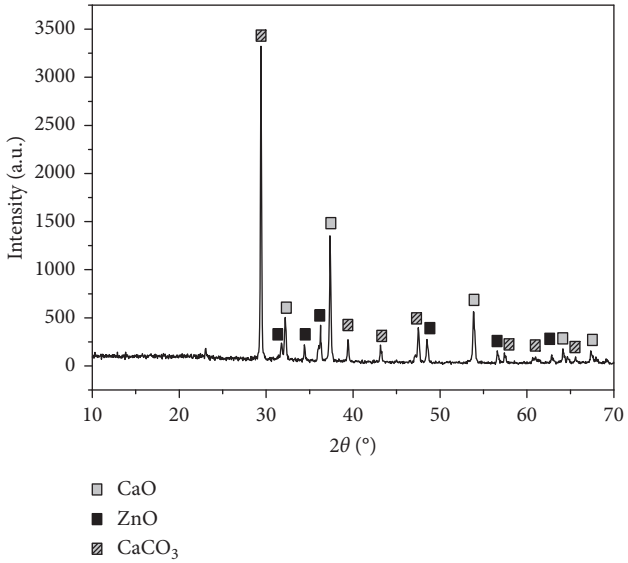

Figure 3: XRD diffractogram of the CaO-ZnO catalyst.

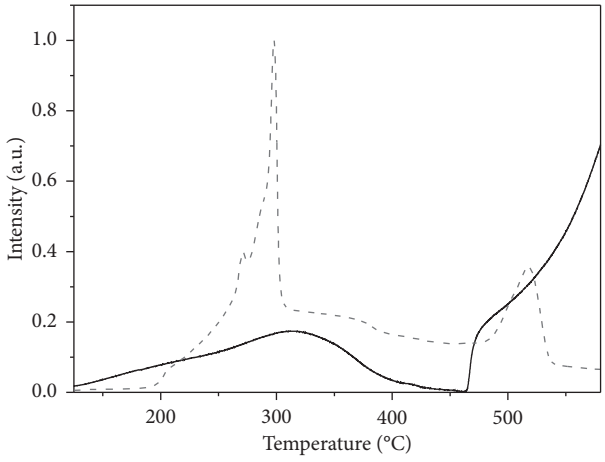

Figure 4: Temperature-programmed reduction experiment: CaO + ZnO oxide mixture (doted line); CaO-ZnO catalyst (continuous line).

3.2. Biodiesel Synthesis. The biodiesel synthesis was performed as described in the experimental section. After the reaction, the phases were separated, the excess of alcohol was removed, and the amounts of both phases were weighed to estimate the conversion of esters according to equation (2). The results are shown in Table 1.

From the analysis of the results, it can be concluded that a change in the catalyst/oil ratio (10 and 30% w/w) does not

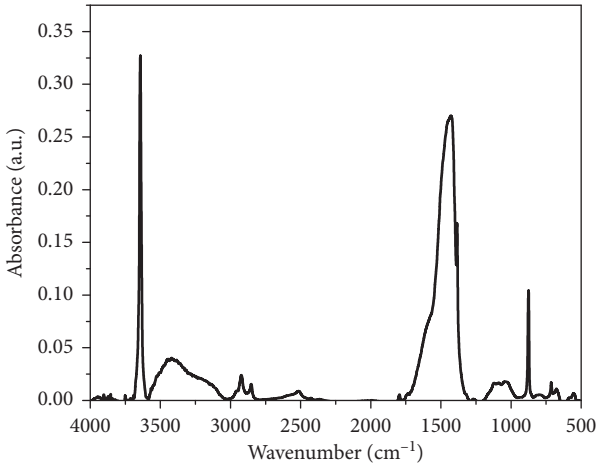

Figure 5: Infrared spectra of the CaO-ZnO catalyst.

Table 1: Percentage of ethyl esters generated by biodiesel synthesis using mixed CaO-ZnO as a catalyst.

Catalyst	% EE
Fresh (10%)	73 ± 0.5
Fresh (30%)	77 ± 0.6
Washed (10%)	64 ± 0.7

Reaction conditions: oil/alcohol molar ratio 1 : 40, 60°C, and 800 rpm for 6 hours.

improve the BD conversion (Table 1). For this reason, it is more efficient and economical to produce BD with only 10% w/w catalyst.

Considering that the regeneration and reuse of the catalyst is one of the most important aspects in industrial applications, the catalyst reusability for BD production was studied. The CaO-ZnO catalyst reused yields 64% EE (Table 1). These results show that the catalyst presents high performance and it is possible to reuse it without a significant activity loss.

The Ca(II) and Zn(II) concentration obtained by atomic absorption spectroscopy in the reaction mixture was 0.31% w/w and 0.15% w/w, respectively. These results allow concluding that the leaching of the catalyst is negligible and the decrease in the yield may be due to the catalyst poisoning.

For the experiment with 10% catalyst, the found values of free and total glycerol, according to AOCS method Ca 14-56, for the fresh catalyst (TG 1.18 ± 0.03%, FG 0.83 ± 0.01%) and the washed catalyst (TG 1.40 ± 0.03%, FG 1.00 ± 0.02%), were similar. These results demonstrate the good performance of the reused catalyst for the BD production.

Furthermore, the SEM image of the reused (washed) catalyst does not show structural changes in the surface as compared to the fresh catalyst (Figure 6).

Alba-Rubio et al. have reported a similar zinc oxide catalyst manufactured from the thermal decomposition of zinc oxalate impregnated with different amounts of calcium oxide [46]. The ZnO-CaO catalysts synthesized by these authors were thermally activated at 1073 K. The FAME yield was ≈80% in 5 h (using ZnO and CaO 4 wt.%)

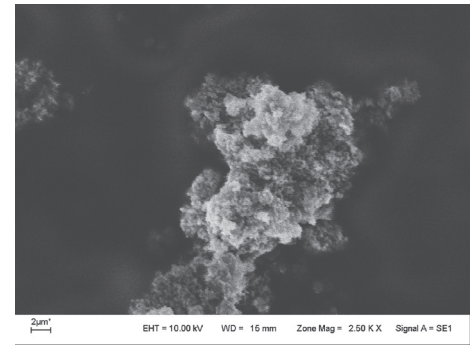

Figure 6: SEM image of the recovered catalyst.

and ≈50% (using ZnO and CaO 6 wt.%) in 3 h using methanol [46, 47].

It is known that the synthesis of esters using methanol produces better yields than using ethanol. Nearly employing half quantity of the catalyst and one hour less of reaction, the final yield is almost the same as that obtained in our experiments. However, the efforts to substitute nonrenewable (fossil) raw materials for sustainable ones, such as ethanol, are well known [48].

Recently, Hassan et al. [29] found similar results. The synthesis of FAMEs catalyzed by CaO showed conversions of 64–81% employing different concentrations of precursors in the catalyst synthesized by the sol-gel method. The BD reaction conditions were as follows: 60°C for 3 hours, ratio of palm oil to methanol 1 : 9, and 4% of CaO. The similar conversions achieved by these authors, with a lower concentration of catalyst and a lower alcohol-to-oil ratio compared to this work, can be explained with greater efficiency due to the active sites distributed in an improved mesoporous structure produced by the synthesis route of the used catalyst and the use of methanol instead of ethanol, which is well known as a less efficient alcohol for the transesterification reaction [29, 48].

The catalyst prepared by Navas et al. [33] was synthesized by precipitation of the precursors: calcium, magnesium, and zinc nitrates in the presence of alumina and then by calcination at 600–750°C. The biodiesel synthesis was carried out using 5 wt.% catalyst under the following reaction conditions: oil-to-methanol ratio 1 : 6, 6 hours of reaction time, and 60°C. It is remarkable how the presence of alumina increases the FAME conversion for all the precursors used, mainly for MgO (13%–60%). In the case of CaO catalyst, the conversion varies from 38% without alumina to 50% by adding alumina prior to the calcination step. It seems that the supported oxides in the alumina provide higher concentration of basic sites and the catalyst is more efficient [47].

The results presented in this work are comparable to those published elsewhere and show an acceptable performance of ethanol as alcohol for the transesterification of vegetable oils using this new heterogeneous CaO-ZnO catalyst prepared in a single step.

These promising results can be taken as a starting point for new developments and optimization of reaction conditions, catalyst preparation, and heterogeneous transesterification reaction.

4. Conclusion

In the present study, an easy one-step synthesis of a novel material to generate a biodiesel catalyst is shown. In addition, it is demonstrated that ethanol is an appropriate alcohol to use as a short-chain alcohol in substitution to methanol. The CaO-ZnO particles of the synthesized catalyst are 2 μm in size. The procedure of synthesis presents an enormous advantage over other techniques due to the CaO-ZnO catalyst is manufactured in only one step. Moreover, this catalyst presents a good performance for the biodiesel synthesis using ethanol. Also, the catalyst can be reused as it maintains its catalytic activity and morphological properties.

Data Availability

The data supporting the conclusions in this work are included in this manuscript. Other datasets generated and analysed during the current work are available from the corresponding author on reasonable request.

Conflicts of Interest

The authors declare that they have no conflicts of interest.

Acknowledgments

The authors acknowledge the National Research Council of Argentina (CONICET), the National Agency for Scientific Promotion (ANPCyT PICT 2144/11 and PICT 0367/13), the National University of San Luis (UNSL), and the National University of Río Cuarto (UNRC) for their financial support.

References

[1] G. Antolín, F. V. Tinaut, Y. Briceño, V. Castaño, C. Pérez, and A. I. Ramírez, "Optimisation of biodiesel production by sunflower oil transesterification," *Bioresource Technology*, vol. 83, no. 2, pp. 111–114, 2002.

[2] F. Ma and M. A. Hanna, "Biodiesel production: a review1-Journal series #12109, Agricultural Research Division, Institute of Agriculture and Natural Resources, University of Nebraska-Lincoln.1," *Bioresource Technology*, vol. 70, no. 1, pp. 1–15, 1999.

[3] A. Ramadhas, S. Jayaraj, and C. Muraleedharan, "Biodiesel production from high FFA rubber seed oil," *Fuel*, vol. 84, no. 4, pp. 335–340, 2005.

[4] A. Demirbas and S. Karslioglu, "Biodiesel production facilities from vegetable oils and animal fats," *Energy Sources, Part A: Recovery, Utilization, and Environmental Effects*, vol. 29, no. 2, pp. 133–141, 2007.

[5] G. Mendow, N. S. Veizaga, and C. A. Querini, "Ethyl ester production by homogeneous alkaline transesterification: influence of the catalyst," *Bioresource Technology*, vol. 102, no. 11, pp. 6385–6391, 2011.

[6] G. Mendow and C. A. Querini, "High performance purification process of methyl and ethyl esters produced by transesterification," *Chemical Engineering Journal*, vol. 228, pp. 93–101, 2013.

[7] L. K. Patrylak, K. I. Patrylak, M. V. Okhrimenko et al., "Ethanol containing ethyl esters of fatty acids as perspective environment like fuel," *Fuel*, vol. 113, pp. 650–653, 2013.

[8] M. D. Serio, R. Tesser, L. Pengmei, and E. Santacesaria, "Heterogeneous catalysts for biodiesel production," *Energy & Fuels*, vol. 22, no. 1, pp. 207–217, 2008.

[9] G. Guan, K. Kusakabe, and S. Yamasaki, "Tri-potassium phosphate as a solid catalyst for biodiesel production from waste cooking oil," *Fuel Processing Technology*, vol. 90, no. 4, pp. 520–524, 2009.

[10] F. Guo, Z.-G. Peng, J.-Y. Dai, and Z.-L. Xiu, "Calcined sodium silicate as solid base catalyst for biodiesel production," *Fuel Processing Technology*, vol. 91, no. 3, pp. 322–328, 2010.

[11] P. C. Mazo and L. A. Rios, "Esterification and transesterification assisted by microwaves of crude palm oil. homogeneous catalysis," *Latin American Applied Research*, vol. 40, no. 4, pp. 337–342, 2010.

[12] C. Ngamcharussrivichai, P. Nunthasanti, S. Tanachai, and K. Bunyakiat, "Biodiesel production through transesterification over natural calciums," *Fuel Processing Technology*, vol. 91, no. 11, pp. 1409–1415, 2010.

[13] J. Boro, A. J. Thakur, and D. Deka, "Solid oxide derived from waste shells of turbonilla striatula as a renewable catalyst for biodiesel production," *Fuel Processing Technology*, vol. 92, no. 10, pp. 2061–2067, 2011.

[14] G. W. Huber, S. Iborra, and A. Corma, "Synthesis of transportation fuels from biomass: chemistry, catalysts, and engineering," *Chemical Review*, vol. 106, no. 9, pp. 4044–4098, 2006.

[15] D. Kumar and A. Ali, "Potassium ion impregnated calcium oxide as a nanocrystalline solid catalyst for biodiesel production from waste cotton seed oil," *Energy Sources, Part A: Recovery, Utilization, and Environmental Effects*, vol. 36, no. 10, pp. 1093–1102, 2014.

[16] M. Canakci and J. Van Gerpen, "Biodiesel production viaacid catalysis," *Transactions of the ASAE*, vol. 42, no. 5, pp. 1203–1210, 1999.

[17] V. G. Deshmane, P. R. Gogate, and A. B. Pandit, "Ultrasound-assisted synthesis of biodiesel from palm fatty acid distillate," *Industrial & Engineering Chemistry Research*, vol. 48, no. 17, pp. 7923–7927, 2009.

[18] S. M. Hingu, P. R. Gogate, and V. K. Rathod, "Synthesis of biodiesel from waste cooking oil using sonochemical reactors," *Ultrasonics Sonochemistry*, vol. 17, no. 5, pp. 827–832, 2010.

[19] V. L. Gole and P. R. Gogate, "Intensification of synthesis of biodiesel from nonedible oils using sonochemical reactors," *Industrial & Engineering Chemistry Research*, vol. 51, no. 37, pp. 11866–11874, 2012.

[20] G. L. Maddikeri, A. B. Pandit, and P. R. Gogate, "Intensification approaches for biodiesel synthesis from waste cooking oil: a review," *Industrial & Engineering Chemistry Research*, vol. 51, no. 45, pp. 14610–14628, 2012.

[21] E. E. Kwon, J. Seo, and H. Yi, "Transforming animal fats into biodiesel using charcoal and CO_2," *Green Chemistry*, vol. 14, no. 6, p. 1799, 2012.

[22] R. S. Watkins, A. F. Lee, and K. Wilson, "Li-CaO catalysed triglyceride transesterification for biodiesel applications," *Green Chemistry*, vol. 6, no. 7, pp. 335–340, 2004.

[23] A. D'Cruz, M. G. Kulkarni, L. C. Meher, and A. K. Dalai, "Synthesis of biodiesel from canola oil using heterogeneous base catalyst," *Journal of the American Oil Chemists' Society*, vol. 84, no. 10, pp. 937–943, 2007.

[24] M. Kouzu, T. Kasuno, M. Tajika, Y. Sugimoto, S. Yamanaka, and J. Hidaka, "Calcium oxide as a solid base catalyst for transesterification of soybean oil and its application to biodiesel production," *Fuel*, vol. 87, no. 12, pp. 2798–2806, 2008.

[25] F.-J. Li, H.-Q. Li, L.-G. Wang, and Y. Cao, "Waste carbide slag as a solid base catalyst for effective synthesis of biodiesel via transesterification of soybean oil with methanol," *Fuel Processing Technology*, vol. 131, pp. 421–429, 2015.

[26] S. Yan, H. Lu, and B. Liang, "Supported CaO catalysts used in the transesterification of rapeseed oil for the purpose of biodiesel production," *Energy & Fuels*, vol. 22, no. 1, pp. 646–651, 2008.

[27] L. C. Meher, M. G. Kulkarni, A. K. Dalai, and S. N. Naik, "Transesterification of karanja (*Pongamia pinnata*) oil by solid basic catalysts," *European Journal of Lipid Science and Technology*, vol. 108, no. 5, pp. 389–397, 2006.

[28] C. Reddy, V. Reddy, R. Oshel, and J. G. Verkade, "Room-temperature conversion of soybean oil and poultry fat to biodiesel catalyzed by nanocrystalline calcium oxides," *Energy & Fuels*, vol. 20, no. 3, pp. 1310–1314, 2006.

[29] N. Hassan, K. N. Ismail, K. H. Ku Hamid, and A. Hadi, "CaO nanocatalyst for transesterification reaction of palm oil to biodiesel: effect of precursor's concentration on the catalyst behavior," *IOP Conference Series: Materials Science and Engineering*, vol. 358, article 012059, 2018.

[30] S. K. Karmee and A. Chadha, "Preparation of biodiesel from crude oil of *Pongamia pinnata*," *Bioresource Technology*, vol. 96, no. 13, pp. 1425–1429, 2005.

[31] J. Jitputti, B. Kitiyanan, P. Rangsunvigit, K. Bunyakiat, L. Attanatho, and P. Jenvanitpanjakul, "Transesterification of crude palm kernel oil and crude coconut oil by different solid catalysts," *Chemical Engineering Journal*, vol. 116, no. 1, pp. 61–66, 2006.

[32] A. K. Singh and S. D. Fernando, "Reaction kinetics of soybean oil transesterification using heterogeneous metal oxide catalysts," *Chemical Engineering & Technology*, vol. 30, no. 12, pp. 1716–1720, 2007.

[33] M. B. Navas, I. D. Lick, P. A. Bolla, M. L. Casella, and J. F. Ruggera, "Transesterification of soybean and castor oil with methanol and butanol using heterogeneous basic catalysts to obtain biodiesel," *Chemical Engineering Science*, vol. 187, pp. 444–454, 2018.

[34] W. Xie and X. Huang, "Synthesis of biodiesel from soybean oil using heterogeneous KF/ZnO catalyst," *Catalysis Letters*, vol. 107, no. 1-2, pp. 53–59, 2006.

[35] C. Ngamcharussrivichai, P. Totarat, and K. Bunyakiat, "Ca and Zn mixed oxide as a heterogeneous base catalyst for transesterification of palm kernel oil," *Applied Catalysis A: General*, vol. 341, no. 1-2, pp. 77–85, 2008.

[36] Ž. Kesić, I. Lukić, D. Brkić et al., "Mechanochemical preparation and characterization of CaO·ZnO used as catalyst for biodiesel synthesis," *Applied Catalysis A: General*, vol. 427-428, pp. 58–65, 2012.

[37] A. Molaei Dehkordi and M. Ghasemi, "Transesterification of waste cooking oil to biodiesel using Ca and Zr mixed oxides as heterogeneous base catalysts," *Fuel Processing Technology*, vol. 97, pp. 45–51, 2012.

[38] Z. Kesic, I. Lukic, M. Zdujic, C. Jovalekic, H. Liu, and D. Skala, "Mechanochemical synthesis of $CaO{\cdot}ZnO{\cdot}K_2CO_3$ catalyst: characterization and activity for methanolysis of sunflower oil," *Chemical Industry and Chemical Engineering Quarterly*, vol. 21, no. 1-1, pp. 1–12, 2015.

[39] D. Kumar and A. Ali, "Transesterification of low-quality triglycerides over a Zn/CaO heterogeneous catalyst: kinetics and reusability studies," *Energy & Fuels*, vol. 27, no. 7, pp. 3758–3768, 2013.

[40] F. Blatter, P. A. V. D. Schaaf, and M. Szelagiewicz, *Crystalline Forms of Rosuvastatin Calcium Salt*, BASF SE, Quincy, FL, USA, 2011.

[41] H. Kumar and R. Rani, "Structural and optical characterization of ZnO nanoparticles synthesized by microemulsion route," *International Letters of Chemistry, Physics and Astronomy*, vol. 19, pp. 26–36, 2013.

[42] K. Nakamoto, *Infrared and Raman Spectra of Inorganic and Coordination Compounds: Theory and Applications in Inorganic Chemistry*, Wiley, Hoboken, NJ, USA, 2009.

[43] O. Koper, Y.-X. Li, and K. J. Klabunde, "Destructive adsorption of chlorinated hydrocarbons on ultrafine (nanoscale) particles of calcium oxide," *Chemistry of Materials*, vol. 5, no. 4, pp. 500–505, 1993.

[44] O. B. Koper, I. Lagadic, A. Volodin, and K. J. Klabunde, "Alkaline-earth oxide nanoparticles obtained by aerogel methods. characterization and rational for unexpectedly high surface chemical reactivities," *Chemistry of Materials*, vol. 9, no. 11, pp. 2468–2480, 1997.

[45] Z. Yang and W. Xie, "Soybean oil transesterification over zinc oxide modified with alkali earth metals," *Fuel Processing Technology*, vol. 88, no. 6, pp. 631–638, 2007.

[46] A. C. Alba-Rubio, J. Santamaría-González, J. M. Mérida-Robles et al., "Heterogeneous transesterification processes by using CaO supported on zinc oxide as basic catalysts," *Catalysis Today*, vol. 149, no. 3-4, pp. 281–287, 2010.

[47] Z. Kesic, I. Lukic, M. Zdujic, L. Mojovic, and D. Skala, "Calcium oxide based catalysts for biodiesel production: a review," *Chemical Industry and Chemical Engineering Quarterly*, vol. 22, no. 4, pp. 391–408, 2016.

[48] G. Anastopoulos, Y. Zannikou, S. Stournas, and S. Kalligeros, "Transesterification of vegetable oils with ethanol and characterization of the key fuel properties of ethyl esters," *Energies*, vol. 2, no. 2, 2009.

Hindawi
International Journal of Chemical Engineering
Volume 2019, Article ID 7135235, 10 pages
https://doi.org/10.1155/2019/7135235

Research Article

Effect of Metal Chlorides on the Pyrolysis of Wheat Straw

Yury V. Lugovoy, Kirill V. Chalov, Yury Yu Kosivtsov, Antonina A. Stepacheva, and Esther M. Sulman

Department of Biotechnology and Chemistry, Tver State Technical University, A. Nikitin Str. 22, Tver 170024, Russia

Correspondence should be addressed to Esther M. Sulman; sulman@online.tver.ru

Received 30 November 2018; Revised 25 January 2019; Accepted 11 February 2019; Published 10 March 2019

Guest Editor: Hu Li

In this paper, the results of the study on the influence of the addition of 10 wt.% of $FeCl_3$, $CoCl_2$, $NiCl_2$, $ZnCl_2$, $SnCl_2$, and $CuCl_2$ on the wheat straw pyrolysis process are presented. The studied chlorides were found to affect the pyrolysis process; however, the highest activity was observed while using $CuCl_2$. The presence of the copper chloride led to the decrease in the temperature of the initial destruction of hemicellulose fraction of wheat straw by 64°C. Besides, the use of $CuCl_2$ allowed increasing the yield of liquid and solid pyrolysis products as well as decreasing the molecular weight distribution of the volatiles. Moreover, the increase in the hydrogen and decrease in carbon dioxide concentration were also observed in the presence of copper chloride. The analysis of the solid residue obtained in the wheat straw pyrolysis in the presence of $CuCl_2$ showed the increase in the specific surface area of the carbon residue from 24 up to 63.5 m^2/g in comparison with that obtained for the noncatalytic process.

1. Introduction

The limitation of natural fuels and the environmental problems rised during their use increase the interest in the processing of biomass in order to produce transportation fuels, energy sources, and chemicals [1]. The advantages of biomass application compared to fossil fuels are low sulfur and nitrogen content, as well as the absence of the effect on the CO_2 balance in the atmosphere. Agricultural wastes from plants are the available biomass source which is produced annually in large amounts throughout the world [2]. In developing countries, a large amount of agricultural waste is currently used either as a raw material for the paper industry or as a source of animal feed. The collection and disposal of such wastes are complex and expensive processes. Thus, the degree of its rational use remains sufficiently low.

In the Russian Federation, the amount of crop waste, which can be effectively used for energy purposes without concurrence with the agricultural needs, exceeds 50 million tons of fuel equivalent per year [3]. The highest amount of grains produced in the Russian Federation belongs to wheat (more than 55%). Meanwhile, the yield of the straw is in the range from 80 to 130% of wheat grain production [4].

According to history, agricultural plant waste can be used to generate heat and electricity. This is confirmed by a large number of industrial plants in countries such as Denmark, Sweden, Spain, Germany, Poland, Canada, the USA, and China [5]. Thus, the development of the fundamental principles of effective processing methods allowing the use of biomass for energy purposes is an urgent task.

Despite the existence of different methods and approaches to the processing of agricultural plant waste, scientists are currently attracted by various modifications of the pyrolysis methods since traditional pyrolysis is not fully capable of solving the problems of the efficient conversion of plant biomass waste for energy purposes [6]. The composition of the pyrolysis products for the plant biomass strongly depends on the feedstock composition, in particular, the content of cellulose, hemicelluloses, and lignin. First, hemicelluloses undergo thermal destruction at a temperature of 170–260°C; then, the cellulose is decomposed at 240–350°C. At last, the decomposition of lignin takes place at 280–500°C. The highest amount of the gaseous products is formed during the thermal decomposition of polysaccharides. Lignin is the most stable component of biomass because of its aromatic composition and a sufficiently high

degree of polymerization [1]. In comparison with the wood biomass, the plant biomass including the agricultural wastes is characterized by the high ash and extractive content. This can lead to the acceleration of the plant biomass pyrolysis as well as promote the formation of carbon-containing residues [2]. The final products of the pyrolysis of plant biomass can be applied as the heat suppliers, gaseous and liquid fuels, and the feedstock for chemicals. For example, during the thermal destruction of cellulose and hemicelluloses, a large number of gaseous hydrocarbons (methane, ethane, ethylene, etc.), hydrogen, and carbon monoxide and dioxide, as well as methanol and acetic acid, are formed. The decomposition of lignin components leads to the formation of phenolic and aromatic compounds. The carbon-containing residue can be applied as the absorbent or filler [1–6]. Moreover, the solid residue containing transition metals can be applied as effective catalysts.

The increase in the efficiency of pyrolysis processes, as well as the quality of the final products obtained, can be reached by the use of catalysis. Therefore, the study of the effect of various compounds on the process of thermal destruction of plant biomass is an important task [7]. The catalyst in the pyrolysis process not only affects the reaction rate but can serve as the heat supplier that leads to the decrease in the process temperature. Besides, the catalyst increases the selectivity to the desired products as well as allows its upgrading. Nowadays, there are numerous studies on the pyrolysis catalysts. Among the different catalysts applied in the biomass pyrolysis process, the soluble salts and oxides of the alkali and transition metals are the most frequently used [8–31]. It is well known that the alkali metal chlorides, particularly K which is present in the plant biomass, increase the rate of the cellulose destruction and promote char formation [8–10]. The presence of NaCl decreases the pyrolysis temperature and increases the yield of low-molecular products [11–14]. The chlorides of alkaline earth metals mainly decrease the pyrolysis temperature [12,15–20]. The treatment of the plant biomass with the solution of $ZnCl_2$ increases the yield of furfural and formic acid. Besides, zinc chloride accelerates the dehydration reactions [21–24]. The chlorides of manganese, iron, nickel, cobalt, and copper increase significantly the formation of carbon-containing residue and decrease the pyrolysis temperature [25, 26]. Moreover, the acid character of the transition metal chlorides significantly accelerates the pyrolysis reactions, leading to the changes in the gaseous product composition [27, 28]. It should be noted that the data on the effect of these compounds are available for the individual components of plant biomass (hemicellulose, cellulose, and lignin). However, the effect of the metal chlorides on the pyrolysis of real feedstock practically was not studied. Thus, the study of the effect of transition metal chlorides ($FeCl_3$, $CoCl_2$, $NiCl_2$, $ZnCl_2$, $SnCl_2$, and $CuCl_2$) on the process of pyrolysis of wheat straw is of theoretical and practical interest.

2. Materials and Methods

The wheat straw used in the current work as a feedstock was collected in July 2017 in the Bologoe district of Tver region, Russia. As the composition of the raw material plays an important role in the pyrolysis process, the determination of moisture and ash content was carried out. Moreover, the content of the main components of wheat straw—extractives, hemicellulose, cellulose, and lignin—was estimated by extraction according to the methods described in [32].

In order to estimate the moisture content in the wheat straw, a weighed portion of the feedstock particles with the mean size of 0.45 mm was dried at 150°C for 1.5 h till the constant mass in a calcinatory. The cooled samples were weighed, and the moisture content (W) was calculated as the relative differences in the weight of initial and dried samples:

$$W = \frac{(m - m_1) \cdot 100}{m}, \quad (1)$$

where m is the feedstock weight in g and m_1 is the feedstock weight after drying in g.

The ash content was measured as the following: a weighed portion of the feedstock particles with the mean size of 0.45 mm was placed in a calcinatory; then, the calcinatory was covered by a cone of the ash-free filter and placed in a muffle furnace at a temperature 550–650°C for 1 h. The ash content (X) was calculated according to

$$X = \frac{m_1 \cdot 100 \cdot 100}{m_2 \cdot (100 - W)}, \quad (2)$$

where m_1 is the ash weight in g, m_2 is the feedstock weight in g, and W is the moisture content in %.

For the measurement of the content of the extractives, a weighed portion of the feedstock particles with the mean size of 0.45 mm was boiled in 50 mL of 70% ethanol for 2 h using reflux condenser; then, the mixture was cooled to the room temperature and filtered. The obtained filtrate was evaporated, and the dried residue was weighed. The extractive content (E) was calculated using

$$E = \frac{m \cdot 200 \cdot 100}{m_1 \cdot (100 - W)}, \quad (3)$$

where m is the weight of the dried residue in g, m_1 is the feedstock weight in g, and W is the moisture content in %.

In order to estimate the effect of transition metal salts on the pyrolysis process of wheat straw, the following compounds were selected: $ZnCl_2{\cdot}6H_2O$, $SnCl_2{\cdot}4H_2O$, $CuCl_2{\cdot}2H_2O$, $NiCl_2{\cdot}6H_2O$, $CoCl_2{\cdot}6H_2O$, and $FeCl_3{\cdot}6H_2O$. The salts were used in dry form by direct application into the samples of wheat straw. The salt concentration in the sample varied from 1 to 10 wt.% according to the preliminary experiments and literature data. The influence of the $CuCl_2$ concentration on the pyrolysis process was studied. In order to estimate the activity of a copper ion in the wheat straw pyrolysis, the thermogravimetric study of the influence of copper salts ($CuSO_4{\cdot}5H_2O$, $Cu_2OH_2CO_3$) was performed.

The pyrolysis process of samples containing the inorganic salts and the sample without additives was studied using a NETZSCH TG 209 F1 thermal analyzer. The conditions of thermogravimetric analysis were similar for all samples. The process was carried out in an inert argon atmosphere in the temperature range from 50 to 600°C with a heating rate of 5°C/min. The composition of the volatile products obtained in the thermal destruction process was

studied using the NETZSCH QMS 403 D MS device for a sample containing 10 wt.% of $CuCl_2$ and the wheat straw without additives.

Based on the preliminary results, copper chloride was also chosen for the experiments in a laboratory pyrolysis unit. The experimental setup (Figure 1) consists of the periodic steel reactor (length 150 mm, diameter 30 mm, and wall thickness 3 mm) with a fixed substrate layer, electric furnace, sealing trap, and eudiometer [32]. The pyrolysis process was carried out at a temperature of 550°C for one hour in a nitrogen atmosphere. The solid and liquid product masses were calculated via differences between the reactor and the liquid trap masses, respectively. The relative error of the mass measurements of pyrolysis products was 0.5 wt.%.

The composition of the gaseous pyrolysis products formed in the thermal decomposition of the wheat straw samples with 10 wt.% $CuCl_2$, as well as the sample without additives, was studied by the chromatographic determination using a unique analytical complex including gas chromatographs (Crystallux 4000M, GAZOKHROM 2000) and a specially developed analyzer of the specific heat of combustion on the base of a flame-temperature detector. The chromatographic analysis of hydrocarbons in the gaseous mixture was carried out on the chromatograph Crystallux 4000M under the following conditions: the consumption of gas carrier (nitrogen) 120 mL/min; gas-carrier pressure 1.5 kgs/sm^3; duration of the analysis 30 min; sample volume 1 mL; carrier silica gel 0.4 mm; column length 1 m; column temperature 50°C; detector temperature 100°C. Volume concentrations of nitrogen, carbon oxide, and methane were analyzed on the chromatograph GAZOKHROM 2000. The flow rate of the gas carrier (helium) was 30 cm^3/min, sample volume of the gas was 0.5 cm^3, and thermostat temperature was 40°C [33].

Solid pyrolysis residues were analyzed by X-ray fluorescence analysis (XFA), X-ray photoelectron spectroscopy (XPS), and low-temperature nitrogen adsorption. XFA was used for the study of catalyst metal migration into the solid carbon residue. The metal content in the solid pyrolysis product was analyzed using a Spectroscan-Maks-GF1E spectrometer (Spectron, St-Petersburg, Russia) equipped with Mo anode, LiF crystal analyzer, and SZ detector. The analysis was based on the Co Ka line. XPS was used to analyze the surface chemical compositions of the solid carbon-containing pyrolysis product. The spectra were obtained with a spectrometer (ES 2403 M-Y IAI RAS). Characteristic MgKa radiation ($h\nu = 1253.6$ eV) was used. The radiation power was 100 W. The spectra were recorded at pressures below 10^{-9} Torr. The specific surface area of the solid pyrolysis product was measured using a Coulter SA 3100 Series Surface Area and Pore Size Analyzers (Beckman Coulter Company). The analysis was conducted for four hours at 200°C, a pressure of 10^{-5} to 10^{-6} Pa, and under constant nitrogen flow at a rate of 1 mL·min^{-1} [32].

3. Results and Discussion

The composition of the wheat straw varies depending on the habitat and growth conditions as well as the season of collection. Difference between the compositions of the feedstock can be significant. Thus, we provided experiments on the estimation of the moisture, ash, extractive content, and the composition of main biomass compounds (Table 1). The experimental data obtained in the current work are in accordance with the literature data [34–38]. The moisture and ash content of wheat straw was found to be 7.2 ± 0.1 and 4.7 ± 0.1 wt.%, respectively. The content of extractives in the wheat straw was estimated as 5.6 ± 0.1 wt.%. The amount of hemicellulose in the raw material, which was calculated as the difference between the weight of the sample before and after the extraction of the sample, was equal to 41.1 ± 0.1 wt.%. The cellulose content was determined by the weight difference of the biomass components and the initial wheat straw weight. Thus, the cellulose content in the wheat straw was found to be 31.7 ± 0.1 wt.%. The total lignin content (9.8 ± 0.1 wt.%) was determined to be the sum of acid-insoluble lignin and acid-soluble lignin.

The mechanism of the metal chloride impact in the thermal destruction process can be described by the formation of carbocations according to the scheme presented in Figure 2 [33]. The studied metal salts are the aprotonic acid centres with the medium strength which are characterized by the relatively high activity and high selectivity in the processes of thermal destruction of hydrocarbon materials [38]. The difference between the influences of the studied chlorides on the wheat straw pyrolysis process consists of the difference in the electronic structure of the metals used which determines the difference in the catalytic properties.

According to the scheme presented in [39, 40], the possible mechanism of the catalytic effect of the aprotonic acid sites of metal chlorides can be described by the scheme (Figure 3).

In order to account for the previously presented mechanisms, the activation of the surface cellulose molecule by metal chlorides should include both solid-state hydrolysis and the glycosidic bond cleavage [41].

In order to estimate the influence of metal chlorides on the wheat straw pyrolysis, the preliminary thermogravimetric experiments of the feedstock without catalysts and with 10 wt.% of salts were performed. As shown by the experimental data (Figure 4), all the studied metal chlorides differently influenced the pyrolysis process of wheat straw. Basically, the presence of metal chlorides had the highest effect on the shift towards lower temperatures of the hemicellulose destruction and the lowest impact on the cellulose destruction temperature. Thus, based on the shift of the hemicellulose destruction temperature peaks towards lower temperatures, the studied transition metal chlorides can be ranked in order of decreasing effects: $CuCl_2 > SnCl_2 > ZnCl_2 > FeCl_3 > CoCl_2 > NiCl_2$. In terms of the effect on the shift of the cellulose destruction temperature peak towards lower temperatures, the studied transition metal chlorides can be arranged in a row slightly different from the above-presented: $CuCl_2 > FeCl_3 > ZnCl_2 > SnCl_2 > NiCl_2 > CoCl_2$.

It should be noted that in the case of using $FeCl_3$ and $ZnCl_2$, besides the shift of the hemicellulose weight loss peak towards lower temperatures, a broadening of the peak was observed. This may be due to the nonselective effect of these

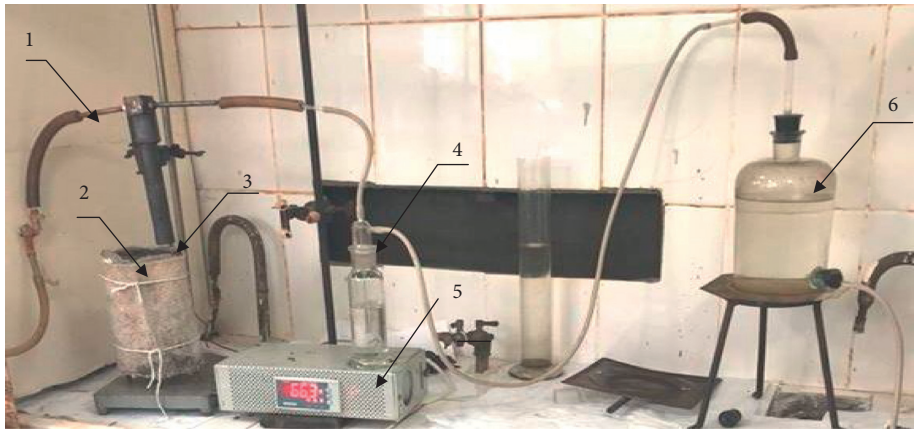

Figure 1: Laboratory equipment for the pyrolysis process: (1) nitrogen purging; (2) electric furnace; (3) reactor; (4) sealing trap; (5) temperature controller; and (6) eudiometer.

Table 1: Wheat straw composition according to the literature and experimental data.

Parameter	Experimental results	Literature data			
		[34]	[35]	[36]	[37]
Moisture content (wt.%)	7.2 ± 0.1	—	—	10.23	8.30
Ash content (wt.%)	4.7 ± 0.1	12.78	8.0	6.99	4.77
Calorific value (MJ/kg)	18.04 ± 0.01	17.10	—	17.38	17.73
Extractives (wt.%)	4.5 ± 0.1	—	5.4	—	—
Hemicelluloses (wt.%)	41.1 ± 0.1	—	23.60	—	26.30
Cellulose (wt.%)	31.6 ± 0.1	—	32.30	—	45.2
Lignin (wt.%)	9.8 ± 0.1	—	17.10	—	10.90
Elemental composition (wt.%)					
C	41.6 ± 0.1	42.49	—	45.48	47.12
H	4.8 ± 0.1	5.12	—	6.12	5.78
N	0.6 ± 0.1	0.68	—	0.52	0.47
O	39.7 ± 0.1	36.52	—	39.96	40.20
S	0.2 ± 0.05	0.39	—	0.13	0.19

substances on the various components of hemicellulose, which ultimately led to a "blurring" of the destruction process for this component and, accordingly, reduced the maximum rate of destruction.

In the presence of $ZnCl_2$, $CoCl_2$, and $NiCl_2$, a decrease in the mass of the solid carbon residue of wheat straw pyrolysis by 14.2 ± 0.05, 5.7 ± 0.03, and 2.8 ± 0.02 %, respectively, was observed. In the case of using $CuCl_2$, $FeCl_3$, and $SnCl_2$, the weight of the solid residue, in contrast, increased by 15.2 ± 0.05, 14.4 ± 0.05, and 4.7 ± 0.02%, respectively. This calculation took into account the weight loss of the chlorides used during heating under conditions similar to the experiment.

As copper ion has the highest impact in the wheat straw destruction temperature, it was chosen for the further experiments. According to the data described in [40], based on the decrease in the biomass thermal destruction temperature and the apparent activation energy, inorganic salts can be ranked as the following: $CuSO_4 > NaOH > Na_2CO_3 > NiCl_2 > ZnCl_2 > NaCl$. This data confirms the high activity of copper compounds in the plant biomass pyrolysis. The experiments on the influence of the copper salts on the wheat straw pyrolysis process (Figure 5) allowed ranking the Cu-containing catalysts as follows: $CuCl_2 > CuSO_4 > Cu_2OH_2CO_3$.

As it is seen in Figure 5, among the studied compounds, copper chloride has the highest activity in the wheat straw pyrolysis process. This can be explained by the higher strength of the acid aprotonic center of Cu^{2+} in the copper chloride [33, 42].

As it was shown by the results of mass spectrometry study of volatile products of wheat straw pyrolysis in the presence of $CuCl_2$, a decrease in the molecular weight distribution and a decrease in the molecular weight of volatile products were observed. It may be of practical interest in purifying volatile products from the resins (Figure 6).

The catalyst content strongly influences the pyrolysis process. In order to estimate the effect of copper chloride content on the wheat straw thermal destruction, the concentration range of 1–10 wt.% was chosen according to the literature [43]. The thermogravimetric study (Figure 7) showed that 10 wt.% of $CuCl_2$ was optimal for the wheat straw pyrolysis using laboratory setup.

As $CuCl_2$ had the highest effect on the process of wheat straw destruction, this chloride with the concentration of

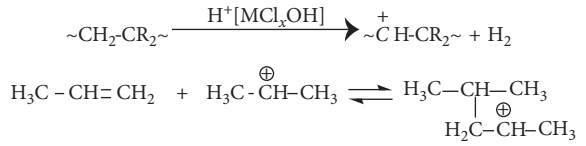

Figure 2: Scheme of the pyrolysis mechanism in the presence of metal chlorides.

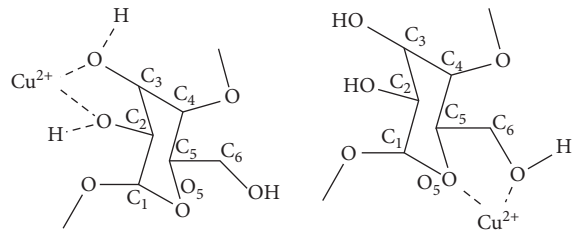

Figure 3: Scheme of the pyrolysis mechanism in the presence aprotonic acid centers.

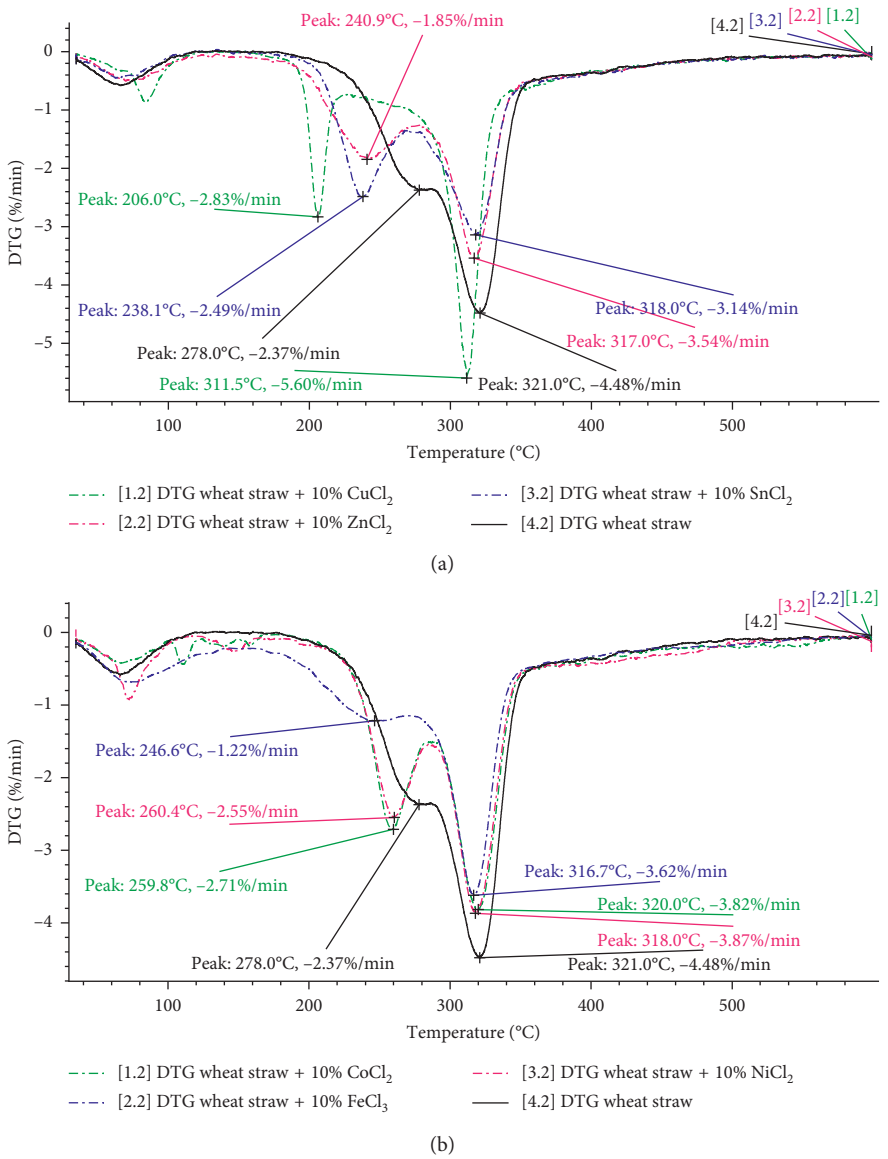

Figure 4: DTG curves obtained as a result of pyrolysis of wheat straw in the presence of copper, tin, and zinc chlorides (a); iron, cobalt, and nickel chlorides (b); and a sample of straw without additives.

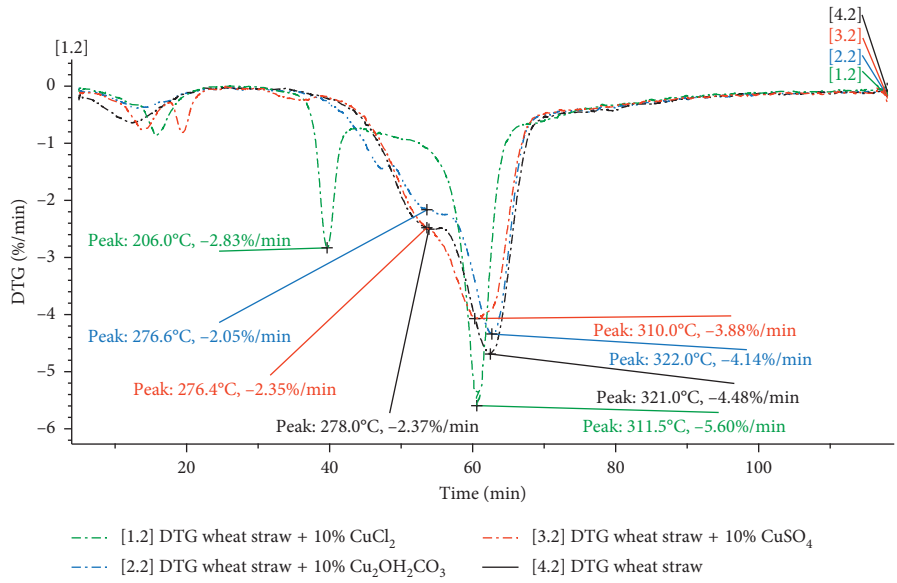

Figure 5: DTG curves obtained as a result of pyrolysis of wheat straw in the presence of copper salts.

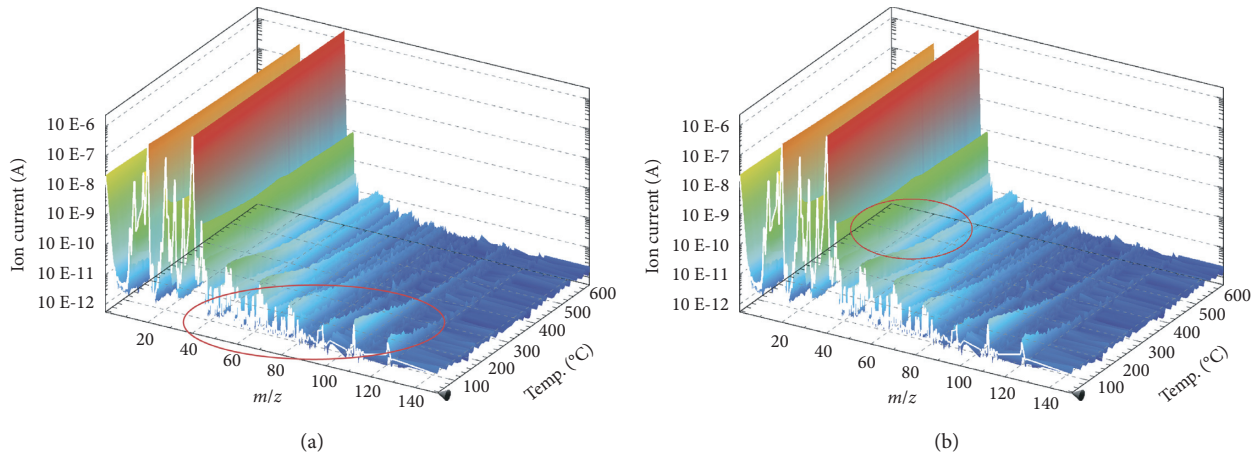

Figure 6: Mass spectrometric study of volatile products of wheat straw pyrolysis without additives (a) and with 10 wt.% $CuCl_2$ (b).

10 wt.% was used in the study at the laboratory pyrolysis unit. It should be noted that in the case of a noncatalytic pyrolysis process, the weights of gaseous, liquid, and solid products were found to be 35.9, 26.1, and 38.0 wt.%, respectively. The use of copper chloride (10 wt.%) led to an increase in the weight of liquid and solid products by the factor of 1.35 and 1.11, respectively, by reducing the weight of gaseous products by the factor of 1.36. It is noteworthy that no decrease in the volume of gaseous products was observed. This should logically lead to a decrease in the average molecular weight of the pyrolysis gas, which is confirmed by chromatographic analysis of gaseous products. In the presence of $CuCl_2$, the hydrogen content during the process increases from 5 to 20 vol. %; meanwhile, the total CO_2 content in the gaseous products decreases from 11.5 to 0.3 vol.%.

The analysis of solid carbon residue obtained in the wheat straw pyrolysis experiment in the presence of $CuCl_2$ by the XPS method results in a survey photoelectron spectra shown in Figure 8(a) and high-resolution photoelectron spectra of the Cu 2p sublevel shown in Figure 8(b). Carbon, nitrogen, oxygen, copper, calcium, silicon, phosphorus, chlorine, and potassium were found on the surface of the solid carbon residue. Carbon, oxygen, calcium, silicon, phosphorus, and chlorine were found in a large amount that can be explained by the presence of these elements in the raw material.

The analysis of Cu 2p3/2 high-resolution spectra shows that copper chloride added to a wheat straw as a catalyst was completely transformed into metallic copper (932.4 eV) and copper oxide (933.7 eV), as well as partially oxidized copper (933.0 eV).

The analysis of high-resolution photoelectron spectra for C 1s sublevel (Figure 9) allows concluding that the major amount of carbon on the solid residue surface is presented by the graphite and some aromatics (284.6 eV), as well as the

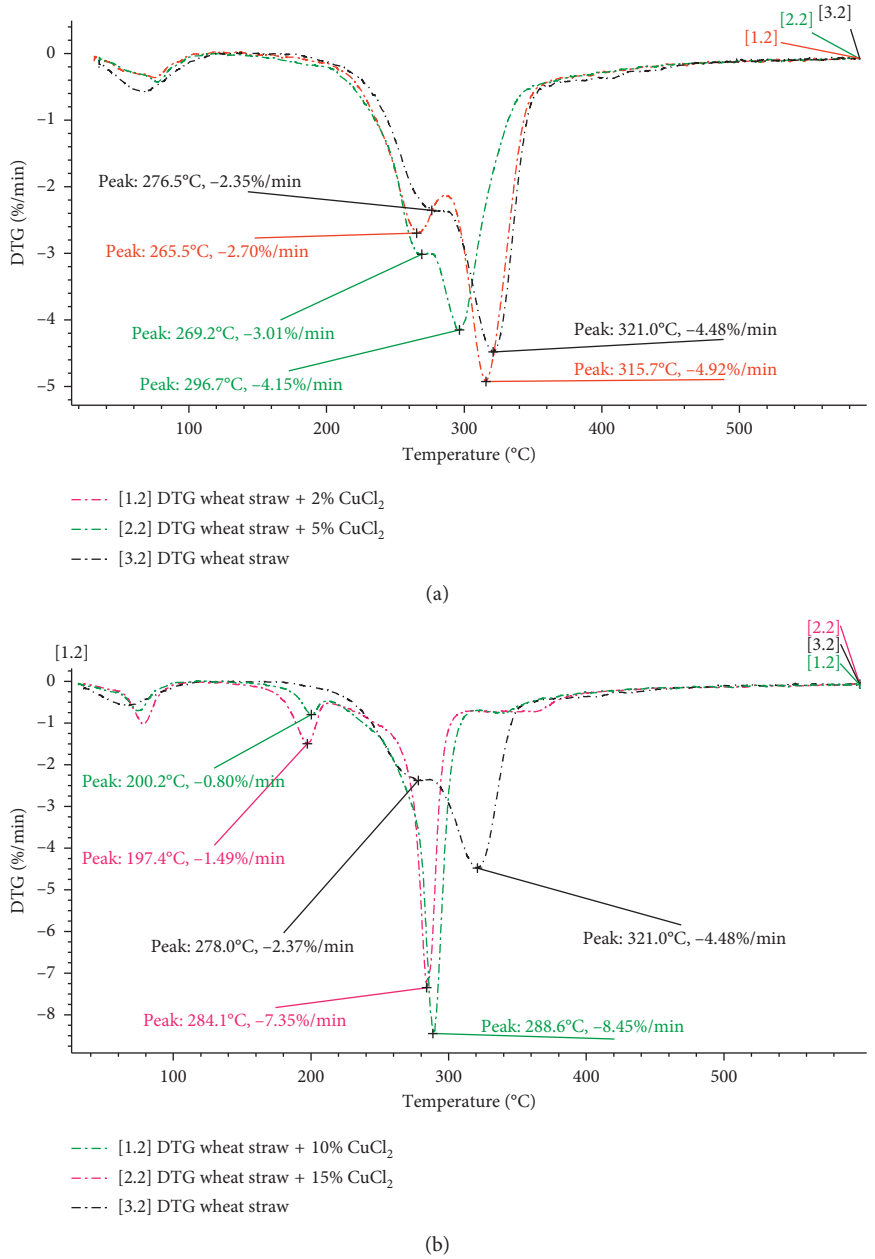

Figure 7: Thermogravimetric study of the $CuCl_2$ concentration effect on the wheat straw pyrolysis: (a) concentration range 2–5 wt.%; (b) concentration range 10–15 wt.%.

alcohol compounds (285.7 eV) and carbonyl and carboxylic groups (286.7 and 289.0 eV).

Thus, the solid residue obtained by wheat straw pyrolysis in the presence of copper chloride, the carbonaceous matrix containing graphite, and condensed aromatic rings impregnated by copper phase was produced.

The study of the solid carbon residue of wheat straw pyrolysis using the XFA method showed that the copper content in the solid pyrolysis residue was 0.31 wt.%. It may indicate a slight copper migration into the internals of the carbon residue.

The results of the study of solid residues obtained in the pyrolysis without the catalyst and in the presence of $CuCl_2$ showed that the presence of the catalyst leads to the increase in the specific surface area from 24 ± 0.1 to 63.5 ± 0.1 m^2/g due to an increase in the total pore volume. The pore size distribution and the surface area of the wheat straw and the carbon-containing residue obtained during noncatalytic and catalytic pyrolysis are presented in Table 2.

4. Conclusions

The studied metal chlorides were found to accelerate the thermal decomposition of the hemicellulosic components of wheat straw in different degrees. $CuCl_2$ had the highest influence on the pyrolysis process of wheat straw. The use of

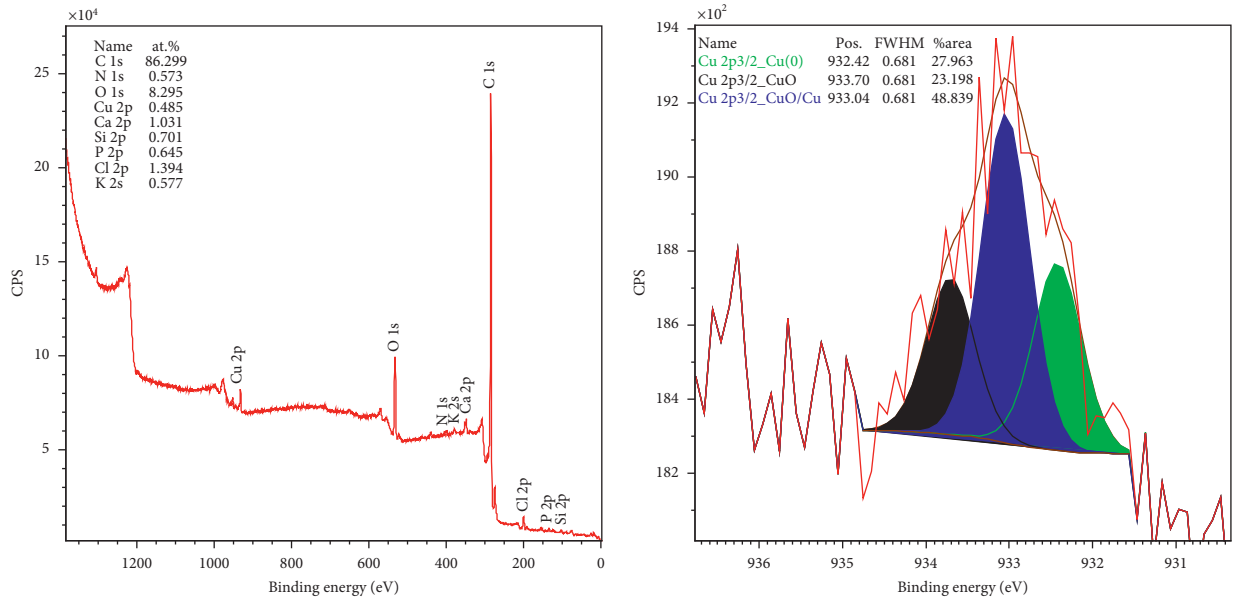

(a) (b)

Figure 8: Survey photoelectron spectra of wheat straw pyrolysis solid carbon residue in the presence of $CuCl_2$ (a) and high-resolution photoelectron spectra of the Cu 2p3/2 sublevel (b).

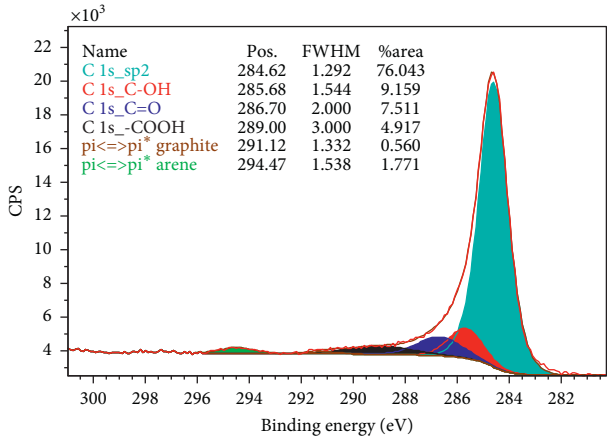

Figure 9: High-resolution photoelectron spectra of the C 1s sublevel.

Table 2: Analysis of the porosity of the initial wheat straw and pyrolysis solid residues.

Sample	Wheat straw		Carbonaceous residue of wheat straw pyrolysis		Carbonaceous residue of wheat straw pyrolysis + $CuCl_2$ 10 wt. %	
Pore diameter range (nm)	Pore volume (mL/g)	(%)	Pore volume (mL/g)	(%)	Pore volume (mL/g)	(%)
Under 6	0.00648	28.94	0.00642	27.41	0.01639	27.80
6–8	0.00311	13.90	0.00305	13.02	0.00844	14.32
8–10	0.00164	7.31	0.00167	7.14	0.00449	7.61
10–12	0.00176	7.87	0.00176	7.51	0.00481	8.16
12–16	0.00172	7.66	0.00188	8.05	0.00541	9.18
16–20	0.00163	7.29	0.00173	7.38	0.00479	8.12
20–80	0.00471	21.05	0.00544	23.23	0.01116	18.93
Over 80	0.00134	5.98	0.00147	6.26	0.00346	5.88
Total	0.02240	100.0	0.02341	100.00	0.05896	100.00
t-Plot surface area (m^2/g)	20.6 ± 0.1		24.0 ± 0.1		63.5 ± 0.1	

copper chloride during the pyrolysis resulted in a decrease in the molecular weight distribution of volatile products, as well as a decrease in the yield of gaseous pyrolysis products due to an increase in the yield of liquid and solid products. The use of copper chloride also led to an increase in the specific surface area of the solid pyrolysis residue, which is probably due to the intense coke formation. XPS data indicate a change in the composition of $CuCl_2$ during the pyrolysis of wheat straw. This indicates the initiating role of this compound in the presented process. The resulting copper-containing carbon residue can potentially be used as a catalyst for the conversion of furfuryl alcohol to 2-methylfuran.

Data Availability

The experimental data used to support the findings of this study are included in the article and in [17].

Conflicts of Interest

The authors declare that there are no conflicts of interest regarding the publication of this paper.

Acknowledgments

This work was financially supported by the Russian Foundation for Basic Researche (grants 18-08-00794 and 17-08-00660). The authors thank Dr. Alexey V. Bykov and Prof. Alexander I. Sidorov for the analysis of the solid residue samples.

References

[1] K. Lazdovica, V. Kampars, L. Liepina, and M. Vilka, "Comparative study on thermal pyrolysis of buckwheat and wheat straws by using TGA-FTIR and Py-GC/MS methods," *Journal of Analytical and Applied Pyrolysis*, vol. 124, pp. 1–15, 2017.

[2] B. Liepina, N. Pandey, Y. Bisht, R. Singh, J. Kumar, and T. Bhaskar, "Pyrolysis of agricultural biomass residues: comparative study of corn cob, wheat straw, rice straw and rice husk," *Bioresource Technology*, vol. 237, pp. 57–63, 2017.

[3] S. Perederi, "Prospects for the use of biofuels from wood raw materials," *LesPromInform*, vol. 98, no. 8, p. 174, 2013.

[4] A. V. Nikitin, *Agro-Industrial Complex of Russia as a Strategic Source of Resources for Biofuel Energy*, Open-Access Journal Youth Scientific Herald, vol. 4, pp. 1–6, 2017.

[5] S. Jones, P. Meyer, L. Snowden-Swan et al., "Process design and economics for the conversion of lignocellulosic biomass to hydrocarbon fuels: fast pyrolysis and hydrotreating bio-oil pathway," National Renewable Energy Laboratory (NREL), Golden, CO, USA, 2013.

[6] S. Eibner, F. Broust, J. Blin et al., "Catalytic effect of metal nitrate salts during pyrolysis of impregnated biomass," *Journal of Analytical and Applied Pyrolysis*, vol. 113, pp. 143–152, 2014.

[7] F. Suárez-García, A. Martínez-Alonso, and J. M. D. Tascón, "Pyrolysis of apple pulp: effect of operation conditions and chemical additives," *Journal of Analytical and Applied Pyrolysis*, vol. 62, no. 1, pp. 93–109, 2002.

[8] A. Jensen, K. Dam-Johansen, M. A. Wójtowicz, and M. A. Seiro, "TG-FTIR study of the influence of potassium chloride on wheat straw pyrolysis," *Energy & Fuels*, vol. 12, no. 5, pp. 929–938, 1998.

[9] D. L. Serio, K. H. Kim, and R. C. Brown, "The influence of alkali and alkaline earth metals on char and volatile aromatics from fast pyrolysis of lignin," *Journal of Analytical and Applied Pyrolysis*, vol. 127, pp. 385–393, 2017.

[10] W.-P. Pan and G. N. Richards, "Influence of metal ions on volatile products of pyrolysis of wood," *Journal of Analytical and Applied Pyrolysis*, vol. 16, no. 2, pp. 117–126, 1989.

[11] J. A. Santana, N. G. Sousa, C. R. Cardoso, W. S. Carvalho, and C. H. Carvalho, "Sodium, zinc and magnesium chlorides as additives for soybean hulls pyrolysis," *Journal of Thermal Analysis and Calorimetry*, vol. 125, no. 1, pp. 471–481, 2016.

[12] G. Varhegyi, M. J. Antal, T. Szekely, and P. Szabo, "Kinetics of the thermal decomposition of cellulose, hemicellulose, and sugarcane bagasse," *Energy & Fuels*, vol. 3, no. 3, pp. 329–335, 1989.

[13] G. N. Szabo, F. Shafizadeh, and T. T. Stevenson, "Influence of sodium chloride on volatile products formed by pyrolysis of cellulose: identification of hydroxybenzenes and 1-hydroxy-2-propanone as major products," *Carbohydrate Research*, vol. 117, pp. 322–327, 1983.

[14] M. Kleen and G. Gellerstedt, "Influence of inorganic species on the formation of polysaccharide and lignin degradation products in the analytical pyrolysis of pulps," *Journal of Analytical and Applied Pyrolysis*, vol. 35, no. 1, pp. 15–41, 1995.

[15] G. N. Richards and G. Zheng, "Influence of metal ions and of salts on products from pyrolysis of wood: applications to thermochemical processing of newsprint and biomass," *Journal of Analytical and Applied Pyrolysis*, vol. 21, no. 1-2, pp. 133–146, 1991.

[16] A. Aho, N. DeMartini, A. Pranovich et al., "Pyrolysis of pine and gasification of pine chars-influence of organically bound metals," *Bioresource Technology*, vol. 128, pp. 22–29, 2013.

[17] J. Chen, J. Sun, and Y. Wang, "Catalysts for steam reforming of bio-oil: a review," *Industrial & Engineering Chemistry Research*, vol. 56, no. 16, pp. 4627–4637, 2017.

[18] O. A. Augustine, A. A. Opeyemi, M. O. Oyinlola et al., "Compositional analysis of lignocellulosic materials: evaluation of an economically viable method suitable for woody and non-woody biomass," *American Journal of Engineering Research*, vol. 4, pp. 14–19, 2015.

[19] G. Varhegyi, M. J. Antal, T. Szekely, F. Till, E. Jakab, and P. Szabo, "Simultaneous thermogravimetric-mass spectrometric studies of the thermal decomposition of biopolymers. 2. Sugarcane bagasse in the presence and absence of catalysts," *Energy & Fuels*, vol. 2, no. 3, pp. 273–277, 1988.

[20] N. Shimada, H. Kawamoto, and S. Saka, "Different action of alkali/alkaline earth metal chlorides on cellulose pyrolysis," *Journal of Analytical and Applied Pyrolysis*, vol. 81, no. 1, pp. 80–87, 2008.

[21] C. D. Blasi, C. Branca, and A. Galgano, "Products and global weight loss rates of wood decomposition catalyzed by zinc chloride," *Energy & Fuels*, vol. 22, no. 1, pp. 663–670, 2008.

[22] Q. Lu, C.-Q. Dong, X.-M. Zhang, H.-Y. Tian, Y.-P. Tian, and X.-F. Zhu, "Selective fast pyrolysis of biomass impregnated with $ZnCl_2$ to produce furfural: analytical Py-GC/MS study," *Journal of Analytical and Applied Pyrolysis*, vol. 90, no. 2, pp. 204–212, 2011.

[23] P. Rutkowski, "Catalytic effects of copper(II) chloride and aluminum chloride on the pyrolytic behavior of cellulose,"

Journal of Analytical and Applied Pyrolysis, vol. 98, pp. 86–97, 2012.

[24] Q. Lu, Z. Wang, C.-Q. Dong et al., "Selective fast pyrolysis of biomass impregnated with $ZnCl_2$: furfural production together with acetic acid and activated carbon as by-products," *Journal of Analytical and Applied Pyrolysis*, vol. 91, no. 1, pp. 273–279, 2011.

[25] D. Fabbri, C. Torri, and V. Baravelli, "Effect of zeolites and nanopowder metal oxides on the distribution of chiral anhydrosugars evolved from pyrolysis of cellulose: an analytical study," *Journal of Analytical and Applied Pyrolysis*, vol. 80, no. 1, pp. 24–29, 2007.

[26] Y. Zhang and C. Liu, "A new horizon on effects of alkalis metal ions during biomass pyrolysis based on density function theory study," *Journal of Analytical and Applied Pyrolysis*, vol. 110, pp. 297–304, 2014.

[27] G. Dobele, G. Rossinskaja, G. Telysheva, D. Meier, and O. Faix, "Cellulose dehydration and depolymerization reactions during pyrolysis in the presence of phosphoric acid," *Journal of Analytical and Applied Pyrolysis*, vol. 49, no. 1-2, pp. 307–317, 1999.

[28] A. Nzihou, B. Stanmore, N. Lyczko, and D. P. Minh, "The catalytic effect of inherent and adsorbed metals on the fast/flash pyrolysis of biomass: a review," *Energy*, vol. 170, pp. 326–337, 2019.

[29] S. D. Minh and J. S. Hargreaves, *Metal Oxide Catalysis*, Wiley Online Library, Hoboken, NJ, USA, 2009.

[30] J. L. G. Fierro, *Metal Oxides: Chemistry and Applications*, CRC Press, Boca Raton, FL, USA, 2006.

[31] I. E. Wachs, "Recent conceptual advances in the catalysis science of mixed metal oxide catalytic materials," *Catalysis Today*, vol. 100, no. 1-2, pp. 79–94, 2005.

[32] Y. V. Lugovoy, K. V. Chalov, O. P. Tkachenko, E. M. Sulman, J. Wärnå, and D. Y. Murzin, "Effect of iron-subgroup metal salts on polymer cord pyrolysis," *RSC Advances*, vol. 5, no. 70, pp. 56460–56469, 2015.

[33] K. V. Chalov, Y. V. Lugovoy, V. Y. Doluda et al., "Influence of metals chlorides on oil-slime thermocatalytic processing," *Chemical Engineering Journal*, vol. 238, pp. 219–226, 2014.

[34] B. M. Jenkins, R. R. Bakker, and J. B. Wei, "On the properties of washed straw," *Biomass and Bioenergy*, vol. 10, no. 4, pp. 177–200, 1996.

[35] D. Montane, X. Farriol, J. Salvadó, P. Jollez, and E. Chornet, "Application of steam explosion to the fractionation and rapid vapor-phase alkaline pulping of wheat straw," *Biomass and Bioenergy*, vol. 14, no. 3, pp. 261–276, 1998.

[36] G. Jang, G. A. Husseini, L. L. Baxter et al., "Analysis of straw by X-ray photoelectron spectroscopy," *Surface Science Spectra*, vol. 11, pp. 91–96, 2004.

[37] M. Adamovic, G. Grubić, I. Milenković et al., "The biodegradation of wheat straw by Pleurotusostreatus mushrooms and its use in cattle feeding," *Animal Feed Science and Technology*, vol. 71, no. 3-4, pp. 357–362, 1998.

[38] C. Yang, X. Lu, W. Lin, X. Yang, and J. Yao, "TG-FTIR study on corn straw pyrolysis-influence of Minerals 1," *Chemical Research in Chinese Universities*, vol. 22, no. 4, pp. 524–532, 2006.

[39] K. Triantafyllidis, A. Lappas, and M. Stöcker, *The Role of Catalysis for the Sustainable Production of Bio-Fuels and Bio-Chemicals*, Elsevier, Amsterdam, Netherlands, 1st edition, 2013.

[40] F. Shafizadeh, R. H. Furneaux, T. G. Cochran, J. P. Scholl, and Y. Sakai, "Production of levoglucosan and glucose from pyrolysis of cellulosic materials," *Journal of Applied Polymer Science*, vol. 23, no. 12, pp. 3525–3539, 1979.

[41] K. S. Minsker, S. R. Ivanova, and R. Z. Biglova, "Complexes of metal chlorides with proton donors-promising polyfunctional catalysts for electrophilic processes," *Russian Chemical Reviews*, vol. 64, no. 5, pp. 429–444, 1995.

[42] P. T. Williams and P. A. Horne, "The role of metal salts in the pyrolysis of biomass," *Renewable Energy*, vol. 4, no. 1, pp. 1–13, 1994.

[43] P. Rutkowski, "Pyrolysis of cellulose, xylan and lignin with the K_2CO_3 and $ZnCl_2$ addition for bio-oil production," *Fuel Processing Technology*, vol. 92, no. 3, pp. 517–522, 2011.

Hindawi
International Journal of Chemical Engineering
Volume 2019, Article ID 4936292, 11 pages
https://doi.org/10.1155/2019/4936292

Research Article

Ethanol Dehydration over WO_3/TiO_2 Catalysts Using Titania Derived from Sol-Gel and Solvothermal Methods

Anchale Tresatayawed,[1] Peangpit Glinrun,[2] and Bunjerd Jongsomjit[1]

[1]*Center of Excellence on Catalysis and Catalytic Reaction Engineering, Department of Chemical Engineering, Faculty of Engineering, Chulalongkorn University, Bangkok 10330, Thailand*
[2]*Department of Petrochemicals and Environmental Management, Faculty of Engineering, Pathumwan Institute of Technology, Phathumwan, Bangkok 10330, Thailand*

Correspondence should be addressed to Bunjerd Jongsomjit; bunjerd.j@chula.ac.th

Received 23 November 2018; Accepted 12 February 2019; Published 3 March 2019

Guest Editor: Masaru Watanabe

The present study aims to investigate the catalytic ethanol dehydration to higher value products including ethylene, diethyl ether (DEE), and acetaldehyde. The catalysts used for this reaction were WO_3/TiO_2 catalysts having W loading of 13.5 wt.%. For a comparative study, the TiO_2 supports employed were varied by two different preparation methods including the sol-gel and solvothermal-derived TiO_2 supports, denoted as TiO_2-SG and TiO_2-SV, respectively. It is obvious that the different preparation methods essentially altered the physicochemical properties of TiO_2 supports. It was found that the TiO_2-SV exhibited higher surface area and pore volume and larger amounts of acid sites than those of TiO_2-SG. As a consequence, different characteristics of support apparently affected the catalytic properties of WO_3/TiO_2 catalysts. As expected, both catalysts WO_3/TiO_2-SG and WO_3/TiO_2-SV exhibited increased ethanol conversion with increasing temperatures from 200 to 400°C. It appeared that the highest ethanol conversion (ca. 88%) at 400°C was achieved by the WO_3/TiO_2-SV catalysts due to its high acidity. It is worth noting that the presence of WO_3 onto TiO_2-SV yielded a remarkable increase in DEE selectivity (ca. 68%) at 250°C. In summary, WO_3/TiO_2-SV catalyst is promising to convert ethanol into ethylene and DEE, having the highest ethylene yield of ca. 77% at 400°C and highest DEE yield of ca. 26% at 250°C. These can be attributed to proper pore structure, acidity, and distribution of WO_3.

1. Introduction

Recently, catalytic ethanol dehydration to produce ethylene and diethyl ether (DEE) has been paid attention due to its cleaner technology and efficient utilization of ethanol, which is a renewable raw material obtained from fermentation of biomass. For instance, the production of ethylene from ethanol is considered as an alternative way to produce ethylene, which is currently produced by the catalytic thermal cracking of petroleum feed stocks such as naphtha and dehydrogenation of ethane from natural gas. In fact, dehydration of ethanol to ethylene is a cleaner technology due to lower operating temperature, uncomplicated process, and less impurity. It is well known that ethylene is one of the most important raw materials for petrochemical industry, which is used as a starting material for production of polyethylene, ethylene oxide, vinyl acetate, ethyl benzene, etc. Considering the production of commercialized DEE at present, although it is produced from dehydration of ethanol, the process is not benign since it uses mineral liquid acids such as H_2SO_4 to catalyze the reaction. Thus, further separation and purification are required. In this case, the solid acid catalysts are preferred since they are reusable and easy to separate from the product. Although the use of DEE is much lesser than ethylene, it is very important chemical. In particular, DEE is mainly employed as a solvent for fragrance and pharmaceutical industries. In transport fuel function, DEE is applied as an ignition-improving additive in engines according to its high volatility and cetane and octane number. The blending of DEE in diesel improves the

performance-emission characteristics with thermal efficiency and reduced emission of NOx, CO, and HC [1]. Hence, the production of ethylene and DEE from ethanol using suitable solid catalysts is very captivating.

Theoretically, the catalytic ethanol dehydration to ethylene and DEE requires acid sites. This reaction essentially undergoes via thermodynamic and kinetic controls. The formation of ethylene is dominated by high reaction temperature since it is an endothermic reaction, whereas DEE mainly occurs at lower reaction temperature due to its exothermic reaction. However, during dehydration of ethanol, a side reaction such as dehydrogenation can occur resulting in the formation of acetaldehyde as a byproduct. From previous works, many solid acid catalysts have been investigated in ethanol dehydration reaction including the transition metal oxides [2–4], zeolites [5], silica-alumina [6, 7], and heteropolyacids [8]. Many researchers found that the transition metal oxides such as TiO_2, ZrO_2, SiO_2, and Nb_2O_5 play an important role in heterogeneous catalysis acting as an active phase, promoter, or support of solid catalysts. Those solid catalysts have been developed on structure characteristics and acid properties to build up the product selectivity, catalytic activity, and stability. Among the transition metal oxides, TiO_2 has been widely used as a support in heterogeneous catalysts due to its suitable surface areas, thermal stability and mechanical resistance [9, 10]. Furthermore, the modification by doping of the active noble and transition metals such as Cs [11], Au/Ag/Cu [12], Al [13], Ru [14], Pt, Pd [15], Mo [16], and W [17, 18] into catalyst supports apparently affected the catalyst selectivity and activity.

In addition, the presence of tungsten (W) metal was found to be very interesting since it contributes Brønsted acid site and increases the catalyst stability and activity [19–21]. It is reported that WO_3/TiO_2 catalyst is widely used in various reactions and processes including glycerol hydrogenation, reforming, oxidation of dibenzothiophene [22], selective catalytic reduction [23], dehydration [24], and photoelectrocatalytic degradation [25]. Phung et al. [26] also reported that WO_3/TiO_2 is promising for the catalytic dehydration of ethanol to ethylene and especially DEE at low temperature. They reported that the addition of tungsten on transition metal oxide provided the Brønsted acids sites that are active to the ethanol dehydration reaction to produce ethylene and DEE and also prevent the formation of byproducts such as acetaldehyde and higher hydrocarbons. In addition, with various tungsten loadings on TiO_2, ZrO_2 and SiO_2 support, the WO_3/TiO_2 catalyst was found to be the most active in this reaction giving the highest yield of DEE. However, besides the active metals, one needs to consider on the properties of a wide variety of supports themselves. The variations of support characteristics mostly arise from different preparation methods. There are many reports focusing on using different methods to prepare various metal oxide supports including the sol-gel [27, 28] and solvothermal methods [29, 30]. In most cases, they found that different preparation methods can alter the properties of support and consequently, different catalytic properties were observed. Therefore, the effect of different preparation methods on the properties of support is crucial for better understanding.

Similarly to Phung et al. [26] study, the WO_3/TiO_2 catalyst was employed in ethanol dehydration reaction. They examined the difference in some support metal oxides such as ZrO_2 and SiO_2. However, the main goal of this present study is to develop a better understanding on different preparation methods including the sol-gel and solvothermal methods to synthesize the TiO_2 supports for WO_3 catalysts used in catalytic ethanol dehydration to ethylene and DEE. The different characteristics of TiO_2 supports and WO_3/TiO_2 catalysts were determined using various characterization techniques. The change in catalytic properties was also investigated via the catalytic ethanol dehydration in a fixed-bed microreactor at the temperature range of 200 to 400°C. Ethanol conversion and product selectivity of different WO_3/TiO_2 catalysts were reported and discussed further.

2. Experimental

2.1. Materials. Chemicals used for preparation of the catalysts were titanium ethoxide (Ti ~ 20%) purchased from Aldrich, ethanol (99.99%) from Merck Company Ltd., titanium (IV) *n*-butoxide (97%), 1,4–butanediol, and tungsten (VI) chloride (99.9+% metals) from Aldrich. For the reaction study, ultrahigh purity nitrogen gas (99.99%) from Linde (Thailand) Public Company Ltd. was employed.

2.2. Preparation of TiO_2 Supports and WO_3/TiO_2 Catalysts. In this study, TiO_2 supports were synthesized using two different methods including the sol-gel and solvothermal methods as reported by Panpranot et al. [29] for a comparative study. For the sol-gel method, titanium ethoxide was used as the precursor. First, the precursor was dissolved in the excess ethanol before added to deionized water with the molar ratio of 165. The mixture solution was stirred under 20 rpm/min at room temperature at least for 2 h. The white precipitates of hydrous oxides formed instantly and separated by centrifugation. The product was redispersed in the ethanol at least 5 times following with centrifugation. The sample was dried and calcined at 450°C for 2 h at the heating rate of 10°C/min. Finally, the white powder of TiO_2 prepared by the sol-gel method was obtained and denoted as TiO_2-SG.

For the solvothermal method, 25 g of titanium (IV) *n*-butoxide (TNB) was used as the precursor. TNB was suspended in 100 ml of 1,4-butanediol in a test tube and placed in the autoclave. The autoclave was completely purged with nitrogen at a pressure of 30 bars before increasing the temperature to 320°C at a heating rate of 2.5°C/min and further held at that temperature for 6 h. Autogenous pressure during the reaction gradually increased as the temperature increased. After the reaction, the autoclave was cooled down to room temperature. The white powder was collected and then washed with ethanol followed by centrifugation at least 5 times. The powder was dried overnight at 110°C, and finally the white powder of TiO_2 prepared

by the solvothermal method was obtained and denoted as TiO_2-SV.

In order to prepare the WO_3/TiO_2 catalysts having W loading of 13.5 wt.%, the simple incipient wetness impregnation was used. The TiO_2-SG and TiO_2-SV supports obtained as mentioned above were used. It was accomplished using the tungsten (VI) chloride as a precursor, followed by drying the catalyst sample overnight at 110°C and calcined at 400°C with a heating rate of 10°C/min for 3 h. Consequently, the obtained WO_3/TiO_2 catalysts are denoted as WO_3/TiO_2-SG and WO_3/TiO_2-SV upon the TiO_2 supports employed.

2.3. Catalysts Characterization. The support and catalysts were characterized by several techniques, which are as follows.

2.3.1. Powder X-Ray Diffraction (XRD). The SIEMENS D-5000 X-ray diffractometer using CuK_α radiation ($\lambda = 1.54439$ Å) was used to determine the crystalline phase structure of supports and catalysts. The crystalline domain sizes were calculated from the Scherrer equation. The supports and catalysts were scanned at a rate of 2.4 min^{-1} in the range 2θ from 20 to 80 degrees with the resolution of 0.02°.

2.3.2. N_2 Physisorption. The adsorptiometer Micromeritics ASAP 2010 automated system instrument was used to determine surface area (BET method), pore volume/diameter, and pore size distribution (BJH method) by nitrogen gas adsorption-desorption at liquid nitrogen temperature at −196°C.

2.3.3. Temperature-Programmed Desorption of Ammonia (NH_3-TPD) and Carbon Dioxide (CO_2-TPD). The Micromeritics Chemisorb 2750 Pulse chemisorption system instrument was employed to identify the acidity and basicity on supports and catalysts. The 0.03 g quartz wool and 0.05 g catalysts were packed in a quartz tube and pretreated at 500°C under He flow for 1 hr. Next, the catalyst surface was saturated with NH_3 or CO_2 in He at 40°C for 30 min. Then, the excess adsorbed gas (the physisorbed NH_3 or CO_2) was purged with He until the baseline was constant. Afterwards, the catalysts was heated from 40°C to 500°C at a heating rate of 10°C/min to desorb NH_3 or CO_2. The amount of NH_3 or CO_2 in effluent was measured via the thermal conductivity detector (TCD) signal as a function of temperature.

2.3.4. Scanning Electron Microscopy (SEM) and Energy Dispersive X-Ray Spectroscopy (EDX). The SEM model JEOL mode JSM-6400 and EDX with stand Link Isis series 300 program were operated for analysis the morphology, element composition, and distributions over supports and catalysts.

2.3.5. X-Ray Fluorescence Analysis (XRF). The Olympus model Vanta M Series was performed to determine the amount of tungsten loading on catalysts. XRF spectrometer has an X-ray tube with Rh anode. The spectra were collected during 120 s, with the tube operating with a current of 100 μA and a voltage of 40 kV.

2.3.6. Catalytic Ethanol Dehydration Reaction. Essentially, the ethanol dehydration reaction system reported by Krutpijit and Jongsomjit was used [31]. It was performed in a fixed-bed continuous flow microreactor having an inside diameter of 0.7 cm and length of 33 cm length. First, 0.01 g of quartz wool and 0.05 g of catalyst (or support) were packed in the middle of reactor. The catalyst was preheated by flowing N_2 with a flow rate of 60 ml/min at 200°C for 1 h under atmospheric pressure to remove the moisture and impurity on surface of catalyst prior reaction. Afterwards, the reaction was started by feeding vaporized ethanol and N_2 stream as carrier gas. The ethanol flow rate was maintained at 1.45 ml/h (weight hourly space velocity (WHSV) = 22.9 ($g_{ethanol} \cdot g_{cat}{}^{-1} \cdot h^{-1}$)) controlled by a syringe pump injection. The reaction was operated at temperature varied from 200 to 400°C. After reaching steady-state condition, the reaction product compositions at reactor effluent were analyzed by a Shimadzu gas chromatography (GC8A) with flame ionization detector (FID) using DB-5 capillary column. Nitrogen with the pressure at 260 kPa was used as carrier gas in GC using the temperature of injector and detector at 150°C. The ethanol conversion was defined as follows:

$$X_{\mathrm{EtOH}} = \frac{n_{\mathrm{EtOH(in)}} - n_{\mathrm{EtOH(out)}}}{n_{\mathrm{EtOH(in)}}} \times 100. \quad (1)$$

The selectivity to i product was defined as follows:

$$S_{\mathrm{ethylene}} = \frac{n_{\mathrm{ethylene}}}{\sum n_i} \times 100,$$

$$S_{\mathrm{DEE}} = \frac{n_{\mathrm{DEE}}}{\sum n_i} \times 100, \quad (2)$$

$$S_{\mathrm{acetaldehyde}} = \frac{n_{\mathrm{acetaldehyde}}}{\sum n_i} \times 100.$$

The yield to i product was defined as follows:

$$Y_{\mathrm{ethylene}} = \frac{S_{\mathrm{ethylene}} \times X_{\mathrm{EtOH}}}{100},$$

$$Y_{\mathrm{DEE}} = \frac{S_{\mathrm{DEE}} \times X_{\mathrm{EtOH}}}{100}, \quad (3)$$

$$Y_{\mathrm{acetaldehyde}} = \frac{S_{\mathrm{acetaldehyde}} \times X_{\mathrm{EtOH}}}{100},$$

where $n_{\mathrm{EtOH(in)}}$ and $n_{\mathrm{EtOH(out)}}$ are defined as the molar flow rate (mmol/min) of ethanol in feed and product, respectively. n_{Ethylene}, n_{DEE}, $n_{\mathrm{Acetaldehyde}}$, and $\sum n_i$ were defined as the molar flow rate of ethylene, DEE, acetaldehyde, and total products (mmol/min), respectively.

3. Results and Discussion

3.1. Characteristics. The XRD patterns of both TiO_2 supports and WO_3/TiO_2 catalysts are illustrated in Figure 1.

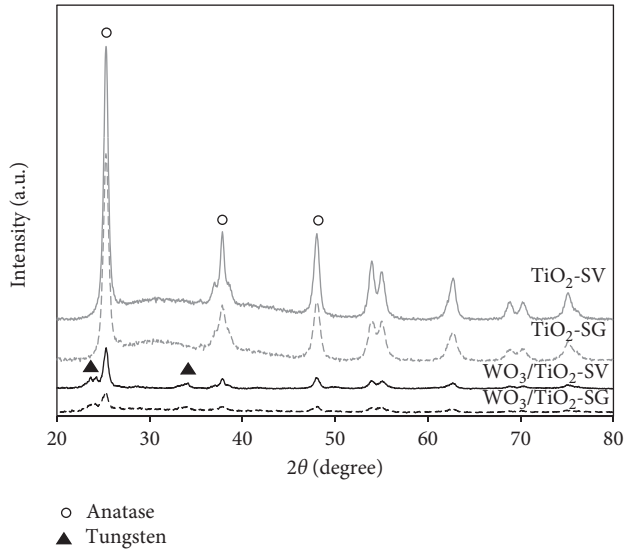

Figure 1: X-ray powder diffraction patterns of supports and catalysts.

Considering the XRD patterns of the supports including TiO_2-SG and TiO_2-SV, they exhibited the similar XRD patterns having the strong diffraction peaks located at 2θ degree of 25° (major), 38°, and 48°, which are assigned to the tetragonal anatase phase of crystalline TiO_2 [32, 33]. When the support was impregnated with 13.5 wt.% of tungsten, the XRD patterns were also similar with those of titania supports. The intensities were lower indicating the smaller crystallite size of WO_3/TiO_2 catalysts than the TiO_2 supports. Besides, the low intensity peaks were observed at 24° and 34° for both WO_3/TiO_2-SG and WO_3/TiO_2-SV catalysts, which were assigned to the formation of the WO_3 crystals with tetragonal phase [34, 35]. When compared the intensity of XRD peaks between WO_3/TiO_2-SG and WO_3/TiO_2-SV, it appeared that WO_3/TiO_2-SG exhibited lower intensity than WO_3/TiO_2-SV suggesting that the crystalline size of the former was smaller than the latter. Based on the Scherrer equation, the average crystalline size of WO_3/TiO_2-SG was smaller than WO_3/TiO_2-SV as seen in Table 1, where the TiO_2 crystalline size was in the range of 10.7–14.3 nm.

The BET surface area (S_{BET}), pore volume, and pore size diameter of TiO_2 supports and WO_3/TiO_2 catalysts analyzed by N_2 physisorption are shown in Table 1. The results revealed that the TiO_2-SG exhibited smaller surface area (73 m^2/g) and pore volume (0.13 cm^3/g) than those of TiO_2-SV BET surface area (85 m^2/g) and pore volume (0.42 cm^3/g). The large surface area essentially enhances catalytic activity in ethanol dehydration by increasing possibility of ethanol to attach on the acid site [28]. In addition, the surface area, pore volume, and pore size diameter decreased with the presence of tungsten due to some pore blockage [36].

Figure 2 showed the N_2 adsorption-desorption isotherms at −196°C for the TiO_2 supports and WO_3/TiO_2 catalysts. The results displayed the Type IV adsorption isotherms with the H1 hysteresis loop indicating the mesoporous structure according to the IUPACS. After loading tungsten to obtain WO_3/TiO_2-SG and WO_3/TiO_2-SV, it was found that the Type IV isotherm was still observed. The hysteresis loop moved toward lower pressure for WO_3/TiO_2-SG and WO_3/TiO_2-SV suggesting that the addition of tungsten onto TiO_2 support catalyst resulted in decreased pore volume. The pore size distribution (PSD) for the TiO_2 support catalysts and catalysts are shown in Figure 3. All catalysts were in the average pore diameter range of 2–50 nm classified as mesoporous particles. The TiO_2-SG showed the narrower pore size distribution than that of TiO_2-SV. The average pore sizes for all samples calculated by Barrett–Joyner–Halenda (BJH) are shown in Table 1, which were corresponding to the results from N_2 adsorption-desorption isotherm as seen from Figure 2.

The morphology of supports and catalysts prepared by different methods showed the different morphologies. The TiO_2-SG formed irregular shape particles, while TiO_2-SV formed small agglomerated spherical and porous particles. When impregnated with tungsten on TiO_2-SG and TiO_2-SV supports, both samples exhibited more porous particles. This suggested that the presence of tungsten into TiO_2 resulted in an increase of porosity. The EDX mapping of WO_3/TiO_2-SG and WO_3/TiO_2-SV catalysts are illustrated in Figure 4. It shows the elemental distribution of Ti, O, and W dispersing on the external surface of catalysts.

The tungsten was well dispersed at the outer surface of both TiO_2-SG and TiO_2-SV. The weight ratios of W/Ti are also listed in Table 2. The amount of tungsten present at outer surface of TiO_2-SG was larger than TiO_2-SV. Nevertheless, according to the XRF analysis the amount of tungsten in the bulk of TiO_2-SV catalyst was larger than TiO_2-SG indicating that the distribution of tungsten for TiO_2-SV catalyst was mostly located inside the pore of catalyst.

It is well known that acidity is the key factor relating to the activity of dehydration catalysts. The acidity of

Table 1: Physical properties of TiO_2 supports and catalysts.

Sample	S_{BET} (m^2/g)	Pore volume (cm^3/g)	Pore diameter (nm)	Crystallite TiO_2 size[a] (nm)	Crystallite WO_3 size[a] (nm)	W content[b] (wt.%)
TiO_2-SG	73	0.13	4.8	12.4	—	—
TiO_2-SV	85	0.42	16.5	15.3	—	—
WO_3/TiO_2-SG	61	0.11	5.1	10.7	6.1	16.3
WO_3/TiO_2-SV	78	0.30	13.0	14.3	9.0	18.9

[a]Measured by XRD using the Scherrer equation, [b]measured by XRF.

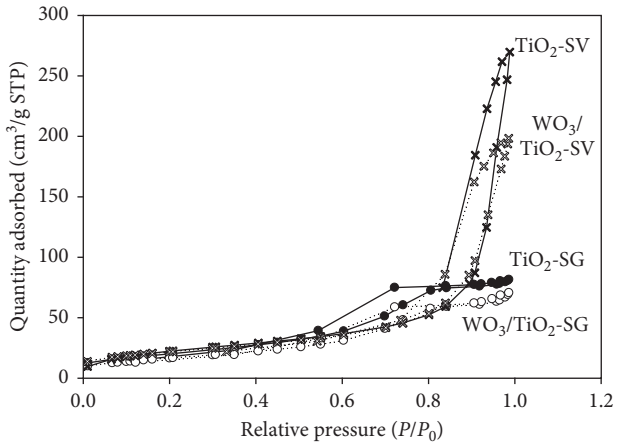

Figure 2: Nitrogen adsorption-desorption isotherms for supports and catalysts.

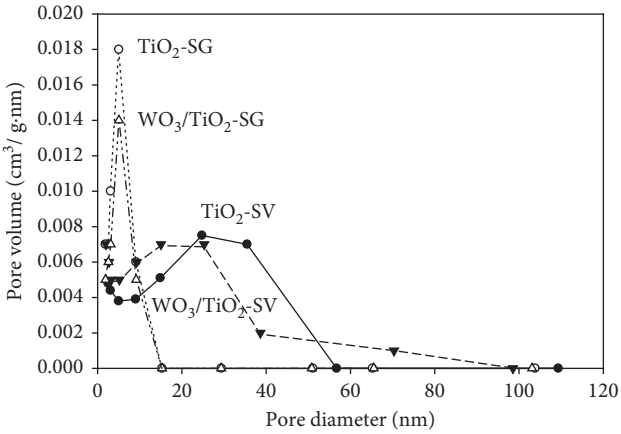

Figure 3: The pore size distribution for supports and catalysts.

supports and catalysts was evaluated by NH_3-temperature-programmed desorption as shown in Figure 5. As observed, the NH_3-TPD profiles for all samples exhibited the broad desorption peaks in range of 150–500°C.

It is known that the NH_3-TPD desorption temperature of acidic sites are classified as 3 categories. The desorption of NH_3 between 150 and 300°C is assigned as weak acidic sites, whereas the desorption between 300 and 450°C is moderate acid sites and the desorption above 450°C is strong acid sites [37]. As seen in Table 3, it indicated that the TiO_2-SG exhibited lower amount of acid site than the TiO_2-SV. However, with tungsten loading on both supports, it showed significant increase in weak and total acid sites for both WO_3/TiO_2-SG and WO_3/TiO_2-SV catalysts, which is necessary for enhancing the production of ethylene and DEE [38, 39]. In addition, it can be observed that the WO_3/TiO_2-SV catalyst exhibited the highest amount of total acid sites at 3645 μmol/g cat.

Considering the CO_2-TPD profiles as shown in Figure 6, the desorption peak displayed the narrow desorption in the temperature range of 50–200°C. Both TiO_2 supports exhibited low temperature CO_2 desorption around 87°C assigned to weak basic sites [40, 41]. The addition of tungsten into support catalysts resulted in a decrease of peak intensity around 80°C. It also revealed that WO_3/TiO_2-SG had the higher amount of basicity site than WO_3/TiO_2-SV as seen in Table 4.

The amounts of carbon deposition after reaction obtained by EDX measurement are shown in Table 5. The WO_3/TiO_2-SG and WO_3/TiO_2-SV exhibited higher amounts of carbon deposition than those of the TiO_2 supports due to their higher acidity. It is well known that high acidity yields high amount of carbon deposition.

3.2. Ethanol Dehydration Reaction. To investigate the catalytic activity and product distribution for all catalysts, the ethanol dehydration reaction in gas phase at atmospheric pressure and temperature ranging from 200°C to 400°C was performed. As seen in Table 6, the ethanol conversion for all samples increased with increasing reaction temperature indicating no deactivation of supports and catalysts. The highest ethanol conversion was achieved at 400°C for all samples. The ethanol conversion was found in order of WO_3/TiO_2-SV (87.6%) > TiO_2-SV (56.3%) > WO_3/TiO_2-SG (45.4%) > TiO_2-SG (33.9%), which are related to total amount acid sites of catalysts. It should be noted that the conversion of TiO_2-SV was still higher than that of WO_3/TiO_2-SG, which is quite interesting.

The selectivity to ethylene, DEE, and acetaldehyde are presented in Table 6. It can be observed that the TiO_2 rendered acetaldehyde as a major product. However, with the introduction of tungsten into TiO_2 supports, ethylene and DEE are turned out to be the major products at different temperature. In general, ethanol dehydration reaction can produce ethylene and DEE in 2 competitive pathways:

$$C_2H_5OH \longrightarrow C_2H_4 + H_2O + 44.9 \text{ kJ/mol} \quad (4)$$

$$2C_2H_5OH \longrightarrow C_2H_5OC_2H_5 + H_2O - 25.1 \text{ kJ/mol} \quad (5)$$

The reaction (4) is endothermic and favors the moderate to high temperature between 320°C and 500°C, while

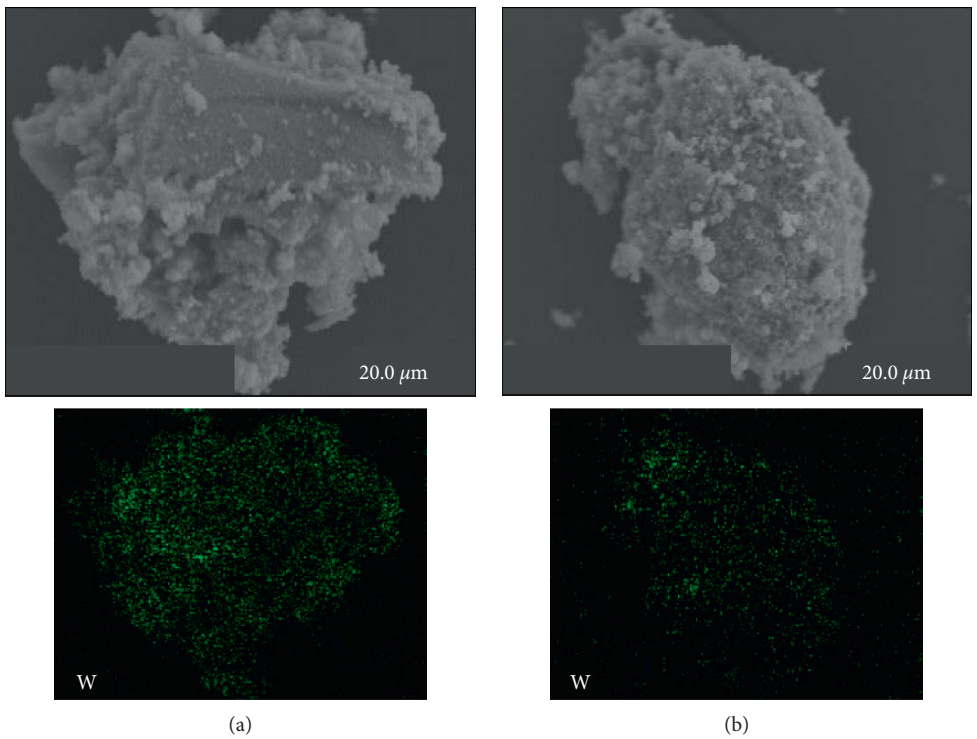

Figure 4: Elemental distribution by EDX mapping for (a) WO_3/TiO_2-SG and (b) WO_3/TiO_2-SV catalyst.

Table 2: Elemental compositions (wt.%) on external surface of catalysts obtained from EDX.

Sample	O	Ti	W	Cl	W/Ti
TiO_2-SG	44.67	55.33	n.a.	n.a.	n.a
TiO_2-SV	44.37	55.63	n.a.	n.a.	n.a
WO_3/TiO_2-SG	30.71	35.17	33.84	0.28	0.96
WO_3/TiO_2-SV	39.00	48.25	12.36	0.39	0.26

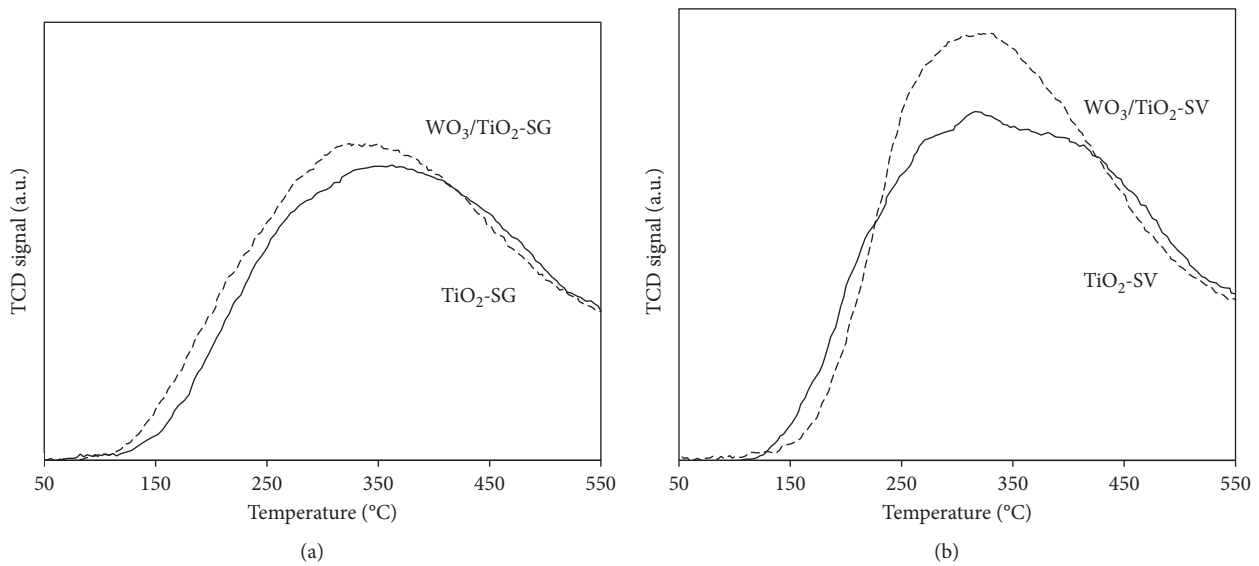

Figure 5: NH_3-TPD profiles of TiO_2 supports and WO_3/TiO_2 catalysts.

Table 3: The amount of surface acidity of supports and catalysts measured by NH_3-TPD.

Sample	NH_3 desorption (μmol/g cat)			Total acidity (μmol/g cat)
	Weak	Medium	Strong	
TiO_2-SG	895	662	717	2274
TiO_2-SV	1152	1232	841	3224
WO_3/TiO_2-SG	1030	1054	681	2765
WO_3/TiO_2-SV	1558	1263	823	3645

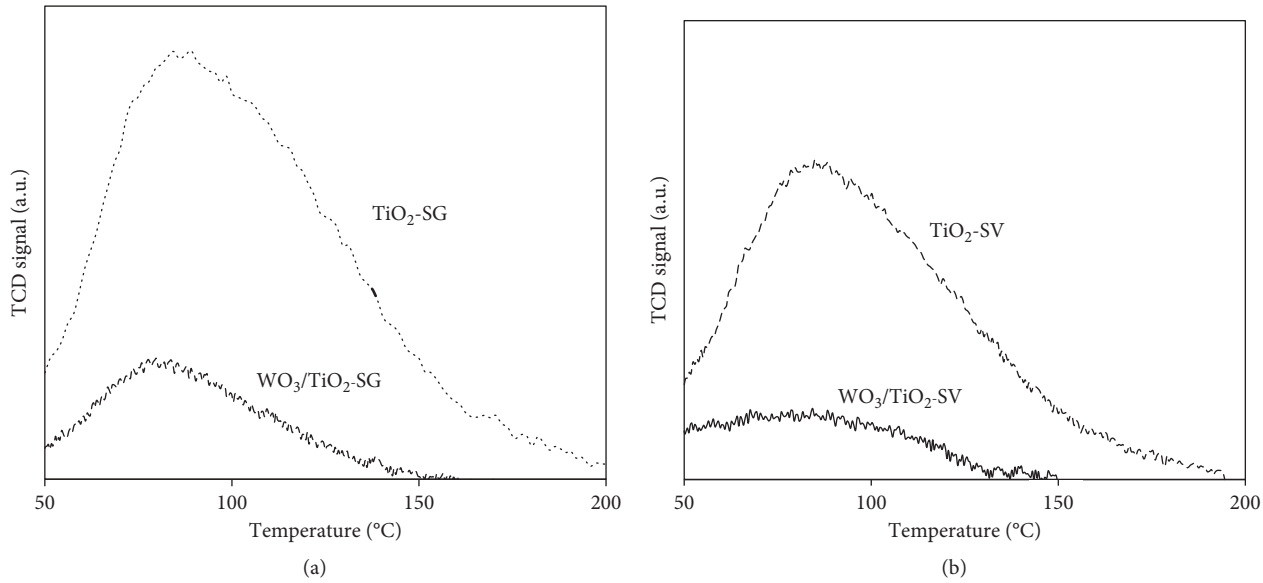

Figure 6: CO_2-TPD profile of TiO_2 supports and WO_3/TiO_2 catalysts.

Table 4: The amount of surface basicity of supports and catalysts measured by CO_2-TPD.

Sample	CO_2 desorption (μmol/g cat)		Total basicity (μmol/g cat)
	Weak	Medium/strong	
TiO_2-SG	27	4	31
TiO_2-SV	18	2	20
WO_3/TiO_2-SG	6	1	7
WO_3/TiO_2-SV	4	0	4

Table 5: The amount of carbon elemental compositions (wt.%) on external surface supports and catalysts after reaction obtained from EDX (the spent catalyst used in the reaction condition at $T = 200$–400°C for 8.5 hr).

Sample	TiO_2-SG	TiO_2-SV	WO_3/TiO_2-SG	WO_3/TiO_2-SV
C (%)	1.0	1.2	1.8	4.5

reaction (5) is exothermic and favors the low to moderate temperature between 150°C and 300°C [42]. The formation of the ethylene occurs by acid catalyst protonating to hydroxyl group of ethanol molecule (proton transfers from acid to O atom to form alkyloxonium ion), and then the water molecules is generated. Subsequently, an ethoxide surface group forms and deprotonates its methyl group to produce the ethylene. The DEE formation proceeds via either dissociative pathway or associative pathway [43]. The dissociative pathway is happened by one ethanol adsorption on catalyst and water elimination providing an adsorbed ethyl group. After that, the ethyl group reacts with the second ethanol and finally the DEE is formed. The associative pathway takes place from coadsorption of two ethanol reacted and formed into DEE. It is recognized that the dehydration of alcohol essentially takes place on Brønsted acid sites [39, 44], while Lewis acid sites rarely contribute for this reaction [45, 46]. The mechanism of ethanol dehydration to ethylene and DEE over the WO_3/TiO_2 catalysts is illustrated in Schemes 1 and 2, respectively. Besides, acetaldehyde is produced under the side reaction or dehydrogenation reaction in reaction (6), which is favored on the basic sites:

$$C_2H_5OH \longrightarrow C_2H_4O + H_2 + 52.4 \text{ kJ/mol} \quad (6)$$

According to the experiment, it was observed that TiO_2-SG and TiO_2-SV support catalysts still showed high acetaldehyde selectivity at ca. 81°C and ca. 71°C, respectively. This is perhaps due to the high reaction temperature or the heat treatment effect to an oxidation of Lewis oxygen in pure TiO_2 structure with the basic site is more dominant than acid as seen from the pure SBA-15 catalyst used in ethanol dehydration reported by Autthanit and Jongsomjit in 2018 [47]. The mechanism of ethanol dehydrogenation to acetaldehyde over TiO_2 support is illustrated in Scheme 3. Acetaldehyde occurs by ethanol molecule firstly adsorbed on the catalyst surface. An

Table 6: Ethanol conversion, product selectivity, and product yield as a function of reaction temperature (the reaction condition: $T = 200–400^{\circ}C$, WHSV = 22.9 $g_{ethanol} \cdot g_{cat}^{-1} \cdot h^{-1}$, and catalyst weight = 0.05 (g)).

Catalyst	Temp (°C)	Ethanol conversion (%)	Product selectivity (%)			Product yield (%)		
			Ethylene	DEE	Acetaldehyde	Ethylene	DEE	Acetaldehyde
TIO_2-SG	200	4.5	0.0	0.0	100.0	0.0	0.0	4.5
	250	8.6	1.8	0.0	98.2	0.2	0.0	8.5
	300	13.2	4.0	2.6	93.4	0.5	0.3	12.3
	350	32.3	11.4	1.6	87.0	3.7	0.5	28.1
	400	33.9	17.7	0.9	81.4	6.0	0.3	27.6
TIO_2-SV	200	21.1	0.0	0.0	100.0	0.0	0.0	21.1
	250	23.2	0.0	0.0	100.0	0.0	0.0	23.2
	300	35.7	2.5	2.1	95.3	0.9	0.8	34.1
	350	54.3	9.7	2.4	87.8	5.3	1.3	47.7
	400	56.3	25.5	3.4	71.1	14.4	1.9	40.0
WO_3/TiO_2-SG	200	12.4	4.7	37.4	57.9	0.6	4.6	7.2
	250	16.4	17.1	40.9	42.0	2.8	6.7	6.9
	300	25.0	39.5	10.4	50.1	9.9	2.6	12.5
	350	33.4	54.5	3.3	42.3	18.2	1.1	14.1
	400	45.4	64.6	1.3	34.1	29.3	0.6	15.5
WO_3/TiO_2-SV	200	33.2	5.2	42.6	52.2	1.7	14.2	17.3
	250	37.7	22.4	67.7	10.0	8.4	25.5	3.8
	300	51.8	52.6	42.4	5.0	27.3	22.0	2.6
	350	71.7	76.4	17.8	5.8	54.8	12.8	4.1
	400	87.6	88.2	3.5	8.3	77.2	3.1	7.3

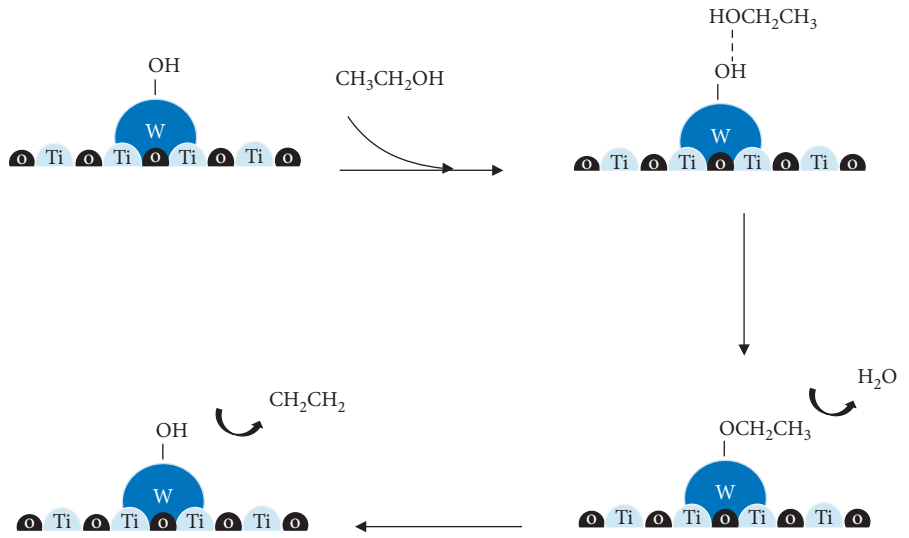

Scheme 1: Ethanol dehydration to ethylene over WO_3/TiO_2 catalyst.

ethoxy group is further generated and converted into acetaldehyde. When impregnated the tungsten on the TiO_2 supports, it revealed increased ethylene selectivity at high temperature and increased DEE selectivity at low temperature. The ethylene and DEE selectivities over WO_3/TiO_2-SV catalyst were higher than those of WO_3/TiO_2-SG catalyst. It was found that the highest ethylene selectivity of ca. 88% under the reaction temperature at 400°C and the highest DEE selectivity of ca. 68% under the reaction temperature at 250°C for WO_3/TiO_2-SV. The factor to increase the ethylene and DEE selectivity is the high amount of weak acid or Brønsted acid, which is the active site for ethanol dehydration after adding the tungsten on TiO_2 supports. As shown in Table 3, the weak acid sites for WO_3/TiO_2 catalyst were significantly higher than TiO_2 support catalyst, whereas the strong acid sites for TiO_2 were higher than the WO_3/TiO_2 catalyst. It is familiar that amount of weak acid site is probably correlated to Brønsted acid site, while the Lewis acid site may correlate to the strong acid site [47].

Besides two products, the acetaldehyde was formed as byproduct over WO_3/TiO_2-SG and WO_3/TiO_2-SV catalysts.

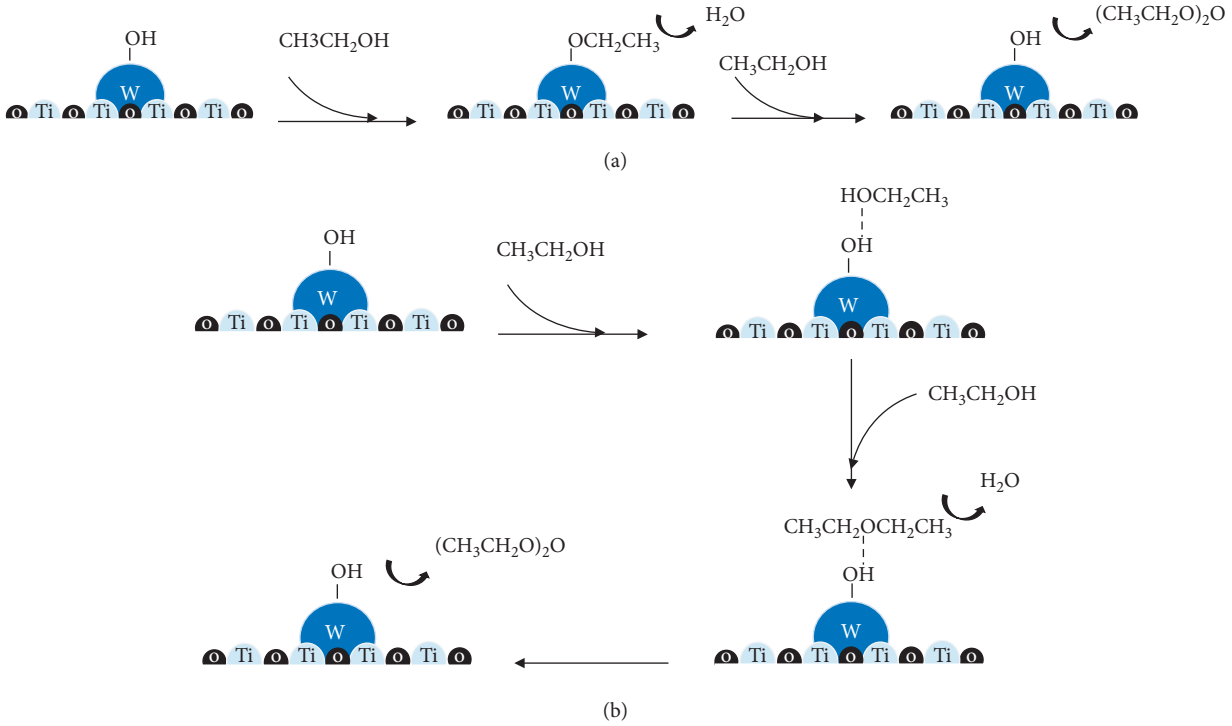

Scheme 2: Ethanol dehydration to DEE with (a) dissociative and (b) associative pathways over WO_3/TiO_2 catalyst.

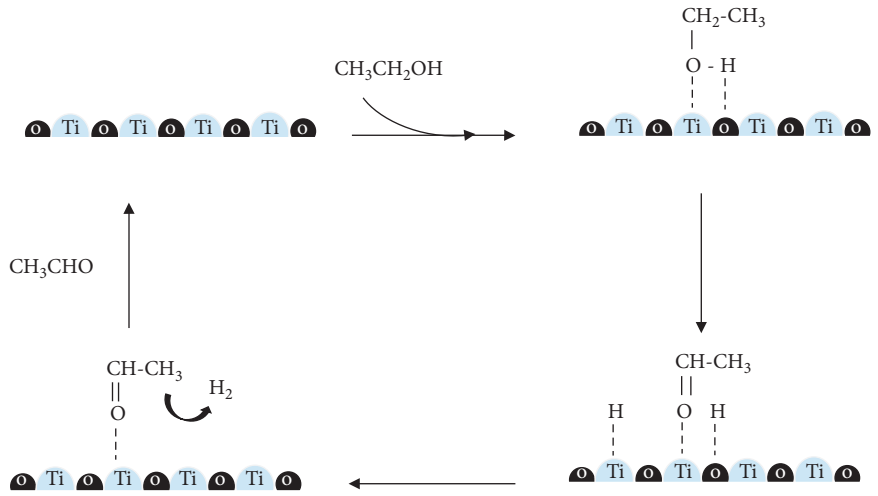

Scheme 3: Ethanol dehydrogenation to acetaldehyde over TiO2 support catalyst.

The acetaldehyde selectivity over WO_3/TiO_2-SG was higher than that of WO_3/TiO_2-SV relating to higher amounts of basic site present in WO_3/TiO_2-SG catalyst. The mass balance (carbon balance) in the reaction test typically closed to 90%. Such a deviation may occur due to mainly from coke formation.

The comparison of product yield for each temperature over supports and catalysts is reported in Table 6. It showed that presence of tungsten essentially improved the ethylene and DEE yield. The highest ethylene yield was found to be ca. 77% at 400°C over WO_3/TiO_2-SV. Moreover, it was observed that the highest DEE yield of ca. 26% at 250°C was obtained with WO_3/TiO_2-SV. However, DEE yield was rather small due to the low conversion at low temperature. It should be mentioned that the highest acetaldehyde yield of ca. 48% at 350°C obtained from TiO_2-SV was observed, which is quite interesting.

4. Conclusion

The WO_3/TiO_2-SV catalyst is promising for dehydration of ethanol to ethylene and DEE having the highest ethylene of 77% at 400°C and the highest yield of 26% at 250°C. It showed that the more efficient method to synthesize TiO_2

support was the solvothermal method due to high acidity and surface area. It is worth noting that the TiO_2-SV itself also rendered the highest yield of acetaldehyde at 48% at 350°C. This support can be potentially used as support for a catalyst in dehydrogenation of ethanol to acetaldehyde.

Data Availability

The data used to support the findings of this study are included within the article.

Conflicts of Interest

The authors declare that there are no conflicts of interest regarding the publication of this paper.

Acknowledgments

The authors thank the Grant for International Research Integration: Chula Research Scholar, Ratchadaphiseksomphot Endowment Fund, Endowment Fund, Grant for Research: Government Budget, Chulalongkorn University (2018), and the National Research Council of Thailand (NRCT) for their financial support of this project.

References

[1] A. Paul, R. S. Panua, D. Debroy, and P. K. Bose, "Effect of diethyl ether and ethanol on performance, combustion, and emission of single-cylinder compression ignition engine," *International Journal of Ambient Energy*, vol. 38, no. 1, pp. 2–13, 2014.

[2] M. R. Mostafa, A. M. Youssef, and S. M. Hassan, "Conversion of ethanol and isopropanol on alumina, titaniaand alumina-titania catalysts," *Materials Letters*, vol. 12, no. 3, pp. 207–213, 1999.

[3] H. Nair, J. E. Gatt, J. T. Miller, and C. D. Baertsch, "Mechanistic insights into the formation of acetaldehyde and diethyl ether from ethanol over supported VO*x*, MoO*x*, and WO*x* catalysts," *Journal of Catalysis*, vol. 279, no. 1, pp. 144–154, 2011.

[4] T. Zaki, "Catalytic dehydration of ethanol using transition metal oxide catalysts," *Journal of Colloid and Interface Science*, vol. 284, no. 2, pp. 606–613, 2005.

[5] Y. Xiao, X. Li, Z. Yuan, J. Li, and Y. Chen, "Catalytic dehydration of ethanol to ethylene on TiO_2/4A zeolite composite catalysts," *Catalysis Letters*, vol. 130, no. 3-4, pp. 308–311, 2009.

[6] I. Rossetti, M. Compagnoni, E. Finocchio et al., "Ethylene production via catalytic dehydration of diluted bioethanol: a step towards an integrated biorefinery," *Applied Catalysis B: Environmental*, vol. 210, pp. 407–420, 2017.

[7] T. K. Phung and G. Busca, "Ethanol dehydration on silica-aluminas: active sites and ethylene/diethyl ether selectivities," *Catalysis Communications*, vol. 68, pp. 110–115, 2015.

[8] A. Popa and V. Sasca, "The influence of surface coverage on the catalytic activity of silica-supported heteropolyacids," *Reaction Kinetics, Mechanisms and Catalysis*, vol. 117, no. 1, pp. 205–221, 2015.

[9] S. Bagheri, N. Muhd Julkapli, and S. Bee Abd Hamid, "Titanium dioxide as a catalyst support in heterogeneous catalysis," *Scientific World Journal*, vol. 2014, Article ID 727496, 21 pages, 2014.

[10] M. Dalil, D. Carnevali, J.-L. Dubois, and G. S. Patience, "Transient acrolein selectivity and carbon deposition study of glycerol dehydration over WO_3/TiO_2 catalyst," *Chemical Engineering Journal*, vol. 270, pp. 557–563, 2015.

[11] U. Filek, A. Kirpsza, A. Micek-Ilnicka, E. Lalik, and A. Bielański, "Ethanol conversion over cesium-doped mono- and bi-cationic aluminum and gallium H3PW12O40 salts," *Journal of Molecular Catalysis A: Chemical*, vol. 407, pp. 152–162, 2015.

[12] D. T. Mai, I. I. Mikhalenko, and A. I. Pylinina, "Hydrothermal ethanol conversion on Ag, Cu, Au/TiO_2," *Russian Journal of Physical Chemistry A*, vol. 88, no. 10, pp. 1637–1642, 2014.

[13] G. Pérez-López, R. Ramírez-López, and T. Viveros, "Acidic properties of Si- and Al- promoted TiO_2 catalysts: effect on 2-propanol dehydration activity," *Catalysis Today*, vol. 305, pp. 182–191, 2018.

[14] T. Kamsuwan, P. Praserthdam, and B. Jongsomjit, "Diethyl ether production during catalytic dehydration of ethanol over Ru- and Pt- modified H-beta zeolite catalysts," *Journal of Oleo Science*, vol. 66, no. 2, pp. 199–207, 2017.

[15] M. Sudhakar, V. V. Kumar, G. Naresh, M. L. Kantam, S. K. Bhargava, and A. Venugopal, "Vapor phase hydrogenation of aqueous levulinic acid over hydroxyapatite supported metal (M = Pd, Pt, Ru, Cu, Ni) catalysts," *Applied Catalysis B: Environmental*, vol. 180, pp. 113–120, 2016.

[16] T. Inmanee, P. Pinthong, and B. Jongsomjit, "Effect of calcination temperatures and Mo modification on nanocrystalline (γ-χ)-Al_2O_3 catalysts for catalytic ethanol dehydration," *Journal of Nanomaterials*, vol. 2017, pp. 1–9, 2017.

[17] J. Chauvin, K. Thomas, G. Clet, and M. Houalla, "Comparative influence of surface tungstate species and bulk amorphous WO_3 particles on the acidity and catalytic activity of tungsten oxide supported on silica," *Journal of Physical Chemistry C*, vol. 119, no. 22, pp. 12345–12355, 2015.

[18] P. Lauriol-Garbey, S. Loridant, V. Bellière-Baca, P. Rey, and J.-M. M. Millet, "Gas phase dehydration of glycerol to acrolein over WO_3/ZrO_2 catalysts: improvement of selectivity and stability by doping with SiO_2," *Catalysis Communications*, vol. 16, no. 1, pp. 170–174, 2011.

[19] J. A. Cecilia, C. García-Sancho, J. M. Mérida-Robles, J. Santamaría González, R. Moreno-Tost, and P. Maireles-Torres, "WO_3 supported on Zr doped mesoporous SBA-15 silica for glycerol dehydration to acrolein," *Applied Catalysis A: General*, vol. 516, pp. 30–40, 2016.

[20] M. Ai, "The activity of WO_3-based mixed-oxide catalysts: I. Acidic properties of WO_3-based catalysts and correlation with catalytic activity," *Journal of Catalysis*, vol. 49, no. 3, pp. 305–312, 1977.

[21] V. Lebarbier, G. Clet, and M. Houalla, "Relations between structure, acidity, and activity of WO_x/TiO_2: influence of the initial state of the support, titanium oxyhydroxide, or titanium oxide," *Journal of Physical Chemistry B*, vol. 110, no. 45, pp. 22608–22617, 2006.

[22] Y. Qin, S. Xun, L. Zhan et al., "Synthesis of mesoporous WO_3/TiO_2 catalyst and its excellent catalytic performance for the oxidation of dibenzothiophene," *New Journal of Chemistry*, vol. 41, no. 2, pp. 569–578, 2017.

[23] X. Zhao, L. Mao, and G. Dong, "Mn-Ce-V-WO_x/TiO_2 SCR catalysts: catalytic activity, stability and interaction among catalytic oxides," *Catalysts*, vol. 8, no. 2, p. 76, 2018.

[24] C. Liebig, S. Paul, B. Katryniok et al., "Glycerol conversion to acrylonitrile by consecutive dehydration over WO_3/TiO_2 and

ammoxidation over Sb-(Fe, V)-O," *Applied Catalysis B: Environmental*, vol. 132-133, pp. 170–182, 2013.

[25] Y. M. Hunge, M. A. Mahadik, A. V. Moholkar, and C. H. Bhosale, "Photoelectrocatalytic degradation of oxalic acid using WO_3 and stratified WO_3/TiO_2 photocatalysts under sunlight illumination," *Ultrasonics Sonochemistry*, vol. 35, pp. 233–242, 2017.

[26] T. K. Phung, L. Proietti Hernández, and G. Busca, "Conversion of ethanol over transition metal oxide catalysts: effect of tungsta addition on catalytic behaviour of titania and zirconia," *Applied Catalysis A: General*, vol. 489, pp. 180–187, 2015.

[27] H. V. Fajardo, E. Longo, E. R. Leite, R. Libanori, L. F. D. Probst, and N. L. V. Carreño, "Synthesis, characterization and catalytic properties of nanocrystaline $Y2O_3$-coated TiO_2 in the ethanol dehydration reaction," *Materials Research*, vol. 15, no. 2, pp. 285–290, 2012.

[28] M. Wannaborworn, P. Praserthdam, and B. Jongsomjit, "A comparative study of solvothermal and sol-gel-derived nanocrystalline alumina catalysts for ethanol dehydration," *Journal of Nanomaterials*, vol. 2015, Article ID 519425, 11 pages, 2015.

[29] J. Panpranot, K. Kontapakdee, and P. Praserthdam, "Selective hydrogenation of acetylene in excess ethylene on micron-sized and nanocrystalline TiO_2 supported Pd catalysts," *Applied Catalysis A: General*, vol. 314, no. 1, pp. 128–133, 2006.

[30] C. M. Gómez-Gutiérrez, P. A. Luque, G. Guerra-Rivas et al., "Solvothermal synthesis of nickel-tungsten sulfides for 2-propanol dehydration," *Scanning*, vol. 37, no. 3, pp. 165–171, 2015.

[31] C. Krutpijit and B. Jongsomjit, "Catalytic ethanol dehydration over different acid-activated montmorillonite clays," *Journal of Oleo Science*, vol. 65, no. 4, pp. 347–355, 2016.

[32] K. Thamaphat, P. Limsuwan, and B. Ngotawornchai, "Phase characterization of TiO_2 powder by XRD and TEM," *Natural Science*, vol. 42, pp. 357–361, 2008.

[33] B. S. Shirke, P. V. Korake, P. P. Hankare, S. R. Bamane, and K. M. Garadkar, "Synthesis and characterization of pure anatase TiO_2 nanoparticles," *Journal of Materials Science: Materials in Electronics*, vol. 22, no. 7, pp. 821–824, 2010.

[34] A. A. Said, M. M. M. Abd El-Wahab, and M. Abd El-Aal, "The role of acid sites in the catalytic performance of tungsten oxide during the dehydration of isopropyl and methyl alcohols," *Chemical and Materials Engineering*, vol. 4, no. 2, pp. 17–25, 2016.

[35] S. Maksasithorn, P. Praserthdam, K. Suriye, and D. P. Debecker, "Preparation of super-microporous WO_3-SiO_2 olefin metathesis catalysts by the aerosol-assisted sol-gel process," *Microporous and Mesoporous Materials*, vol. 213, pp. 125–133, 2015.

[36] R. E. M. Abdennouri, A. Elmhammedi, A. Galadi et al., "Influence of tungsten on the anatase-rutile phase transition of sol-gel synthesized TiO_2 and on its activity in the photocatalytic degradation of pesticides," *Journal of Materials and Environmental Science*, vol. 4, no. 6, pp. 953–960, 2013.

[37] M. Almohalla, I. Rodríguez-Ramos, and A. Guerrero-Ruiz, "Comparative study of three heteropolyacids supported on carbon materials as catalysts for ethylene production from bioethanol," *Catalysis Science & Technology*, vol. 7, no. 9, pp. 1892–1901, 2017.

[38] T. Kamsuwan and B. Jongsomjit, "A comparative study of different Al-based solid acid catalysts for catalytic dehydration of ethanol," *Engineering Journal*, vol. 20, no. 3, pp. 63–75, 2016.

[39] H. Xin, X. Li, Y. Fang et al., "Catalytic dehydration of ethanol over post-treated ZSM-5 zeolites," *Journal of Catalysis*, vol. 312, pp. 204–215, 2014.

[40] K.-M. C. David Raju Burri, S.-C. Han, A. Burri, and S.-E. Park, "Dehydrogenation of ethylbenzene to styrene with CO_2 over TiO_2-ZrO_2 bifunctional catalyst," *Bulletin of the Korean Chemical Society*, vol. 28, no. 1, pp. 53–58, 2007.

[41] D. Chen, D. Mao, J. Xiao, X. Guo, and J. Yu, "CO_2 hydrogenation to methanol over CuO-ZnO-TiO_2-ZrO_2: a comparison of catalysts prepared by sol-gel, solid-state reaction and solution-combustion," *Journal of Sol-Gel Science and Technology*, vol. 86, no. 3, pp. 719–730, 2018.

[42] S. L. Chong, J. C. Soh, and C. K. Cheng, "Production of ethylene from ethanol dehydration over H_3PO_4- modified cerium oxide catalyst," *Malaysian Journal of Analytical Sciences*, vol. 21, no. 4, pp. 839–848, 2017.

[43] W. Alharbi, E. Brown, E. F. Kozhevnikova, and I. V. Kozhevnikov, "Dehydration of ethanol over heteropoly acid catalysts in the gas phase," *Journal of Catalysis*, vol. 319, pp. 174–181, 2014.

[44] E. Hong, H.-I. Sim, and C.-H. Shin, "The effect of Brønsted acidity of WO_3/ZrO_2 catalysts in dehydration reactions of C_3 and C_4 alcohols," *Chemical Engineering Journal*, vol. 292, pp. 156–162, 2016.

[45] W. R. Moser, R. W. Thompson, C.-C. Chang, and H. Tong, "Silicon-rich H-ZSM-5 catalyzed conversion of aqueous ethanol to ethylene," *Journal of Catalysis*, vol. 117, no. 1, pp. 19–32, 1989.

[46] C. P. Nash, A. Ramanathan, D. A. Ruddy et al., "Mixed alcohol dehydration over Brønsted and Lewis acidic catalysts," *Applied Catalysis A: General*, vol. 510, pp. 110–124, 2016.

[47] C. Autthanit and B. Jongsomjit, "Production of ethylene through ethanol dehydration on SBA-15 catalysts synthesized by sol-gel and one-step hydrothermal methods," *Journal of Oleo Science*, vol. 67, no. 2, pp. 235–243, 2018.

Hindawi
International Journal of Chemical Engineering
Volume 2019, Article ID 4102646, 10 pages
https://doi.org/10.1155/2019/4102646

Research Article

Carbon-Based Catalyst from Pyrolysis of Waste Tire for Catalytic Ethanol Dehydration to Ethylene and Diethyl Ether

Ekrachan Chaichana,[1] Weeraphat Wiwatthanodom,[2] and Bunjerd Jongsomjit[2]

[1]*Research Center of Natural Materials and Products, Chemistry Program, Faculty of Science and Technology, Nakhon Pathom Rajabhat University, Muang, Nakhon Pathom 73000, Thailand*
[2]*Center of Excellence on Catalysis and Catalytic Reaction Engineering, Department of Chemical Engineering, Faculty of Engineering, Chulalongkorn University, Bangkok 10330, Thailand*

Correspondence should be addressed to Bunjerd Jongsomjit; bunjerd.j@chula.ac.th

Received 12 November 2018; Revised 1 January 2019; Accepted 8 January 2019; Published 5 February 2019

Guest Editor: Hu Li

This work investigated the use of waste tire as a source of carbon in preparation of carbon-based catalysts for applying in ethanol dehydration. The pyrolysis of waste tire was performed to obtain the solid carbon, and then it was treated with two different acids including HCl and HNO_3 prior to the activation process with different temperatures to gain suitable carbon catalysts. All carbon catalysts were characterized using nitrogen physisorption, XRD, FTIR, and acid-base titration. The catalysts were tested for catalytic ethanol dehydration in a micropacked-bed reactor under the temperature range from 200°C to 400°C. It revealed that the ethanol conversion increased with increasing the reaction temperature for all catalysts. The carbon catalyst treated with HCl and calcined at 420°C (AC_H420) exhibited the highest ethanol conversion of 36.2% at 400°C having ethylene and diethyl ether selectivity of 65.9 and 33.5%, respectively. The high activity of this catalyst can be attributed to the high acid density at the surface (18.5 μmol/m^2), which was significantly higher than those of most other catalysts (less than 8.0 μmol/m^2).

1. Introduction

It has been reported that global tire manufacturing output is estimated to be over 17 million tons in 2016 and is growing nearly by 4% per year through 2022 [1]. This leads to large amounts of waste tires produced annually. A common way for disposal of these waste tires is land filling. However, due to their large volume and high void space (about 75%), they consume a considerable amount of space if directly dumped into landfill [2]. Burning waste tires also release various harmful gases such as CO_2 and CO, and volatile organic compounds such as benzene, styrene, butadiene, and phenol-like substances [3].

One of the most interesting and dynamically developing methods for reducing waste tires is a pyrolysis process [4]. The pyrolysis process is not only the waste disposal, but also produces alternative fuel for internal combustion engines. In addition, the pyrolysis is nontoxic without emission of harmful gas, unlike incineration [5]. The proportions of pyrolysis products including gas, oil, and solid carbon depend on the rate of temperature rise, time of decomposition, temperature, and pressure [6].

In general, flash pyrolysis process (heating rate around 100°C/s to 10,000°C/s) produces 45–75 wt% of liquid, 15–25 wt% of solid, and 10–20 wt% of noncondensable gases [7]. The obtained pyrolysis gas and liquid can be efficiently used as fuel. In general, the pyrolysis liquid has an average heating value of 12 MJ/kg and the pyrolysis gas has an average heating value of 23–26.3 MJ/kg. For the obtained pyrolysis solid (solid carbon), it can be used to produce low-grade carbon black, and also adsorbent materials after applying an activation step (known as activated carbon, AC) [8]. Thus, the use of solid carbon from waste tire as a catalyst or a catalyst support is also an alternative way for valorization of waste tires. Sanchez-Olmos *et al.* [9] prepared a new acid catalyst based from a solid carbon from waste tire pyrolysis.

The solid carbon was functionalized using sulfuric acid as source of $-SO_3H$ acid groups prior using in biodiesel production. It was found that this catalyst exhibited a high catalytic performance, which required shorter times, low temperature, and significantly a low amount of methanol compared to other studies for the biodiesel production. Hood et al. [10] compared waste tire-derived carbons prepared using two different methods including the treatment with concentrated sulfuric and a newly developed method involving the sequential treatment with L-cysteine, dithiothreitol, and H_2O_2 under mild conditions. The catalysts were applied for the waste to biofuel conversion. It was found that both catalysts could also effectively convert oleic acid or a mixture of fatty acids and soybean oil to usable biofuels.

In addition, one of the interesting reactions in which carbon-based catalyst from pyrolysis could be employed is catalytic ethanol dehydration that converts ethanol into ethylene and diethyl ether (DEE) [11–14]. This reaction undergoes via suitable solid acid catalysts. Ethylene is one of the most usable upstream chemicals, while DEE is mostly used as a solvent in chemical processes including fragrance and pharmaceutical processes. However, only a few research works studied in the catalytic ethanol dehydration with using the carbon-based catalyst. Bedia et al. [15] used acid carbon catalyst derived from olive stone activated with phosphoric acid (H_3PO_4) for catalytic decomposition of ethanol, which yields mainly dehydration products, mostly ethylene with lower amounts of diethyl ether. It was also found that characteristic of the carbon catalyst such as surface functional groups significantly affected the catalytic activity during the reactions. The mentioned characteristics varied with the activation temperature and the chemical concentration in impregnation step. Therefore, adjusting conditions in preparation processes of carbon catalyst can tailor the reaction and obtain the desired products.

Hence, in this study, waste tires were used to prepare carbon-based catalysts via pyrolysis with various conditions including activation temperatures and types of treatment acid (HCl and H_2SO_4). All prepared carbons were then activated with H_3PO_4 prior to sulfonating with H_2SO_4 to obtain the acidic carbon-based catalysts for ethanol dehydration to ethylene and diethyl ether. The carbon catalysts were characterized with different techniques such as N_2 physisorption, acid-based titration, Fourier transform infrared spectroscopy (FTIR), and X-ray diffraction (XRD). The catalysts were then tested in the gas-phase ethanol dehydration under a reaction temperature of 200°C to 400°C. The catalytic performance for all catalysts in terms of catalytic activity and product selectivity was determined and further discussed.

2. Materials and Methods

2.1. Materials. Waste tires were obtained from the local supplier in Bangkok, Thailand. Hydrochloric acid (HCl), nitric acid (HNO_3), and phosphoric acid (H_3PO_4) were purchased from QRëC, New Zealand. The proximate analysis of waste tire is shown in Table 1.

Table 1: Proximate analysis of waste tires.

Item	Value (%)
Moisture	2.81
Volatile matter	1.86
Ash	15.42
Fixed carbon	79.91

2.2. Pyrolysis of Waste Tire. Waste tires were washed, dried, and cut into pieces. They were then pyrolyzed at 400°C in nitrogen with a heating rate of 10°C/min and held at that temperature for 1 h. Products from pyrolysis included three phases: liquid (bio-oil), solid (carbon), and gas. In this study, only solid carbon was further investigated.

2.3. Preparation of Carbon Catalyst. At first, waste tires were pyrolyzed at 420°C in 0.5 batch reactor with N_2 flowing at 50 mL/min. The pyrolysis process was conducted as illustrated in Scheme 1.

All solid material from the pyrolysis of waste tires known as solid carbon was brought into a magnetic separator to remove the tire wire. After that, the carbon was treated with 3 M hydrochloric (HCl) or nitric acid (HNO_3) at 125°C for 1 h, neutralized with water, and dried. The activation process was carried out with 1 M phosphoric acid (1 : 2 w/v) at three different temperatures including 420, 520, and 620°C for 3 h in a vacuum oven.

Six carbon catalysts are donated as follows:

$$\mathbf{AC\_XY}, \quad (1)$$

where X refers to hydrochloric (H) or nitric acid (N) treatment and Y is the activation temperatures. For instance, **AC_H420** refers to the catalyst obtained using hydrochloric acid, activated at 420°C.

2.4. Sulfonating of Catalyst. The prepared carbon catalyst was mixed with sulfuric acid (98 %) in the ratio of 1 g carbon per 1 mL acid. The mixture was stirred at 125°C for 20 h. The obtained catalyst was washed with water until it become neutral, and then dried at 125°C for 6 h.

2.5. Characterization of Carbon Catalyst

2.5.1. Nitrogen Physisorption. The surface area and pore characteristics of all catalysts were determined by the nitrogen physisorption technique using Micromeritics ASAP 2020 surface area and porosity analyzer. The catalyst sample was thermally heated at 150°C for 1 h before nitrogen adsorption at the temperature of −196°C.

2.5.2. Iodine Adsorption Test. The adsorption of iodine was determined using 0.5 N standardized iodine solution and conducted according to ASTM D1510 [16].

2.5.3. X-Ray Diffraction (XRD). XRD was used to determine the bulk crystalline phases of all catalysts using a SIEMENS

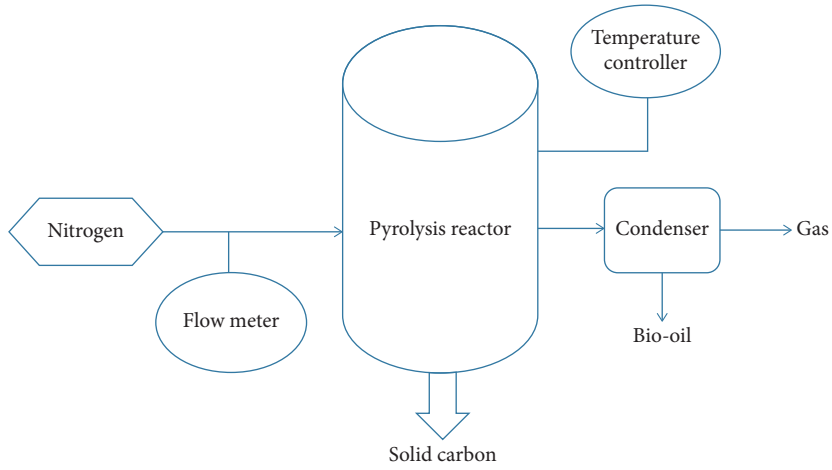

Scheme 1: Pyrolysis process.

D5000 X-ray diffractometer with CuK_α radiation through an Ni filter in the 2θ range of 20° to 80° [17].

2.5.4. Acidity Determination. 0.1 g of catalyst was soaked in 60 ml of 0.08 M sodium hydroxide (NaOH) for 24 h at room temperature. A few drops of phenolphthalein were added into the mixture, and then titrated with 0.02 M HCl until the equivalent point was reached.

2.5.5. Scanning Electron Microscopy (SEM). The morphology of the catalysts was investigated with using JEOL JSM-35F scanning electron microscope (SEM). The sample was conductive to prevent charging by coating with gold particle by ion 45 sputtering device.

2.5.6. Fourier Transform Infrared Spectroscopy (FTIR). The functional groups of the catalysts were determined by a Nicolet 6700 FTIR spectrometer. The infrared spectra were recorded under the wavenumber scanning from 400 to 4,000 cm^{-1} with a scanning frequency of 64 times.

2.6. Reaction Study. The ethanol dehydration process was conducted in a fixed-bed continuous flow reactor with 0.7 cm inside diameter. First, 0.01 g of quartz wool and 0.05 g of catalyst were packed into the middle of reactor. The process began with pretreating the catalyst with argon (50 ml/min) at 200°C for 1 h under atmospheric pressure (WHSV = 8.4 h^{-1}). The reaction was carried out in the temperature range from 200°C to 400°C. The obtained products were analyzed by a Shimadzu GC14B gas chromatographer with capillary column (DB-5 for separation of ethylene, diethyl ether, and acetaldehyde) and FID detector. The catalytic ethanol dehydration system (Scheme 2) was conducted as reported in our previous work [12].

3. Results and Discussion

3.1. Characterization. Characterization results of the carbon catalysts prepared from pyrolysis of waste tires treated with two different acids (HCl and HNO_3), and activated with phosphoric acid at various temperatures are shown in Table 2. From a nitrogen adsorption-desorption technique, which gave details of surface and pore characteristics, it was found that surface areas and pore volume of all activated carbons increased with increasing the activation temperature indicating no sintering occurred. The higher temperatures enhance a removal of organic volatile compounds and also noncarbon atom remained in the activated carbons resulting in the additional pores inside the structure, thus leading to the higher pore volume and the larger surface [18]. However, the small new pores dragged the average pore values of the activated carbons down as seen from the result. Similar trends were found for both types of activated carbons, treated with HCl or HNO_3.

It was observed that iodine adsorption capacities of the catalysts did not linearly increase with increasing of surface area. Change in pore size could affect the adsorption capacity of the catalyst. Decrease of pore size in the catalysts activated at higher temperature obstructs the adsorption of iodine molecules onto the catalyst surface. Even though the iodine molecules are relatively smaller (0.6 nm, [19]) than the average pore sizes of the catalyst, the new pores generated at the high activation temperature may be smaller than or nearly the same size as the iodine molecules, thus hindering the adsorption process. Shimada et al. [20] also found a remarkable decrease in the iodine adsorption number which is attributed to the collapse of pores by the excessive activation and an increase in the ash content in the activated carbon. Change in adsorption characteristic could influence the performance of catalysts, especially when catalysts have to be immobilized prior to use.

Adsorption isotherms of the catalysts were also obtained from a nitrogen adsorption-desorption technique. It can be observed that all samples exhibited type IV isotherm with a hysteresis loop indicating to a mesoporous structure of the materials according to the IUPAC classification (Figure 1).

Crystal structures of the catalyst samples were detected with an X-ray diffractometer (XRD). It can be seen from the

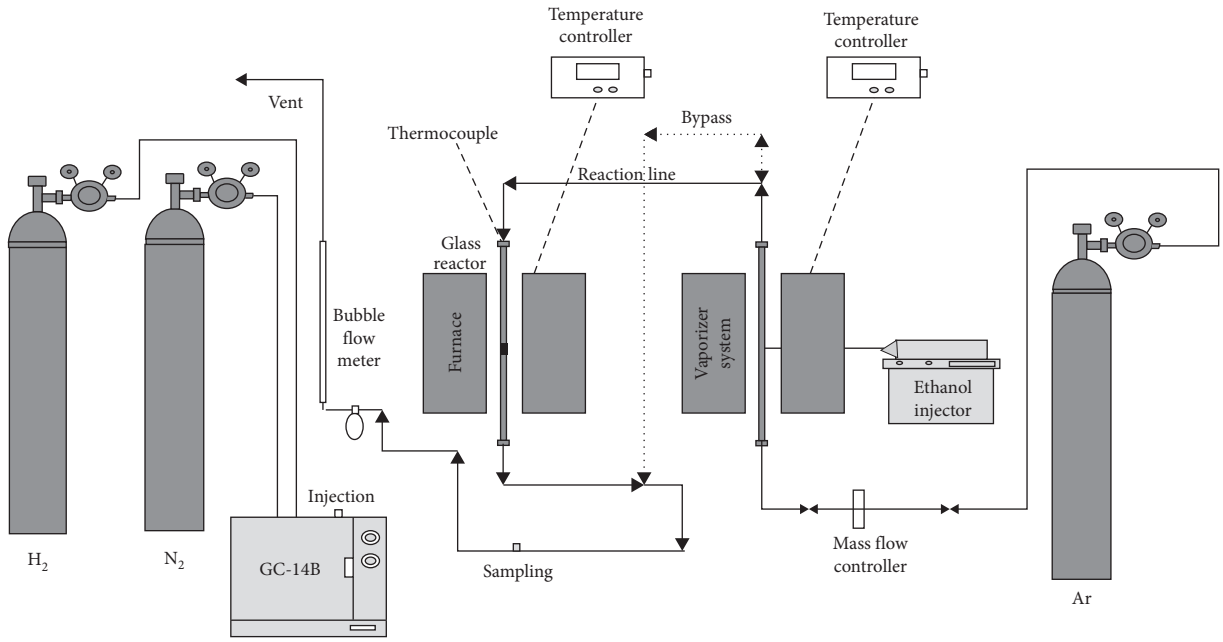

Scheme 2: Ethanol dehydration system.

Table 2: Surface areas, pore characteristics, and iodine adsorption of carbon catalysts.

Sample	Surface area (m^2/g)	Pore volume (cm^3/g)	Pore size (nm)	Iodine adsorption (mg/g)
AC_H420	119.2	0.85	28.3	125
AC_H520	273.6	1.49	23.4	129
AC_H620	293.3	1.81	20.4	139
AC_N420	105.8	0.85	32	124
AC_N520	263.6	1.34	23.9	126
AC_N620	290.0	1.62	21.3	129

XRD patterns in Figure 2 that all samples exhibited the similar crystal structures revealing the characteristic peaks of graphite at around $2\theta = 26$ [21]. The sharper peaks appeared with the higher activation temperature. This suggests that the higher activation temperature causes more crystallinity to the samples.

Morphologies of the catalysts were investigated with a scanning electron microscope (SEM) as shown in the SEM micrographs in Figure 3. It can be observed that all catalysts exhibited spherical-like particles with smooth surface. No differences in morphologies caused by different activation temperatures or acids were observed.

For efficient use in the ethanol dehydration, the acidity of the catalysts was improved by sulfonating with H_2SO_4 onto the carbon. The finished catalysts were then investigated with the FTIR to detect functional groups on the catalyst surface. The FTIR spectra of all catalysts are shown in Figure 4. It can be seen that all catalysts clearly exhibited peaks around 1184 cm^1, which are attributed to sulfate groups (S=O) from the substitution of hydrogen in surface hydroxyl groups (−O−H). This is evident for the presence of acid groups derived from sulfonation with H_2SO_4 on the catalyst surfaces. The peaks attributed to alcohols (R−OH) around 3400–3600 cm^{-1} and carboxylic (C=O) around 1711 cm^{-1} were also observed in all catalysts.

The acidity of the catalysts was determined by back titration with NaOH. The result of acidity determination with regard to surface acidity (moles of acidic sites) and acid density is shown in Table 3. It was observed that the surface acidities of all catalysts are nearly similar probably due to same amount of sulfonic acid sites present on all catalysts. This indicates that all catalysts have similar adsorption capacities for sulfonic acid, in consistent with the adsorption capacities of iodine as observed previously. The differences in surface areas of the catalysts insignificantly affected the acidity of the catalyst. However, as a result of the differences in surface areas of the catalysts, it leads to the variation of acid density among all catalysts. The highest acid density belonged to the catalysts activated at the low temperature (400°C) for both series of catalysts (previously treated with HCl or HNO_3) due to their low surface areas. These acid properties may influence catalytic performances of the catalyst during ethanol dehydration, which will be further discussed in the next part.

3.2. Reaction Study. The catalytic ethanol dehydration was conducted under temperature programming from 200°C to 400°C for all catalysts to evaluate their catalytic performance

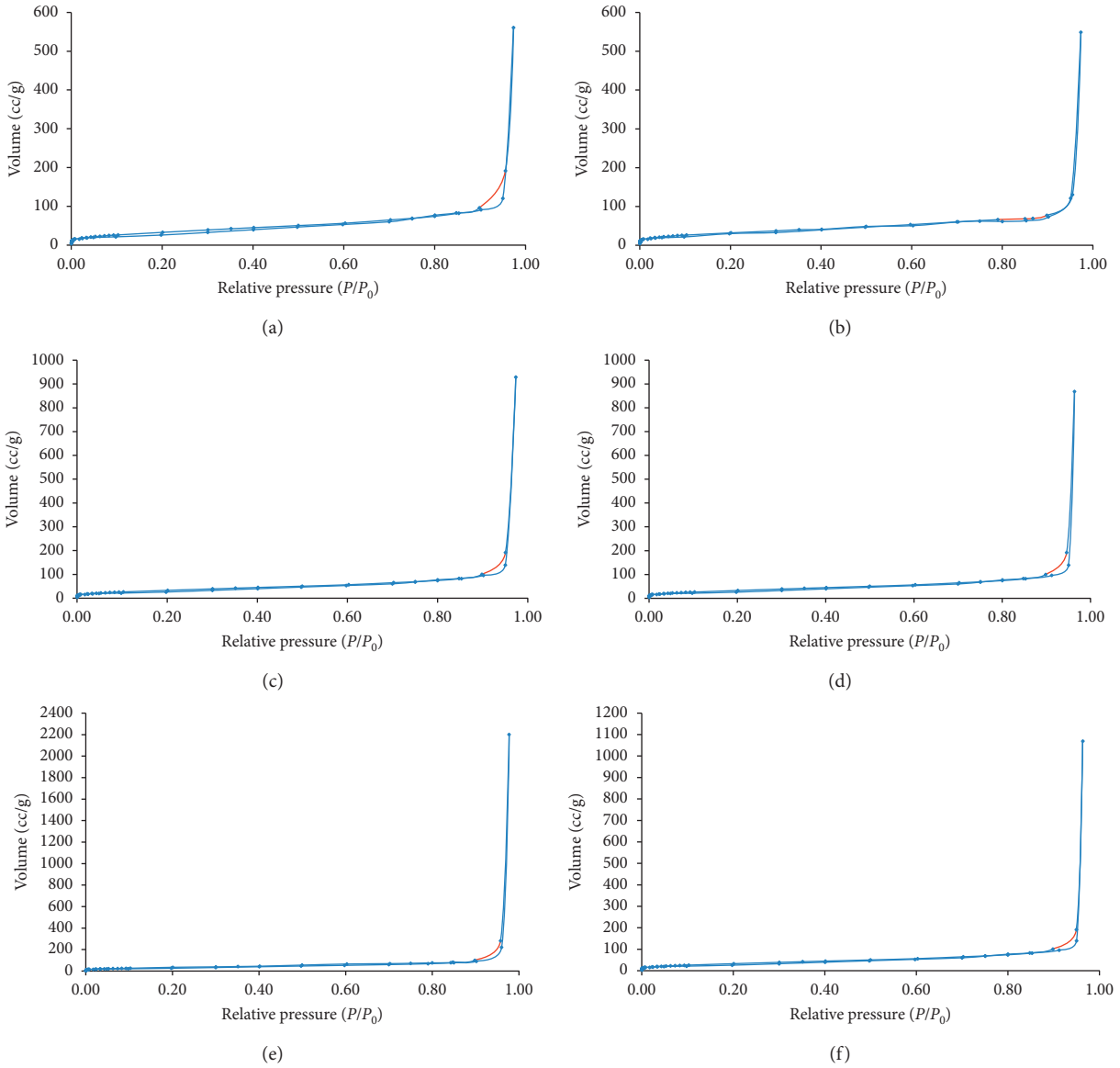

Figure 1: N_2 adsorption/desorption isotherms of the catalysts.

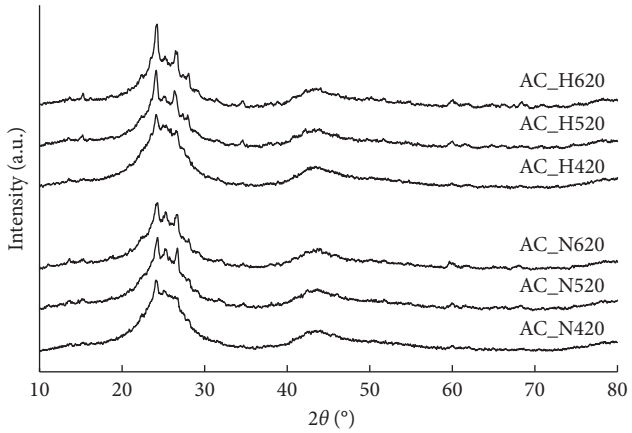

Figure 2: XRD patterns of the catalysts.

in terms of catalytic activity (% ethanol conversion) and product selectivity. The ethanol conversions of all catalysts at various temperatures are shown in Figure 5. The ethanol conversions at 400°C (the best condition) are also listed in Table 3 along with the product selectivities at this temperature.

From Figure 5, it can be observed that for all catalysts except AC_N620, the ethanol conversion increased with reaction temperatures. This could be an effect of an endothermic reaction which favors high temperature. The synthesis pathway of ethanol into ethylene is considered an endothermic reaction as proposed in reaction (2) [22]. Therefore, the results confirm the existence of this reaction.

$$C_2H_5OH \longrightarrow C_2H_4 + H_2O \longrightarrow (\Delta H = +44.9\,\text{kJ/mol}) \quad (2)$$

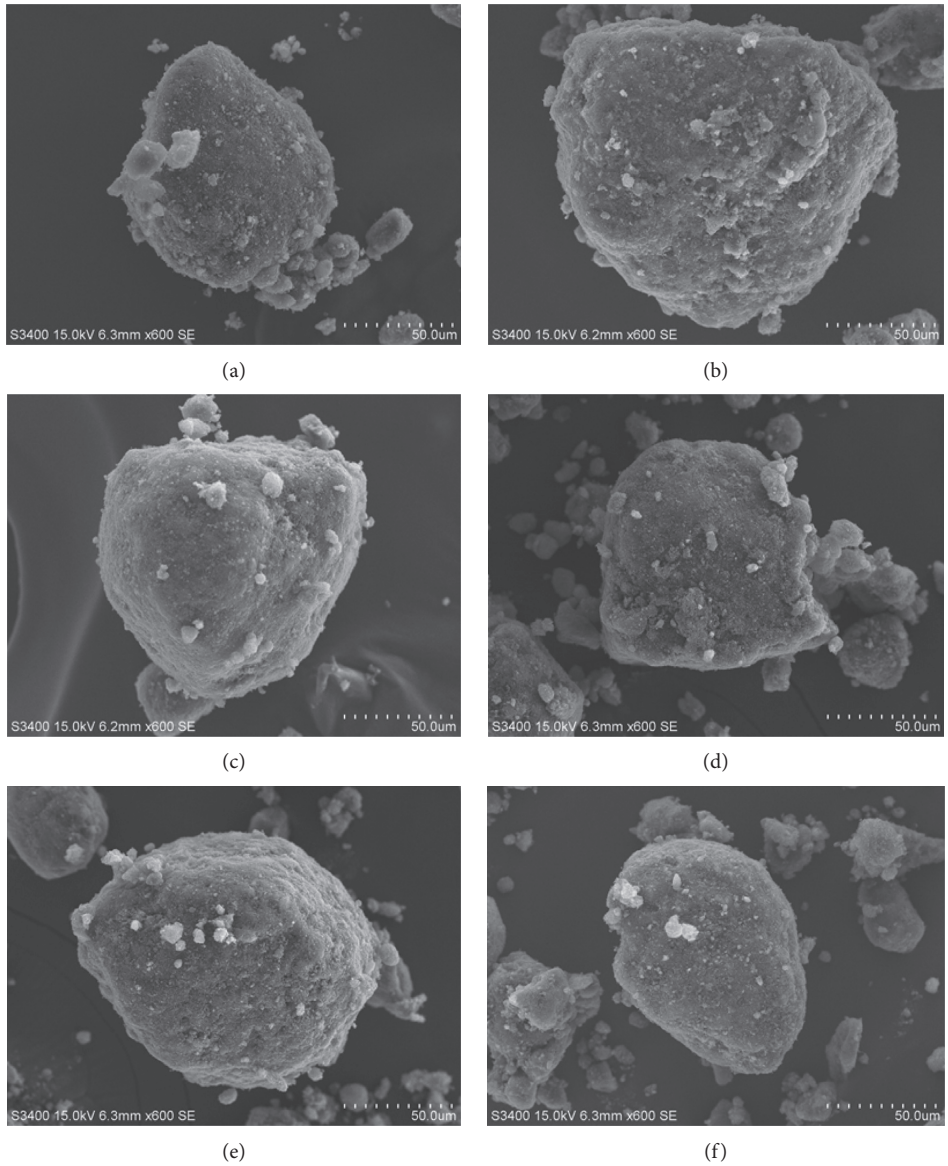

Figure 3: SEM micrographs of the catalysts: (a) AC_H420, (b) AC_H520, (c) AC_H620, (d) AC_N420, (e) AC_N520, and (f) AC_N620.

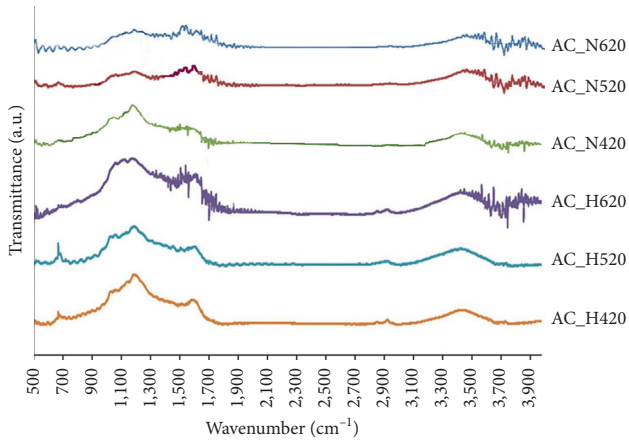

Figure 4: FTIR spectra of the catalysts.

Considering the ethanol conversions at 400°C in Table 3, it was found that for both series of catalysts, the ethanol conversions increased with surface acidity and acid density of the catalysts. Nevertheless, the acid density apparently influenced the ethanol conversion more than the total acidity. It has been known that the dehydration process increases with increased total acidity of the carbon surfaces and takes place mainly at the active centers of the Brønsted acid. Accordingly, sulfonic groups on the catalysts, which easily give up a proton can be classified as the Brønsted acid, essentially enhance catalytic activities of the catalysts. Thus, high acidity (Brønsted acid sites) of the catalysts increased the ethanol conversion as expected. The reaction pathway of ethanol dehydration with the sulfonic acid carbon-based catalyst can be proposed as Figure 6. In the first step, protonation takes place at alcoholic oxygen in the ethanol

Table 3: Surface acidity, total conversion, and product selectivity of carbon-based catalysts at 400°C.

Sample	Acidity (μmol/g)	Acid density (μmol/m^2)	Ethanol conversion (%)	Selectivity (%)		
				Ethylene	Diethyl ether	Acetaldehyde
AC_H420	2210	18.5	36.2	65.9	33.5	0.6
AC_H520	2200	8.0	19.9	66.2	33.1	0.7
AC_H620	2170	7.4	14.3	69.0	30.5	0.4
AC_N420	2270	21.5	29.1	69.4	29.9	0.7
AC_N520	2040	7.7	22.7	75.6	23.6	0.8
AC_N620	1980	6.8	22.1	73.9	25.5	0.6

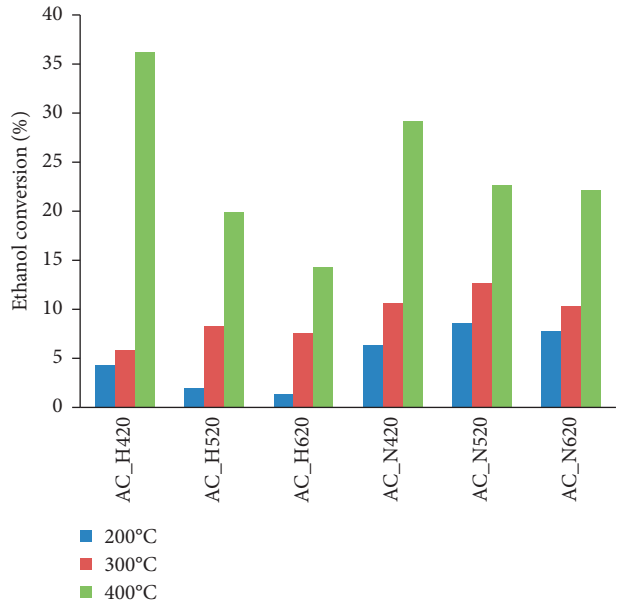

Figure 5: Ethanol conversion of the catalysts for ethanol dehydration at various temperatures.

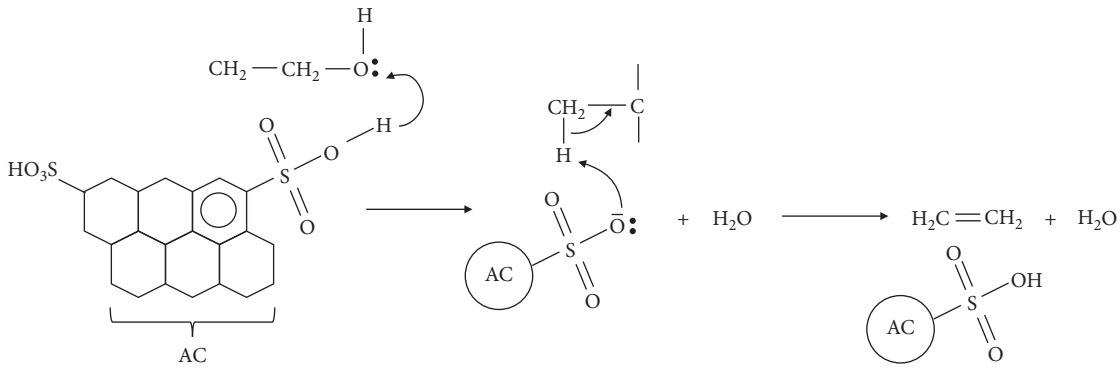

Figure 6: The mechanism of ethanol dehydration to ethylene.

molecule. Then, the C-O bond is broken causing the loss of a water molecule and resulting in a carbocation intermediate. Finally, a hydrogen ion is removed from the carbocation, forming a double bond of ethylene.

For the effect of acid density, it can be seen that the ethanol conversion of the catalysts significantly increased with the acid density. This effect was also observed in our previous study [23], which revealed that high acid density of the alumina catalysts apparently results in high catalytic activity in the ethanol dehydration. This is because the shorter distances between two nearby neighboring acid sites (high acid density) probably lead to rapidly react to form diethyl ether. The diethyl ether can be formed through a bimolecular nucleophilic substitution mechanism which is preferred with two adjacent ethanol molecules adsorbed on the catalyst surface as shown in Figure 7. It can be see that

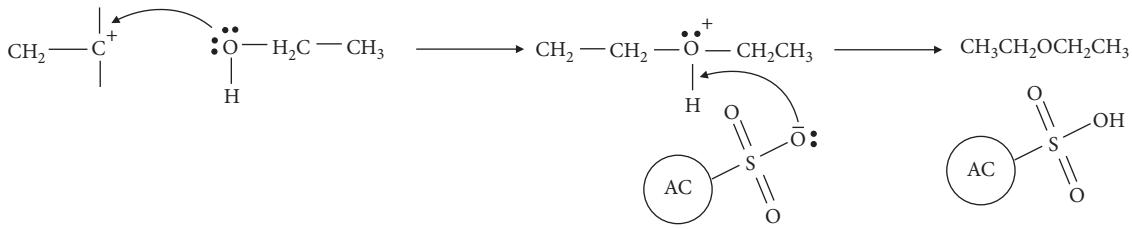

Figure 7: The mechanism of ethanol dehydration to diethyl ether.

the intermediate carbocation combines with the near ethanol molecule and then produces diethyl ether. Converting the ethanol into diethyl ether can increase the ethanol conversion. In addition, diethyl ether also acts as reaction intermediate and is subsequently decomposed to ethylene [24]. Nevertheless, this process still increased the catalytic activity anyway.

It should be noted that the catalytic activity also decreased with increasing of the activation temperature of the catalysts. The reason may be a gradual decomposition of carboxyl groups present on the carbon surface prior to sulfonation, which already becomes unstable at 180°C [25]. It has also been reported that heat treatment will create unsaturated surfaces as a result of thermal desorption of acidic functional groups [26]. Several researchers found that the decomposition of oxygen functional groups occurs at elevated temperatures and leads to an increase in basicity of the carbon surface [27–29]. Therefore, an increase of the activation temperature led to lower acidity on the catalyst and consequently reduced the ethanol conversion. This indicates that the other acidic functional groups such as carboxyl group could involve in the reaction mechanism of the ethanol dehydration besides sulfonic acid on the catalyst surface.

When comparing between two series of the catalysts, it was found that with the high activation temperatures (520°C and 620°C) the HNO_3-treated catalysts gave the higher catalytic activity than the HCl-treated catalysts. However, at 420°C, the HCl-treated catalyst (AC_H420) conversely gave the higher catalytic activity than the HNO_3-treated catalyst (AC_N420). This was because at the same activation temperatures (520°C and 620°C), the HNO_3-treated activated carbons have a slightly larger pore diameter than the HCl-treated activated carbons (Table 1). Therefore, after sulfonation the sulfonic acid sites located inside the pores of the HNO_3-treated catalysts could be more easily access than those of the HCl-treated catalysts. This is attributed to the higher catalytic activity of the HNO_3-treated catalysts. Nevertheless, at 420°C both types of activated carbons (AC_H420 and AC_N420) have the relatively larger pore diameter, thus an effect of pore diameter becoming lower. The higher catalytic activity of AC_H420 than AC_N420 was due to that HNO_3 having a higher oxidizing strength that destroyed the pore walls to a large extent, fixing a large amount of oxygen surface groups [30]. The higher degree of oxidization at the catalyst surface could convert surface hydroxyl groups into other oxygen contained groups, thus consequently affecting the addition of the sulfonic groups through hydroxyl groups during sulfonation. This leads to the higher active acidic centers on the surface of AC_H420 than AC_N420, and then provided the higher catalytic activity.

With regard to the product selectivity of the catalyst, it was found that all HNO_3-treated catalysts had higher ethylene selectivities than those obtained from HCl-treated catalysts. The opposite was true for the diethyl ether selectivities. The acetaldehyde selectivities were insignificant for both series of catalysts. The different natures of catalysts, which were previously treated with different acids, may be the reasons for the different selectivities. It is generally accepted that the ethanol conversion to ethylene occurs on weak acid sites [24, 31]. Therefore, this suggests that the HNO_3-treated catalysts have the higher proportion of weak acid sites than the HCl-treated catalysts. From the results of the reaction study, it can be concluded that the types of acid used in treatment process, and also the activation temperatures, influence the catalytic performance of the solid carbon catalysts prepared from the pyrolysis of waste tire. Therefore, tuning the ethanol dehydration production with solid carbon catalysts by variation of the acid types would be plausible and worth further investigation.

In Table 4, summarized reports of catalytic performance for ethanol dehydration to ethylene over various catalysts are compared. It can be seen that the solid carbon catalysts in this study exhibited the lower catalytic activity than most catalysts in the previous studies. Nevertheless, when comparing among the carbon-based catalysts, the waste tire-derived carbon is still comparable. Thus, waste tires have the considerable potential to be developed as a catalyst for ethanol dehydration.

4. Conclusion

Waste tires were pyrolyzed to obtain carbon and then sulfonated to achieve the carbon-based catalysts. The catalysts were divided into two series according to the acid types in the treatment process. Both series of catalysts have the same trends that increasing the activation temperature decreased the catalytic activity due to the reduction of acid density. The HNO_3-treated catalysts had higher catalytic activities than the HCl-treated catalysts except at the activation temperature of 400°C. The ethylene selectivities of the HNO_3-treated catalysts were rather higher than those of

Table 4: Comparison of catalysts for ethylene dehydration and their catalytic ability.

Catalyst			Reaction temperature (°C)	Ethanol conversion (%)	Ethylene selectivity (%)	Ref.
HBZ			200–400	7–100	1–100	[17]
Al-HBZ			200–400	9–92	0–98	[17]
M-Al			200–400	12–92	0–96	[17]
H-ZSM-5			400	99	10	[32]
20HP-ZSM-5			250–450	25–100	3–98	[32]
γ-Al_2O_3			400–550	70–100	40–95	[11]
TiO_2/γ-Al_2O_3			360–550	70–100	50–99	[11]
SAPO-34			500	100	100	[33]
Carbon based	Activator	Modifier				
Bacterial cellulose			200–400	41–65	0–65	[34]
Olive stone	Steam	$(NH_4)_2S_2O_8$	180	1–22	16–26	[35]
		HNO_3	150–450	n.a.	0–50*	[24]
		CH_3COOOH	150–450	n.a.	0–15*	[25]
Polish brown coal	HCl, HF	H_2SO_4	150–450	n.a.	0–14*	[25]
		Air	150–450	n.a.	0–18*	[25]
		Cl_2	150–450	n.a.	0–5*	[25]
Waste tire	HCl	H_2SO_4	200–400	14–36	65–69	This work
	HNO_3	H_2SO_4	200–400	22–29	69–75	This work

*Based on the ethanol conversion to ethylene only and the values are approximate.

HCl-treated catalysts. This was probably resulted from the higher proportion of weak acid sites.

Data Availability

The data used to support the findings of this study are included within the article.

Conflicts of Interest

The authors declare that they have no conflicts of interest.

Acknowledgments

The authors thank the Grant for International Research Integration: Chula Research Scholar, Ratchadaphiseksomphot Endowment Fund for financial support of this project.

References

[1] Smithers Groups, *The Future of Tire Manufacturing to 2022*, 2017, https://www.smithersrapra.com/market-reports/tire-industry-market-reports/the-future-of-tire-manufacturing-to-2022.

[2] I. de Marco Rodriguez, M. F. Laresgoiti, M. A. Cabrero, A. Torres, M. J. Chomón, and B. Caballero, "Pyrolysis of scrap tyres," *Fuel Processing Technology*, vol. 72, no. 1, pp. 9–22, 2001.

[3] J. I. Reisman and P. M. Lemieux, *Air Emissions from Scrap Tire Combustion*, EPA, Washington, D.C., USA, 1997.

[4] M. Ryms, K. Januszewicz, W. M. Lewandowski, and E. Klugmann-Radziemska, "Pyrolysis process of whole waste tires as A biomass energy recycling/piroliza opon samochodowych jako energetyczny recykling biomasy," *Ecological Chemistry and Engineering S*, vol. 20, no. 1, pp. 93–107, 2013.

[5] J. Scheirs and W. Kaminsky, *Feedstock Recycling and Pyrolysis of Waste Pastic: Converting Waste Plastics into Diesel and Other Fuels*, John Wiley and Sons, Chichester, England, 2006.

[6] M. N. Islam, M. N. Islam, and M. R. A. Beg, "The fuel properties of pyrolysis liquid derived from urban solid wastes in Bangladesh," *Bioresource Technology*, vol. 92, no. 2, pp. 181–186, 2004.

[7] N. Punsuwan and C. Tangsathitkulchai, "Product characterization and kinetics of biomass pyrolysis in a three-zone free-fall reactor," *International Journal of Chemical Engineering*, vol. 2014, Article ID 986719, 10 pages, 2014.

[8] J. D. Martínez, N. Puy, R. Murillo, T. García, M. V. Navarro, and A. M. Mastral, "Waste tyre pyrolysis - a review," *Renewable and Sustainable Energy Reviews*, vol. 23, pp. 179–213, 2013.

[9] L. A. Sánchez-Olmos, J. Medina-Valtierra, K. Sathish-Kumar, and M. Sánchez Cardenas, "Sulfonated char from waste tire rubber used as strong acid catalyst for biodiesel production," *Environmental Progress and Sustainable Energy*, vol. 36, no. 2, pp. 619–626, 2016.

[10] Z. D. Hood, S. P. Adhikari, Y. Li et al., "Novel acid catalysts from waste-tire-derived carbon: application in waste-to-biofuel conversion," *ChemistrySelect*, vol. 2, no. 18, pp. 4975–4982, 2017.

[11] G. Chen, S. Li, F. Jiao, and Q. Yuan, "Catalytic dehydration of bioethanol to ethylene over TiO2/γ-Al2O3 catalysts in microchannel reactors," *Catalysis Today*, vol. 125, no. 1-2, pp. 111–119, 2007.

[12] C. Krutpijit and B. Jongsomjit, "Catalytic ethanol dehydration over different acid-activated montmorillonite clays," *Journal of Oleo Science*, vol. 65, no. 4, pp. 347–355, 2016.

[13] I. Takahara, M. Saito, M. Inaba, and K. Murata, "Dehydration of ethanol into ethylene over solid acid catalysts," *Catalysis Letters*, vol. 105, no. 3-4, pp. 249–252, 2005.

[14] A. M. Nadeem, G. I. N. Waterhouse, and H. Idriss, "The reactions of ethanol on TiO_2 and Au/TiO_2 anatase catalysts," *Catalysis Today*, vol. 182, no. 1, pp. 16–24, 2012.

[15] J. Bedia, R. Barrionuevo, J. Rodríguez-Mirasol, and T. Cordero, "Ethanol dehydration to ethylene on acid carbon catalysts," *Applied Catalysis B: Environmental*, vol. 103, no. 3-4, pp. 302–310, 2011.

[16] ASTM D1510, *Standard Test Method for Carbon Black—Iodine Adsorption Number*, ASTM International, West Conshohocken, PA, USA, 1999.

[17] T. Kamsuwan and B. Jongsomjit, "A comparative study of different Al-based solid acid catalysts for catalytic dehydration

of ethanol," *Engineering Journal*, vol. 20, no. 3, pp. 63–75, 2016.

[18] W. Liu and G. Zhao, "Effect of temperature and time on microstructure and surface functional groups of activated carbon fibers prepared from liquefied wood," *BioResource*, vol. 7, no. 4, pp. 5552–5567, 2012.

[19] Y. Yue, Q. Lin, M. Irfan et al., "Characteristics and potential values of bio-products derived from switchgrass grown in a saline soil using a fixed-bed slow pyrolysis system," *BioResource*, vol. 12, no. 3, pp. 6529–6544, 2017.

[20] M. Shimada, T. Iida, K. Kawarada et al., "Pore structure and adsorption properties of activated carbon prepared from granular molded waste paper," *Journal of Material Cycles and Waste Management*, vol. 6, no. 2, pp. 111–118, 2004.

[21] C. H. Manoratine, S. R. D. Rosa, and I. R. M. Kottegoda, "XRD-HTA, UV Visible, FTIR and SEM interpretation of reduced graphene oxide synthesized from high purity vein graphite," *Material Science Research India*, vol. 14, no. 1, pp. 19–30, 2017.

[22] Y. Chen, Y. Wu, L. Tao et al., "Dehydration reaction of bio-ethanol to ethylene over modified SAPO catalysts," *Journal of Industrial and Engineering Chemistry*, vol. 16, no. 5, pp. 717–722, 2010.

[23] J. Janlamool and B. Jongsomjit, "Catalytic ethanol dehydration to ethylene over nanocrystalline χ- and γ-Al_2O_3 catalysts," *Journal of Oleo Science*, vol. 66, no. 9, pp. 1029–1039, 2017.

[24] M. Zhang and Y. Yu, "Dehydration of ethanol to ethylene," *Industrial and Engineering Chemistry Research*, vol. 52, no. 28, pp. 9505–9514, 2013.

[25] J. Jasińska, B. Krzyżyńska, and M. Kozłowski, "Influence of activated carbon modifications on their catalytic activity in methanol and ethanol conversion reactions," *Open Chemistry*, vol. 9, no. 5, pp. 925–931, 2011.

[26] M. S. Shafeeyan, W. M. A. W. Daud, A. Houshmand, and A. Shamiri, "A review on surface modification of activated carbon for carbon dioxide adsorption," *Journal of Analytical and Applied Pyrolysis*, vol. 89, no. 2, pp. 143–151, 2010.

[27] Y. Otake and R. G. Jenkins, "Characterization of oxygen-containing surface complexes created on a microporous carbon by air and nitric acid treatment," *Carbon*, vol. 31, no. 1, pp. 109–121, 1993.

[28] H. Darmstadt and C. Roy, "Surface spectroscopic study of basic sites on carbon blacks," *Carbon*, vol. 41, no. 13, pp. 2662–2665, 2003.

[29] S. A. Dastgheib and T. Karanfil, "Adsorption of oxygen by heat-treated granular and fibrous activated carbons," *Journal of Colloid and Interface Science*, vol. 274, no. 1, pp. 1–8, 2004.

[30] C. Moreno-castilla, F. Carrasco-marín, F. J. Maldonado-hódar, and J. Rivera-utrilla, "Effects of non-oxidant and oxidant acid treatments on the surface properties of an activated carbon with very low ash content," *Carbon*, vol. 36, no. 1, pp. 145–151, 1998.

[31] K. K. Ramasamy and Y. Wang, "Catalyst activity comparison of alcohols over zeolites," *Journal of Energy Chemistry*, vol. 22, no. 1, pp. 65–71, 2013.

[32] K. Ramesh, L. Hui, Y. Han, and A. Borgna, "Structure and reactivity of phosphorous modified HZSM-5 catalysts for ethanol dehydration," *Catalysis Communications*, vol. 10, no. 5, pp. 567–571, 2009.

[33] C. Duan, X. Zhang, R. Zhou et al., "Comparative studies of ethanol to propylene over HZSM-5/SAPO-34 catalysts prepared by hydrothermal synthesis and physical mixture," *Fuel Processing Technology*, vol. 108, pp. 31–40, 2013.

[34] M. Ibnu Abdulwahab, A. Khamkeaw, B. Jongsomjit, and M. Phisalaphong, "Bacterial cellulose supported alumina catalyst for ethanol dehydration," *Catalysis Letters*, vol. 147, no. 9, pp. 2462–2472, 2017.

[35] F. Carrasco-Marín, A. Mueden, and C. Moreno-Castilla, "Surface-treated activated carbons as catalysts for the dehydration and dehydrogenation reactions of ethanol," *Journal of Physical Chemistry B*, vol. 102, no. 46, pp. 9239–9244, 1998.

Hindawi
International Journal of Chemical Engineering
Volume 2019, Article ID 1734507, 10 pages
https://doi.org/10.1155/2019/1734507

Research Article

Influence of Ethanol Organosolv Pulping Conditions on Physicochemical Lignin Properties of European Larch

Markus Hochegger,[1] **Betty Cottyn-Boitte**,[2] **Laurent Cézard**,[2] **Sigurd Schober**,[1] **and Martin Mittelbach**[1]

[1]*Institute of Chemistry, NAWI Graz, CentralLab Biobased Materials, University of Graz, 8010 Graz, Austria*
[2]*Institut Jean-Pierre Bourgin, INRA, AgroParisTech, CNRS, Université Paris-Saclay, 78000 Versailles, France*

Correspondence should be addressed to Martin Mittelbach; martin.mittelbach@uni-graz.at

Received 30 November 2018; Accepted 9 January 2019; Published 3 February 2019

Guest Editor: Hu Li

Over the years, the organosolv pulping process has proven to be a valuable pretreatment method for various lignocellulosic feedstocks. The objective of this study was to characterize and assess the potential applicability of the organosolv lignin fraction from European larch sawdust, as no research has been conducted in this field so far. Eight different samples were prepared from the European larch sawdust under varied reaction conditions and one milled wood lignin sample as reference. The reaction temperature and sulfuric acid loading were varied between 420 and 460 K and 0.00 and 1.10% (w/w on dry wood basis) H_2SO_4, respectively. The antiradical potential (via DPPH$^\bullet$ method), chemical structure (via ATR-FTIR, ^{1}H NMR, ^{31}P NMR, and thioacidolysis), as well as the molecular weight distribution of the isolated lignins were analyzed and compared. Results from thioacidolysis show a direct correlation between the amount of β-ether bonds broken and pulping process severity. Similarly, both antiradical potential and phenolic hydroxyl group content exhibit a direct relationship to reaction temperature and catalyst loading. On the contrary, the content of aliphatic hydroxyl groups and the average molecular weights both decreased with increasing process severity. The high content of phenolic hydroxyl groups and antioxidative potential of the larch organosolv fractions, especially for the sample isolated at 460 K and 1.10% H_2SO_4 loading, indicate good applicability as antioxidants as well as feedstocks for further downstream valorization and require additional research in this area.

1. Introduction

The impending depletion of fossil resources has incited a rise of interest in converting renewable resources, such as lignocellulosic feedstocks, to chemicals and fuels. Lignin is an excellent candidate to fulfil that role, being the largest naturally occurring source of aromatic compounds and a major component of lignocellulose. Lignin is built up from methoxylated hydroxy phenylpropanoid units via random radical polymerization, leading to a complex, amorphous, and water-insoluble polymer with a multitude of chemically distinct binding motifs [1].

The organosolv pulping process is one option of biorefinery concepts that can efficiently separate biomass into cellulose-, hemicellulose-, and lignin-rich fractions. It was developed over 80 years ago by Kleinert and Tayenthal [2] for the fractionation of multiple types of lignocellulosic feedstocks, including wood and agricultural wastes, using low-boiling point water-miscible solvents as pulping agents. The resulting organosolv lignin has a low content of residual carbohydrates as well as high potential for valorization, besides producing a cellulose-rich fraction of high quality comparable to that of the kraft process [3].

Several studies have been conducted recently on the organosolv pulping of softwoods. Lesar et al. studied the uncatalyzed pulping of mixed softwood from recycling companies. The maximum lignin removal of 51% was achieved at 493 K with 196 min of reaction time and 65% aq. EtOH [4]. Nitsos et al. focused on acid-catalyzed organosolv pulping of spruce. They reached a feedstock delignification

of 62% at 456 K, 60 min, and 60% aq. EtOH and a sulfuric acid loading of 1% [5]. Løhre et al. tested a flow-through organosolv fractionation of mixed softwood. The maximum lignin removal of 83.1% was achieved at 448 K, 63% aq. EtOH with 6.00 mol·m^{-3} H_2SO_4 [6]. Smit et al. studied a novel acid-catalyzed acetone organosolv fractionation process of spruce and pine, amongst other lignocellulosic feedstocks, as pretreatment for enzymatic sugar production. However, the applied reaction conditions of 413 K, 50% aq. acetone, 120 min, and 40 mM of H_2SO_4 proved to be too benign, as delignification was just 31.6% for pine and 29.7% for spruce, respectively [7].

Furthermore, multiple studies have been published recently on possible applications for organosolv lignins. It was proposed that it can be used as an adhesive in wood panel production [8], a monomer in a biopolymer [9], a possible antioxidant [10, 11], and a pesticide [10].

European larch (*Larix decidua* Mill) is one of the most important wood species of Central Europe that mainly occurs in mountainous regions (Alps, Carpathians, and Sudetes). It typically reaches 45 m with a diameter of up to 1.5–2.5 m and a lifespan of up to 800 years [12, 13]. Its natural habitat spans approximately 5000 km^2 with a further 5000 km^2 of plantations in the Central and Western Europe together with Japanese and hybrid larch species [14]. The European larch is one of the fastest growing conifer trees with more than 10 m^3·ha^{-1}·y^{-1} and additionally possesses a low susceptibility to pests, high wood durability, and good fiber characteristics [12, 13]. It is largely used in carpentry, façade building, as well as naval construction [15]. Several studies have been conducted on European larch wood, including lignin and extractive content [16] and distribution in the heartwood [17], as well as its correlation to decay resistance [18].

However, no study has been conducted yet on the influence of organosolv pulping conditions on the properties of the lignin fraction of European larch. Research into the valorization of side products of the wood industry, such as sawdust, seems promising due to the high relevance of larch timber on the European market.

Eight lignin preparations were extracted from the European larch under varied conditions using an ethanol organosolv process with conditions derived from the literature [19–21]. Additionally, one milled wood lignin sample was isolated as reference. Furthermore, the correlations between the pulping conditions and the physicochemical characteristics of the organosolv lignin samples were studied. The lignin structure was elucidated using ATR-FTIR, thioacidolysis, and HPSEC. The functional group content was assessed using ^{1}H NMR and ^{31}P NMR, and the antioxidative potential was determined via the DPPH method.

2. Materials and Methods

2.1. Feedstock. The European larch sawdust was provided by Sägewerk/Hobelwerk Alfred Seebacher GmbH & Co. KG located in Gnesau (Carinthia), Austria. The trees were harvested at approximately 100 years of age between November 2016 and March 2017 from the Nockberge region, Carinthia, at least 1000 m above sea level. The logs were sawn in October 2017 without previous debarking.

The sawdust was directly collected and transported to our laboratory in a 100 L plastic bag. The sawdust was screened, and the fraction smaller than 1.5 mm × 1.5 mm and larger than 100 μm × 100 μm was collected as feedstock for the organosolv fractionation experiments and stored in a refrigerator at 277 K in closed glass containers. Part of the sawdust was ground using an MF 10 basic microfine grinder (IKA, Germany) equipped with an MF 10.1 cutting-grinding head, from which the fraction smaller than 0.5 mm was retained for chemical analysis.

2.2. Organosolv Fractionation. Organosolv pretreatment of the pinaceous sawdust was performed in a 0.5 L stirred batch reactor, made of HastelloyC® (Paar Instrument Company, Series 4575A HP/HT). A split ring closure system with a flexible graphite gasket was used to maintain the reaction pressure and a thermowell to measure the internal temperature. The reactor was loaded with 36 g of sawdust on dry-wood basis, filled with 250 mL of a 75% v/v aqueous ethanol solution (liquid-to-solid ratio 7 : 1 v/w) with either sulfuric acid as a catalyst (0.75–1.65% w/w) or autocatalytic. The reactions were performed at 440, 450, 455, and 460 K, respectively, at a heating rate of 8–10 K/min, with 30 min of reaction time at the respective temperature [19–21]. After the fractionation process, the reaction mixture was filtered over a Whatman No. 5 filter paper in a Büchner funnel to separate the solid cellulose-rich substrate from the lignin-rich liquor. The solid phase was washed with a total of 165 mL (3 × 55 mL) of warm (333 K) aqueous ethanol solution and combined it with the initial filtrate, followed by warm (333 K) water washing (3 × 50 mL) which was discarded. The combined liquid phase was poured into three times the volume of distilled water (1.25 L) to precipitate the ethanol organosolv lignin fraction. In the case of the autocatalytic reaction, the water was acidified to pH 3 with conc. HCl to ease lignin precipitation. The crude larch organosolv lignin was separated from the liquid fraction once again via filtration and consequent warm water washing (333 K, 3 × 75 mL). Afterwards, both the lignin fraction and pulp fraction were freeze dried for 24 h and stored for further analysis (Figure 1).

Furthermore, catalyst loading, treatment temperature, and duration were merged into a combined severity factor (CSF), developed by Abatzoglou et al. [22], to be able to more easily compare different fractionation experiments, as shown in the following equation:

$$\mathrm{CSF} = \log_{10}\left[t \times \exp\left(\frac{T(t) - 373}{14.75}\right)\right] - \mathrm{pH}, \quad (1)$$

where t denotes the treatment time, $T(t)$ is the treatment temperature in K; 373 is the reference temperature in K, and 14.75 is a constant describing the role of temperature in a catalyzed reaction system [22].

2.3. Milled Wood Lignin. Milled wood lignin (MWL) was prepared based on a method published by Holtman et al.

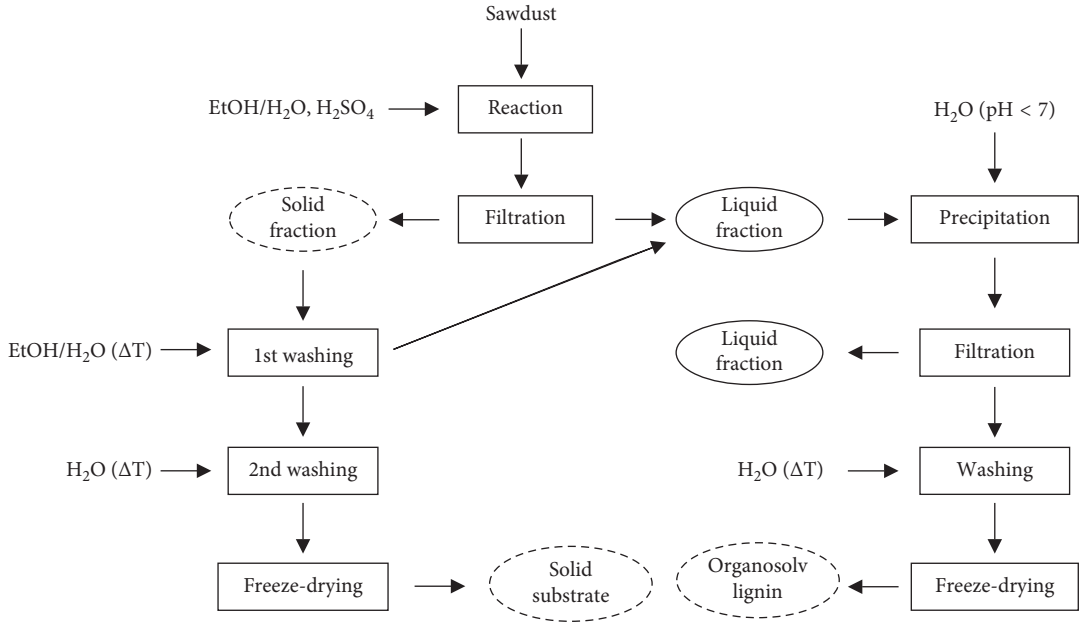

Figure 1: Schematic drawing of the organosolv fractionation and workup procedure. Product fractions are written in bold, dashed lines indicate solid fractions, whereas solid lines indicate liquid fractions.

[23] with minor modifications. For a detailed description of the method, please see Supplementary Materials. The yield of purified milled wood lignin was 4.0% based on dry extractive-free wood.

2.4. Analytical Protocols

2.4.1. Chemical Characterization. The humidity of the softwood sawdust was determined using an MA23 infrared moisture analyzer (Satorius AG, Germany). Klason lignin and acid-soluble lignin [24] of the feedstock and cellulose-rich organosolv fraction, hot-water- and acetone-soluble extractives [25], and ash content [26] of the feedstock were analyzed in accordance to standards published by the Technical Association of the Pulp and Paper Industry (TAPPI). Carbohydrate content of the larch sawdust was determined based to a multistep-method, comprising sawdust hydrolysis, reduction of released monosaccharides to the corresponding alditols, acetylation of the resulting polyols, liquid-liquid separation, and GC-FID analysis [27]. The results from the chemical characterization of larch sawdust are summarized in Table 1. Part of the organosolv lignin fraction was crudely purified for further analysis. In detail, 1.5 g of lignins was dissolved in 10 mL of HPLC-grade acetone and filtered through a 0.45 μm nylon syringe filter (Ø 33 mm, Carl Roth, Germany) before solvent removal via a rotary evaporator and drying in a vacuum desiccator.

2.4.2. Attenuated Total Reflection Fourier-Transformed Infrared Spectroscopy (ATR-FTIR). Structural features of the larch organosolv samples were analyzed using infrared spectroscopy on an FTIR spectrometer (Cary 630 FTIR, Agilent) equipped with the diamond ATR accessory running on MicroLab FTIR Software. 32 background scans and 64 sample scans were collected, at a resolution of 2 cm^{-1} from 4000 to 600 cm^{-1}. The spectra were further processed using SpectraGryph v1.2.10 software.

Table 1: Chemical composition of larch sawdust, reported as mean ($n = 3$) ± standard deviation.

Component	Content (% (w/w))
Ash	0.17 ± 0.02
Extractives (water + acetone)	12.02 ± 0.12
Klason lignin	26.90 ± 0.10
Acid soluble lignin	0.30 ± 0.02
Carbohydrates (as monomers)	
Glucose	51.15 ± 0.33
Arabinose	0.99 ± 0.02
Galactose	4.97 ± 0.25
Mannose	7.39 ± 0.07
Xylose	3.12 ± 0.14

2.4.3. Nuclear Magnetic Resonance (NMR) Analysis. The semiquantification of functional groups via ^{1}H NMR was performed based on analysis protocols published by Pan et al. [28] with minor modifications. In detail, 1 g of the purified organosolv lignin was acetylated using 20 mL of a 1 : 1 pyridine : acetic anhydride mixture, reacting for 84 h at room temperature in dark, under constant shaking in a incubating mini shaker (VWR, USA). Afterwards, the mixture was added dropwise to 200 mL of constantly stirred ice-cold water that was acidified with 2 mL of concentrated HCl. The acetylated lignin was isolated over a Büchner funnel glass frit (porosity 3), washed with distilled water until the filtrate was pH neutral, and dried in vacuum over $CaCl_2$. 50 mg of the acetylated organosolv lignins were dissolved in 600 μL DMSO-d_6, and 10 mg of p-nitrobenzaldehyde (Sigma Aldrich, USA) were added as internal

standard. All NMR spectra were recorded on a Bruker Avance III 300 MHz NMR spectrometer equipped with a 5 mm TXI probe at 298 K. For the 1D ^{1}H NMR spectra, 16 scans were acquired and multiplied with an exponential windows function with a line broadening of 0.3 Hz prior to Fourier transformation. The spectra were integrated in MestreNova 8. The content of hydroxyl groups (in mmol·g^{-1}) was calculated on the basis of hydrogen atoms contained in the internal standard compared to that of acetyl and methoxyl groups, respectively, and by integration of the following spectral regions: internal standard (8.45–7.98 ppm), aliphatic acetyl (2.17–1.70 ppm), phenolic acetyl (2.50–2.17 ppm), and methoxyl groups (4.10–3.10 ppm). Furthermore, the content of carboxylic acid groups (COOH) was determined via ^{31}P NMR; for a detailed description, see Supplementary Materials.

2.4.4. Molecular Weight Analysis. The molecular weight was estimated through high-performance size-exclusion chromatography (HPSEC) using a styrene-divinylbenzene PLgel column (Polymer Laboratories, 5 mm, 100 Å, 600 mm length, 7.5 mm inner diameter) with a photodiode array detector (Dionex Ultimate 3000 UV/vis detector) set to 280 nm UV and tetrahydrofuran (1 mL·min^{-1}) as eluent. A calibration curve based on polyethylene oxide standards (Igepal, Sigma Aldrich) and injection of pure coniferyl alcohol monomers and dimers was used for quantitative assessment. The organosolv lignins were dissolved in tetrahydrofuran and filtered through a 0.45 mm PTFE membrane filter before analysis via HPSEC.

2.4.5. Thioacidolysis. Thioacidolysis followed by GC-MS analysis was conducted based on a method published by Aguié-Béghin et al. [11]. In detail, the lignin-derived thioacidolysis monomers, namely, guaiacyl (G), p-hydroxyphenyl (H), and syringyl (S) were analyzed as trimethylsilyl derivatives via GC-MS (Saturn 2100, Varian, Agilent, USA) equipped with a poly(dimethylsiloxane) column (30 m × 0.25 mm; PB-1, Supelco, Sigma Aldrich, USA) using 5 mg of sample and 0.20 mg heneicosane ($C_{21}H_{44}$, Fluka) as internal standard. The temperature program was 313 to 453 K at 30 K·min^{-1}, followed by 453 to 533 K at 2 K·min^{-1}. An ion trap was used as a mass spectrometer set to an ionization energy of 70 eV and positive detection mode. Quantitative determination of the G and vanillin monomers (no H and S units found) was performed from ion chromatograms reconstructed at *m/z* 269, as compared with the signal from the internal standard measured from the ion chromatogram reconstructed at *m/z* (57 + 71 + 85).

2.4.6. Determination of the Antioxidative Potential. The radical-scavenging capability of the of the organosolv lignins was assessed as an indicator for the antioxidative potential, based on a method published by Dizhbite et al. [29] and was applied with minor modifications. In detail, 800 μL of ethanolic $6{,}00 \times 10^{-5}$ mol/l 1,1-diphenyl-2-picrylhydrazyl (DPPH$^{\bullet}$) (Sigma Aldrich, USA) was mixed with 200 μL of a 9 : 1 aqueous dioxane solution containing varying lignin concentrations (1–250 μg/mL) in 1 mL single-use microBRAND® UV cuvettes (1 cm path length; Sigma Aldrich, USA). The reaction mixture was stored in darkness at room temperature under periodical shaking for 18 min, and the absorption was consequently determined at 517 nm (λ_{max}) with a Cary 60 UV/VIS spectrometer (Agilent, USA).

To determine the quenching percentage (Q), the sample absorption (A_0) was corrected by the absorption of both the diluted lignin samples in the corresponding concentration without DPPH (A_{ref}) and of the DPPH$^{\bullet}$ solution without lignin (A_0):

$$Q = \frac{A - (A_{ref} + A_0)}{A_0} \times 100. \quad (2)$$

By plotting the quenching percentage against the lignin concentration, the EC_{50} can be determined, which is defined as the value at 50% Q. The radical-scavenging capability of the organosolv lignin samples was assessed in terms of antiradical power (ARP), defined as the reciprocal value of EC_{50} [30]. The ARPs of 3,5-di-tert-butyl-4-hydroxytoluene (BHT) and 2/3-*t*-butyl-4-hydroxyanisole (BHA) were determined as reference. All samples were analyzed in triplicate, and the mean values ± standard deviation are reported.

3. Results and Discussion

3.1. Yield of Organosolv Fractionation Experiments. Ethanol organosolv pretreatment is known to be effective at separating cellulose from lignin as well as hemicellulose in multiple feedstocks, including woody biomass [31]. Results from the catalyzed and autocatalyzed organosolv fractionation experiments of larch sawdust are summarized in Table 2. The moisture content of the larch sawdust was 19.1 ± 0.5% for all experiments. No predrying was performed because high moisture content facilitates feedstock impregnation with pulping liquor and thus increases the delignification rate [32]. The pretreatment time was set to 0.5 h as preliminary experiments have shown that there is no significant difference in lignin yield between 0.5 and 1.0 h (not shown). The maximum yield of ethanol organosolv lignin (EOL), 21.82% (w/w), was achieved at 460 K with a catalyst loading of 1.65% (w/w). The results also indicate that an increase of both temperature (440 to 460 K) and catalyst loading (0.00% to 1.65%) lead to an increase of organosolv lignin yield as well as acid-soluble lignin (ASL) in the aqueous phase. The increase in lignin yield is due to more excessive ether bond cleavage at higher process severities [11]. Similarly, the increase in ASL is caused by further fragmentation of dissolved lignin polymers to more water-soluble species. The yield of solid substrate decreased with both increasing temperature and catalyst loading due to increased delignification as well as carbohydrate degradation. The Klason lignin content of the solid substrate first decreased with increasing temperature and catalyst loading, reaching a minimum at 455 K at 0.75% (w/w) H_2SO_4. However, with increasing process severity, the rate of

Table 2: Process parameters, mass flows of the organosolv extraction experiments, and lignin content of the solid substrate.

	Process parameters[a]			Mass flows (% w/w)			KL of substrate
	T^b (K)	C (wt%.)	CSF	S	EOL	ASL	(% w/w)
OS-A	440	1.10	1.65	47.49	16.36	4.62	18.16
OS-B	445	1.10	1.80	44.52	17.61	4.77	16.54
OS-C	450	1.10	1.95	38.56	19.12	5.40	14.16
OS-D	455	0.75	1.93	38.68	19.06	5.45	14.14
OS-E	455	1.10	2.10	34.14	20.01	5.64	16.05
OS-F	460	1.10	2.24	29.74	20.83	5.85	19.76
OS-G	460	1.65	2.42	22.42	21.82	6.14	29.24
AC-OS	460	0.00	—	80.11	6.47	3.05	24.59

[a]36 g of feedstock (on dry basis), 250 mL of 75% aq. ethanol, and 30 min residence time. [b]T, temperature; C, catalyst loading on dry wood basis; CSF, combined severity factor; S, solid substrate; EOL, ethanol organosolv lignin; ASL, acid-soluble lignin in the aqueous phase; KL, Klason lignin; AC-OS, autocatalyzed organosolv.

carbohydrate degradation surpassed that of delignification and the content of Klason lignin increased, to reach a maximum of 29.24%.

Nitsos et al. [5] reported a maximum lignin yield of 16.80% for acid-catalyzed organosolv pulping of spruce wood at a CSF of 2.23 (456 K, 60 min, 1% (on dry wood basis (odw)) H_2SO_4, 60% EtOH). A significantly higher yield was achieved in this study, 20.83%, at a CSF of 2.24. However, Pan et al. [19] reported a maximum lignin yield of 24.96% for lodgepole pine, at a CSF of 2.48 (453 K, 70 min, 1.10% (odw) H_2SO_4, 75% EtOH), surpassing this work by 3.14% at a comparable CSF of 2.42.

As the ethanol organosolv fractionations were performed at both low pH and high temperature, it is possible that pseudolignins were formed. They are hypothesized to form primarily from sugar degradation products, such as furfural and 5-hydroxymethylfurfural, via first rearrangement reactions followed by oxidation, polymerization, and condensation reactions to yield aromatic components [33, 34]. These aromatic components can increase the Klason lignin content of the pulp phase and furthermore reduce enzymatic digestibility by unproductive binding with enzymes. This phenomenon is most likely to have occurred in the high severity pulping runs, OS-F and OS-G, since significant amounts of carbohydrates could not be retained in the solid substrate phase.

Furthermore, the lignin yield of the autocatalyzed fractionation experiment was low (6.47% (w/w)). Lesar et al. [4] reported a lignin yield of 17.3% for softwood under autocatalyzed conditions. However, these results were achieved under more severe conditions (493 K, 196 min, 65% EtOH). Thus, with proper reaction optimization, higher removal efficiency is possible, but still inferior to the catalyzed organosolv experiments.

CSF analysis was used to be able to easily compare and correlate ethanol organosolv fractionation yields and physicochemical characteristics of the isolated larch lignins. However, CSF was not used to analyze the processing conditions of the autocatalyzed experiment, as no acidic catalyst was used.

3.2. Influence of Process Parameters on Characteristics of Larch Organosolv Lignin. FT-IR analysis is a commonly used technique to analyze structural features of lignin, due to its speed and simplicity. In Figure 2, five IR spectra are shown, including organosolv lignin from low (OS-A), mid (OS-D), and high severity (OS-G) fractionation as well as autocatalyzed organosolv lignin (AC-OS) and milled wood lignin (MWL). All spectra look similar, albeit small differences, indicating comparable chemical structures. The absorption bands of the lignin samples were assigned based on published studies [35, 36], which are summarized in Table S1 in the Supplementary Materials. The strong broad signals at 3420 cm^{-1} are ascribed to hydroxyl bond (O-H) stretching. The signals at 2930 and 3855 cm^{-1} correspond to C-H bond stretching in methyl- and methylene groups. The band at 1700 cm^{-1} is ascribed to C=O bond stretching in unconjugated systems. Three peaks associated with aromatic skeletal vibrations are also found, at 1600, 1510, and 1420 cm^{-1}. A relative decrease of all three peaks in the organosolv lignins compared to MWL indicates that structural degradation of the lignin structure occurred during the fractionation process. The band at 1360 cm^{-1} is assigned to phenolic hydroxyl vibrations. The peak at 1264 cm^{-1} is characteristic for ring vibrations of guaiacyl monomers. Four bands correspond to aromatic C-H bond vibrations typically found in guaiacyl monomers, 1140 cm^{-1}, 1030 cm^{-1}, 850 cm^{-1}, and 813 cm^{-1}. The lack of characteristic syringyl (S) vibrations at 1330 and 1120 cm^{-1} and of p-hydroxyphenyl (H) vibrations at 1168 and 833 cm^{-1} in all IR spectra prove that lignin in European larch is indeed G-type. The peaks at 1215 and 1126 cm^{-1} can both be ascribed to C=O stretching vibrations, whereas the former also includes C-C and C-H bond stretching vibrations in CH_3.

High-performance size-exclusion chromatography was performed, to assess the impact of treatment severity on molecular mass distribution of the resulting organosolv lignin fraction. Although average molecular mass estimation based on a polystyrene calibration is by no means able to produce accurate absolute masses, it is indeed a valid tool for comparative purposes. Results listed in Table 3 indicate that the differences between number average molecular weights (M_n) of organosolv lignins from low (440 K, 1.10 % H_2SO_4) and high severity (460 K, 1.65% H_2SO_4) fractionation experiments are insignificant, 1058 g·mol^{-1} and 932 g·mol^{-1}, respectively. Weight average molecular weights (M_w) decrease with increasing process severity, from 2501 g·mol^{-1} (OS-A) to 1980 g·mol^{-1} (OS-G). As expected, larch organosolv lignin from the autocatalyzed pulping run exhibits the lowest M_w (1655 g·mol^{-1}) as it is less efficient at removing lignin from the feedstock. The average molecular weights and their variance between low and high severity fractionation experiments are significantly smaller compared to previously published data with similar fractionation conditions, with M_w ranging from 3.2×10^3 to 6.5×10^3 [37] and 2,240 to 4,600 [20], respectively.

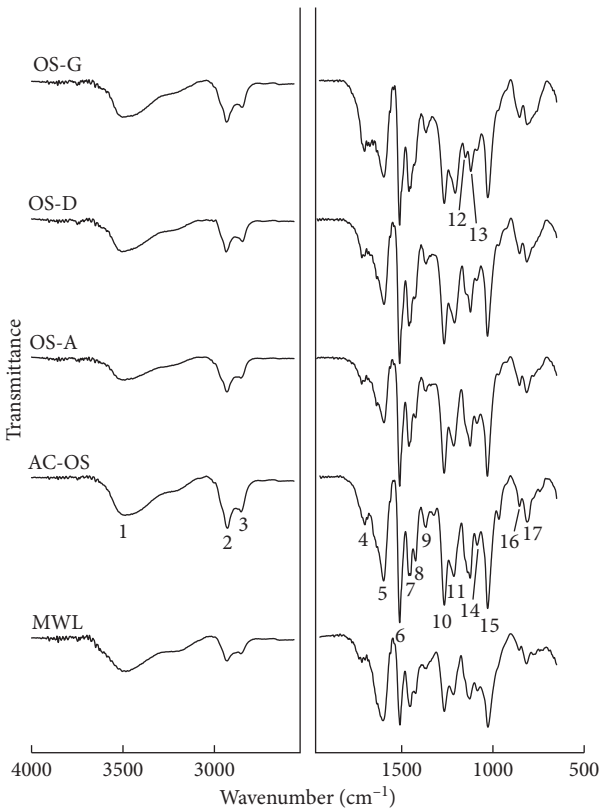

Figure 2: ATR-FTIR spectra of larch lignin samples; for peak identification, see Supplementary Materials.

Table 3: Results from molecular weight analysis of larch organosolv samples.

	CSF	M_n (g·mol^{-1})	M_w (g·mol^{-1})	M_w/M_n
OS-A	1.65	1058	2501	2.36
OS-B	1.80	1096	2296	2.09
OS-C	1.95	1117	2403	2.15
OS-D	1.93	1063	2281	2.15
OS-E	2.10	1064	2223	2.09
OS-F	2.24	970	2022	2.08
OS-G	2.42	932	1981	2.13
AC-OS	—	998	1655	1.66

Proton NMR analysis is known to be a reliable tool to semiquantify the content of functional groups of acetylated lignin samples, specifically phenolic (PhOH) and aliphatic hydroxyl groups (AlkOH) as well as methoxyl groups (MeO) [38, 39]. The result shown in Table 4 indicates a direct correlation ($r = 0.9894$) between process severity and content of phenolic hydroxyl groups, increasing from 3.15 mmol·g^{-1} (OS-A) to 4.15 mmol·g^{-1} (OS-G). This increase can be attributed to a more efficient cleavage of α- and β-aryl ether bonds at higher temperatures and catalyst loading [40]. These results are in good accordance with the literature, where PhOH contents for organosolv lignins from 3.01 to 4.25 mmol·g^{-1} for lodgepole pine [20], 2.34 to 4.04 mmol·g^{-1} for *Miscanthus x giganteus* [37], and 2.21 to 4.38 mmol·g^{-1} for hybrid poplar [28] were reported.

On the contrary, the content of aliphatic hydroxyl groups is decreasing with increasing severity, from 4.15 to 3.25 mmol·g^{-1}. It was proposed by McDonough [41] that this phenomenon is also associated with acid-catalyzed β-aryl ether cleavage. In detail, a γ-hydroxymethyl group is released as formaldehyde, forming an enol ether bond on the lignin side chain that is consequently broken [42]. Thus, the same mechanisms leading to an increase of PhOH groups during the organosolv fractionation process led to a decrease of AlkOH groups. Additionally, during organosolv pulping, the whole side chain can be cleaved off, reducing the AlkOH content further. The determined concentration range for aliphatic hydroxyl groups corresponds well to literature values, ranging from 3.77 to 4.72 mmol·g^{-1} for lodgepole pine [20], 1.07 to 3.11 mmol·g^{-1} for *Miscanthus x giganteus* [37], and 2.73 to 5.01 mmol·g^{-1} for hybrid poplar [28].

As can be seen in Table 4, the total amount of free hydroxyl groups does indeed not change significantly between all the acid-catalyzed fractionation experiments, just a slight increase from OS-C to OS-G can be observed. Both the MWL and the autocatalyzed organosolv lignin contain a significantly higher amount of total hydroxyl groups, 9.12 mmol/g and 8.65 mmol/g, respectively, which is in good accordance with the literature [43]. Furthermore, the content of free carboxylic acid groups was low in all larch organosolv fractions, ranging from 0.07 to 0.2 mmol·g^{-1}. The highest content was achieved in the autocatalyzed sample because of its comparably least severe method of extraction. However, no significant difference can be observed within the acid-catalyzed organosolv samples.

Methoxyl group content ranges from 5.77 to 6.27 mmol·g^{-1}. Pearson correlation analysis indicates that the content of MeO in larch organosolv lignin is independent of the pulping conditions ($r = -0.4644$). These observations are consistent with data published by Pan et al. [28] on the correlation of organosolv fractionation conditions to physicochemical lignin properties of hybrid poplar and Gilarranz et al. [40] on autocatalyzed methanol pulping of Tasmanian blue gum. The MWL sample exhibits the lowest content of PhOH and the highest content of AlkOH. This is well documented in the literature, as the Björkman method [44] is the most benign lignin extraction process, conserving most of its natural structural features. Additionally, the content of methoxyl groups is significantly lower in both MWL and the autocatalyzed organosolv lignin compared to the sulfuric acid catalyzed organosolv samples. This can be explained by nucleophilic addition of ethanol on the benzylic position during acid catalyst pulping and a general higher lignin extraction efficiency [45]. The high content of AlkOH in the autocatalyzed organosolv sample despite its comparably high content of PhOH can be explained due to the absence of an acidic catalyst as described above. Of the eight different organosolv lignins investigated in this study, OS-G probably has the highest applicability as it contains the highest amount of phenolic hydroxyl groups. A higher content of free hydroxyl groups correlates increased chemical reactivity, thus making OS-G an excellent candidate for use as an antioxidant or as a monomer for biopolymer production.

Table 4: Functional group content of the larch organosolv samples. PhOH-, AlkOH-, and MeO contents were determined via ^{1}H NMR and COOH content via ^{31}P NMR.

	CSF	PhOH[a] ($mmol \cdot g^{-1}$)	AlkOH ($mmol \cdot g^{-1}$)	Total OH ($mmol \cdot g^{-1}$)	PhOH/AlkOH ratio	MeO ($mmol \cdot g^{-1}$)	COOH ($mmol \cdot g^{-1}$)
OS-A	1.65	3.15	4.15	7.30	0.76	6.27	0.09
OS-B	1.80	3.45	3.91	7.36	0.88	6.05	0.07
OS-C	1.95	3.50	3.72	7.22	0.94	5.92	0.07
OS-D	1.93	3.47	3.73	7.20	0.93	5.77	0.07
OS-E	2.10	3.74	3.60	7.34	1.04	6.09	0.09
OS-F	2.24	3.91	3.51	7.42	1.11	5.71	0.09
OS-G	2.42	4.15	3.25	7.40	1.28	6.01	0.1
AC-OS	—	3.60	5.05	8.65	0.71	4.78	0.2
MWL	—	3.08	6.04	9.12	0.51	4.16	—[b]

[a]PhOH, phenolic hydroxyl groups; AlkOH, aliphatic hydroxyl groups; MeO, methoxyl groups; COOH, carboxylic acid groups. [b]Not analyzed via ^{31}P NMR.

To get a more complete view on the influence of pulping conditions on changes in the lignin structure, thioacidolysis of the larch organosolv samples was performed, and the results are summarized in Table 5. Thioacidolysis is based on acid-catalyzed depolymerization of lignins with a high specificity to aryl ether bonds. A high content of releasable monomers therefore indicates more benign extraction conditions and consequently a less altered lignin structure [46]. Additionally, a high content of releasable monomers correlates to a low content of phenolic hydroxyl groups, as they are primarily formed during β-ether bond cleavage. Only guaiacyl (G) thioacidolysis monomers and vanillin, an oxidized guaiacyl derivate, were detected, neither p-hydroxyphenyl-(H) nor syringyl (S) monomers. This can be explained by the limited natural occurrence of both monomers in conifers of maximum 8 % and 2 %, respectively [47], in addition to a higher liability of syringyl units towards ether cleavage. The content of releasable G-units and vanillin both decreases with increasing processing severity from 171 $\mu mol \cdot g^{-1}$ to 242 $\mu mol \cdot g^{-1}$ (OS-B) to 11 $\mu mol \cdot g^{-1}$ and 99 $\mu mol \cdot g^{-1}$ (OS-G), respectively. This trend is in good accordance with the results of ^{1}H NMR analysis, and the maximum content of releasable monomers correlates to the minimum of PhOH hydroxyl groups and vice versa. The lower thioacidolysis yields of OS-A compared to OS-B could be explained due to the less-efficient lignin extraction in the presence of the same sulfuric acid loading. As expected, the content of releasable monomers is highest in the autocatalyzed lignin sample due to the relatively benign extraction conditions.

Table 5: Yields from thioacidolysis and GC-MS of the thioethylated guaiacyl (G) monomer derivatives (mean of two independent analyses).

	CSF	G-units ($\mu mol \cdot g^{-1}$)	Vanillin·($\mu mol\ g^{-1}$)
OS-A	1.65	136	298
OS-B	1.80	171	242
OS-C	1.95	156	209
OS-D	1.93	116	232
OS-E	2.10	58	175
OS-F	2.24	24	127
OS-G	2.42	11	99
AC-OS	—	344	233

3.3. Correlation between Process Parameters and Antiradical Potential. As parameter to assess the reactivity of isolated larch organosolv lignins, their respective antiradical potential (ARP) was chosen. The ARP was analyzed using DPPH$^{\bullet}$ as a radical source in aqueous dioxane and the loss of absorption at 517 nm as indicator for the scavenging capability. As can be seen in Figure 3, the pulping conditions do have a significant impact on the ARP of the resulting organosolv lignin fractions. Larch sawdust extracted under the most benign conditions (440 K, 1.10% H_2SO_4) yielded in organosolv lignin with the smallest ARP of 66.1, corresponding to the highest EC50 of 15.6 $\mu g \cdot mL^{-1}$. With increasing process severity, the radical scavenging capability also rises, up to a maximum of 100.7 (460 K, 1.10 wt% H_2OS_4), equal to an EC50 of 9.9 $\mu g \cdot mL^{-1}$. The autocatalyzed organosolv lignin sample (AC-OS) achieved an ARP of 82.0, comparable to the samples isolated at 455 K at 0.75 (OS-D) and 1.10% (w/w) H_2SO_4 (OS-E), respectively. Statistical analysis of the relationship between process severity and ARP demonstrate a strong direct correlation ($r = 0.9976$). This finding is in good accordance with previously published data on organosolv lignins of *Miscanthus x giganteus* [37], hybrid polar [28], and aspen, spruce, and birch wood [29].

The content of nonetherified phenolic hydroxyl groups is primarily responsible for the antioxidative potential of lignin [29, 48]. Indeed, as can be seen in Figure 3, the organosolv sample with the lowest content of PhOH exhibits the lowest antioxidative potential and vice versa (66.1/3.15 $mmol \cdot g^{-1}$ vs. 100.7/4.15 $mmol \cdot g^{-1}$). As expected, the content of aliphatic hydroxyl groups is indirectly correlated ($r = -0.9844$) to ARP because of their indirect relationship to PhOH. Results further indicate that the contribution of methoxyl group to ARP is negligible. However, more recent findings by Ponomarenko et al. [48] indicate that o-methoxyl groups indeed have a positive effect on DPPH$^{\bullet}$ scavenging capacity. This discrepancy can be explained by the large variety of lignins used in the aforementioned study, including grass, hardwood, and softwood lignins from different technical processes.

Furthermore, results from this study show that average molecular weights and antioxidant activity have a weak to very weak indirect correlation ($r(\mathrm{Mn}) = -0.7564$,

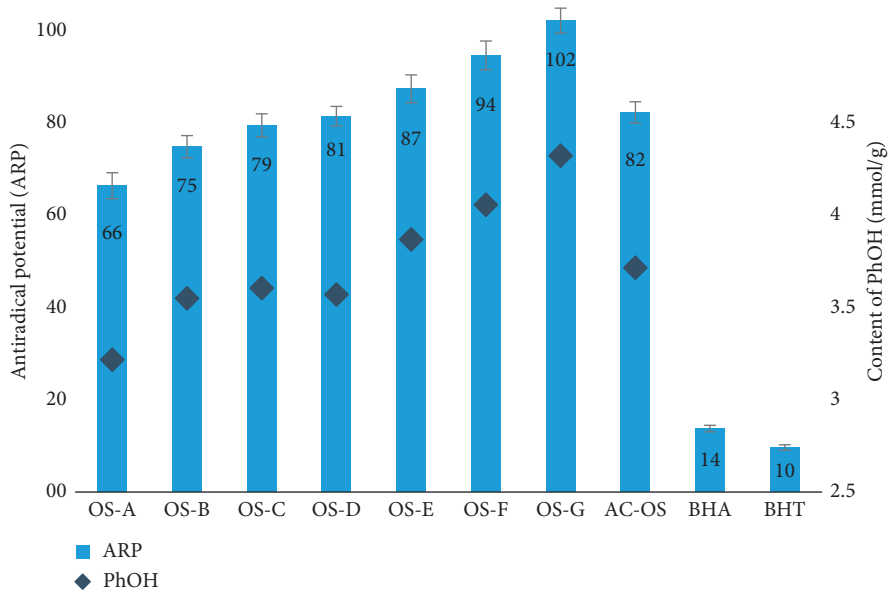

Figure 3: Relationship between antiradical potential and content of phenolic hydroxyl groups; ARP is reported as mean ($n = 3$), and the error bars represent the standard deviation.

$r(\mathrm{Mw}) = -0.5722$). The difference in average molecular weights between low and high severity pulping conditions is quite low, as discussed above, and significantly smaller compared to previously reported results [28, 37, 49]. Thus, the average molecular weights cannot be used as proper indicator for the potential antioxidative potential of larch organosolv lignins.

However, a direct comparison of antioxidative potential is typically complicated by distinct differences in the DPPH$^{\bullet}$ analysis conditions, such as radical concentration, reaction time, and solvent ratio/volume. The results by Pan et al. [28] were achieved under quite similar conditions. Their results for EC_{50} of hybrid poplar organosolv lignins range from 8.2 to 80.0 $\mu g \cdot mL^{-1}$, compared to 9.9 to 15.6 $\mu g \cdot mL^{-1}$ for the European larch in this study. This parity indicates that under similar pulping conditions, organosolv lignin from the European larch can achieve antioxidative potentials similar to that of hardwood lignins.

4. Conclusion

In this study, for the first time, the relationship between physicochemical characteristics and pulping conditions of ethanol organosolv lignins from the European larch are investigated. This study should serve as the initial step for possible future applications of larch organosolv lignins as antioxidant or feedstock for biopolymer production. ATR-FTIR, ^{1}H NMR, ^{31}P NMR, HPSEC, thioacidolysis, and an antioxidative assay are used as analytical tools. The harshest reaction conditions (OS-G), 460 K and 1.10 % (w/w) H_2SO_4, resulted in the highest yield of organosolv lignin (21.82%). Additionally, OS-G has the highest content of phenolic hydroxyl groups (4.15 $mmol \cdot g^{-1}$) and antiradical potential as well as the lowest content of releasable guaiacyl monomers by thioacidolysis (11 $\mu mol \cdot g^{-1}$). OS-A shows the lowest PhOH content (3.15 $mmol \cdot g^{-1}$), lowest antiradical potential, and highest content of releasable guaiacyl monomers (484 $\mu mol \cdot g^{-1}$). The autocatalyzed organosolv lignin exhibited the highest aliphatic hydroxyl group (5.05 $mmol \cdot g^{-1}$) content and lowest weight average molecular weight. Both the high antiradical potential and content of free phenolic hydroxyl groups indicate that larch organosolv lignin indeed has potential for further valorization.

Further investigations are planned, to properly assess potential future applicability of the material. These include method optimization for the organosolv pulping process, alternative fractionation methods, such as Kraft, Organocell, and γ-valerolactone pulping, and additional analysis techniques, such as zeta potential, 2D HSQC NMR, and thermal analyses.

Data Availability

The data used to support the findings of this study are available from the corresponding author upon request.

Conflicts of Interest

The authors declare no conflicts of interest.

Acknowledgments

The authors would like to thank Prof. Anton Huber for his various suggestions and fruitful discussions, Prof. Klaus Zangger for his expertise in NMR spectroscopy, and Ing. Bernd Werner for analyzing the lignin samples via NMR.

Supplementary Materials

The supplementary materials contain a detailed description of milled wood lignin isolation and purification, ^{31}P NMR analysis, and a table containing a detailed assignment of the

absorption bands from the IR analysis of the lignin samples. (*Supplementary Materials*)

References

[1] J. Ralph, "Hydroxycinnamates in lignification," *Phytochemistry Reviews*, vol. 9, no. 1, pp. 65–83, 2010.

[2] T. Kleinert and K. Tayenthal, "Process of decomposing vegetable fibrous matter for the purpose of the simultaneous recovery both of the cellulose and the incrusting ingredients," 1930, U.S. Patent.

[3] J. H. Lora and W. G. Glasser, "Recent industrial applications of lignin: a sustainable alternative to nonrenewable materials," *Journal of Polymers and the Environment*, vol. 10, no. 1-2, pp. 39–48, 2002.

[4] B. Lesar, M. Humar, G. Hora et al., "Utilization of recycled wood in biorefineries: preliminary results of steam explosion and ethanol/water organosolv pulping without a catalyst," *European Journal of Wood and Wood Products*, vol. 74, no. 5, pp. 711–723, 2016.

[5] C. Nitsos, R. Stoklosa, A. Karnaouri et al., "Isolation and characterization of organosolv and alkaline lignins from hardwood and softwood biomass," *ACS Sustainable Chemistry and Engineering*, vol. 4, no. 10, pp. 5181–5193, 2016.

[6] C. Løhre, M. Kleinert, and T. Barth, "Organosolv extraction of softwood combined with lignin-to-liquid-solvolysis as a semi-continuous percolation reactor," *Biomass and Bioenergy*, vol. 99, pp. 147–155, 2017.

[7] A. Smit and W. Huijgen, "Effective fractionation of lignocellulose in herbaceous biomass and hardwood using a mild acetone organosolv process," *Green Chemistry*, vol. 19, no. 22, pp. 5505–5514, 2017.

[8] G. Koumba-Yoya and T. Stevanovic, "Study of organosolv lignins as adhesives in wood panel production," *Polymers*, vol. 9, no. 12, p. 46, 2017.

[9] S. B. Harris, U. W. Tschirner, A. Gillespie et al., "Characteristic properties of novel prganosolv lignin/polylactide/delta-valerolactone terpolymers," *Journal of Polymers and the Environment*, vol. 26, no. 8, pp. 3262–3271, 2018.

[10] A. García, G. Spigno, and J. Labidi, "Antioxidant and biocide behaviour of lignin fractions from apple tree pruning residues," *Industrial Crops and Products*, vol. 104, pp. 242–252, 2017.

[11] V. Aguié-Béghin, L. Foulon, P. Soto et al., "Use of food and packaging model matrices to investigate the antioxidant properties of biorefinery grass lignins," *Journal of Agricultural and Food Chemistry*, vol. 63, no. 45, pp. 10022–10031, 2015.

[12] A. Farjon, *A Handbook of the World's Conifers (Two Vol. Set)*, Brill Academic Publishers, Leiden, Netherlands, 2010.

[13] T. Geburek, "Larix decidua," in *Enzyklopädie der Holzgewächse: Handbuch und Atlas der Dendrologie*, B. Stimm, A. Roloff, H. Weisgerber et al., Eds., Wiley VCH, Weinheim, Germany, 2018.

[14] J. Matras and L. Pâques, *EUFORGEN Technical Guidelines for Genetic Conservation and Use for European Larch (Larix Decidua)*, Bioversity International, Rome, Italy, 2008.

[15] A. Praciak, *The CABI Encyclopedia of Forest Trees*, CABI, Wallingford, UK, 2013.

[16] M. Grabner, R. Wimmer, N. Gierlinger et al., "Heartwood extractives in larch and effects on X-ray densitometry," *Canadian Journal of Forest Research*, vol. 35, no. 12, pp. 2781–2786, 2005.

[17] N. Gierlinger and R. Wimmer, "Radial distribution of heartwood extractives and lignin in mature European larch," *Wood and Fiber Science*, vol. 36, no. 3, pp. 387–394, 2004.

[18] N. Gierlinger, D. Jacques, R. Wimmer et al., "Heartwood extractives and lignin content of different larch species (Larix sp.) and relationships to brown-rot decay-resistance," *Trees-Structure and Function*, vol. 18, no. 2, pp. 230–236, 2004.

[19] X. Pan, D. Xie, R. W. Yu et al., "Pretreatment of lodgepole pine killed by mountain pine beetle using the ethanol organosolv process: fractionation and process optimization," *Industrial and Engineering Chemistry Research*, vol. 46, no. 8, pp. 2609–2617, 2007.

[20] X. Pan, D. Xie, R. W. Yu, and J. N. Saddler, "The bioconversion of mountain pine beetle-killed lodgepole pine to fuel ethanol using the organosolv process," *Biotechnology and bioengineering*, vol. 101, no. 1, pp. 39–48, 2008.

[21] S.-K. Jang, H.-Y. Kim, H.-S. Jeong, J.-Y. Kim, H. Yeo, and I.-G. Choi, "Effect of ethanol organosolv pretreatment factors on enzymatic digestibility and ethanol organosolv lignin structure from Liriodendron tulipifera in specific combined severity factors," *Renewable Energy*, vol. 87, pp. 599–606, 2016.

[22] N. Abatzoglou, E. Chornet, K. Belkacemi, and R. P. Overend, "Phenomenological kinetics of complex systems: the development of a generalized severity parameter and its application to lignocellulosics fractionation," *Chemical Engineering Science*, vol. 47, no. 5, pp. 1109–1122, 1992.

[23] K. M. Holtman, H. m. Chang, H. Jameel, and J. F. Kadla, "Quantitative13C NMR characterization of milled wood lignins isolated by different milling techniques," *Journal of Wood Chemistry and Technology*, vol. 26, no. 1, pp. 21–34, 2006.

[24] TAPPI Standards, *Acid-Insoluble Lignin in Wood and Pulp: T 222 om-15*, 2015.

[25] TAPPI Standards, *Solvent Extractives of Wood and Pulp: T204 cm-17*, 2009.

[26] TAPPI Standards, *Ash in Wood, Pulp, Paper, and Paperboard: Combustion at 525°C: T 211 om-16*, 2016.

[27] T. Renders, S. Van den Bosch, T. Vangeel et al., "Synergetic effects of alcohol/water mixing on the catalytic reductive fractionation of poplar wood," *ACS Sustainable Chemistry & Engineering*, vol. 4, no. 12, pp. 6894–6904, 2016.

[28] X. Pan, J. F. Kadla, K. Ehara, N. Gilkes, and J. N. Saddler, "Organosolv ethanol lignin from hybrid poplar as a radical scavenger: relationship between lignin structure, extraction conditions, and antioxidant activity," *Journal of agricultural and food chemistry*, vol. 54, no. 16, pp. 5806–5813, 2006.

[29] T. Dizhbite, G. Telysheva, V. Jurkjane et al., "Characterization of the radical scavenging activity of lignins-natural antioxidants," *Bioresource Technology*, vol. 95, no. 3, pp. 309–317, 2004.

[30] W. Brand-Williams, M. E. Cuvelier, and C. Berset, "Use of a free radical method to evaluate antioxidant activity," *LWT-Food Science and Technology*, vol. 28, no. 1, pp. 25–30, 1995.

[31] A. K. Tolbert, C. G. Yoo, and A. J. Ragauskas, "Understanding the changes to biomass surface characteristics after ammonia and organosolv pretreatments by using time-of-flight secondary-ion mass spectrometry (TOF-SIMS)," *ChemPlusChem*, vol. 82, no. 5, pp. 686–690, 2017.

[32] T. Kleinert, "Ethanol-water delignification of wood-rate constant and activation energy," *Tappi*, vol. 58, no. 8, pp. 170-171, 1975.

[33] F. Hu, S. Jung, and A. Ragauskas, "Pseudo-lignin formation and its impact on enzymatic hydrolysis," *Bioresource technology*, vol. 117, pp. 7–12, 2012.

[34] S. D. Shinde, X. Meng, R. Kumar, and A. J. Ragauskas, "Recent advances in understanding the pseudo-lignin formation in a lignocellulosic biorefinery," *Green Chemistry*, vol. 20, no. 10, pp. 2192–2205, 2018.

[35] O. Faix, "Classification of lignins from different botanical origins by FT-IR spectroscopy," *Holzforschung*, vol. 45, no. s1, pp. 21–28, 1991.

[36] J.-L. Wen, S.-L. Sun, B.-L. Xue, and R.-C. Sun, "Recent advances in characterization of lignin polymer by solution-state nuclear magnetic resonance (NMR) methodology," *Materials*, vol. 6, no. 1, pp. 359–391, 2013.

[37] R. E. Hage, D. Perrin, and N. Brosse, "Effect of the pretreatment severity on the antioxidant properties of ethanol organosolv *Miscanthus x giganteus* lignin," *Natural Resources*, vol. 03, no. 02, pp. 29–34, 2012.

[38] G. Wang and H. Chen, "Fractionation and characterization of lignin from steam-exploded corn stalk by sequential dissolution in ethanol-water solvent," *Separation and Purification Technology*, vol. 120, pp. 402–409, 2013.

[39] C. Fernández-Costas, S. Gouveia, M. A. Sanromán, and D. Moldes, "Structural characterization of Kraft lignins from different spent cooking liquors by 1D and 2D nuclear magnetic resonance spectroscopy," *Biomass and Bioenergy*, vol. 63, pp. 156–166, 2014.

[40] M. A. Gilarranz, F. Rodríguez, and M. Oliet, "Lignin behavior during the autocatalyzed methanol pulping of eucalyptus globulus changes in molecular weight and functionality," *Holzforschung*, vol. 54, no. 4, pp. 373–380, 2000.

[41] T. J. McDonough, "The chemistry of organosolv delignification," *Tappi Journal*, vol. 76, pp. 186–193, 1993.

[42] Y. Guo, J. Zhou, J. Wen, G. Sun, and Y. Sun, "Structural transformations of triploid of populus tomentosa carr. lignin during auto-catalyzed ethanol organosolv pretreatment," *Industrial Crops and Products*, vol. 76, pp. 522–529, 2015.

[43] L. Yao, C. Chen, C. G. Yoo et al., "Insights of ethanol organosolv pretreatment on lignin properties of *Broussonetia papyrifera*," *ACS Sustainable Chemistry and Engineering*, vol. 6, no. 11, pp. 14767–14773, 2018.

[44] A. Björkman, "Studies on finely divided wood. Part 1. Extraction of lignin with neutral solvents," *Sven Papperstidn*, vol. 59, pp. 477–485, 1956.

[45] R. El Hage, N. Brosse, P. Sannigrahi, and A. Ragauskas, "Effects of process severity on the chemical structure of Miscanthus ethanol organosolv lignin," *Polymer Degradation and Stability*, vol. 95, no. 6, pp. 997–1003, 2010.

[46] P. Albersheim, *Plant Cell Walls: From Chemistry to Biology*, Garland Science, New York, NY, USA, 2011.

[47] E. Adler, "Lignin chemistry-past, present and future," *Wood Science and Technology*, vol. 11, no. 3, pp. 167–218, 1977.

[48] J. Ponomarenko, T. Dizhbite, M. Lauberts, A. Volperts, G. Dobele, and G. Telysheva, "Analytical pyrolysis - a tool for revealing of lignin structure-antioxidant activity relationship," *Journal of Analytical and Applied Pyrolysis*, vol. 113, pp. 360–369, 2015.

[49] H. Sadeghifar, T. Wells, R. K. Le, F. Sadeghifar, J. S. Yuan, and A. Jonas Ragauskas, "Fractionation of organosolv lignin using acetone:water and properties of the obtained fractions," *ACS Sustainable Chemistry and Engineering*, vol. 5, no. 1, pp. 580–587, 2016.

Hindawi
International Journal of Chemical Engineering
Volume 2018, Article ID 2316939, 10 pages
https://doi.org/10.1155/2018/2316939

Review Article

Upgrading of Carbohydrates to the Biofuel Candidate 5-Ethoxymethylfurfural (EMF)

Xiaofang Liu and Rui Wang

Guizhou Engineering Research Center for Fruit Processing, Food and Pharmaceutical Engineering Institute, Guiyang University, Guiyang 550005, China

Correspondence should be addressed to Xiaofang Liu; liuxfzap@163.com

Received 16 September 2018; Revised 8 November 2018; Accepted 19 November 2018; Published 17 December 2018

Guest Editor: Masaru Watanabe

5-Ethoxymethylfurfural (EMF), one of the significant platform molecular derivatives, is regarded as a promising biofuel and additive for diesel, owing to its high energy density (8.7 $kWh \cdot L^{-1}$). Several catalytic materials have been developed for the synthesis of EMF derived from different feedstocks under relatively mild reaction conditions. Although a great quantity of research has been conducted over the past decades, the unsatisfactory production selectivity mostly limited to the range 50%–70%, and the classic fructose used as the substrate restricted its application for fuel manufacture in large scale. To address these production improvements, this review pays attention to evaluate the activity of various catalysts (e.g., mineral salts, zeolites, heteropolyacid-based hybrids, sulfonic acid-functionalized materials, and ionic liquids), providing potential research directions for the design of novel catalysts for the achievement of further improved EMF yields.

1. Introduction

Diminishing fossil reserves and growing environmental problems have determined research for sustainable, green, and environmentally benign resources for liquid fuels and chemicals [1–3]. Biomass is widely available, inexpensive, and a CO_2-neutral source of carbon, the catalytic conversion of which to platform chemicals has potential to substitute the products from nonrenewable fossil sources [4–6]. A large number of strategies have been investigated for the conversion of carbohydrates in lignocellulosic biomass into chemicals and fuels [7–9]. The choice of an appropriate catalyst plays a significant role in observing high conversion and selectivity to the target chemicals in a sustainable, green, and economic process [10].

The main purpose of this review is to evaluate the activity of various catalysts (e.g., mineral salts, zeolites, heteropolyacid-based hybrids, sulfonic acid group-functionalized materials, and ionic liquids) with different catalytic effects and functional groups for the production of EMF from HMF, fructose, glucose, and other carbohydrates under the applied reaction conditions, providing potential research directions for the design of novel catalysts for the achievement of further improved EMF yields. Fossil fuels and the derived chemicals have been produced from the limited natural sources. Increasing demand for limited fossil fuels and environmental degradation is gradually severe. Thus, replacing the fossil fuels with alternative and sustainable energy sources is imperative [11, 12]. Biomass is regarded as the only sustainable source of organic carbon compounds that have been suggested as the ideal equivalent to petroleum for the synthesis of fuels and chemicals. Biomass is widely existing and available as a proper feedstock, whose production estimates 1.0×10^{11} tons per year. Extensive research and studies have been conducted to produce biofuels and biodegradable products from biomass [13–15].

Among multiple furan derivatives derived from biomass, EMF is recognized as an excellent additive for regular diesel with promising properties as follows:

(i) With high boiling point (508 K) in comparison with diesel fuel.

(ii) High energy density (30.3 $MJ \cdot L^{-1}$) is similar to regular gasoline (31.9 $MJ \cdot L^{-1}$) and is compared to diesel fuel (33.6 $MJ \cdot L^{-1}$), which is notably higher than ethanol (21 $MJ \cdot L^{-1}$) [16].

(iii) Due to its low toxicity, EMF can be used as a flavor and aroma ingredient in the food beverage industries [17–21].

(iv) To blend EMF with diesel fuel in a diesel engine reduces the formation of particulate contamination, SO_2 emissions, and soot. Meanwhile, EMF-blended fuel can make the engine run smoothly for hours [11, 12, 22, 23].

(v) Ethers that included EMF have a high cetane number [16], which is a very important factor for combustion performance and emission.

(vi) No hydrogenation step is required in EMF production, which is an advantage over other fuel additives (e.g., DMF) obtained from HMF production.

Considering the fact that EMF plays a significant role as a fuel candidate, diesel fuel additive [24], FDCA, or cyclopentenones precursor [25, 26], it is vital to review their different production aspects with detailed attention. Thus, recent progress in EMF synthesis is summarized in this review.

2. Synthesis of EMF

In order to produce EMF, HMF should participate in the etherification reaction with ethanol in the presence of an acid catalyst. Fructose or glucose may also be used as an initiator feed in large scale because their price is considerably low compared to fructose and HMF. Production of EMF from disaccharides, polysaccharides, and biomass through a "one-pot" approach is economically desirable due to the fact that the costs of saccharification, sugar isolation, and purification can be eliminated. However, the yield of synthesized EMF decreases significantly when HMF or fructose has not been used as the feed, and the possible reaction pathways for the synthesis of EMF from carbohydrates are presented in Scheme 1. The proposed reaction mechanism of hexose conversion to EMF is shown in Scheme 2.

Another method to produce EMF from different feedstocks is to follow a multistep mechanism. In the first step of the mechanism, an intermediate is produced, and then the intermediate is converted to EMF at very high yield. A representative example of the multistep method is found in the preparation of halomethylfurfural, namely, 5-chloromethylfurfural (CMF), where the reaction of biomass, polysaccharides, or C6 sugars with HCl leads to the production of CMF, and then, EMF is produced by nucleophilic substitution of CMF with ethanol [27]. Herein, we reviewed and compared different acid catalysts and their efficacies on the production yields of EMF from various feedstocks. Optimal reaction conditions for the case were presented.

2.1. Homogeneous Mineral Salts. Soluble catalysts or the homogeneous catalysts possessed excellent catalytic performance and the fast reaction rate, the existent ions of which are highly dispersed through the medium to enhance the availability of active sites with reactants. Generally, mineral salts acted as Lewis acid in favor of converting the glucose-based substrates to synthesize EMF. However, the separation and recycle wasted energy are not catered to the green and sustainable development.

Additionally, the heterogeneous catalytic reaction caused lower corrosion for the environment and equipment. Therefore, much more researchers concentrated on solid acid catalysts and enhanced their performances and activities [28–30]. Reaction temperature plays a crucial role in carbohydrates transformation and EMF synthesis, and the temperature ranges from 70°C to 160°C. The major byproducts existing in the system were EL, 5-(ethoxymethyl) furfural diethylacetal (EMFDEA) [17], and 5,5′(oxybis(methylene))bis-2-furfural (OBMF) [31].

Metal chloride always is a commercially available Lewis acid with low toxicity and a high catalytic activity for the conversion of hexoses. Series of metal chlorides have been introduced for the production of EMF (Scheme 3). Initially, Liu et al. [32] examined various inorganic salts to promote fructose into EMF with NH_4Br, $CuCl_2 \cdot 4H_2O$, and $NiCl_2 \cdot 6H_2O$ giving low yields of EMF. Among those mentioned above, NH_4Cl demonstrated superior catalytic activity with 42% total yield of HMF and EMF under optimum reaction condition. Simultaneously, Yang et al. [33] chose the $AlCl_3 \cdot 6H_2O$ as a catalyst for carbohydrates including glucose, sucrose, maltose, cellobiose, starch, and cellulose and converted to EMF in ethanol/water binary solvents. The higher total furans yield (included HMF and EMF) of 57% was obtained, and a moderate EMF yield of 40% was derived from sucrose. However, the conversion efficiencies of other carbohydrates to furan were low. The highest EMF yield through single step reaction from HMF was proved to be 92.9% catalyzed by $AlCl_3$ at 100°C for 5 h by Liu et al. [31]. With the same carbohydrates conversion system, Yu et al. [34] performed the use of large-scale common metal salts as catalysts for the preparation of EMF to understand the catalytic mechanism. According to the research, $AlCl_3$ gave good catalytic activity for producing EMF from fructose at 140°C, while $CuSO_4$ and $Fe_2(SO_4)_3$ provided comparable EMF yields at 110 to 120°C, and the latter favored the EL formation.

To enhance the catalytic performance, Jia et al. [35] explored combinations of $AlCl_3$ with different cocatalysts such as $B(OH)_3$ and $BF_3 \cdot (Et)_2O$ or halide salts such as NaF, NaCl, and NaBr. The result of $BF_3 \cdot (Et)_2O/AlCl_3 \cdot 6H_2O$ proved to be significantly superior to other catalysts; 55.0%, 45.4%, and 23.9% high yields of EMF derived from fructose, inulin, and sucrose were achieved, respectively, under the optimized conditions. Later, Zhou et al. [36] studied the reactivity of $FeCl_3$, $CrCl_2$, $GeCl_4$, $IrCl_3$, and so on for the production of EMF. The presented toxicity, high price, and instability drawbacks of other metal chlorides affect the further exploration. In the presence of $FeCl_3$, a maximum EMF yield of 30.1% was obtained in the mixture solvent composed of [Bmim]Cl and ethanol.

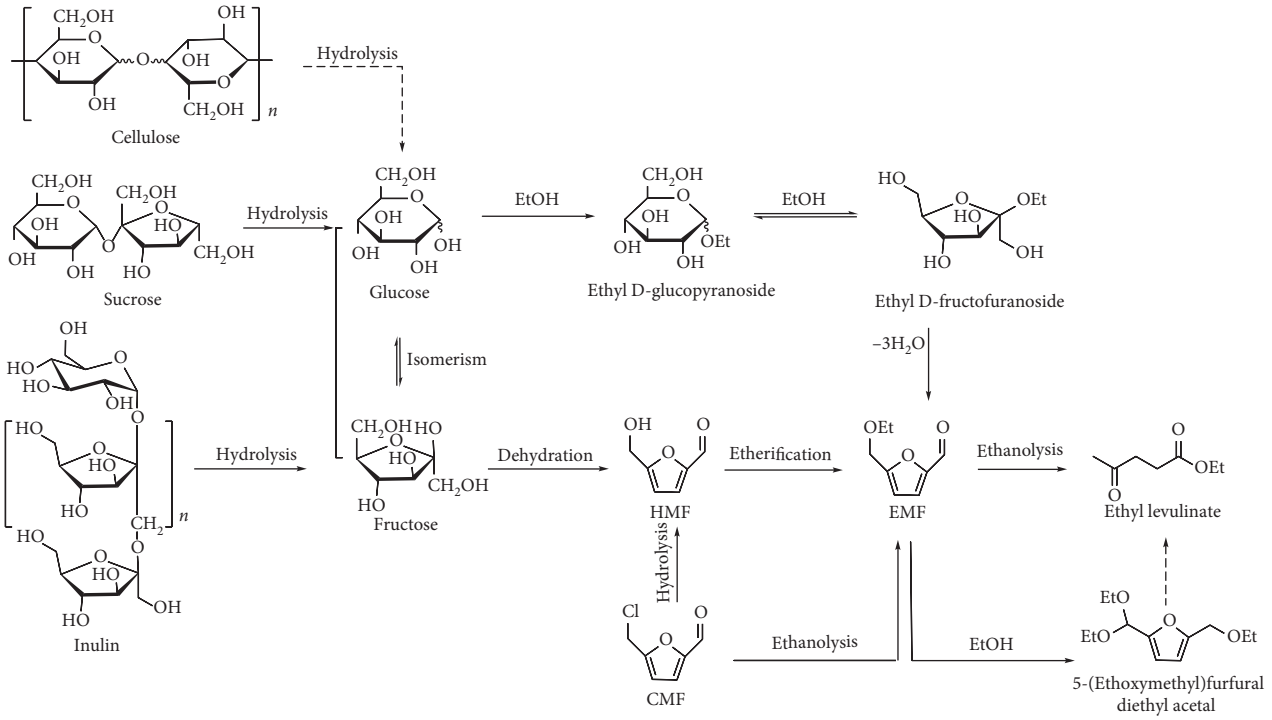

Scheme 1: Reaction pathways for the synthesis of EMF from carbohydrates.

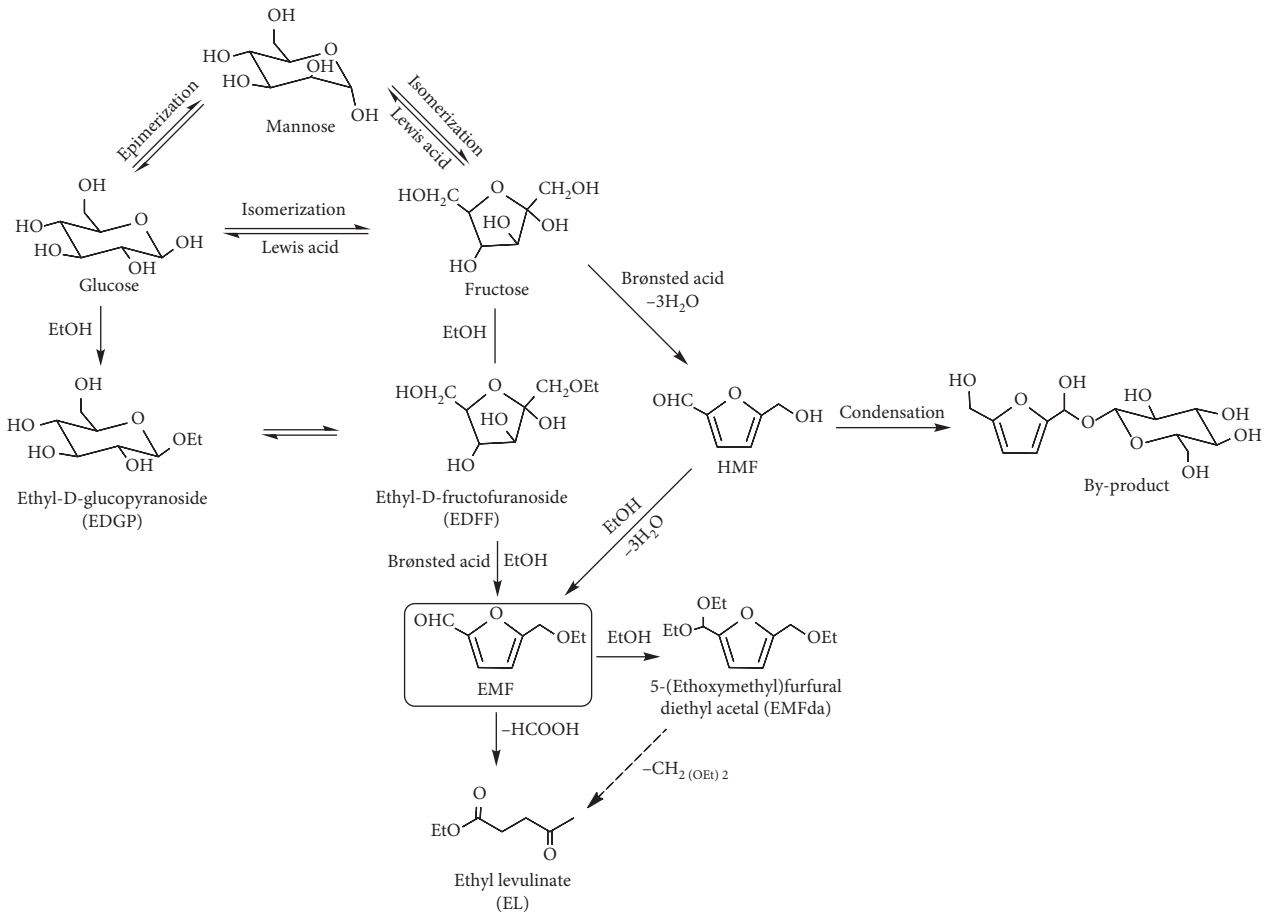

Scheme 2: Proposed mechanism for one-pot conversion of hexose to EMF.

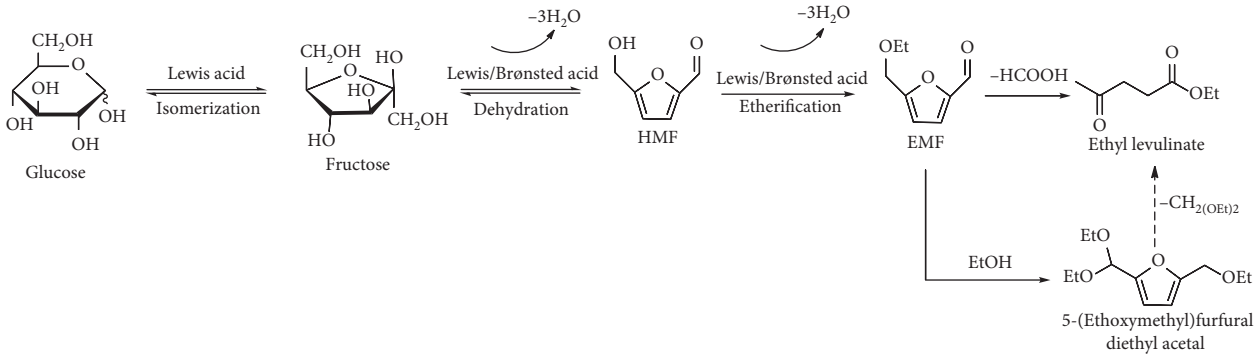

Scheme 3: Reaction pathways for the conversion of hexose to EMF catalyzed by Lewis acid.

2.2. Heterogeneous Catalysts

2.2.1. Zeolitic Catalysts. Zeolites with the highly dispersed and uniform channel microporous structure typically restrict the formation of large and unwanted by-product for the EMF preparation system. Meanwhile, the micropores also limit the effective diffusion of HMF and EMF due to the molecular sizes and small pore openings of zeolites [37, 38]. Expansion of the pore sizes needed to be further explored for the application in more areas.

The enlarged pore sizes play an important role for these materials. For instance, Lanzafame et al. [29] conducted the efficient etherification of HMF catalyzed by mesoporous Al-MCM-41 (with different Si/Al ratios), zirconia, or sulfated zirconia immobilized on SBA-15. Strong Lewis acid sites ZrO_2 and isolated Al^{3+} sites were explained to be beneficial for EMF production. In addition, strong Brønsted acid sites led to the formation of ethyl 4-oxopentanoate. Investigation on mesoporous aluminosilicates by further introducing aluminum into the framework Al-TUD-1 (Si/Al ratio: 21) was carried out by Neves et al. [39]. Based on the unique and regular channel of MCM-41, Che et al. [30] illustrated a nanosphere catalyst with highly dispersed $H_4SiW_{12}O_{40}$/MCM-41 for the etherification of the hydroxyl group of HMF. Comparing the catalytic performance with *p*-TSA, H_2SO_4, Amberlyst-15, and H_3PO_4, $H_4SiW_{12}O_{40}$/MCM-41 showed 84.1% selectivity to EMF with 92.0% conversion of HMF under mild conditions. Meanwhile, the intermediate 5,5′(oxybis(methylene))bis-2-furfural could also be converted to target product EMF. They found that, with the strength of acids and heteropoly anion effects, the effective catalytic performance of $H_4SiW_{12}O_{40}$/MCM-41 was obtained. In this regards, Liu et al. [40] developed MCM-41-HPW with different dosages of phosphotungstic acid (HPW) supporting on MCM-41. The optimal 40 wt.% MCM-41-HPW achieved a high EMF yield of 83.4%, converted from HMF at 100°C for 12 h.

Inspired by the published results that tin-containing zeolite (Sn-BEA) was effective for the glucose-fructose-HMF conversion, Lew et al. [41] further employed Sn-BEA combined with Amberlyst-131 for one-pot glucose-to-fructose-to-HMF-to-EMF conversion, giving 31% yield of EMF. Li et al. [42] found DeAl-H-beta could provide a moderate EMF yield (43%) from sucrose, and the EMF yield was improved up to 50% by a one-pot two-step method. However, poor catalytic performance was achieved using cellobiose as a substrate for EMF. Lewis et al. [43] explored a series of zeolites including Hf-, Zr-, Ti-, Ta-, Nb-, and Sn-Beta that could promote the etherification reaction of HMF. Under batch conditions, Ta-Beta and Al-Beta showed comparable EMF yields of 56% and 41%, respectively.

Product selectivity depends on the control of active sites strength. Barbera et al. [44] introduced NH_4-exchanged zeolites, and the NH_4 was used to block the strong sites, thus preventing the secondary reactions. The results proved that NH^{4+} effectively increased the product selectivity of NH_4-BEA catalyst for HMF etherification reaction. Recently, Bai et al. [45] exhibited the glucose conversion to EMF catalyzed by multifunctional MFI-Sn/Al zeolite with dual meso-/microporosity and dual Lewis and Brønsted acidity. Combination of Lewis acidic Sn and Al sites and Brønsted acidic Al-O(H)-Si sites was efficient for the cascade isomerization-dehydration-etherification reaction, affording 44% EMF yield.

2.2.2. Heteropolyacid-Based Hybrid Catalysts. Heteropolyacids have several advantages such as strong Brønsted acidity, tunable acid-base properties, and high proton mobility. But, they tend to dissolve in water and polar solvents and possess low surface area and low thermal stability, which limits their application in catalytic conversion. Supporting a solid support is a method that has been used by different groups.

Originally, Yang et al. [46] investigated the fructose-EMF transformation in a mixed ethanol/THF (tetrahydrofuran) medium catalyzed by $H_3PW_{12}O_{40}$ (HPW). The microwave offered EMF in yield of 76% under the optimum reaction condition, and the cosolvent THF significantly increased fructose conversion. Wang et al. [47] compared the activity of HPW, phosphomolybdic acid (HPM), $AlCl_3$, H_3PO_4, and Amberlyst-15 for production of EMF from fructose in an ethanol/DMSO mixture. Results indicated that HPW and HPM exhibited superior catalytic activities than $AlCl_3$, H_3PO_4, and Amberlyst-15, and the former formed 64% EMF within 130 min at 140°C. In this regard, Ren et al. [48] exchanged H^+ ion of HPW with Ag^+ and achieved Ag_1H_2PW, which presented a high activity and EMF yield of 88.7%. Further replacing another H^+ in the

Ag_1H_2PW, the acid strength of the catalyst decreased. Ren et al. used Ag_1H_2PW catalyst for fructose dehydration and HMF etherification, and a relatively high yield of EMF (69.5%) was obtained.

Stability and efficient separation are crucial criteria to be the catalyst support. Addition of heteropolyacid into Fe_3O_4@SiO_2, simultaneously with the introduction of the silica layer could modify the MNPs-formed inert surface. Fe_3O_4@SiO_2-HPW catalyzed the reaction of HMF with ethanol, and therefore, the activity increased dramatically and the production of EMF yield reached 83.6% [49]. Wang et al. [50] also applied Fe_3O_4@SiO_2-HPW for EMF production from HMF to obtain the same effect, which was in accordance with the results of Liu and Zhang [51]. Besides, Fe_3O_4@SiO_2-HPW achieved an EMF yield of 54.8% derived from fructose.

Organic-inorganic hybrid materials become the hotspot to be the catalyst, for instance, HPA-based $[MIMBS]_3PW_{12}O_{40}$ hybrid catalyst reported by Liu et al. [52] for the preparation of EMF. Combination of IL with $H_3PW_{12}O_{40}$ enhanced the EMF yield to 90.7% with 98.1% conversion of HMF under the optimum reaction condition at 70°C within 24 h. Wang et al. [53] studied the uniform nanospheric hybrids by controlling the molar ratio of phosphotungstic acid (HPW) and pyridine (PY) or trimethylamine (TEA) in different nanosizes. Particularly, PY-PW-1 showed an excellent catalytic activity with 90% of EMF, which attribute to the relatively strong acidity and regular pore size. With the prepared nanosphere PY-PW-1, fructose was also converted to EMF in one-pot reaction process and obtained a moderate yield of 55% with the enhanced temperature at 120°C.

The synthesized K-10 clay-HPW not only avoided the HPW being dissolved into polar organic solvents and expressed the high activity. Liu et al. [54] used 30 wt.% of K-10 clay-HPW for HMF-EMF transformation. Under the optimum reaction conditions (100°C, 10 h), catalytic activity was increased to 91.5% yield, whereas for one-pot fructose conversion to EMF, 61.5% yield of EMF was gained. The prepared catalyst with high stability could be reused several times without loss of catalytic performance. MCM-41 with uniform channel structure and pore size was suitable to support 12-tungstophosphoric acid that allowed the one-pot conversion of fructose directly into EMF, leading to 42.9% EMF by 40 wt.% MCM-41-HPW [40].

Apart from K-10 clay and MCM-41, MOF-based [Cu-BTC][HPM] (NENU-5) was also efficient for the etherification of HMF to EMF with up to 68.4% yield under normal pressure and optimized conditions (Figure 1). Benefiting from the unique structure, MOFs can provide adsorption sites for HPM to avoid HPM dissolving into solvents, making the catalysts be recyclable with 55% EMF yield [55].

The addition of cosolvent exhibits improvement in EMF yield as compared with the single solvent, and enhanced yield of EMF ranges from 5 to 20 percentages. Xu et al. [56] explored the ethanol/*n*-hexane mixture solvent indicating that the introduction of *n*-hexane could enhance the yield of EMF to 66.3% with optimum volume ratio (ethanol : *n*-hexane, 6 : 4), conducted at 120°C within 180 min. With the ethanol-DMSO mixture, Li et al. [57] also developed acid-base bifunctional hybrid nanosphere catalyst Lys/PW that possessed an optimal reaction activity of 76.6% EMF yield from fructose, implying that the base sites of the catalysts play an important role in increasing EMF stability.

Combination of Lewis acid $AlCl_3 \cdot 6H_2O$ and Brønsted solid acid PTSA-POM proved cooperative effect for glucose transformation into EMF and generated 30.6% EMF under the ethanol-water (9 : 1) system. [58].

The appropriate supports play a vital role in heteropolyacid as the active center producing EMF. Partial substitution of protons is another effective approach to change the property of heteropolyacid for better catalytic activity. Raveendra et al. [59] reported the cesium-exchanged silicotungstic acid to enhance the surface area and acidity and finally obtained 91% EMF yield with Cs_2STA at 120°C for 2.5 h.

2.2.3. Sulfonic Acid-Functionalized Catalysts. The strong acidity of sulfonic acid groups can be immobilized onto the diverse supporter by sulfonation reactions and hence gain multiple sulfonic acid-functionalized catalysts. Simultaneously, the acidic density can be flexibly controlled by the dosage of sulfonic sources. Considering the green and sustainable development request, loss of element S was not catered for the present development.

Magnetic carriers to load sulfonic acid groups can be easily separated by a permanent magnet and recycled for times without loss of activity attracting much attention of scientists. Zhang et al. [60] chose Fe_3O_4@SiO_2 for preparation supporting a high yield (up to 89.3%) of EMF converted from HMF. Magnetic nanoparticles (MNPs) and amorphous carbon were selected to immobilize sulfonic acid groups ($-SO_3H$) which act as a solid acid catalyst for EMF production [61]. Successfully, Fe_3O_4@C-SO_3H shared active catalytic properties in HMF-EMF, fructose-EMF, sucrose-EMF, and inulin-EMF systems, and considerable yields of 88.4%, 67.8%, 33.2%, and 58.4% were obtained, respectively. Among those, the low yield of EMF was produced from sucrose owing to the composition of sucrose, which contains one fructose and glucose unit, and glucose cannot be converted to EMF directly. The more deep-seated research was carried out by Fe_3O_4@SiO_2-SH-Im-HSO_4 [62] and facilitated by it, indicating that EMF yields derived from inulin (56.1%) and fructose were consistent while glucose always promoted to ethyl glucoside. Soon afterward, Wang et al. [63] illustrated the smooth conversion of sucrose and inulin with superior catalytic performance offering 53.6% and 26.8% EMF yields, respectively, at 140°C for 24 h. Excellent catalytic performance of OMC-SO_3H indicated its promising application for biomass conversion into value-added chemicals and liquid fuels.

Considering the sustainable and green development trend, the same magnetic Fe_3O_4@C-SO_3H prepared from wheat straw biomass afforded comparable EMF yield of 64.2% in DMSO-ethanol binary solvent. Bearing multiple

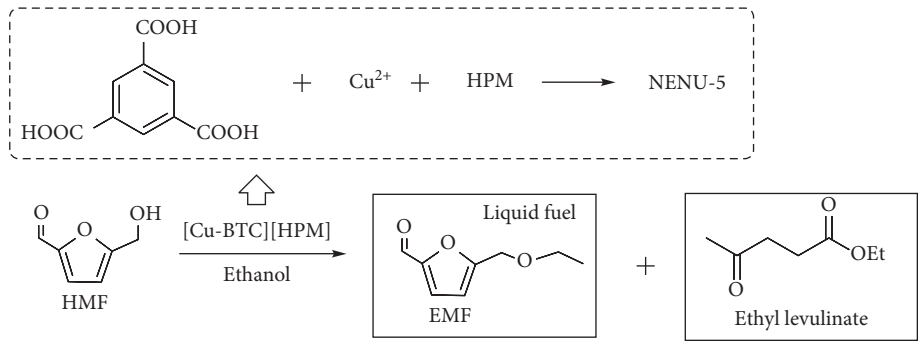

Figure 1: Schematic of the catalyst preparation and catalytic procedure.

-COOH, -SO_3H, and -OH groups, the authors described the progress of fructose or HMF to EMF in relatively high yields with 64.2% and 85.6% [64].

Grafting sulfonic acid onto the inorganic insoluble supports is a technique to prepare high-performance heterogeneous solid acidic catalysts. Liu and Zhang [51] studied the grafting of sulfonic acid onto the mesoporous silica and utilized for effective etherification of HMF for EMF with 83.8% under the optimal conditions (100°C, 10 h), while the high yields of 63.1% and 60.7% were synthesized by one-pot transformation of fructose and inulin. However, the aldose-based carbohydrates such as glucose were mainly turned to ethyl D-glucopyranoside with a high yield of 91.7%. The unique properties such as 2D structure, high stability, and high surface areas decided GO as a promising catalytic material that was oxidized by Hummers' method clarified the engineered catalytic performance for the conversion of HMF into EMF with high yield of EMF (92%), while EMF yield was decreased when fructose replaced HMF as a starting material [65] (Figure 2). Under mixture solvent ethanol-DMSO in 3 : 7, furan selectivity enhanced to 71% EMF yield and 34%, and 66% EMF yields were achieved when sucrose and inulin were used as the substrates. Partially reducing GO, amorphous carbon black (CB), and carbon nanotubes (CNTs) by sulfuric acid (S-RGO) were conducted for the synthesis of EMF converted from HMF. The catalytic activity of S-RGO proved to be superior to S-CB, S-CNTs, and even the classic Amberlyst-15 [66].

Besides, new solid acid catalysts obtained by sulfonating natural biopolymers met the green trend for biomass conversion to high value-added chemicals. Liu et al. [67] developed the cellulose sulfuric acid for the etherification of HMF for the synthesis of EMF and observed high yield (84.4%) under optimized condition. Similarly, application of glucose-derived magnetic solid acid, glu-Fe_3O_4-SO_3H, also acted as an etherification catalyst and generated 92% isolated yield EMF [68]. With the optimal 50 wt.% loading rate of glu-Fe_3O_4-SO_3H, EMF from fructose was effectively produced by 81% yield.

Amberlyst-15 as one of the standard solid acid catalysts was applied in various reaction systems and first explored by Zhu et al. [69] for the HMF-5-methoxymethylfurfural (MMF) conversion in low-boiling point solvent. The presence of cosolvent THF enhanced the contact of -SO_3H of Amberlyst-15 leading to promoting the catalytic progress

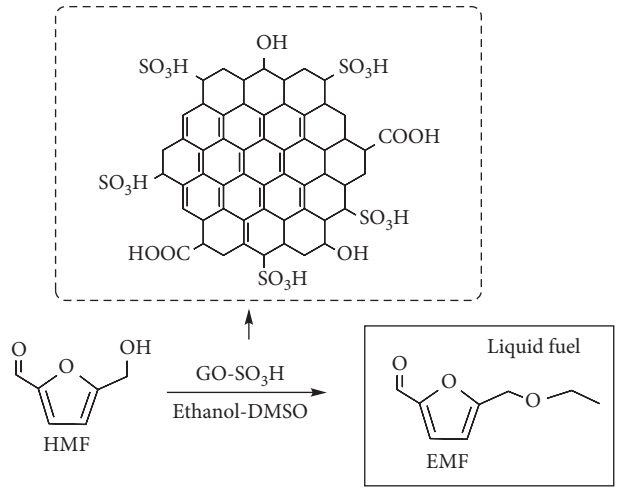

Figure 2: The conversion of HMF to EMF catalyzed by GO-SO_3H.

and accumulating the target molecules. Because of short of the high surface area and the limited contact of active sites and substrate, the catalytic performance of Amberlyst-15 was dissatisfactory. MOF provided large enough specific surface area and acidic density, and MIL-101-SO_3H(100) showed a better catalytic performance with 89.2% conversion of fructose and 67.7% EMF yield in the ethanol and THF mixture.

Well-defined structure and uniform distribution of active sites catalyst arenesulfonic acid-modified SBA-15 Ar-SO_3H-SBA-15 was studied for the conversion of fructose to EMF in binary ethanol-DMSO solvent in optimizing reaction conditions (e.g., temperature, catalyst loading, and DMSO concentration), demonstrating the maximum EMF yield of 63.4% [70]. Li et al. [71] generated a series of SO_3H-functionalized polymer solid acid catalysts for successive fructose dehydration and HMF etherification, and an EMF yield of 72.8% was achieved with the optimal catalyst poly(VMPS)-PW at 110°C within 10 h.

2.2.4. Ionic Liquid Catalysts. Due to the tailored design, good thermal and chemical stability, low melting point, and good solubility of acidic ionic liquids, the investigation of

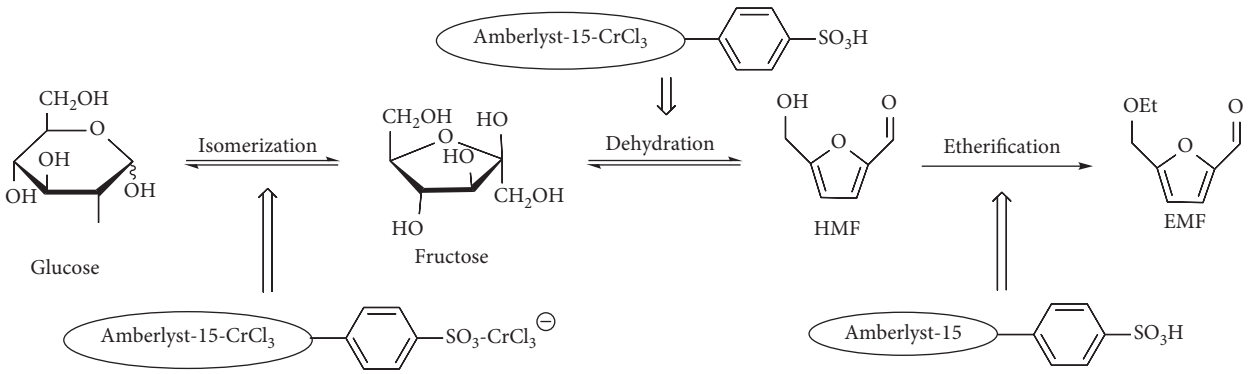

Figure 3: Schematic illustration of the catalysis progress.

them attracts much attention. The problem of high cost and recycle is urgently to be solved.

Kraus and Guney [72] appointed the sulfonic acid-functionalized IL to catalyze the conversion of fructose for the EMF fabrication in a one-pot procedure without the addition of solvent or acid catalysts. The application of 1-butyl-3-(3-sulfopropyl)-imidazolium chloride (4) and 1-methyl-3-(3-sulfopropyl)-imidazolium chloride (5) for EMF provided comparable 55% and 54% yields under the mild condition (100°C, 80 min), and the novel biphasic medium assembly of hexanes and IL enhanced the EMF yields to a certain extent.

The Brønsted acidic IL $[DMA]^+[CH_3SO_3]^-$ was effective for fructose-EMF conversion with a relatively high yield of 64%, while one-pot cellulose transformation gave 22% yield of EMF [73]. Alam et al. [37] further showed EMF production directly from Foxtail and Red nut sedge weeds in presence of $[DMA]^+[CH_3SO_3]^-$, which was better than $[NMP]^+[CH_3SO_3]^-$ when converting foxtail to EMF.

Except the ionic liquid catalysts, functionalized ionic liquids can also act as the reaction medium to afford efficient EMF yield. Guo et al. [74] chose hydrogen sulfate ionic liquid as a homogeneous catalyst and mixed with ethanol as a reaction solvent for efficient preparation of EMF. Catalyzed by the $[C_4mim][HSO_4]$-ethanol system, high yield of 83% EMF was observed from fructose at 130°C within 20 min, which could be attributed to the acidity of $[C_4mim][HSO_4]$, the viscosity of the mixture system, and the formed hydrogen bonds between $[C_4mim][HSO_4]$, ethanol solvent, and fructose.

Due to the superior physical and chemical properties and benefits of acidic ILs, an effective progress for EMF derived from carbohydrates by deep eutectic solvent (DES) mixture as a solvent was proposed [75]. 77.3% EMF yield was gained with fructose as substrate catalyzed by Amberlyst-15, and more excellent catalytic performance afforded a high EMF yield of 46.7% obtained from glucose with $CrCl_3$-modified Amberlyst-15 (Figure 3).

2.2.5. Others. Except for the mentioned catalysts in the previous section, there exist many other effective materials such as Zr-Mont, Co(*x*)Pc, $MoO_2Cl_2(H_2O)_2$, and a combination of metal chloride with resins which could be also used for carbohydrates transformation to EMF.

Acidic Zr-montmorillonite (Zr-Mont) catalyst was utilized for synthesis mixture of EMF and 2-(diethoxymethyl)-5-(ethoxymethyl)furan by Shined and Rode [76], and the latter can turn into EMF by conducting in water with the same Zr-Mont. Under the optimized reaction conditions, EMF was observed in the highest yields of 91% by etherification HMF with ethanol. Yadav et al. [77] investigated the use of cobalt (I, II, III) phthalocyanine (Co(*x*)Pc) for the isomerization of glucose to fructose, for fructose dehydration, and in the subsequent etherification. It was noted that Co(*x*)Pc was effective for the direct conversion of carbohydrates to EMF in [EMIM]Cl ionic liquid, and Co(III) Pc exhibited much higher catalytic activity. The levulinate could be reduced by the waste and basic additive oil shale ash, which is formed by burning oil shale in power plants, while it was efficient for the preparation of EMF with high yield and purity [78]. The final product EMF syntheses starting from 5-bromomethylfurfural (BMF) afforded 88% yield without further purification which reacted under room temperature for 17 h in 96% ethanol.

Considering the excellent catalytic property for the reduction reaction, high valent oxomolybdenum complexes were investigated for the synthesis of EMF by one-pot fructose conversion in ethanol/THF (5 : 2) mixture and optimal yield of 53% was achieved within 17 h at 120°C. With the efficient catalyst, 40% and 23% yield of EMF were produced from inulin and sucrose, respectively [79].

Marine carbohydrate agar derived from red algae was reported for production of EMF in the presence of [EMIM]Cl, $CrCl_2$, and Dowex resin mixture, afford isolate 3.9 g of EMF and EL (EMF to EL mole ratio: 5 : 2) from 10 g of agar [80]. Similarly, biomass wheat straw was directly converted by alcoholysis reaction in 94% (w/w) ethanol with 30 mM H_2SO_4 at 200°C, and yields for EMF and by-product EL were 20% and 25%, respectively [81].

3. Conclusions

As mentioned above, various Lewis and Brønsted acid catalysts have been conducted to convert HMF, fructose, and inulin in high yields without extra costs for isolation and purification. It is worth noting that HMF is not affordable as

a feed for EMF production regardless of the high yields of 70%–95% reported for HMF etherification to EMF by different groups. The technoeconomic analysis carried out by Torres et al. [82] estimated the HMF price of 2.16 $/kg based on the process proposed by Roman-Leshkov et al. [83]. EMF synthesis from fructose at a desirable yield of 50%–70%, but high reaction temperature (90–130°C) and retention time (6–24 h), is needed compared to the HMF cases. In general, EMF production derived from sucrose did not gain high yields, because of the fact that glucose obtained from sucrose conversion was not converted to EMF in good yields. Nevertheless, the fructose polymer inulin exhibited better performance and produced EMF at high yields. One-pot transformation of cellulose or biomass to EMF led to low yields, due to their complex structures with the low glucose conversion to EMF. Ethanol/THF or ethanol/DMSO mixture is applied as a reaction medium for EMF synthesis from fructose. In a series of reactions, EMF may also participate in the rehydration reaction to produce EL.

Conflicts of Interest

The authors declare that there are no conflicts of interest regarding the publication of this paper.

Acknowledgments

This work was financially supported by the Joint Science and Technology Funds of the Youth Growth S&T Personnel Foundation of Guizhou Education Department (No. KY [2018]292), the Special Funding of Guiyang Science and Technology Bureau and Guiyang University (GYU-KYZ [2018]01-12), and the Technical Talent Support Program of Guizhou Education Department (No. KY[2018]069).

References

[1] E. L. Kunkes, D. A. Simonetti, R. M. West, J. C. Serrano-Ruiz, C. A. Gartner, and J. A. Dumesic, "Catalytic conversion of biomass to monofunctional hydrocarbons and targeted liquid-fuel classes," *Science*, vol. 322, no. 5900, pp. 417–421, 2008.

[2] D. R. Dodds and R. A. Gross, "Chemicals from biomass," *Science*, vol. 318, no. 5854, pp. 1250-1251, 2007.

[3] P. Gallezot, "Conversion of biomass to selected chemical products," *Chemical Society Reviews*, vol. 41, no. 4, pp. 1538–1558, 2012.

[4] R. J. Putten, J. C. Waal, E. Jong, C. B. Rasrendra, H. J. Heeres, and J. G. Vries, "Hydroxymethylfurfural, a versatile platform chemical made from renewable resources," *Chemical Reviews*, vol. 113, no. 3, pp. 1499–1597, 2013.

[5] J. C. Serrano-Ruiz, R. Luque, and A. Sepúlveda-Escribano, "Transformations of biomass-derived platform molecules: from high added-value chemicals to fuelsvia aqueous-phase processing," *Chemical Society Reviews*, vol. 40, no. 11, pp. 5266–5281, 2011.

[6] K. Yan, G. Wu, T. Lafleur, and C. Jarvis, "Production, properties and catalytic hydrogenation of furfural to fuel additives and value-added chemicals Renewable Sustainable," *Renewable and Sustainable Energy Reviews*, vol. 38, pp. 663–676, 2014.

[7] J. B. Binder and R. T. Raines, "Simple chemical transformation of lignocellulosic biomass into furans for fuels and chemicals," *Journal of the American Chemical Society*, vol. 131, no. 5, pp. 1979–1985, 2009.

[8] J. N. Chheda, G. W. Huber, and J. A. Dumesic, "Liquid-phase catalytic processing of biomass-derived oxygenated hydrocarbons to fuels and chemicals *Angew*," *Angewandte Chemie International Edition*, vol. 46, no. 38, pp. 7164–7183, 2007.

[9] Y. Zhang, Z. Xue, J. Wang et al., "Controlled deposition of Pt nanoparticles on Fe_3O_4@carbon microspheres for efficient oxidation of 5-hydroxymethylfurfural," *RSC Advances*, vol. 6, no. 56, pp. 51229–51237, 2016.

[10] E. Taarning, I. S. Nielsen, K. Egeblad, R. Madsen, and Christensen, "Chemicals from renewables: aerobic oxidation of furfural and hydroxymethylfurfural over gold catalysts," *ChemSusChem*, vol. 1, no. 1-2, pp. 75–78, 2008.

[11] H. Omidvarborna, A. Kumar, and D. S. Kim, "Recent studies on soot modeling for diesel combustion," *Renewable and Sustainable Energy Reviews*, vol. 48, pp. 635–647, 2015.

[12] H. Omidvarborna, A. Kumar, and D. S. Kim, "Characterization of particulate matter emitted from transit fueled with B20 in idle modes," *Journal of Environmental Chemical Engineering*, vol. 2, no. 4, pp. 2335–2342, 2014.

[13] G. W. Huber, S. Iborra, and A. Corma, "Synthesis of transportation fuels from biomass: chemistry, catalysts, and engineering," *Chemical Reviews*, vol. 106, no. 9, pp. 4044–4098, 2006.

[14] T. Werpy, G. Petersen, A. Aden, J. Bozell, J. Holladay, and J. White, *Top Value Added Chemicals from Biomass. Volume 1-Results of Screening for Potential Candidates from Sugars and Synthesis Gas*, Department of Energy Washington DC, Washington, DC, USA, 2004.

[15] B. Kamm, P. R. Gruber, and M. Kamm, *Biorefineries-Industrial Processes and Products*, John Wiley & Sons, Hoboken, NY, USA, 2007.

[16] M. J. Murphy, J. D. Taylor, and R. L. McCormick, "Compendium of experimental cetane number data," NREL/SR-540-36805, National Renewable Energy Laboratory, Golden, Colorado, 2004.

[17] J. S. Câmara, M. A. Alves, and J. C. Marques, "Changes in volatile composition of Madeira wines during their oxidative ageing," *Analytica Chimica Acta*, vol. 563, no. 1-2, pp. 188–197, 2006.

[18] B. Vanderhaegen, H. Neven, S. Coghe, K. J. Verstrepen, H. Verachtert, and G. Derdelinckx, "Evolution of chemical and sensory properties during aging of top-fermented beer," *Journal of Agricultural and Food Chemistry*, vol. 51, no. 23, pp. 6782–6790, 2003.

[19] M. S. Pérez-Coello, M. A. González-Viñas, E. Garcıa-Romero, M. C. Dıaz-Maroto, and M. D. Cabezudo, "Influence of storage temperature on the volatile compounds of young white wines," *Food Control*, vol. 14, no. 5, pp. 301–306, 2003.

[20] S. H. Oliveira, P. P. Guedes, B. P. Machado, T. Hogg, J. C. Marques, and J. S. Câmara, "Impact of forced-aging process on Madeira wine flavor," *Journal of Agricultural and Food Chemistry*, vol. 56, no. 24, pp. 11989–11996, 2008.

[21] I. Cutzach, P. Chatonnet, and D. Dubourdieu, "Study of the formation mechanisms of some volatile compounds during the aging of sweet fortified wines," *Journal of Agricultural and Food Chemistry*, vol. 47, no. 7, pp. 2837–2846, 1999.

[22] G. J. M. Gruter and F. Dautzenberg, "Method for the synthesis of 5-hydroxy-methylfurfural ethers and their use," U.S. Patent/0082304 A1, 2011.

[23] H. Omidvarborna, A. Kumar, and D. S. Kim, "Variation of diesel soot characteristics by different types and blends of biodiesel in a laboratory combustion chamber," *Science of The Total Environment*, vol. 544, pp. 450–459, 2016.

[24] B. Liu and Z. H. Zhang, "One-pot conversion of carbohydrates into furan derivatives via furfural and 5-hydroxylmethylfurfural as intermediates," *ChemSusChem*, vol. 9, no. 16, pp. 1–23, 2016.

[25] M. E. Janka, D. M. Lange, M. C. Morrow et al., "Oxidation process to produce a crude and/or purified carboxylic acid product," US patent 2012/0302770A1, 2012.

[26] A. Bredihhin, S. Luiga, and L. Vares, "Application of 5-ethoxymethylfurfural (EMF) for the production of cyclopentenones," *Synthesis*, vol. 48, no. 23, pp. 4181–4188, 2016.

[27] S. Alipour, H. Omidvarborna, and D. S. Kim, "A review on synthesis of alkoxymethyl furfural, a biofuel candidate," *Renewable and Sustainable Energy Reviews*, vol. 71, pp. 908–926, 2017.

[28] M. Balakrishnan, E. R. Sacia, and A. T. Bell, "Etherification and reductive etherification of 5-(hydroxymethyl) furfural: 5-(alkoxymethyl) furfurals and 2,5-bis (alkoxymethyl) furans as potential bio-diesel candidates," *Green Chemistry*, vol. 14, no. 6, pp. 1626–1634, 2012.

[29] P. Lanzafame, D. M. Temi, S. Perathoner et al., "Etherification of 5-hydroxymethyl-2-furfural (HMF) with ethanol to biodiesel components using mesoporous solid acidic catalysts," *Catalysis Today*, vol. 175, no. 1, pp. 435–441, 2011.

[30] P. H. Che, F. Lu, J. J. Zhang et al., "Catalytic selective etherification of hydroxyl groups in 5-hydroxymethylfurfural over $H_4SiW_{12}O_{40}$/MCM-41 nanospheres for liquid fuel production," *Bioresource Technology*, vol. 119, pp. 433–436, 2012.

[31] B. Liu, Z. H. Zhang, K. , C. Huang, and Z. F. Fang, "Efficient conversion of carbohydrates into 5-ethoxymethylfurfural in ethanol catalyzed by $AlCl_3$," *Fuel*, vol. 113, pp. 625–631, 2013.

[32] J. T. Liu, Y. Tang, K. G. Wu, C. F. Bi, and Q. Cui, "Conversion of fructose into 5-hydroxymethylfurfural(HMF) and its derivatives promoted by inorganic salt in alcohol," *Carbohydrate Research*, vol. 350, pp. 20–24, 2012.

[33] Y. Yang, C. W. Hu, and M. M. Abu-Omar, "Conversion of glucose into furans in the presence of $AlCl_3$ in an ethanol-water solvent system," *Bioresource Technology*, vol. 116, pp. 190–194, 2012.

[34] X. Yu, X. Y. Gao, R. L. Tao, and L. C. Peng, "Insights into the metal salt Catalyzed 5-ethoxymethylfurfural synthesis from carbohydrates," *Catalysts*, vol. 7, no. 6, pp. 182–192, 2017.

[35] X. Q. Jia, J. P. Ma, P. H. Che et al., "Direct conversion of fructose-based carbohydrates to 5-ethoxymethylfurfural catalyzed by $AlCl_3{\cdot}6H_2O/BF_3(Et)_2O$ in ethanol," *Journal of Energy Chemistry*, vol. 22, no. 1, pp. 93–97, 2013.

[36] X. M. Zhou, Z. H. Zhang, B. Liu, Q. Zhou, S. G. Wang, and K. J. Deng, "Catalytic conversion of fructose into furans using $FeCl_3$ as catalyst," *Journal of Industrial and Engineering Chemistry*, vol. 20, no. 2, pp. 644–649, 2014.

[37] M. I. Alam, S. De, S. Dutta, and B. Saha, "Solid-acid and ionic-liquid catalyzed one-pot transformation of biorenewable substrates into a platform chemical and a promising biofuel," *RSC Advances*, vol. 2, no. 17, pp. 6890–6896, 2012.

[38] S. Saravanamurugan and A. Riisager, "Solid acid catalysed formation of ethyl levulinate and ethyl glucopyranoside from mono-and disaccharides," *Catalysis Communications*, vol. 17, pp. 71–75, 2012.

[39] P. Neves, M. M. Antunes, P. A. Russo et al., "Production of biomass-derived furanic ethers and levulinate esters using heterogeneous acid catalysts," *Green Chemistry*, vol. 15, no. 12, pp. 3367–3376, 2013.

[40] A. Q. Liu, Z. H. Zhang, Z. F. Fang, B. Liu, and K. C. Huang, "Synthesis of 5-ethoxymethylfurfural from 5-hydroxymethylfurfural and fructose in ethanol catalyzed by MCM-41 supported phosphotungstic acid," *Journal of Industrial and Engineering Chemistry*, vol. 20, no. 4, pp. 1977–1984, 2014.

[41] C. M. Lew, N. Rajabbeigi, and M. Tsapatsis, "One-pot synthesis of 5-(ethoxymethyl)furfural from glucose using Sn-BEA and Amberlyst catalysts," *Industrial & Engineering Chemistry Research*, vol. 51, no. 14, pp. 5364–5366, 2012.

[42] H. Li, S. Saravanamurugan, S. Yang, and A. Riisager, "Direct transformation of carbohydrates to the biofuel 5-ethoxymethylfurfural by solid acid catalysts," *Green Chem*, vol. 18, no. 3, pp. 726–734, 2016.

[43] J. D. Lewis, S. V. Vyver, A. J. Crisci et al., "A continuous flow strategy for the coupled transfer hydrogenation and etherification of 5-(hydroxymethyl)furfural using lewis acid zeolites," *ChemSusChem*, vol. 7, no. 8, pp. 2255–2265, 2014.

[44] K. Barbera, P. Lanzafame, S. Perathoner et al., "HMF etherification using NH_4-exchanged zeolites," *New Journal of Chemistry*, vol. 40, no. 5, pp. 4300–4306, 2016.

[45] Y. Y. Bai, L. Wei, M. F. Yang et al., "Three-step cascade over a single catalyst: synthesis of 5-(ethoxymethyl)furfural from glucose over a hierarchical lamellar multi-functional zeolite catalyst," *Journal of Materials Chemistry A*, vol. 6, no. 17, pp. 7693–7705, 2018.

[46] Y. Yang, M. M. Abu-Omar, and C. W. Hu, "Heteropolyacid catalyzed conversion of fructose, sucrose, and inulin to 5-ethoxymethylfurfural, a liquid biofuel candidate," *Appl. Energy*, vol. 99, pp. 80–84, 2012.

[47] H. L. Wang, T. S. Deng, Y. X. Wang, Y. Q. Qi, X. L. Hou, and Y. L. Zhu, "Efficient catalytic system for the conversion of fructose into 5-ethoxymethylfurfural," *Bioresource Technology*, vol. 136, pp. 394–400, 2013.

[48] Y. Ren, B. Liu, Z. Zhang, and J. Lin, "Silver-exchanged heteropolyacid catalyst (Ag_1H_2PW): an efficient heterogeneous catalyst for the synthesis of 5-ethoxymethylfurfural from 5-hydroxymethylfurfural and fructose," *Journal of Industrial and Engineering Chemistry*, vol. 21, pp. 1127–1131, 2015.

[49] L. H. Reddy, J. L. Arias, J. Nicolas, and P. Couvreur, "Magnetic nanoparticles: design and characterization, toxicity and biocompatibility, pharmaceutical and biomedical applications," *Chemical Reviews*, vol. 112, no. 11, pp. 5818–5178, 2012.

[50] S. G. Wang, Z. H. Zhang, B. Liu, and J. L. Li, "Silica coated magnetic Fe_3O_4 nanoparticles supported phosphotungstic acid: a novel environmentally friendly catalyst for the synthesis of 5-ethoxymethylfurfural from 5-hydroxymethylfurfural and fructose," *Catalysis Science & Technology*, vol. 3, no. 8, pp. 2104–2112, 2013.

[51] B. Liu and Z. H. Zhang, "One-pot conversion of carbohydrates into 5-ethoxymethylfurfural and ethyl D-glucopyranoside in ethanol catalyzed by a silica supported sulfonic acid catalyst," *RSC Advances*, vol. 3, no. 30, pp. 12313–12319, 2013.

[52] B. Liu, Z. H. Zhang, and K. J. Deng, "Efficient one-pot synthesis of 5-(ethoxymethyl) furfural from fructose catalyzed by a novel solid catalyst," *Industrial & Engineering Chemistry Research*, vol. 51, no. 47, pp. 15331–15336, 2012.

[53] Z. W. Wang, H. Li, C. J. Fang, W. F. Zhao, T. T. Yang, and S. Yang, "Simply assembled acidic nanospheres for efficient production of 5-ethoxymethylfurfural from 5-hydromethylfurfural and fructose," *Energy Technology*, vol. 5, no. 11, pp. 2046–2054, 2017.

[54] A. Q. Liu, B. Liu, Y. M. Wang, R. S. Ren, and Z. H. Zhang, "Efficient one-pot synthesis of 5-ethoxymethylfurfural from fructose catalyzed by heteropolyacid supported on K-10 clay," *Fuel*, vol. 117, pp. 68–73, 2014.

[55] Z. H. Wang and Q. W. Chen, "Conversion of 5-hydroxymethylfurfural into 5-ethoxymethylfurfural and ethyl levulinate catalyzed by MOF-based heteropolyacid materials," *Green Chemistry*, vol. 18, no. 21, pp. 5884–5889, 2016.

[56] G. Z. Xu, B. L. Chen, Z. B. Zheng, K. Li, and H. G. Tao, "One-pot ethanolysis of carbohydrates to promising biofuels: 5-ethoxymethylfurfural and ethyl levulinate," *Asia-Pacific Journal of Chemical Engineering*, vol. 12, no. 4, pp. 527–535, 2017.

[57] H. Li, K. S. Govind, R. Kotni, S. Shunmugavel, A. Riisager, and S. Yang, "Direct catalytic transformation of carbohydrates into 5-ethoxymethylfurfural with acid-base bifunctional hybrid nanospheres," *Energy Conversion and Management*, vol. 88, pp. 1245–1251, 2014.

[58] H. S. Xin, T. W. Zhang, W. Z. Li et al., "Dehydration of glucose to 5-hydroxymethylfurfural and 5-ethoxymethylfurfural by combining Lewis and Brønsted acid," *RSC Advances*, vol. 7, no. 66, pp. 41546–41551, 2017.

[59] G. Raveendra, A. Rajasekhar, M. Srinivas, P. S. S. Prasad, and N. Lingaiah, "Selective etherification of hydroxymethylfurfural to biofuel additivesover Cs containing silicotungstic acid catalysts G," *Applied Catalysis A: General*, vol. 520, pp. 105–113, 2016.

[60] Z. H. Zhang, Y. M. Wang, Z. F. Fang, and B. Liu, "Synthesis of 5-ethoxymethylfurfural from fructose and inulin catalyzed by a magnetically recoverable acid catalyst," *ChemPlusChem*, vol. 79, no. 2, pp. 233–240, 2014.

[61] Z. L. Yuan, Z. H. Zhang, J. D. Zheng, and J. T. Lin, "Efficient synthesis of promising liquid fuels 5-ethoxymethylfurfural from carbohydrates," *Fuel*, vol. 150, pp. 236–242, 2015.

[62] S. S. Yin, J. Sun, B. Liu, and Z. H. Zhang, "Magnetic material grafted cross-linked imidazolium based polyionic liquids: an efficient acid catalyst for the synthesis of promising liquid fuel 5-ethoxymethylfurfural from carbohydrates," *Journal of Materials Chemistry A*, vol. 3, no. 9, pp. 4992–4999, 2015.

[63] J. M. Wang, Z. H. Zhang, S. W. Jin, and X. Z. Shen, "Efficient conversion of carbohydrates into 5-hydroxylmethylfurfan and 5-ethoxymethylfurfural over sufonic acid-functionalized mesoporous carbon catalyst," *Fuel*, vol. 192, pp. 102–107, 2017.

[64] Y. Yao, A. Gu, Y. Wang, H. J. Wang, and W. Li, "Magnetically recoverable carbonaceous material: an efficient catalyst for the synthesis of 5-hydroxymethylfurfural and 5-ethoxymethylfurfural from carbohydrates," *Russian Journal of General Chemistry*, vol. 86, no. 7, pp. 1698–1704, 2016.

[65] H. L. Wang, T. S. Deng, Y. X. Wang et al., "Graphene oxide as a facile acid catalyst for the one-pot conversion of carbohydrates into 5-ethoxymethylfurfural," *Green Chemistry*, vol. 15, no. 9, pp. 2379–2383, 2013.

[66] M. M. Antunes, P. A. Russo, P. V. Wiper et al., "Sulfonated graphene oxide as effective catalyst for conversion of 5-(hydroxymethyl)-2-furfural into biofuels," *ChemSusChem*, vol. 7, no. 3, pp. 804–812, 2014.

[67] B. Liu, Z. H. Zhang, and K. C. Huang, "Cellulose sulfuric acid as a bio-supported and recyclable solid acid catalyst for the synthesis of 5-hydroxymethylfurfural and 5-ethoxymethylfurfural from fructose," *Cellulose*, vol. 20, no. 4, pp. 2081–2089, 2013.

[68] R. S. Thombal and V. H. Jadhav, "Application of glucose derived magnetic solid acid for etherification of 5-HMF to 5-EMF, dehydration of sorbitol to isosorbide, and esterification of fatty acids," *Tetrahedron Letters*, vol. 57, no. 39, pp. 4398–4400, 2016.

[69] H. Zhu, Q. Cao, C. H. Li, and X. Mu, "Acidic resin-catalysed conversion of fructose into furan derivatives in low boiling point solvents," *Carbohydrate Research*, vol. 346, no. 13, pp. 2016–2018, 2011.

[70] G. Morales, M. Paniagua, J. A. Melero, and J. Iglesias, "Efficient production of 5-ethoxymethylfurfural from fructose by sulfonic mesostructured silica using DMSO as co-solvent," *Catalysis Today*, vol. 279, pp. 305–316, 2017.

[71] H. Li, Q. Y. Zhang, and S. Yang, "Catalytic cascade dehydration-etherification of fructose into 5-ethoxymethylfurfural with SO_3H-functionalized polymers," *International Journal of Chemical Engineering*, vol. 2014, Article ID 481627, 7 pages, 2014.

[72] G. A. Kraus and T. Guney, "A direct synthesis of 5-alkoxymethylfurfural ethers from fructose via sulfonic acid-functionalized ionic liquids," *Green Chemistry*, vol. 14, no. 6, pp. 1593–1596, 2012.

[73] S. De, S. Dutta, and B. Saha, "One-pot conversions of lignocellulosic and algal biomass into liquid fuels," *ChemSusChem*, vol. 5, no. 9, pp. 1826–1833, 2012.

[74] H. X. Guo, X. H. Qi, Y. Y. Hiraga, T. M. Aida, and R. L. Smith, "Efficient conversion of fructose into 5-ethoxymethylfurfural with hydrogen sulfate ionic liquids as co-solvent and catalyst," *Chemical Engineering Journal*, vol. 314, pp. 508–514.

[75] M. Zuo, K. Le, Y. C. Feng et al., "An effective pathway for converting carbohydrates to biofuel 5-ethoxymethylfurfural via 5-hydroxymethylfurfural with deep eutectic solvents (DESs)," *Industrial Crops and Products*, vol. 112, pp. 18–23, 2018.

[76] S. Shinde and C. Rode, "Cascade reductive etherification of bioderived aldehydes over Zr-based catalysts," *ChemSusChem*, vol. 10, no. 20, pp. 4090–4101, 2017.

[77] K. K. Yadav, S. Ahmad, and S. M. S. Chauhan, "Elucidating the role of cobalt phthalocyanine in the dehydration of carbohydrates in ionic liquids," *Journal of Molecular Catalysis A: Chemical*, vol. 394, pp. 170–176, 2014.

[78] I. Viil, A. Bredihhin, U. Mäeorgb, and L. Vares, "Preparation of potential biofuel 5-ethoxymethylfurfural and other 5-alkoxymethylfurfurals in the presence of oil shale ash," *RSC Advances*, vol. 4, no. 11, pp. 5689–5693, 2014.

[79] J. G. Pereira, S. C. A. Sousa, and C. A. Fernandes, "Direct conversion of carbohydrates into 5-ethoxymethylfurfural (EMF) and 5-hydroxymethylfurfural (HMF) catalyzed by oxomolybdenum complexes," *ChemistrySelect*, vol. 2, no. 16, pp. 4516–4521, 2017.

[80] B. Kim, J. Jeong, S. Shin et al., "Facile single-step conversion of macroalgal polymeric carbohydrates into biofuels," *ChemSusChem*, vol. 3, no. 11, pp. 1273–1275, 2010.

[81] R. J. Grisel, J. C. van der Waal, E. de Jong, and W. J. Huijgen, "Acid catalysed alcoholysis of wheat straw: towards second generation furan-derivatives," *Catalysis Today*, vol. 223, pp. 3–10, 2014.

[82] A. I. Torres, P. Daoutidis, and M. Tsapatsis, "Continuous production of 5-hydroxymethylfurfural from fructose: a design case study," *Energy & Environmental Science*, vol. 3, no. 10, pp. 1560–1572, 2010.

[83] Y. Román-Leshkov, J. N. Chheda, and J. A. Dumesic, "Phase modifiers promote efficient production of hydroxymethylfurfural from fructose," *Science*, vol. 312, no. 5782, pp. 1933–1937, 2006.

Hindawi
International Journal of Chemical Engineering
Volume 2018, Article ID 7452817, 7 pages
https://doi.org/10.1155/2018/7452817

Research Article

Synthesis of a New Copper-Based Supramolecular Catalyst and Its Catalytic Performance for Biodiesel Production

Fei Chang,[1] **Chen Yan**,[2] **and Quan Zhou**[3]

[1]*Institute of Comprehensive Utilization of Plant Resources, Kaili University, Kaili 556011, China*
[2]*An Shun City People's Hospital, People's Hospital Republic of China, An Shun 561000, China*
[3]*Pharmaceutical and Bioengineering College, Hunan Chemical Vocational Technology College, Zhuzhou, Hunan 412000, China*

Correspondence should be addressed to Fei Chang; feichang1980@126.com

Received 6 August 2018; Revised 8 October 2018; Accepted 21 October 2018; Published 2 December 2018

Guest Editor: Shunmugavel Saravanamurugan

A new copper-based supramolecular (β-cyclodextrins, β-CD) catalyst was synthesized and used for transesterification of *Xanthium sibiricum* Patr oil to biodiesel. This catalyst exhibited high activity (88.63% FAME yield) in transesterification under the ratio of methanol-oil: 40 : 1; catalyst dosage: 8 wt.%; reaction temperature: 120°C; and reaction time: 9 h. The XRD, SEM, TEM, XPS, and BET characterization results showed that Cu-β-CD catalyst was amorphous and had clear mesoporous structure (17.2 nm) as compared with the native β-CD. This phenomenon is attributed to the coordination of Cu and β-CD.

1. Introduction

With the rapid socioeconomic development, the demand for petrochemical energy is on the increase. At the same time, the shortage of energy and environmental pollution have become the focus [1, 2]. Biodiesel is a good substitute for petrochemical diesel because of its sustainability, biodegradability, and cleanability [3]. Biodiesel, also known as fatty acid monoester, mainly including fatty acid methyl esters (FAME) and fatty acid ethyl esters (FAEE), is typically prepared via esterification or transesterification reactions of animal and vegetable oils with methanol or ethanol in the presence of an acidic and/or basic catalyst [4]. The reaction processes can be divided into homogeneous and heterogeneous ones depending on the type of catalysts, and researchers are more inclined to heterogeneous research for its advantages such as simple steps, easy postprocessing, and less pollution [5, 6]. Heterogeneous catalysts mainly include inorganic acid salts, solid heteropoly acids, metal oxides [7, 8], zeolites [9], and hydrotalcites [10]. Among them, the single and mixed metal oxides were studied by numerous studies due to their environment-friendly, cheap, and efficient catalytic characteristics, which were generally prepared by coprecipitation, sol-gel, impregnation, and hydrothermal methods [11]. In particular, the metal oxides composed of Ca, Mg, and Al were extensively illustrated to be active for biodiesel production [12–14]. However, Cu-based catalysts used for efficient biodiesel preparation have been rarely reported so far.

In this report, a new Cu-based supramolecular catalyst was prepared from $CuSO_4{\cdot}5H_2O$ and β-CD by simple organic synthesis and was applied to biodiesel synthesis. The results showed that the catalyst had obvious mesoporous structure and good catalytic activity. The results of this study fill the gaps of copper-based catalysts for biodiesel production.

2. Experiments

2.1. Materials. *Xanthium sibiricum* Patr oil was extracted with the reported method [15]. Pure fatty acid methyl esters were purchased from Sigma (USA). β-CD was purchased from Hongchang Pharmaceutical Reagent Co., Ltd., Xi'an. Anhydrous methanol, NaOH, and $CuSO_4{\cdot}5H_2O$ are analytically pure (AR) and purchased from Chemical Reagent Co., Ltd., Tianjin.

2.2. Catalyst Preparation. According to previous reports [16, 17], 2.5 g β-CD and 0.8 g NaOH were dissolved into 50 mL distilled water and stirred to completely dissolve at room temperature, and then 50 mL aqueous solution of 0.5 g $CuSO_4 \cdot 5H_2O$ was gradually added at room temperature under magnetic stirring for 1.5 h and filtered. Upon completion, 500 mL ethanol was added to the filtrate, and a precipitate formed, which was filtered and washed with absolute ethanol to give a neutral precipitate. The attained solid was further dried at 80°C for 5 h.

2.3. Catalyst Characterization. TGA analysis was recorded by NETZSCH STA 429 instrument. XRD patterns were measured with the Bruker D8 advanced X-ray diffractometer (XRD) with Cu Kα radiation (λ = 0.154 nm) at 40 kV and 30 mA with a step size of 0.02. The surface morphologies of the catalysts were characterized via FEI inspect F50 type scanning electron microscope (SEM). The internal structure of catalysts was analyzed by the FEI Tecnai G2 F20 S-TWIN 200 kV transmission electron microscope (TEM). XPS analysis was conducted using the Thermo Scientific ESCALAB 250Xi spectrometer employing a monochromatic Al Kα X-ray source (hν = 1486.8 eV) and 500 μm test spot area, 15 kv test tube voltage, 10 mA tube current, and 2×10^{-9} mbar analysis room floor vacuum. The Brunauer–Emmett–Teller (BET) surface areas were measured by N_2 adsorption/desorption apparatus (Micromeritics ASAP 2020), and the pore size and pore volume distributions were calculated using the Barrett–Joyner–Halenda (BJH) model.

2.4. Product Analysis. The appropriate amount of *X. sibiricum* Patr oil, catalyst, and methanol were added into a 25 mL glass three-necked flask with a condensing means and placed in a an oil bath (120°C) with magnetic stirring for a certain time. After the reaction completion, the reaction mixture was cooled down and filtered, while the excess methanol was removed by rotary evaporation. Hereafter, the FAME contents of the samples were determined by the gas chromatography (GC, Agilent 6890 GC), and the FAME contents were calculated according to the methods reported in [18].

3. Results and Discussions

3.1. Catalyst Characterization

3.1.1. TGA Analysis. The TGA analysis results of the Cu-β-CD catalyst are shown in Figure 1. It can be seen that the weight loss of the Cu-β-CD catalyst mainly included three stages, namely, loss of water (50–150°C), catalyst decomposition (150–300°C), and complete decomposition of the catalyst (300–800°C). Evidently, this catalyst was stable until the temperature of around 150°C.

3.1.2. XRD. Usually, the catalytic activity is closely related to the morphology of the catalyst. The catalytic effect of the amorphous material was generally better than the crystal

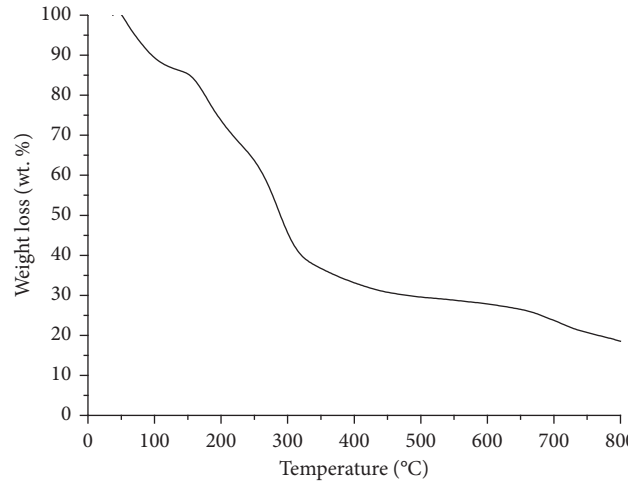

Figure 1: TGA curves of Cu-β-CD catalyst.

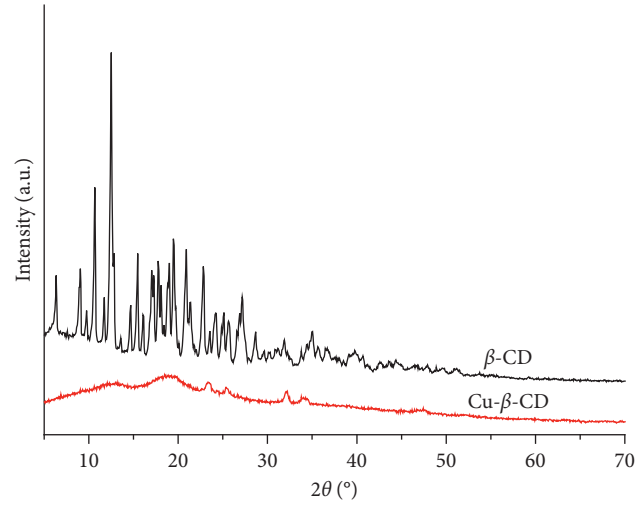

Figure 2: XRD patterns of pure β-CD and Cu-β-CD catalyst.

counterpart [19, 20]. XRD patterns of β-CD and Cu-β-CD are shown in Figure 2, it could be clearly seen that the single β-CD had distinct diffraction peaks, belonging to crystal state material. However, Cu-β-CD did not show significant diffraction peaks but appeared as wave packets. So, the structures were greatly changed when the copper ions were involved, which changed its morphology and increased its specific surface area (Figures 3–5), while improving its catalytic activity. This is consistent with the experimental results (Table 1).

3.1.3. XPS. The valence of copper ions and structure of the complex were determined by XPS spectra (Figure 6). As can be seen from Figures 6(a) and 6(b), Cu ions existed in the Cu-β-CD catalyst. C1s might be divided into three signals in Figure 6(a), namely, C-C (284.7 eV), C-O (286.4 eV), and C=O (287.9 eV), respectively. In addition, it can be seen from Figure 6(b) that the Cu's basic binding energy was 933.3 ev (Cu2p3/2) and 953.6 ev (Cu2p1/2). Therefore, Cu^{2+},

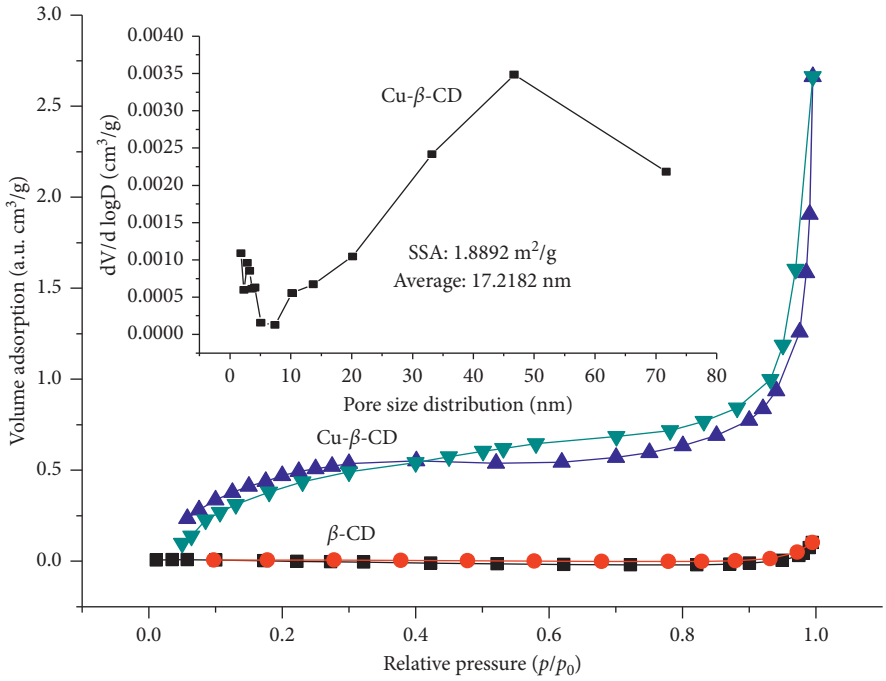

Figure 3: N_2 adsorption-desorption isotherms and pore size distribution of β-CD and Cu-β-CD.

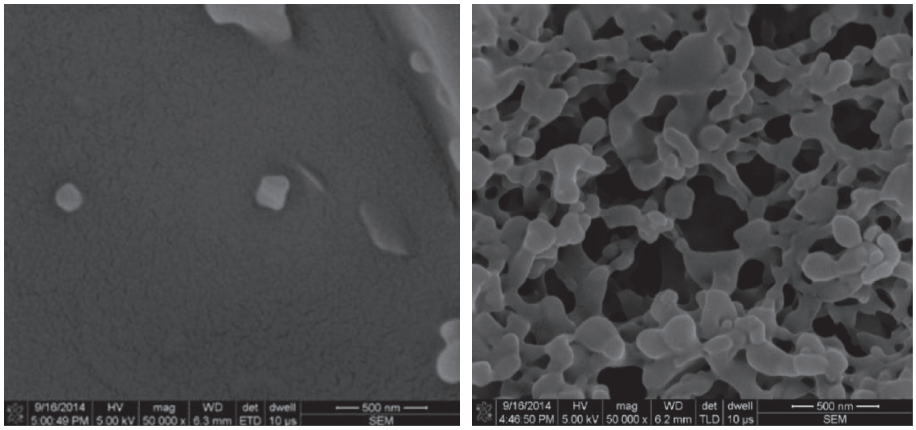

Figure 4: SEM images of pure (a) β-CD and (b) Cu-β-CD catalysts.

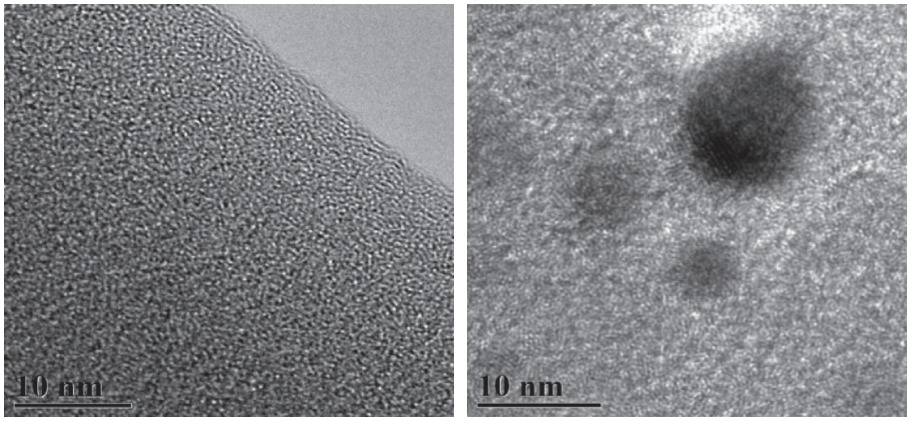

Figure 5: TEM images of pure (a) β-CD and (b) Cu-β-CD samples.

Table 1: The catalytic activity of the catalysts.

Entry	Catalyst	FAME%
1	β-CD (native)	nd
2	$Cu(SO_4)_2{\cdot}5H_2O$	nd
3	$Cu(SO_4)_2{\cdot}5H_2O$+β-CD (simple physical mixture)[a]	nd
4		
5	CuO	nd
6	Cu-β-CD	88.6

Condition of reaction: the ratio of methanol-oil: 40 : 1; the amount of catalyst: 8 wt.%; reaction temperature: 120°C; reaction time: 9 h; [a]physical mixing; nd: not detected; FAME%: the data of biodiesel production percentages.

copper, is predominantly present in this complex, and coordination compounds were formed such as $CuCO_3$ and CuO. For this study, it can be deduced that a similar C-O-Cu bond existed in the Cu-β-CD catalyst. This is consistent with previous reports [21, 22] and FT-IR (Figure 1, supporting information (available here).

3.1.4. N_2 Adsorption-Desorption Isotherm. The specific surface area (SSA) and pore size are also the main factors that affect the activity of the catalyst. So, SSA and pore size distribution of the β-CD and Cu-β-CD were studied via N_2 adsorption-desorption isotherm and calculated by BET and BJH methods, respectively. As can be seen from Figure 3, β-CD did not display apparent hysteresis loops, but hysteresis ring closure point of the Cu-β-CD appeared at p/p_0 = 0.4. In addition, the dramatic increase trend in the high-pressure section indicated that it belongs to the type IV isotherms and type H4 hysteresis ring [22, 23]. These results demonstrated that β-CD had no distribution of pores and the Cu-β-CD possessed slit hole formed by multilayer structure, and its average pore size is 17.2 nm. Those were consistent with SEM and TEM studies. Apart from this, the SSA of Cu-β-CD catalyst was 1.9 m^2/g, which is much larger than that of β-CD (0.1 m^2/g) [24].

3.1.5. SEM and TEM. The morphology of the catalyst is typically correlated to its activity directly [25]. In order to understand the structure of Cu-β-CD, the catalyst was characterized by SEM and TEM, and the results are shown in Figures 4 and 5. The surface of native β-CD is smooth (Figure 4), and the obvious pore structure cannot be observed (Figure 5), but the Cu-β-CD showed multihole structure and heterogeneous mesoporous structure (Figure 4). Furthermore, a uniform worm-like duct structure of the Cu-β-CD was also observed (Figure 5). So, it can be concluded that the Cu-β-CD is a porous mesoporous material, and it can be inferred that Cu-β-CD catalyst has a larger specific surface area (SSA) than β-CD, which was confirmed by the BET test results. As we all know, the catalyst with porous mesoporous structures, small particles, and large SSA can improve the activity of the catalyst [26, 27], and the Cu-β-CD should have a high catalytic activity. Accordingly, the results of catalytic performance of the catalysts are shown in Table 1.

3.2. Catalytic Performance of the Catalysts. Catalytic performance of the relevant catalysts is shown in Table 1 (supporting information). As can be seen from Table 1, β-CD (native), $Cu(SO_4)_2{\cdot}5H_2O$, $Cu(SO_4)_2{\cdot}5H_2O$+β-CD (simple physical mixture), and CuO did not show catalytic activity (Table 1, entries 1–5). In contrast, the Cu-β-CD showed a higher activity (FAME yield: 88.6%, Table 1, entry 6) under 40 : 1 methanol-oil ratio, 8 wt.% catalyst load, 120°C reaction temperature, and 9 h reaction time. In combination with the relevant card results that can be determined its catalytic activity, it can be deduced that the superior activity of Cu-β-CD is mainly due to the Cu^{2+} and β-CD which formed the Cu-OH bonds, and the Cu^{2+} may act as electrophilic species to activate ester. Furthermore, the Cu-OH bonds act as nucleophilic species to attack the carbon of the ester, and two synergies may weaken the ester bond and make $-OCH_3$ attack ester bonds easily [17].

3.3. Effect of Single Factor on the FAME Content. In order to optimize the biodiesel catalytic process of the Cu-β-CD, reaction temperature, methanol/oil molar ratio, catalyst loading, and reaction time were studied, respectively. The results are shown in Figure 7, and in most chemical reactions, reaction temperature is one of the most important parameters. The choice of temperature has a direct effect on the reaction rate and product yield. As can be seen from Figure 7(a), the FAME content is only 20% at 65°C, but it increased with the increase of temperature. When the temperature reached 120°C, the maximum yield is obtained, while continuing to increase the temperature to 140°C leads to no change in the FAME. Figure 7(b) shows the effect of the molar ratio of methanol to oil in the reaction system. When the methanol-oil molar ratio is 10 : 1–50 : 1, it is proportional to the yield of FAME. As the methanol-oil molar ratio is 40 : 1 and 50 : 1, the yield of FAME was 88.39% and 89.11%, respectively. It can be considered that the increase of the ratio of methanol-oil yields of FAME can be neglected. Taking into account the catalyst concentration and cost, the methanol-oil molar ratio need not be further increased; therefore, the optimal molar ratio of methanol to oil is 40 : 1 in this reaction. Such a high molar ratio of methanol to oil is related to the characteristic of β-CD having alcoholicity [28]. The catalyst is the most critical factor in transesterification, and Figure 7(c) shows the yield of FAME under 2 wt.%–8 wt.% catalyst; the content of FAME is lowest with 2 wt.% catalyst amount, and with the increase of the amount of catalyst, the yield of FAME also increases. The yield of FAME reached its maximum when increasing to 8 wt.%. Therefore, the optimal catalyst loading should be chosen to be 8 wt.% for the cost problem. The reaction time is also a key factor affecting the reaction result. The impact of reaction time on the yield of FAME is shown in Figure 7(d). It can be seen from the Figure 7(d) that the conversion rate of FAME reached the maximum after 9 h. This shows that 88.63% FAME conversion was received under the optimized reaction conditions of 40 : 1 molar

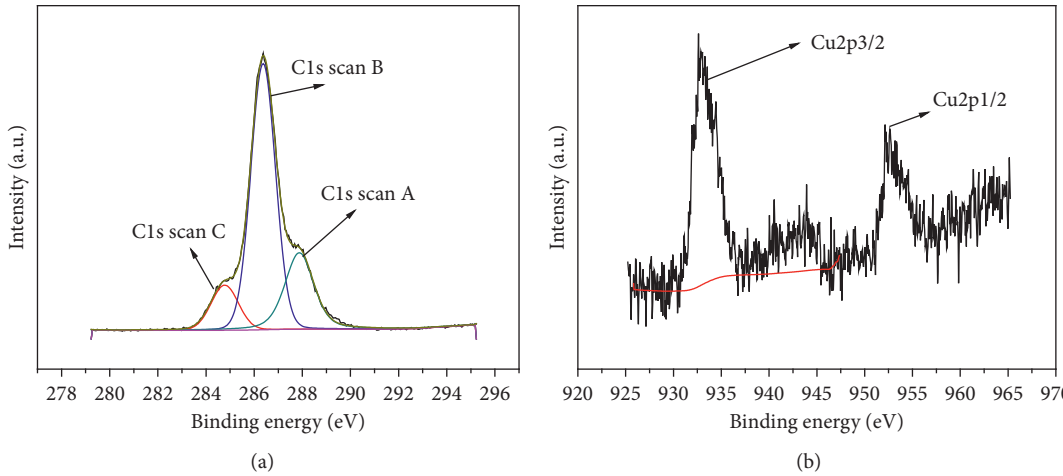

Figure 6: The XPS spectra of Cu-β-CD catalyst.

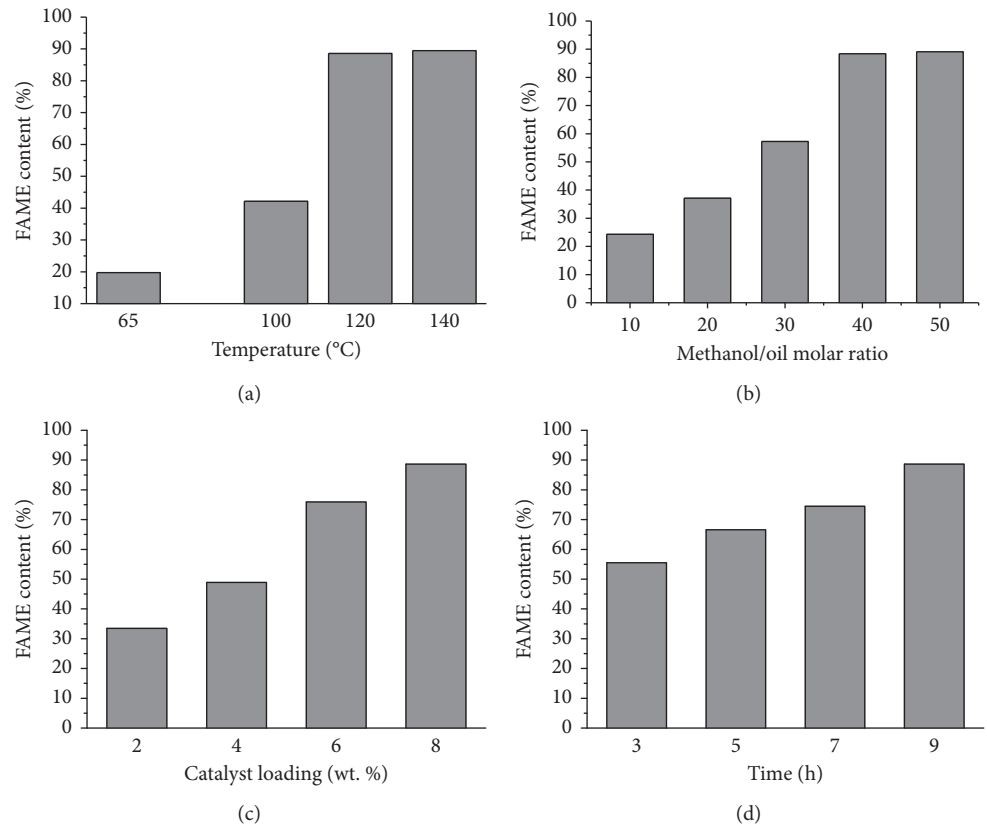

Figure 7: The effect of single factor on the FAME content. (a) Effect of temperature on FAME content (methanol/oil molar ratio = 40 : 1, CA = 8 wt.%, t = 9 h). (b) Effect of methanol/oil molar ratio on FAME content (CA = 8 wt.%, T = 120°C, t = 9 h). (c) Effect of catalyst loading on FAME content (methanol/oil molar ratio = 40 : 1, T = 120°C, t = 9 h). (d) Effect of time on FAME content (methanol/oil molar ratio = 40:1, T = 120°C, CA = 8 wt.%).

ratio of methanol/oil, 8 wt.% Cu-β-CD amount, 120°C, and 9 h.

Overall, Cu-β-CD was stable until around 150°C, which was a mesoporous material having a large SSA (1.8892 m^2/g) compared with β-CD (0.11 m^2/g), and its activity lies in the synergy of β-CD and copper.

4. Conclusions

The Cu-β-CD was prepared by a simple method, which was found to be a kind of uniform worm-like duct and porous mesoporous structured material. It was successfully applied to biodiesel production, giving 88.63% FAME conversion

under optimal conditions. This study further demonstrated that Cu^{2+} and β-CD in the catalyst played a synergistic catalytic role, greatly improving the activity of Cu-based catalyst in transesterification.

Data Availability

The data used to support the findings of this study are available from the corresponding author upon request.

Disclosure

Fei Chang and Chen Yan contributed equally to this work.

Conflicts of Interest

The authors declare that they have no conflicts of interest.

Acknowledgments

This work was financially supported by Guizhou Provincial State University S&T Technology Joint Fund Program (nos. LH[2015]7762 and LH [2015]7752).

Supplementary Materials

FT-IR of β-CD and Cu-β-CD is shown in Figure 1; it could be seen that peaks of the single β-CD and Cu-β-CD did not show significant change, and it is obvious that the Cu-β-CD retains the structure of the β-CD. But, there are obvious differences in 800–400 cm^{-1} and 1600–1200 cm^{-1}; these changes may be caused by the Cu-OH of Cu and cyclodextrin [1–3]. (*Supplementary Materials*)

References

[1] Y. He, S. Wang, and K. K. Lai, "Global economic activity and crude oil prices: a cointegration analysis," *Energy Economics*, vol. 32, no. 4, pp. 868–876, 2010.

[2] S. N. Dodić, S. D. Popov, J. M. Dodić, J. A. Ranković, and Z. Z. Zavargo, "Biomass energy in Vojvodina: market conditions, environment and food security," *Renewable and Sustainable Energy Reviews*, vol. 14, no. 2, pp. 862–867, 2010.

[3] M. Balat, "Production of bioethanol from lignocellulosic materials via the biochemical pathway: a review," *Energy Conversion and Management*, vol. 52, no. 2, pp. 858–875, 2011.

[4] A. D. Lele, K. Anand, and K. Narayanaswamy, *Surrogates for Biodiesel: Review and Challenges*, Springer, Singapore, 2017.

[5] M. R. Avhad and J. M. Marchetti, "A review on recent advancement in catalytic materials for biodiesel production," *Renewable and Sustainable Energy Reviews*, vol. 50, pp. 696–718, 2015.

[6] H. H. Mardhiah, H. C. Ong, H. H. Masjuki, S. Lim, and H. V. Lee, "A review on latest developments and future prospects of heterogeneous catalyst in biodiesel production from non-edible oils," *Renewable and Sustainable Energy Reviews*, vol. 67, pp. 1225–1236, 2017.

[7] F. Chang, Q. Zhou, H. Pan et al., "Solid mixed-metal-oxide catalysts for biodiesel production: a review," *Energy Technology*, vol. 2, no. 11, pp. 865–873, 2014.

[8] N. F. Balsamo, K. Sapag, M. I. Oliva, G. A. Pecchi, G. A. Eimer, and M. E. Crivello, "Mixed oxides tuned with alkaline metals to improve glycerolysis for sustainable biodiesel production," *Catalysis Today*, vol. 279, no. 2, pp. 209–216, 2017.

[9] S. Manadee, O. Sophiphun, N. Osakoo et al., "Identification of potassium phase in catalysts supported on zeolite NaX and performance in transesterification of *Jatropha* seed oil," *Fuel Processing Technology*, vol. 156, pp. 62–67, 2017.

[10] K. G. Georgogianni, A. K. Katsoulidis, P. J. Pomonis, G. Manos, and M. G. Kontominas, "Transesterification of rapeseed oil for the production of biodiesel using homogeneous and heterogeneous catalysis," *Fuel Processing Technology*, vol. 90, no. 7-8, pp. 1016–1022, 2009.

[11] H. V. Lee, J. C. Juan, T. Y. Yun Hin, and H. C. Ong, "Environment-friendly heterogeneous alkaline-based mixed metal oxide catalysts for biodiesel production," *Energies*, vol. 9, no. 8, p. 611, 2016.

[12] G. Tao, Z. Hua, Z. Gao, Y. Zhu, Y. Z. Chen, and J. Shi, "KF-loaded mesoporous Mg-Fe bi-metal oxides: high performance transesterification catalysts for biodiesel production," *Chemical Communications*, vol. 49, no. 73, pp. 8006–8008, 2013.

[13] J. R. Mercury, A. H. De Aza, and P. Pena, "Synthesis of $CaAl_2O_4$ from powders: particle size effect," *Journal of the European Ceramic Society*, vol. 25, no. 14, pp. 3269–3279, 2005.

[14] V. Mandić and S. Kurajica, "The influence of solvents on sol–gel derived calcium aluminate," *Materials Science in Semiconductor Processing*, vol. 38, pp. 306–313, 2015.

[15] F. Chang, M. A. Hanna, D. J. Zhang et al., "Production of biodiesel from non-edible herbaceous vegetable oil: *Xanthium sibiricum* Patr," *Bioresource Technology*, vol. 140, pp. 435–438, 2013.

[16] Y. Matsui, T. Kurita, M. Yagi, T. Okayama, K. Mochida, and Y. Date, "The formation and structure of Copper (II) complexes with cyclodextrins in an alkaline solution," *Bulletin of the Chemical Society of Japan*, vol. 48, no. 7, pp. 2187–2191, 1975.

[17] F. Chang, Q. Zhou, H. Pan, X. F. Liu, H. Zhang, and S. Yang, "Efficient production of biodiesel from Xanthium sibiricum Patr oil via supramolecular catalysis," *Renewable Energy*, vol. 111, pp. 556–560, 2017.

[18] H. Pan, X. F. Liu, H. Zhang, K. Yang, S. Huang, and S. Yang, "Multi-SO_3H functionalized mesoporous polymeric acid catalyst for biodiesel production and fructose-to-biodiesel additive conversion," *Renewable Energy*, vol. 107, pp. 245–252, 2017.

[19] L. M. Correia, R. M. A. Saboya, N. de Sousa Campelo et al., "Characterization of calcium oxide catalysts from natural sources and their application in the transesterification of sunflower oil," *Bioresource Technology*, vol. 151, pp. 207–213, 2014.

[20] W. Suryaputra, I. Winata, N. Indraswati, and S. Ismadji, "Waste capiz (Amusium cristatum) shell as a new heterogeneous catalyst for biodiesel production," *Renewable Energy*, vol. 50, pp. 795–799, 2013.

[21] E. Norkus, G. Grincienė, T. Vuorinen, E. Butkus, and R. Vaitkus, "Stability of a dinuclear Cu(II)–β-Cyclodextrin complex," *Supramolecular Chemistry*, vol. 15, no. 6, pp. 425–431, 2003.

[22] E. Norkus, G. Grincienė, T. Vuorinen, and R. Vaitkus, "Cu(II) ion complexation by excess of β-cyclodextrin in aqueous alkaline solutions," *Journal of Inclusion Phenomena*, vol. 48, no. 3-4, pp. 147–150, 2004.

[23] Y. Chen, Y. Cao, Y. Suo, G. P. Zheng, X. X. Guan, and X. C. Zheng, "Mesoporous solid acid catalysts of 12-tungstosilicic acid anchored to SBA-15: characterization and catalytic properties for esterification of oleic acid with methanol," *Journal of the Taiwan Institute of Chemical Engineers*, vol. 51, pp. 186–192, 2015.

[24] Y. Luo, Z. Mei, N. Liu, H. Wang, C. Han, and S. He, "Synthesis of mesoporous sulfated zirconia nanoparticles with high surface area and their applies for biodiesel production as effective catalysts," *Catalysis Today*, vol. 298, pp. 99–108, 2017.

[25] Y. H. Taufiq-Yap, H. V. Lee, M. Z. Hussein, and R. Yunus, "Calcium-based mixed oxide catalysts for methanolysis of *Jatropha* curcas oil to biodiesel," *Biomass and Bioenergy*, vol. 35, no. 2, pp. 827–834, 2011.

[26] Z. Helwani, M. R. Othman, N. Aziz, W. J. N. Fernando, and J. Kim, "Technologies for production of biodiesel focusing on green catalytic techniques: a review," *Fuel Processing Technology*, vol. 90, no. 12, pp. 1502–1514, 2009.

[27] D. Y. C. Leung, X. Wu, and M. K. H. Leung, "A review on biodiesel production using catalyzed transesterification," *Applied Energy*, vol. 87, no. 4, pp. 1083–1095, 2010.

[28] A. Buvari, J. Szejtli, and L. Barcza, "Complexes of short-chain alcohols with β-cyclodextrin," *Journal of Inclusion Phenomena*, vol. 1, no. 2, pp. 151–157, 1983.

Hindawi
International Journal of Chemical Engineering
Volume 2018, Article ID 7617685, 18 pages
https://doi.org/10.1155/2018/7617685

Review Article

Chemocatalytic Production of Lactates from Biomass-Derived Sugars

Heng Zhang,[1,2] Yulin Hu,[2] Liying Qi,[2] Jian He,[1] Hu Li,[1] and Song Yang[1]

[1]*State Key Laboratory Breeding Base of Green Pesticide & Agricultural Bioengineering, Key Laboratory of Green Pesticide & Agricultural Bioengineering, Ministry of Education, State-Local Joint Laboratory for Comprehensive Utilization of Biomass, Center for Research & Development of Fine Chemicals, Guizhou University, Guiyang, Guizhou 550025, China*
[2]*Institute for Chemicals and Fuels from Alternative Resources (ICFAR), Department of Chemical and Biochemical Engineering, Western University, London, Ontario, Canada, N6A 5B9*

Correspondence should be addressed to Hu Li; hli13@gzu.edu.cn and Song Yang; jhzx.msm@gmail.com

Received 31 July 2018; Accepted 22 October 2018; Published 13 November 2018

Academic Editor: Iftekhar A. Karimi

In recent decades, a great deal of attention has been paid to the exploration of alternative and sustainable resources to produce biofuels and valuable chemicals, with aims of reducing the reliance on depleting confined fossil resources and alleviating serious economic and environmental issues. In line with this, lignocellulosic biomass-derived lactic acid (LA, 2-hydroxypropanoic acid), to be identified as an important biomass-derived commodity chemical, has found wide applications in food, pharmaceuticals, and cosmetics. In spite of the current fermentation of saccharides to produce lactic acid, sustainability issues such as environmental impact and high cost derived from the relative separation and purification process will be growing with the increasing demands of necessary orders. Alternatively, chemocatalytic approaches to manufacture LA from biomass (i.e., inedible cellulose) have attracted extensive attention, which may give rise to higher productivity and lower costs related to product work-up. This work presents a review of the state-of-the-art for the production of LA using homogeneous, heterogeneous acid, and base catalysts, from sugars and real biomass like rice straw, respectively. Furthermore, the corresponding bio-based esters lactate which could serve as green solvents, produced from biomass with chemocatalysis, is also discussed. Advantages of heterogeneous catalytic reaction systems are emphasized. Guidance is suggested to improve the catalytic performance of heterogeneous catalysts for the production of LA.

1. Introduction

Due to the burgeoning world population, demands for energy and chemicals are sharply increasing. Therefore, traditional nonrenewable fossil resources, particularly coal and petroleum, are going to be run out, and their concomitantly environmental and climatological impacts are also urgently needed to be addressed in the meantime [1–4]. With regards to this, alternatively manners to transform renewable, sustainable, and carbon-neutral biomass resources from plants into potential biofuels, polymer building blocks, and value-added chemicals are widely researched. Carbohydrates, the largest fraction of biomass, are being deemed as the main feedstocks in the biorefineries that will derive platform molecules to be served as precursors to the chemical industry [5–8]. In addition, cellulose, composed of glucose units, is recognized as the single most abundant organic compound on Earth, which can be upgraded to glucose and subsequently converted into value-added chemical molecules [9]. Taking the predicted energy demands (30–60 TW in 2050) into account, cellulosic biomass shows the large potential (supply approximately 30 TW) towards satisfying the energy demand of mankind [10]. Consequently, efficiently selective conversion of cellulosic biomass into valuable chemicals as well as biofuels and materials is highly preferable [11–13].

Lactic acid (LA, 2-hydroxypropanoic acid), one of the great appeals among carbohydrate-derived platform

molecules, is an important feedstock for the production of alkyl lactates, biodegradable plastics such as polylactic acid (PLA), and other valuable chemicals under suitable reaction conditions in the assistance of catalytic functionalities. Specially, PLA polymer bearing the advantages of biodegradability, compostability, and biocompatibility could be utilized in a wide range of applications such as eco-friendly packages. In addition, carbon neutral balance is accepted when PLA is disposed to release CO_2 and water. LA was firstly found in 1780 by the Swedish chemist Scheele in acid milk [14, 15]. In spite of its late discovery, LA has found widespread applications in the food industry, and the commercialization of LA-based biopolymers is also of high interest currently [16]. In addition, alkyl lactates (methyl lactate (ML), and ethyl lactate (EL)), important versatile platform chemicals, have also attracted much attention because of their extensive applications including that in nontoxic and biodegradable green solvents, that in plasticizers for cellulose plastics and vinyl resins [17], and being environmental, recyclable, noncorrosive, and economic [18].

It is estimated that LA demand in 2020 will be above 600000 tons [7]. Currently, commercial LA production is manufactured through anaerobic fermentation method (over 90%), showing some merits such as low production temperature, low energy consumption, and high purity via an appropriate strain [19, 20], as illustrated in Scheme 1. Typically, 4 main steps should be processed for the production of LA by traditional fermentation when starting from cellulosic biomass, including (1) pretreatment of feedstocks, (2) anaerobic fermentation, (3) acidulation, and (4) separation and purification of LA. However, the low productivity, need for high price enzymes (strict pH and temperature), and complicated separation along with purification requirements are always accompanied, accordingly. As a consequence, sustainability issues regarding the up-scaling of the present fermentation process are highly required to be disposed via a promising alternative method, chemocatalysis, which could be regarded as the research hotspot in the state-of-the-art development of lactic acid research.

Chemical catalysis (homogeneous or heterogeneous), being considered to be the formidable strategy to transform cellulosic biomass into value-added chemicals with acceptable selectivity, is rising progressively [21]. In particular, in a platform approach, chemocatalysts are playing a vital role in the fundamental and novel production routes of lactic acid (or lactates), using sugars even real lignocellulosic biomass (i.e., cornstalk). However, the chemical production of lactic acid (or esters) generally leads to racemic mixtures, which is not an issue when compounds such as acrylic acid, 2,3-pentanedione, etc. are target compounds to be produced. However, chirality control is very important if lactide (industrial building block of PLA) production is the target as this will determine the properties of the polymer. Chromatographic methods [22, 23], chemical resolution [24] and the combination of the chemo- and biocatalysis [25] are regarded as the means for chiral resolution of racemic lactic acid. Nonetheless, enantioselective chemoproduction of lactic acid from sugars directly has not been reported.

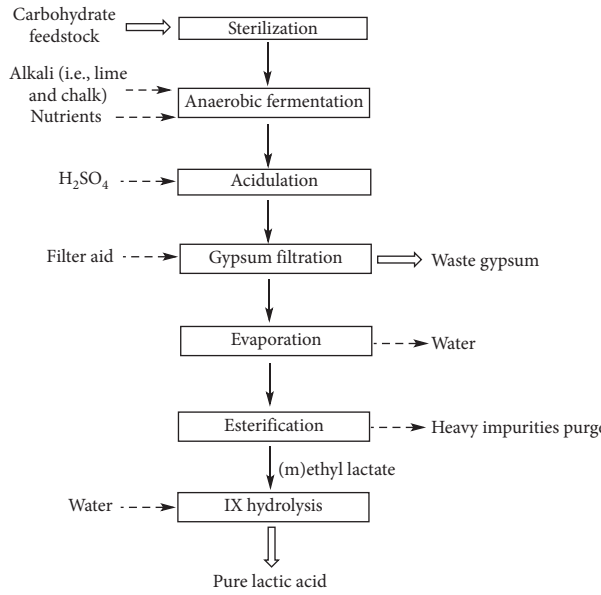

Scheme 1: Conventional fermentative method for producing LA.

Currently, many research groups are employing the chemocatalysts to synthesize lactic acid (in water) or lactates (alcoholic solvents). The main emphasis of this review is to depict the state-of-the-art development of LA or lactates production from sugars and real lignocellulosic biomass resources, with chemocatalysis especially heterogeneously catalysts which have tremendous advantages (i.e., recyclable, reusable, and environmentally benign). Furthermore, structure-function relationships, reaction mechanisms, and guidance on designing heterogeneous acid catalysts for LA or lactates production are also discussed, accordingly.

2. Chemocatalytic Production of LA

2.1. Alkaline Catalytic Manners for LA. The hydrothermal process, one of the most potential approaches, is used in the conversion of biomass into valuable resources, since water can serve as a reaction medium bearing special properties when treated in the high temperature and pressure [26]. With respect to the issue of catalytic transformation of biomass into LA with the hydrothermal process using alkaline catalysts, Jin research group made many valuable contributions to this research theme [26–34]. Initially, they demonstrated that glycolaldehyde, an aldose with two carbon atoms, usually produced via reverse aldol condensation of C_6 sugars, can also generate LA with 28% yield using 0.75 M·NaOH basic catalyst (300°C, 10 min) [26]. After then, they employed glucose as the substrate to produce LA with moderate yield employing NaOH and $Ca(OH)_2$ as the alkaline catalyst, respectively (Table 1, Entry 2). It is worth noting that, on the basis of the viewpoint of economy, $Ca(OH)_2$ was regarded to be more suitable than NaOH [27]. Interestingly, in order to enhance the market values of glycerin, biodiesel byproduct, Jin et al. attempted to convert glycerin into LA under alkali-catalyzed hydrothermal conditions and some valuable results were obtained [28]. After

Table 1: Catalytic transformation of lactic acid from different feedstocks by alkaline.

Entry	Substrate	Catalyst	Reaction conditions	Yield of LA (%)	Reference
1	Glycolaldehyde	NaOH	300°C, 10 min	28.1	[26]
2	Glucose	NaOH	300°C, 1 min	27	[27]
		$Ca(OH)_2$	300°C, 1 min	20	
3	Glycerin	KOH	300°C, 80 min	90	[28]
4	Glucose	NaOH	300°C, 1 min	27	[29]
	Glucose	$Ca(OH)_2$	300°C, 1 min	20	
	Cellulose	$Ca(OH)_2$	300°C, 90 s	19.2	
	Starch	$Ca(OH)_2$	300°C, 90 s	18.7	
5	Cellulose	NaOH + Ni	300°C, 1 min	34.1	[30]
6	Glucose	NaOH + CuO	188°C, 0.15 min	59	[31]
7	Cellulose	NaOH + Zn/Ni/C	300°C, 5 min	42	[32]
8	Glucose	NaOH + $NiCl_2$	300°C, 1 min	25	[33]
9	Glucose	Na_2SiO_3	300°C, 1 min	30	[34]
10	D-Glucose	Hydrotalcite	50°C, 8 h	20.3	[35]
11	D-Glucose	KOH/Al_2O_3 Microwave	180°C, microwave 3.1 $W \cdot g^{-1}$, 40 min	75	[36]
	D-Mannose			41	
	D-Fructose			36	
	D-Ribose			43	
	D-Arabinose			35	
	D-Sucrose			23	
12	Hydroxyacetone	$Pt/MgO\text{-}Al_2O_3\text{-}800$	40°C, 6 h	100 (selectivity)	[37]
13	Glucose	[IMEP]Cl, NaOH	100°C, 30 min, N_2	63	[38]
		[IMEP]Cl, KOH		65.5	
14	Glucose	$Ba(OH)_2$	250°C, 3 min	57	[39]
15	Glucose	$Ba(OH)_2$	Ball milling (solvent-free)	35.6	[40]
16	Glucose	$Ba(OH)_2$	25°C, 48 h	95.4	[41]
	Fructose			83.5	
17	Corn cobs	$Ca(OH)_2$	300°C, 30 min	44.76	[42]
18	Bread residues	$Ca(OH)_2$	300°C, 30 min	73	[43]
19	Rice straw	NaOH, NiO nanoplates	260°C, 2 h	58.81	[44]
20	Alginate	CaO	200°C, 6 h	14.66	[45]

screening the alkali-metal hydroxides and alkaline-earth-metal hydroxides, they presented that KOH exhibited the best activity with 90% yield, using the lower concentration or a shorter reaction time (Table 1, Entry 3). Generally, to clearly present the reaction mechanism is very important to understand the targeted reaction process, to some extent. To our satisfaction, Jin et al. conjectured the mechanism (Figure 1) with regard to converting glucose into LA under alkaline hydrothermal reaction with more economic catalyst $Ca(OH)_2$. To be specific, Ca^{2+} is a divalent cation, whose radius is determined to be larger than that of Na^+. Consequently, Ca^{2+} was believed to be easier to combine with two O atoms, to form complexes than Na^+. These complexes are likely to facilitate the C_3-C_4 bond breaking via reverse aldol condensation. In addition, they also proposed the reaction pathway of glucose transformation to LA under alkaline hydrothermal reaction conditions (Figure 2). Notably, nearly 20% yield of LA could be also obtained using cellulose and starch substrates, respectively [29].

To keep up Jin group's works concerning the conversion of carbohydrates biomass into LA, they added Ni as co-catalyst in the LA production started from cellulose under hydrothermal conditions with NaOH [30]. However, the reaction mechanism was not clearly presented. After then, they conducted a detailed study with respect to converting glucose into LA using 0.01 M·Ni^{2+}, 0.01 M·NaOH as

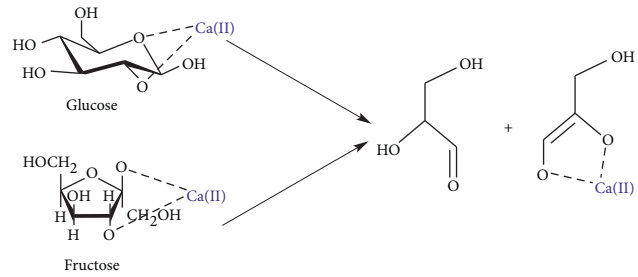

Figure 1: Proposed retro-aldol of glucose and fructose by complexation with Ca^{2+}.

cocatalysts, with 35% water filling at 300°C for 1 min, generating 25% LA yield, accordingly [33]. Most importantly, the detailed reaction mechanism was also clearly demonstrated. To be specific, (1) coordination with Ni^{2+}, (2) nucleophilic attack by OH^-, (3) retro-aldolization, (4) Lobry de Bruyn Alberda van Ekenstein (LBAE) to form double bond, (5) elimination of water, and (6) benzilic acid rearrangement were determined as the main 6 steps during this process. Accordingly, glyceraldehyde was demonstrated to be the key intermediate. Some other interesting works of Jin group regarding the production of LA from biomass are also demonstrated here in Table 1 [31, 32, 34]. It is noteworthy that the low-cost and highly active basic catalyst Na_2SiO_3,

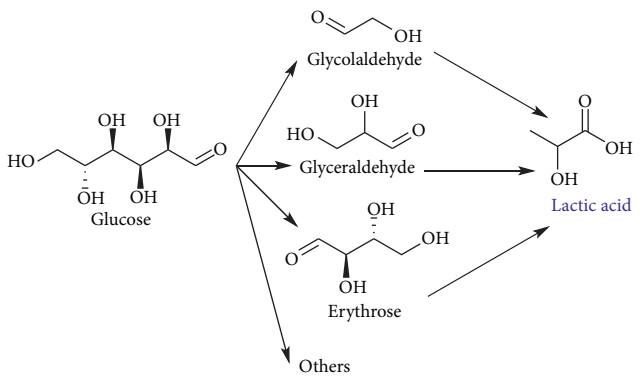

Figure 2: Proposed pathway of formation of LA from glucose by alkaline hydrothermal reaction.

acted as a mild catalyst to address the corrosion issue was researched in detail, giving 30% LA yield [34].

As mentioned above, solid alkaline catalyst bearing low corrosiveness seems to be a better choice, when employed in the production of LA under hydrothermal process. In this regard, versatile activated hydrotalcites were utilized as alkaline catalysts to convert glucose in a flow reactor into LA, giving 20.3% LA yield at 50°C [35]. The results indicated that hydrotalcite (Mg/Al = 2) activated at 723 K contained the most Brønsted-base sites, and a linear increase was determined with respect to LA yield and accessible Brønsted-base sites. Similarly, with slight modifications, Albuquerque et al. employed dual metal/base catalyst systems (Pt-Mg-Al hydrotalcite) to converting hydroxyacetone to LA, under oxidative aqueous-phase reaction conditions [37]. The highly remarkable 100% selectivity to LA with the bifunctional catalysts was determined, which was believed to be based on the proximity of metal and basic centers along with hindering the side reaction of LA to pyruvic acid. Surprisingly, Epane et al. found that microwave as an effective and environmentally friendly means could also make a contribution to the production of LA from saccharides, under solvent-free conditions which was deemed to be within the green chemistry concept [36]. On the basis of the presence of KOH/Al_2O_3 and microwave, high 75% LA yield could be obtained from glucose without solvent, as presented in Table 1, Entry 11.

Unfortunately, the aforementioned hydrothermal process almost adopted relatively high reaction temperatures (i.e., 300°C), thus limiting their promising industrial applications to some extent. For the sake of overcoming this challenge, Wang et al. used the polymeric catalyst (polymerization of imidazole and epichlorohydrin, [IMEP]Cl) as weak Lewis acid along with NaOH/KOH to transform glucose into LA [38]. Several parameters including the base, [IMEP]Cl loading, reaction temperature, and atmosphere were investigated in detail to determine the best reaction conditions. A high 63% LA yield could be obtained from glucose along with a low 62.66 $kJ \cdot mol^{-1}$ activation energy, even only at 100°C for 30 min under N_2. The key reaction mechanism was also studied, and the rate determining step was also determined to be dihydroxyacetone (DHA) to pyruvic aldehyde (PAL), accordingly. The detailed mechanism regarding DHA to PAL involved the coordination of active hydrogens of [IMEP]Cl with the electronegative oxygens on trioses, followed by keto-enol tautomerism through a 1,2-hydride shift to produce LA.

In spite of the LA production using $Ba(OH)_2$ investigated by Jin group before, Esposito and Antonietti also researched the LA manufactured from glucose with $Ba(OH)_2$ in detail [39]. Interestingly, differing from Jin et al.'s results, LA yields up to 57% could be gained within 3 min at 250°C. In connection with the interesting work employing $Ba(OH)_2$ as the basic catalyst in the production of LA from biomass, Qi research group presented two interesting and valuable results (Table 1, Entry 15 and 16). Without harsh conditions is the key innovation point regarding their research works to transform biomass to LA. The first attempt is to use a mechanochemical ball milling method, employing glucose feedstock and $Ba(OH)_2$, giving 35.6% LA yield after 6 h [40]. Valuably, Li et al. reported an effective method to quantitatively converting sugars into LA only at room temperature under a N_2 atmosphere, wherein 95.4% LA yield could be determined from glucose at room temperature for 48 h under 1 bar N_2 [41]. In addition, based on their experimental results, they also proposed the reaction mechanism (Figure 3). To be specific, in addition to the common isomerization and retro-aldol fragmentation, $Ba(OH)_2$ may form the important barium lactate complex via Path II, followed by converting to lactic acid with the addition of H_2SO_4 aqueous solution. The anaerobic environment was determined to play the vital role in hindering the oxidation of glyceraldehyde (GLY) and DHA or other intermediates, into side products according to the detailed results.

As discussed above, sugars can be transformed into LA with acceptable yield under alkaline hydrothermal process. Nonetheless, LA production directly from real biomass is highly more commended without hesitation. As shown in Table 1, corn cobs and bread residues could be treated as the potential feedstocks for the production of LA, giving 44.76% and 73% LA yield using $Ca(OH)_2$, respectively [42, 43]. Furthermore, China's most abundant agricultural waste, rice straw, was also converted into LA of 58.81% yield at 260°C for 2 h, using 1 M·NaOH and 0.052 g NiO nanoplates as cocatalysts [44]. It is noteworthy that marine biomass, considered to be the third-generation promising renewable biomass feedstock, could also be transformed into LA with hydrothermal technique [46, 47]. Starting from alginate biomass, 14.66% LA yield was determined at 200°C for 6 h, using CaO as a solid basic catalyst [45]. The detailed reaction mechanism is illustrated in Figure 4. As investigated according to their experimental results, the hydration of CaO to $Ca(OH)_2$ in an aqueous medium, generating Brønsted bases (OH^-), is the key point during the reaction. Different from Reference [38], they believed that PAL to LA is the rate-determining step wherein CaO could enhance the LA yield from PAL, by benzylic acid Rearrangement.

2.2. LA Production via Acid Catalysis. As discussed above, with the addition of alkaline catalysts especially under hydrothermal reaction conditions, LA could be produced with

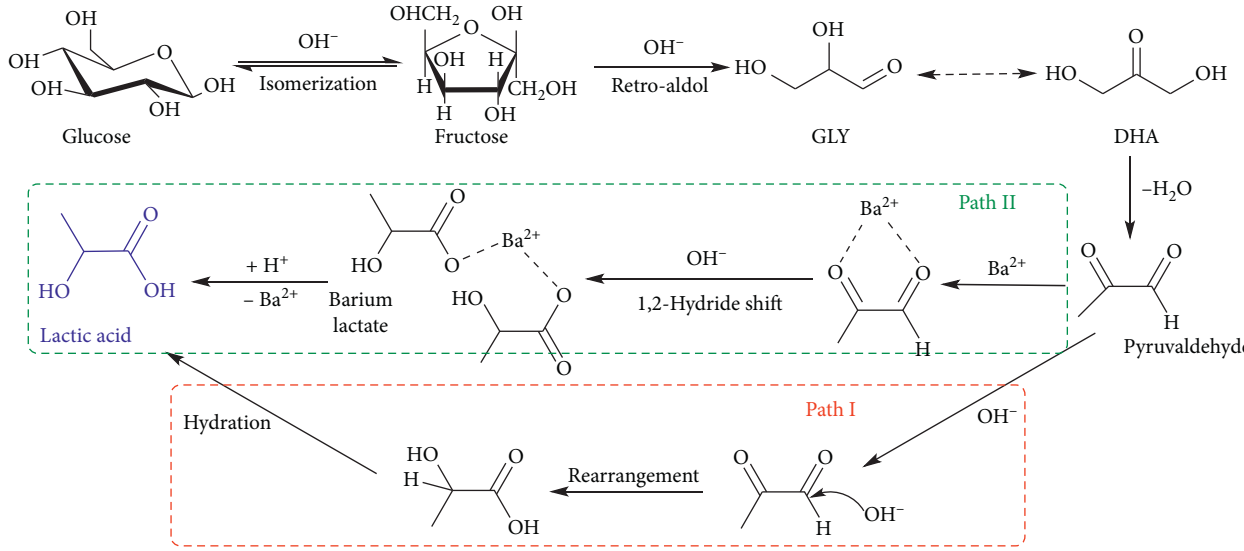

Figure 3: Proposed pathway for the conversion of glucose to lactic acid with the base at room temperature under nitrogen (Path I general base catalyst route; Path II: $Ba(OH)_2$ catalytic-complex route).

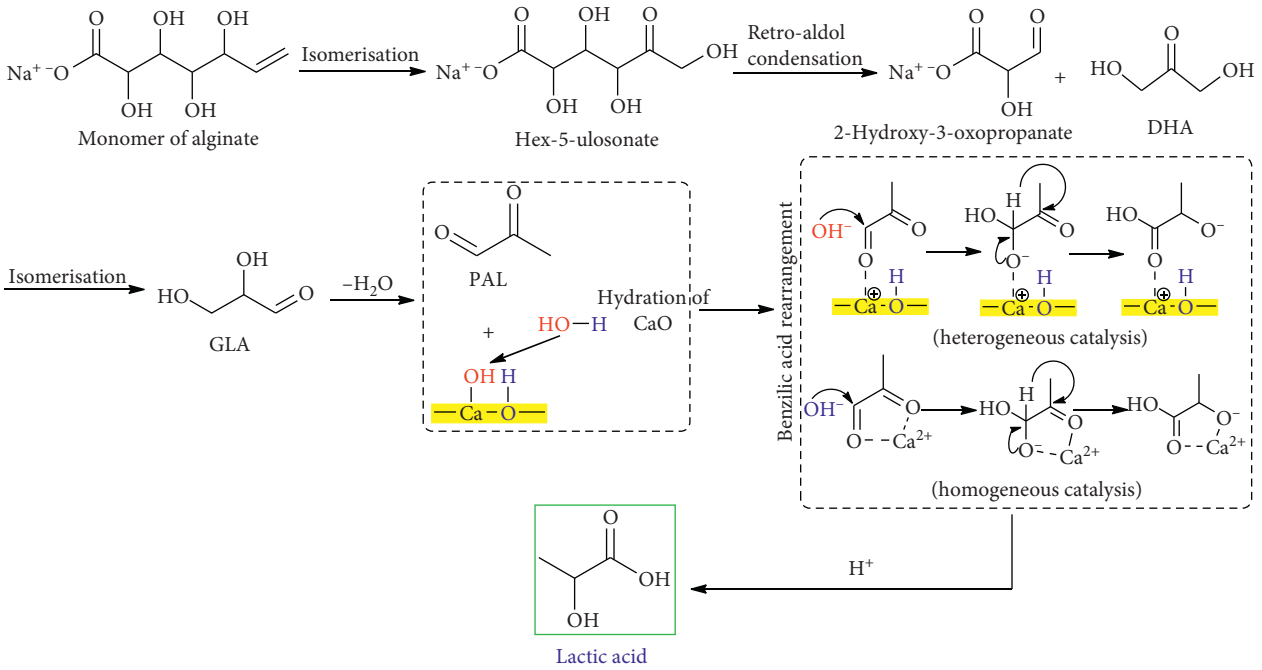

Figure 4: Proposed reaction pathway for catalytic hydrothermal conversion of sodium alginate into lactic acid with hydrated CaO catalyst.

relatively acceptable yield, to some extent. However, acid solution was always needed to employ to neutralize the base, along with hydrolysis the possible lactates to acquire the final product, pure LA. Therefore, acidic catalysts appear to be a better choice to be used in the production of LA and lactates, starting from different types of feedstocks (i.e., C_6, C_3 sugars, and so on), through several specific catalytic reactions. Specifically, Lewis acidic sites are regarded as the key role in the transformation of LA or lactates from different carbohydrates even cellulose. In addition, from the environmental point of view, heterogeneously acidic catalysts which are less corrosive and can be recycled from the products for reutilization are the main discussed objects regarding the LA preparation in the following two parts, accordingly.

2.2.1. Trisaccharides to LA. DHA or GLY is being deemed as the key intermediate with respect to transforming saccharides into LA. As a consequence, illuminating the LA production directly from simply C_3 sugars is important to further understand the reaction of converting C_6 and cellulose to LA. Generally, 100 (DHA) and 120 (GLA) kJ/mol are demanded to be energetically favored, in order to be

isomerized to LA [48]. It is widely believed that DHA/GLY to LA include two steps: (1) DHA is transformed into PAL through the successive keto-enol tautomerization and dehydration [26, 49], catalyzed by both Lewis and Brønsted acids [50, 51]; (2) rehydration of PAL followed by 1,2-hydride shift produces LA wherein Lewis acids are regarded to perform better than Brønsted acids [49, 50, 52]. Some homogeneous catalysts including H_2SO_4 [53], $CrCl_3{\cdot}6H_2O$ [54], $ZnSO_4$ [55], $AlCl_3{\cdot}6H_2O$ [54, 56], $SnCl_2$ [54, 57], and $SnCl_4{\cdot}6H_2O$ [54] have been studied in DHA into LA and its esters. For instance, Rasrendra et al. investigated the 26 metal salts towards LA preparation from DHA in detail, and they found that Al^{III} salts were determined to be the most active, quantitatively with 93% LA yield at 140°C for 90 min [50]. In addition, the detailed reaction pathway was also proposed based on the experimental results, as shown in Figure 5 which is similar to the 2 steps as discussed above. However, they did not explain why Al^{III} salts performed the best and why other metals were less active. The good news is, to continue the interesting work, Jolimaitre et al. [58] investigated the detailed reaction mechanism regarding the best performance of Al^{III} salts for the conversion of DHA into LA, as inspired by the valuable work of commercial OLI Systems (OLI Systems Stream Analyzer Software, OLI Systems, 2012) [59]. According to the thermodynamic analysis and kinetic studies, hydrolysis of aluminium aqua complexes such as $[Al(OH_2)_6]^{3+}$ to form the most active Lewis acids, namely, cationic hydroxyl-aluminium complexes $[Al(OH)_h]^{(3-h)+}$, are believed to be the key active Lewis acidic sites towards PAL into LA.

It is worth noting that during the bioprocessing of biomass upgrading, tunable acidic, thermal stable, and shape-selective zeolites materials are considered to be the most promising heterogeneously solid acidic catalysts with superior catalytic performance [60]. With respect to the transformation of DHA to LA, zeolites as efficient catalysts have also been reported [51, 57, 61, 62]. Taarning et al. firstly used several Lewis-acidic zeolites in the production of LA from DHA and Sn-Beta was found to be highly selective for the isomerization of trioses to LA [51]. In addition, based on Corma's research with respect to NMR evidence [63], the real catalytically active site is determined as the partially hydrolyzed framework tin species. On the basis of Taarning's valuable works, some other interesting studies regarding the LA formation from C_3-sugars using zeolites, such as the H-USY [57], the MFI [61], and the hierarchical tin zeolite with micromesoporous structure [62] were also proposed and investigated for the production of LA from C_3 sugars. Lewis acidic sites are believed to be the key role with regards to isomerization of trioses to LA, along with weak Brønsted acids. After then, based on the excellent reactivity of tin, Wang et al. designed the surfactant-modified SnP catalyst for the isomerization of DHA to LA, and poly (ethylene glycol) (PEG) was found to be the most potential, along with 96.1% LA yield at 140°C for 4 h [63]. Recently, Nakajima et al. presented an interesting study regarding the efficient production of LA from DHA, using Nb_2O_5 with an orthorhombic structure and a high surface area (208 m^2/g) [64]. Thanks to its high water-tolerant Lewis acid sites (0.21 mmol/g) and Brønsted acid sites (0.10 mmol/g), nearly 80% LA yield could be achieved at 100°C within 3 h. As identified in this research, the high density of water-compatible Lewis acid sites should be believed to play the crucial role in the isomerization of PAL to LA (the rate-determining step for the conversion of DHA to LA).

2.2.2. Hexaose to LA. As a consensus, effective LA production from hexoses is more preferable compared to C_3 sugars. In a similar manner, the novel well-aligned Nb_2O_5 nanorod owning highly single crystallinity was also designed to produce LA from glucose [65]. A promising LA yield of 39% could be achieved along with a good reusability among the 4 successive processes. However, Sn-based catalysts have been studied and found to exhibit satisfied reactivity for LA production as presented above. Therefore, to find the modified Sn-based catalysts is a good choice with respect to LA production, accordingly. As illustrated in Table 2 (Entry 2–4), Sn(IV)-based organometallic complexes [66], Zn-Sn-Beta Lewis acid-base catalyst [67], and Pb-Sn-Beta catalyst [68] were investigated in detail to prepare LA from fructose, sucrose, and glucose, respectively. Acceptable LA yields could be obtained using the aforementioned catalysts and Sn species bearing the good Lewis acid character was believed to play the key role regarding the formation of LA step. Nonetheless, leaching of metals was found to lead to the poor reusability.

In addition to these functional materials aforementioned for LA transformation from hexoses, Huang et al. employed the solid Lewis acidic material (Table 2, Entry 5), MIL-100 (Fe), a metal-organic frameworks (MOFs) material with outstanding advantages such as large surface area, extrahigh porosity, highly thermal and chemical stability, and so on [69, 86–88]. 32% LA yield could be reached with MIL-100 (Fe), and the catalytic activities were found to be affected by the framework's metal, surface area, and Lewis acid properties, accordingly. In addition, the MIL-100(Fe) could be reused among 4 successive recycles with a simple dispose. Nevertheless, very few studies researched LA production directly from cellulosic biomass, due to the complexity of biomass structures (i.e., cellulose, hemicellulose, and lignin), along with the catalyst deactivation induced by lignin [89]. Interestingly, Liu et al. presented a valuable work regarding LA production directly from lignocellulosic sugars including levoglucosan, glucose, and xylose with good yields [70]. Using a Lewis acid catalyst, $La(OTf)_3$ which is stable in both aqueous and organic solvent, 61% LA yield for C_5 sugars and >70% LA yield from C_6 sugars could be obtained. On the basis of their studies, two efficient methods including fast pyrolysis combined with retro-aldol condensation of pyrolytic sugars, and ionic liquid pretreatment combined with retro-aldol condensation of the sugar-rich fraction, could be demonstrated to impart significant meaning on biorefinery of lignocellulosic biomass.

2.2.3. Cellulose to LA. The direct transformation of cellulose being the main component of lignocellulosic biomass into valuable chemicals such as LA is highly desired in making

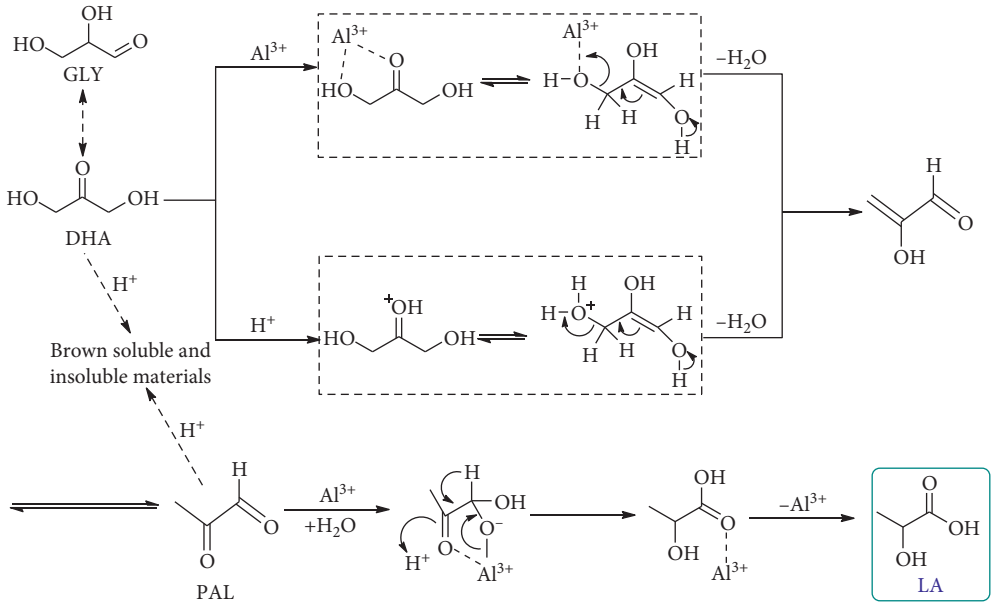

Figure 5: Proposed reaction pathway for converting C_3 sugars to LA in aqueous with Al^{III} salts catalyst.

Table 2: Catalytic transformation of lactic acid from C_6 sugars and cellulose by acids.

Entry	Substrate	Catalyst	Reaction conditions	Yield of LA (%)	Reference
1	Glucose	Nb_2O_5 nanorod	250°C, 4 h	39	[65]
2	Fructose	Sn(IV) organometallic complexes	190°C, 0.5 h	63	[66]
3	Sucrose	Zn-Sn-Beta	190°C, 2 h	54	[67]
4	Glucose	Pb-Sn-Beta	190°C, 2 h	52	[68]
5	Fructose	MIL-100 (Fe)	190°C, 2 h	32	[69]
	Levoglucosan			75	
6	Glucose	$La(OTf)_3$	250°C, 1 h	74	[70]
	Xylose			61	
7	Cellulose	AlW	190°C, 24 h	28	[71]
		ZrW		19	
8	Cellulose	ZrW	190°C, 24 h	3 g/L^{-1}	[72]
	Pine wood sawdust		190°C, 8 h	1.2 g/L^{-1}	
9	Xylose	ZrO_2	200°C, 40 min	42	[73]
	Xylan		200°C, 90 min	30	
10	Cellulose	ZrO_2 (monoclinic)	200°C, 6 h	21.2	[74]
11	Cellulose	$10\%ZrO_2$-Al_2O_3	200°C, 6 h	25.3	[75]
12	Cellulose	$Er(OTf)_3$	240°C, 30 min	89.6	[76]
13	Cellulose	$ErCl_3$	240°C, 30 min	91.1	[77]
14	Cellulose	Er-K10	240°C, 30 min	67.6	[78]
15	Cellulose	Er/deAlβ-zeolite	240°C, 30 min	58	[79]
16	Cellulose	$Pb(NO_3)_2$	190°C, 2 h	71	[80]
17	Cellulose	$VOSO_4$	180°C, 2 h	54	[81]
	Fructose		190°C, 2 h	90	
18	Glucose	$AlCl_3$ + $SnCl_2$	180°C, 2 h	81	[82]
	Cellulose		190°C, 2 h	65	
19	Cellulose	NbF_5-AlF_3	180°C, 2 h	27.3	[83]
20	Cellulose	Nb@CaF_2	180°C, 2 h	15.4	[84]
	Xylose		200°C, 1 h	38	
21	Glucose	$LaCoO_3$ perovskite	200°C, 1 h	40	[85]
	Cellulose		240°C, 1 h	24	

important contributions to biomass-based renewable biorefinery [90]. To be deemed as a pioneer, Chambon et al. investigated the solid Lewis acids, AlW and ZrW, in the direct transformation of cellulose into LA along with a general yield (Table 2, Entry 7) of 28% and 19%, respectively [71]. As derived from the research, the positive synergy between water autoprotolysis and solid Lewis acidic catalyst surface were determined as the key role in directly producing LA from crystalline cellulose. The former function was found to depolymerize cellulose to soluble

intermediates, and LA could be produced by the AlW and ZrW Lewis acids from the soluble intermediates. After then, to continue this interesting work, further study was investigated in detail regarding the direct transformation of raw pine-wood sawdust biomass into LA using ZrW Lewis acid [72]. The advantage of the utilization of real raw biomass instead of isolated cellulose for the production of biochemicals is to avoid costly fractionation processes. Interestingly, based on the LA production of kinetic studies of model cellulose and pine-wood sawdust, lignin/hemicellulose present in raw wood biomass was believed to not hinder the function of ZrW for conversion of LA, which is contrary to general expectations. However, solid Lewis ZrW was determined to deactivate among the two reaction kinds. In spite of this, on the basis of their studies, direct transformation of raw cellulosic biomass into biochemicals such as LA comes to be feasible. Hemicellulosic biomass (xylose or xylan) was also investigated to be converted into LA, using a commercial ZrO_2 catalyst in the pH neutral aqueous solvents [73]. LA yield of 42% and 30% from xylose and xylan, respectively, could be achieved under the optimized reaction conditions, while negligible LA yield was obtained in the absence of ZrO_2. A detailed reaction mechanism regarding the formation of LA from xylose was also studied. Acidic-basic bifunctionality of ZrO_2 was determined to be the key role in LA formation from xylose. To be specific, the carbonyl group of xylose interacts with the Zr^{4+}Lewis acidic site, and the O^{2-} anion on the ZrO_2 surface as weak base adsorbs onto the OH group [91–93]. After then, Zr^{4+}Lewis acidic site activates the carbonyl group of PAL followed by the nucleophilic attack of OH^- from water autodissociation. However, an environmental-friendly method for the production of LA from hemicellulosic biomass in the aqueous catalytic process presents a promising way to transform hemicellulosic biomass. In a similar manner, Wattanapaphawong et al. studied the ZrO_2-based catalysts (Table 2, Entry 10-11) to produce LA from cellulose directly, giving acceptable yield [74, 75]. However, ZrO_2-Al_2O_3 catalysts bearing more Lewis acid sites and far fewer base sites compared to ZrO_2 exhibit a higher LA yield. This suggests that Lewis acid sites played a more important role in producing LA than base sites [75].

In fact, the yield of LA is not very high when using the aforementioned catalysts from cellulose. With respect to this regard, Wang et al. designed the erbium- (Er-) based Lewis acid catalyst for the production of LA directly from cellulose, along with high yields (Table 2, Entry 12–15). Initially, they investigated lanthanide triflates catalysts to prepare LA from cellulose, and $Er(OTf)_3$ was determined to be the best choice with 89.6% LA yield under optimized reaction conditions [76]. In addition, $Er(OTf)_3$ could be recycled and exhibited similar LA yields in up to five consecutive reutilizations. After then, they continued to use $ErCl_3$ as an efficient Lewis acidic catalyst for the production of LA from cellulose, and a 91.1% high LA yield could be achieved [77]. Similarly, $ErCl_3$ was also determined to be stable among the course of the five catalytic runs. To some extent, this simple and environmental-friendly means is of great importance regarding the economical LA production, from lignocellulosic biomass in large-scale applications, importantly, inspired by the remarkable reactivity of Er^{3+} with regard to LA production from cellulose, and heterogeneous catalysis is playing the more and more role in biomass conversion. Combined with the commercially available and cheap montmorillonite K10 clay bearing many advantages such as significant cation-exchange ability, erbium-exchanged montmorillonite K10 clay catalysts were prepared and investigated in the LA production from cellulose [78]. However, to be served as a heterogeneous catalyst, a high LA yield of 67.6% could be obtained under optimized reaction conditions. Unfortunately, LA yield decreased to some extent during recycling study, and erbium metals leaching along with carbon cokes deposition were believed as the main reasons. Recently, Er/deAlβ-zeolite prepared by the same group was also examined for LA production from cellulose, and acceptable LA yield could be also obtained. Encouragingly, a better reusability was determined than Er-K10 [79].

In addition to Dong group, Wang et al. also researched the LA production from cellulose with a high yield using Lewis metal inorganic salts, and detailed reaction mechanism was also demonstrated (Table 2, Entry 16–18). Their pioneering work regarding the LA preparation with 71% yield by the addition of dilute Pb^{2+} ions could be achieved at 190°C in 2 h [80], which was milder than Dong's studies. More importantly, detailed theoretical (cluster-continuum model) and experimental studies were introduced to determine the reaction pathway, wherein Pb^{2+} in combination with water played the key role in isomerization of glucose (cellulose hydrolysis products) to fructose, cleavage of the C_3-C_4 bond of fructose into trioses, and the transformation of trioses to LA. Nonetheless, the toxicity of Pb^{2+} must be taken into account prior to the practical application on the basis of the interesting study. Furthermore, how to efficiently separate and recover the Pb^{2+} without increasing the process cost is also needed to be addressed. After then, to continue their research, a cheaper and less toxic vanadium salt, $VOSO_4$, was found to perform well in both LA or formic acid production from cellulose by simply shifting the reaction atmosphere from N_2 to O_2 [81]. They suggested that under anaerobic conditions, VO^{2+} could catalyze the isomerization of glucose to fructose, the retro-aldol fragmentation of fructose to C_3 sugars, and the isomerization of C_3 sugars into LA. However, to convert cellulose into LA using a more environmental-friendly catalytic system is being highly demanded. With respect to this regard, Wang et al. found that the combination of Al(III) and Sn(II) cations could be served as an efficient and less-corrosive catalyst for the transformation of LA directly from cellulose [82]. Under the optimized conditions, high LA yields could be achieved, accordingly (Table 2, Entry 18). More importantly, on the basis of experimental and computational studies, the detailed reaction pathway (Figure 6) and mechanism (Figure 7) were proposed. It was found that Al(III) was primarily responsible for isomerization of glucose into fructose by 1,2-hydride shift and the conversion of C_3 intermediates into lactic acid, whereas Sn(II) took effect on the retro-aldol fragmentation. On the basis of their valuable studies,

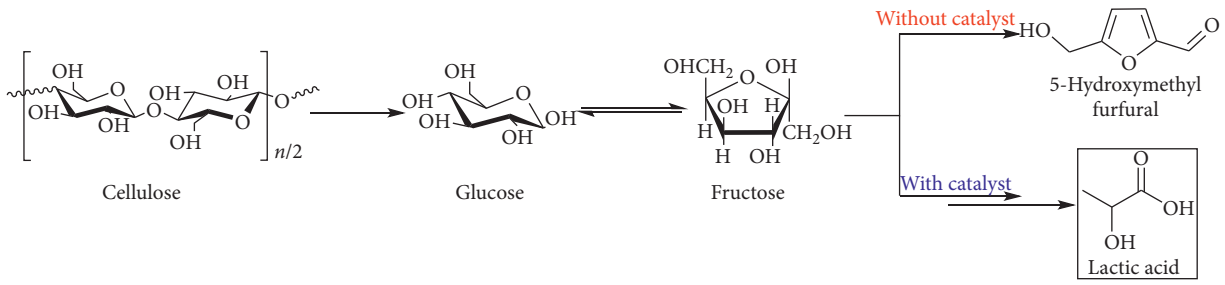

Figure 6: Proposed reaction pathways of the transformation of cellulose in the presence and absence of Al(III)-Sn(II) catalyst.

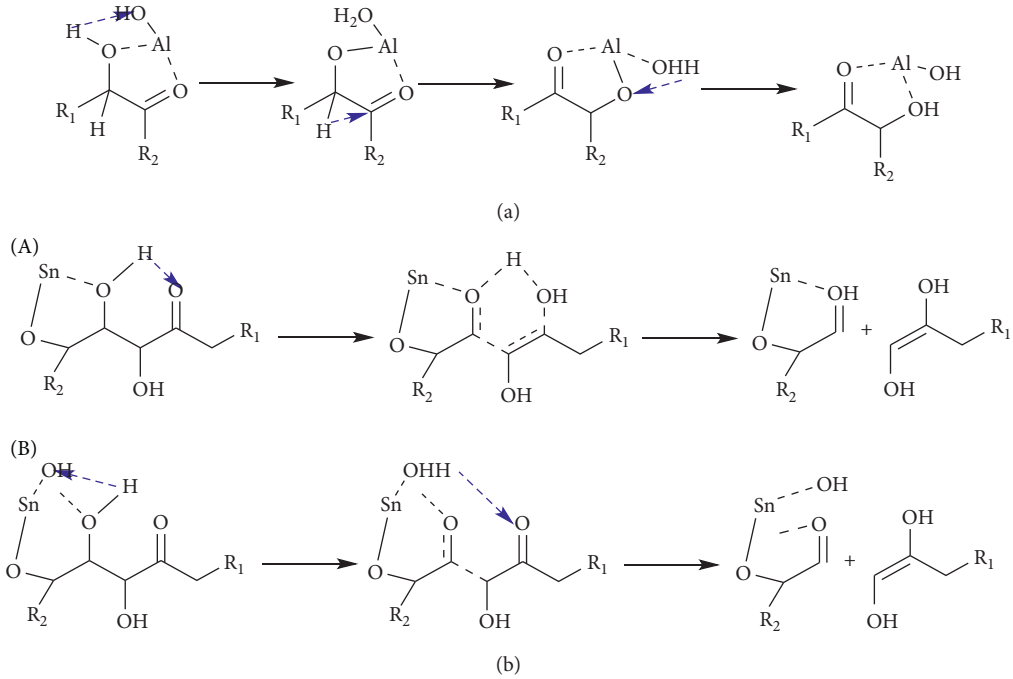

Figure 7: Proposed reaction mechanism of the isomerization and retro-aldol fragmentation with Al(III)-Sn(II) catalyst.

designing the suitable catalysts coupling of multifunctional sites for the chemical reactions with high selectivity, especially biomass transformations which contain complex tandem elementary steps may be feasible to some extent.

As shown above, niobium-based catalysts can catalyze C_3 and C_6 sugars into LA (Section 2.2.1). Therefore, employing niobium-based catalysts to convert cellulose into LA may be feasible. Coman et al. fabricated the Nb-based inorganic fluorides catalysts, NbF_5-AlF_3 and Nb@CaF_2 containing both Brønsted and Lewis acid sites, for the effective one-pot conversion of cellulose into LA, in the aqueous reaction phase [83, 84]. Nb(V)/Nb(IV) species were determined as the key active sites with respect to the mainly tandem steps including glucose isomerization into fructose, fructose retro-aldol condensation, and the triose isomerization to LA. However, solid Lewis acids and bases have been proven to be effective for LA preparation from sugars, utilization of the interesting redox catalysts, and relevant reaction mechanism is barely understood. As for this, Yang et al. demonstrated an important work using $LaCoO_3$ perovskite metal oxides to produce LA, and the detailed reaction mechanism regarding redox properties of $LaCoO_3$ was presented clearly (Figure 8) [85]. Unlike traditional Lewis acid or base catalysis, as illustrated in Figure 8, the redox pathway started from the oxidative decarboxylation of aldose sugars and the lattice oxygen atoms participated in the redox cycles. Firstly, glucose was oxidized into gluconic acid; secondly, gluconic acid took oxidative decarboxylation to form xylose; thirdly, xylose repeated the oxidation step to transform into xylonic acid followed by oxidative decarboxylation to produce C4 aldose and which would be oxidized to hydroxybutyric acid; fourthly, dehydration happened at elevated temperatures to form pyruvic acid; fifthly, through the reduced perovskite structure, $LaCoO_{2.5}$, pyruvic acid was finally reduced to target product LA.

3. Production of Alkyl Lactates

Bio-based methyl/ethyl lactates (ML, EL), nontoxic liquids owning high boiling points, are being served as the potential value-added compounds with a high extent of functionality especially in green alternative solvents [94]. Of particular

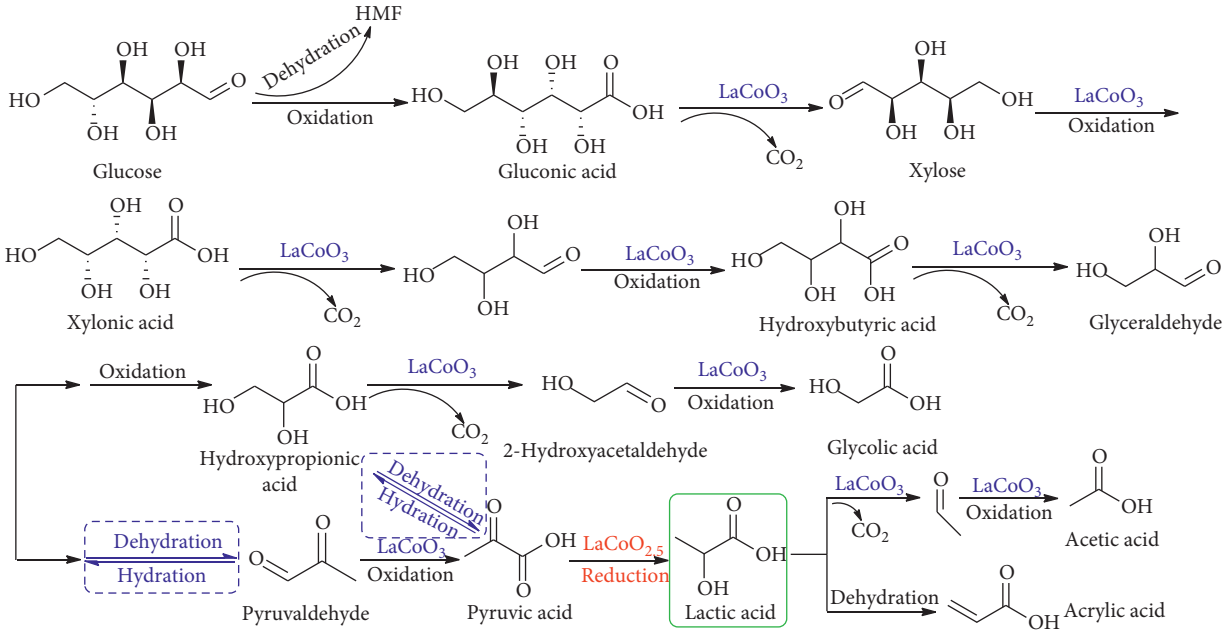

Figure 8: Proposed redox reaction pathway of LA production from glucose using $LaCoO_3$.

interest is to employ renewable biomass feedstocks (i.e., cellulose, sugars, and so on) to synthesis alkyl lactates via a chemical process with high yields. Currently, for the industrial production of lactates, esterification of LA with alcohol is the main method using homogeneous acids [95]. However, the use of the highly corrosive acid catalyst which needs costly neutralization and separation steps will cause environmental issues that conflict with the purport of green chemistry. In order to address this, many researchers have presented valuable studies with respect to the efficient preparation of alkyl lactates from sustainable biomass feedstocks.

3.1. C_3 Sugars to Lactates. Generally, C_3 sugars were usually employed to be the substrates for the production of lactates to serve as the model reaction, with the final aim of using lignocellulose biomass directly. Derived from the relevant studies of mechanism, as illustrated in Figure 9, trioses (DHA or GLA) can be converted into lactates using acids bearing Brønsted/Lewis active sites, wherein Lewis acid is playing the key role in producing lactates. In a similar manner with the production of LA from sugars, zeolites Lewis solid acids showed the most promising application with high reactivity in producing lactates from trioses. Pioneering work was presented by Taarning et al., wherein strong Lewis-acidic Sn-Beta was determined to exhibit the best performance with nearly 100% ML yield at 115°C for 24 h from DHA [51]. In addition, based on their valuable study, during the reaction of trioses in methanol, Lewis acids are believed to be selective towards the ML, whereas Brønsted acids prefer the formation of PADA, accordingly. The reaction pathway involved the Meerwein–Ponndorf–Verley–Oppenauer-type redox reaction of PAL hemiacetal (MeOH), wherein the 1,2-hydride shift takes place in a concerted fashion to form ML, respectively (Figure 10). Inspired by this important research, starting from C_3 sugars, zeolites catalysts including USY CBV600 (ML yield of 82% at 110°C for 4 h) [96], Sn-MCM-41 (EL yield of 98% at 90°C for 6 h) [97], Sn-MWW (ML yield of 99% at 120°C for 24 h) [98], GaUSY (EL selectivity of 82% at 85°C) [99], hierarchical tin zeolites (ML yield of 90% at 80°C for 5 h) [62], and hierarchical niobium-containing zeolites (ML yield of 96% at 80°C for 5 h) [100] were investigated in the alkyl lactates preparation. However, the nature of acidic sites was determined to influence products distribution strongly, wherein Lewis acids favor ML/EL formation which is the same conclusion of Christensen's work.

As discussed above, tin-based acids catalysts showed excellent reactivity towards lactates formation. According to these results, tin ion-exchanged montmorillonites [101], and tin-silicate catalyst synthesized by aerosol-assisted sol-gel method [102] were also prepared and used in lactates production with high activities. More importantly, Pighin et al. showed two interesting studies regarding detailed kinetic and mechanistic lactates formation from C_3 sugars, using Sn/Al_2O_3 catalysts [103–105]. On the basis of the kinetic studies and the proposed pseudohomogeneous mechanism, starting from DHA, ML/EL could be selectively transformed through pyruvic aldehyde hemiacetal intermediates via isomerization by Lewis acids, whereas Brønsted acidic catalysts favored the PADA formation.

3.2. C_6 Sugars to Lactates. Compared to trioses, the transformation of hexoses into lactates through chemocatalysis is more preferable. Some relatively typical homogeneous Lewis acidic catalysts were studied with respect to converting C_6 sugars into lactates, such as $SnCl_4$ [106], $InCl_3{\cdot}4H_2O$-$SnCl_2$ two-component catalyst system [107], and $ZnCl_2$ [108] with

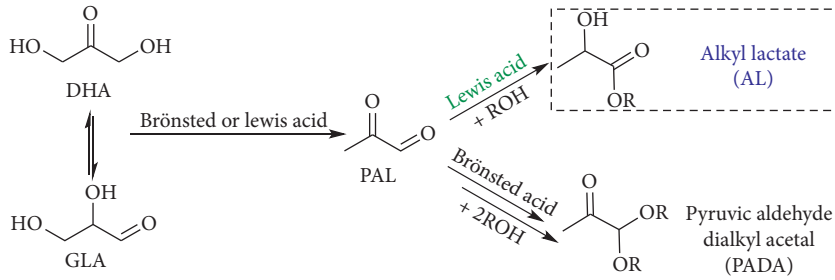

Figure 9: Proposed mechanism for the conversion of DHA to ethyl lactate.

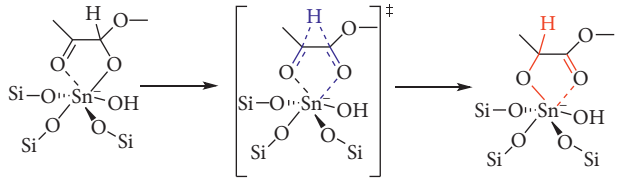

Figure 10: Proposed mechanism of ML formation by Sn-Beta.

high yields, respectively. Encouragingly, Yang et al. used $SnCl_4$-NaOH catalyst system to convert carbohydrates to ML under mild conditions (Table 3, Entry 1). According to the detailed studies, upon neutralizing the protons derived from the methanolysis of $SnCl_4$ with NaOH base, the side reaction of dehydration of C_6 sugars to methyl levulinate was restrained, and ML yield could be improved to some extent by this facile and effective method. More importantly, Nemoto et al. revealed a valuable work regarding the role of $NaBF_4$ salts in the transformation of ML using $InCl_3{\cdot}4H_2O$-$SnCl_2$. Based on hard-soft-acid-base rules [124], Sn species, relative hard acids that could be coordinated with the BF^{4-} anion (a hard base), while could not be coordinated with the Cl^- anion (a borderline base) which would be replaced with MeOH (a hard base). As a consequence, by the addition of $NaBF_4$, the $InCl_3$ and $SnCl_2$ species may exist independent of each other, which would improve about 20% yield of ML, accordingly.

Alternatively, heterogeneously solid Lewis acidic catalysts seem to be a better choice due to their high activity and recyclability. With regard to transformation of lactates from C_6 sugars, Taarning's work is regarded as the most valuable and pioneering research without hesitation (Table 3, Entry 4). For sucrose to be converted into lactates, the reaction mechanism is wherein Lewis acidic sites are determined to play the key role in the isomerization of PAL to ML via 1,2-hydride shift. A high ML yield of 68% using sucrose as a substrate can be achieved at 160°C for 20 h. More importantly, the Lewis acidic zeotypes could be simply filtrated and exhibited high stability for multiple recyclings after a simple handling by calcination only, without any substantial change in terms of product selectivity. Similarly, based on the valuable work regarding the excellent reactivity and stability of tin Lewis acidic zeotypes, many studies for the conversion of carbohydrates into ML using modified tin-based zeolites spring up as presented in Table 3 (Entry 5–7, 9–12). Especially, Tolborg et al. revealed that by the addition of alkali salts during the synthesis of tin zeolite, ML yield could be improved more than two-fold than pure tin beta [112]. They proposed that in the presence of alkali salts, some of the Brønsted acidic sites derived from defects in the framework will be neutralized. As a result, the formation of byproducts could be hindered and the selectivity for ML will be improved, accordingly. Some other modified studies such as hierarchical Sn-Beta zeolites prepared by no fluoride and low concentration tetraethylammonium hydroxide (TEAOH) template [114], hierarchical Sn-Beta zeolites synthesized by the assistant template of poly-diallyldimethylammonium chloride (PDADMA) [116], and Sn-Beta zeolites with nano-size and fewer defects [117] were also investigated in detail to clarify the structure-reactivity relationship. In a similar manner, they all revealed that the modified Sn-Beta bearing the promoting effect of meso-porosity performed better than the microporous Sn-Beta zeolite, in terms of yield and turnover frequency values (TOFs). To some extent, this can contribute to the vital and challenging process of the biorefinery when using large molecules such as cellulose.

However, the aforementioned studies investigated the tin-based zeotypes for efficient production of lactates, and little attention was paid to the systematic investigation of kinetic and mechanistic understanding in the Sn-Beta-catalyzed lactates course. With regard to this, Tosi et al. designed the relatively detailed kinetic analysis of fructose, glucose, and sucrose transformation to ML through typical Sn-Beta [125]. Emphasis was focused on the influence of substrate masking and water using 1D and 2D NMR spectroscopy method. They revealed that most ML was not produced from the substrates directly; however, methyl fructosides were determined as the key intermediates. At 160°C, over 40% of substrate carbon were masked (i.e., reversibly protected in situ) as methyl fructosides within a few minutes when employing hydrothermally synthesized Sn-Beta, while more than 60% methyl fructosides could be formed within a few minutes by post-synthetically treated Sn-Beta. Moreover, the existence of water (to release fructose) could tailor the masking process wherein the addition of small quantities of water was able to accelerate conversion to ML without the decrease of catalyst stability. In addition to tin-based zeolites, another valuable research using bifunctional carbon-silica catalysts (Sn-Si-CSM-773–20.4) bearing both Lewis and weak Brønsted acid sites did make an important contribution to lactates production [118]. Lewis acid sites were introduced through

Table 3: Catalytic production of lactates from C_6 sugars and cellulose via acid-catalysis.

Entry	Substrate	Catalyst	Reaction conditions	Yield of lactates (%)	Reference
1	Glucose	$SnCl_4$-NaOH	160°C, 2.5 h	47	[106]
	Fructose			57	
	Sucrose			51	
2	Fructose	$InCl_3{\cdot}4H_2O$-$SnCl_2$, $NaBF_4$	160°C, 10 h	72	[107]
3	Glucose	$ZnCl_2$	200°C, 3 h	47.7	[108]
	Fructose			51.7	
	Sucrose			47.5	
4	Sucrose	Sn-beta	160°C, 20 h	68	[109]
	Glucose			43	
	Fructose			44	
5	Xylose	Sn-beta	140°C, 20 h	42	[110]
6	Glucose	Sn-MCM-41	160°C, 20 h	43	[111]
7	Sucrose	K-PT-Sn-beta	170°C, 16 h	71	[112]
8	Xylose	Zr-SBA-15	240°C, 6 h	41	[113]
	Fructose			44	
	Glucose			38	
	Sucrose			40	
9	Glucose	Hierarchical Sn-Beta	160°C, 10 h	58	[114]
10	Inulin	Sn-SBA-15	160°C, 20 h	57	[115]
11	Sucrose	Sn-beta-H	160°C, 20 h	72.1	[116]
12	Fructose	Sn-beta-9h	160°C, 10 h	47	[117]
	Mannose			39	
	Sucrose			57	
13	Fructose	Sn-Si-CSM-773–20.4	155°C, 20 h	17	[118]
	Glucose			32	
	Sucrose			45	
14	Sucrose	ZIF-8	160°C, 24 h	42	[119]
15	Glucose	γ-Al_2O_3	160°C, 6 h	34	[120]
16	Cellulose	$SnCl_2{\cdot}2H_2O$-$ZnCl_2$	210°C, 4 h	32.1	[121]
	Sugarcane bagasse		190°C, 6 h	31.2	
17	Cellulose	Zr-SBA-15	240°C, 10 h	28.1	[113]
18	Cellulose	Zr-SBA-15	260°C, 2 h	~33	[122]
19	Cellulose	Ga-doped Zn/H-nanozeolite Y	270°C, 5 h	57.8	[123]
	Glucose		270°C, 1 h	64.0	
	Fructose		270°C, 1 h	67.3	

grafting Sn (IV) to the silica surface, and important Brønsted acid sites (number and strength) were controlled by tailoring the carbon deposition content, pyrolysis temperature, and thermal posttreatment. With this versatile material, the one-pot transformation of fructose, glucose, and sucrose into ML could be proved, along with 32%, 17%, and 45% yield, respectively (Table 3, Entry 13). However, the complicated and longstanding synthetic procedure should be involved to prepare this material, which would influence its industrial application. Similar to ref. 70, ZIF-8 MOFs were also tested in the conversion of hexoses into ML. Successfully transformation of sucrose to ML with a high yield of 42%, at 160°C in 24 h was achieved [119]. It is worth noting that the latest work regarding hexoses conversion into ML was presented by Yamaguchi et al. using an interesting catalyst γ-Al_2O_3 with acid-base bifunctional characters, showing considerable ML yield [120]. It was found that due to the essential high acid and base densities of γ-Al_2O_3, cascade reactions in glucose to ML consisting isomerization, retro-aldol, and dehydration could be successfully carried out, with 34% yield of ML from glucose at 160°C for 6 h.

3.3. Cellulose to Lactates. Generally, the direct utilization of cellulose as feedstocks for the production of lactates is being deemed to be a milestone, especially through the versatile chemocatalysis. With respect to this research, limited studies regarding the efficient transformation of lactates from cellulose via chemocatalysis can be presented, because of the very complex reactions and the inherent rigidity of cellulose. For the homogeneous catalyst used in lactates production from cellulose, $SnCl_2{\cdot}2H_2O$-$ZnCl_2$ was utilized as an efficient catalyst to ML production with 32.1% yield in methanol, at relatively mild reaction conditions with 210°C for 4 h [121]. In addition, 31.2% ML yield could be also obtained from real biomass sugar cane bagasse at 190°C within 6 h. However, lower yields of ML were achieved from glucose (15.7%) and sucrose (14.7%), may be derived from the strong acidity of $SnCl_2{\cdot}2H_2O$-$ZnCl_2$ which would transform many monosaccharides and disaccharides into dark tars. On the other hand, Zr-SBA-15 heterogeneous catalysts developed by Lin group, could not only exhibit good yields of ML form monosaccharides and disaccharides (Table 3, Entry 8) [113], but also perform well from cellulose directly in 95% methanol solvent [113] and in 95% ethanol [122],

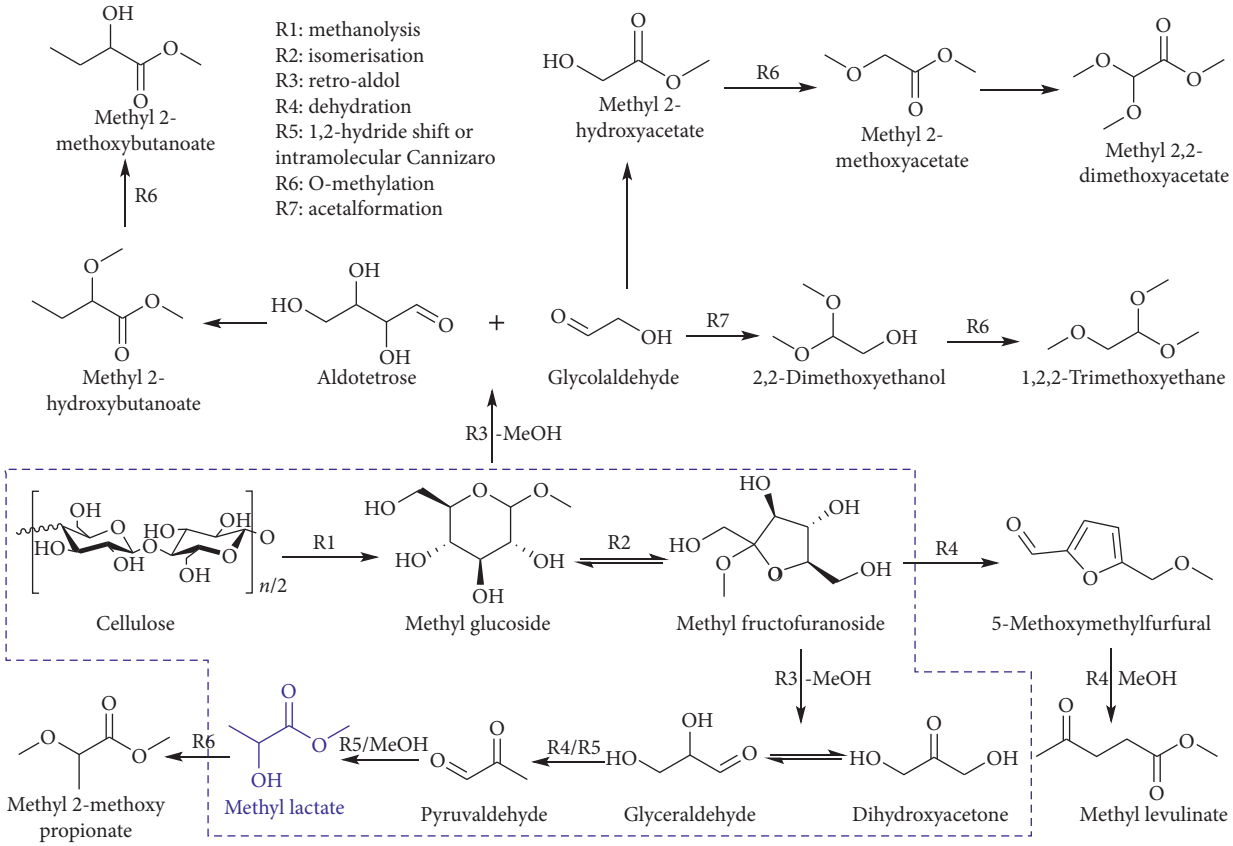

Figure 11: Proposed reaction pathway for the conversion of methyl lactate from cellulose using Ga-doped Zn/HNZY.

respectively. The addition of a little amount of water (5 wt%) along with the weak Brønsted acids of Zr-SBA-15, was believed to facilitate the hydrolysis of cellulose. After then, the Lewis acidic sites of Zr-SBA-15 played the key role in a series of reactions such as isomerization, retro-aldol condensation, and so on. However, despite the high cost of the equipment, the "one-pot" process using water as cosolvent in supercritical alcohol conditions can be regarded as an environmental-friendly way to yield lactates directly from cellulosic biomass.

Nonetheless, the aforementioned catalysts not presented high yields of lactates from cellulose directly. With respect to getting a high productivity of lactates from cellulose, Verma et al. designed the Ga-doped Zn/H-nanozeolite Y catalysts, to be served the most efficient materials so far for converting cellulose directly into ML with 57.8% yield at 270°C, 5 h in supercritical methanol [123]. It is believed that due to the enhancement of Lewis acid sites along with the decrease of Brønsted acid sites which derived from doping of Ga on ZnO, together with large external surface areas of HNZY, were determined as the crucial parameters to highly converting cellulose into lactates. More importantly, the catalyst could be reused in four consecutive cycles, with ignorable selectivity towards ML, highlighting its excellent stability. The detailed reaction pathway was proposed accordingly (Figure 11), including several steps such as methanolysis, isomerization, retro-aldol condensation, and so on. Some other side-products could also be formed by tailoring the reaction parameters; however, Ga-doped Zn/HNZY is determined to be crucial to control the consecutive reaction pathways for the upgrading of cellulose into glucose, retro-aldol condensation into trioses, and intramolecular Cannizzaro reaction into ML.

4. Conclusion and Perspective

Catalytic transformations of valuable organic acids such as lactic acid, levulinic acid, and amino acid from renewable carbon resources including polysaccharides, lignin, and their derivatives is of high interest for a sustainable chemical industry in the future [126, 127]. The development of efficient techniques for commercial lactic acid and alkyl lactates production from lignocellulosic biomass is regarded as an important process of biorefinery, in order to reduce the reliance on petroleum feedstocks. Compared to traditional fermentation methods suffering from waste dispose, costly separation, and the inability to transform cellulosic biomass without costly pretreatments, chemocatalysis is being recognized as an effective formidable strategy to upgrading cellulosic biomass into value-added chemicals with acceptable selectivity. However, the separation of enantiomers is a formidable and tremendous challenge because of the extremely similar physical and chemical properties caused as good as molecular structure. The technical challenge to achieve that is the very low enantiomer selectivity and the limited loss of one of the lactate isomers. Moreover, although

basic catalysts are capable of catalyzing biomass into LA under hydrothermal conditions, the difficulty in acquiring a high LA yield is the main challenge.

From the environmental-friendly point of view, heterogeneously solid acidic catalysts which are less corrosive and can be recycled from the reaction medium for reutilization are considered to be the better choice currently. Sn-based zeotype catalysts bearing strong Lewis acidities have demonstrated excellent performance for the transformation of sugars to lactates. However, long synthesis time especially Sn-β with crystallization time up to 10–20 days and the utilization of some toxic tin precursors may hamper the industrial applications, to some extent. Furthermore, the poor stability at elevated temperatures and the narrow channels of Sn-Beta hindering the large biomass molecules (i.e., cellulose) to contact with active sites should also be taken into consideration. It is worth mentioning that the introduction of weak Brønsted acids is believed to be beneficial to LA and lactates transformation. With respect to the catalyst design, some suggestions based on the literature are presented here:

(i) More attention is recommended to pay on the synthesis of active, selective and durable solid acidic catalysts for the efficient transformation of cellulosic biomass into LA and lactates

(ii) The design of novel multifunctional (i.e., controllable active sites, strong Lewis acidic functional groups with weak Brønsted acidic sites, and acid-base bifunctional sites) heterogeneous catalysts is highly appreciated

(iii) It should be reinforced to design the mesoporous nanocatalysts, bearing large surface area along with large pore size, in order to render reactants contact with the active sites easily

(iv) More studies are demanded to propose a facile method that can prepare the target catalysts in view of large-scale and low-cost

(v) For lactates production, the recyclability of methanol or ethanol solvent should be taken into consideration, which is likely to affect the whole process economics, in order to intensify the sustainable process

(vi) It is indispensable to be devoted into an insightful understanding in terms of the reaction mechanism and structure-properties of the catalysts, which is helpful to understand the reaction pathways and the better design of catalysts

Conflicts of Interest

The authors have no conflicting interests to declare.

Acknowledgments

This work was financially supported by the Natural Science Foundation of China (21576059 and 21666008), the Key Technologies R&D Program of China (2014BAD23B01), and Chinese State Scholarship Fund (No. 201706670012).

References

[1] H. Li, Z. Fang, R. L. Smith Jr., and S. Yang, "Efficient valorization of biomass to biofuels with bifunctional solid catalytic materials," *Progress in Energy and Combustion Science*, vol. 55, pp. 98–194, 2016.

[2] H. Li, P. S. Bhadury, A. Riisager, and S. Yang, "One-pot transformation of polysaccharides via multi-catalytic processes," *Catalysis Science and Technology*, vol. 4, no. 12, pp. 4138–4168, 2014.

[3] H. Zhang, H. Li, H. Pan et al., "Magnetically recyclable acidic polymeric ionic liquids decorated with hydrophobic regulators as highly efficient and stable catalysts for biodiesel production," *Applied Energy*, vol. 223, pp. 416–429, 2018.

[4] H. Zhang, H. Li, H. Pan, A. Wang, C. C. Xu, and S. Yang, "Magnetically recyclable basic polymeric ionic liquids for efficient transesterification of *Firmiana platanifolia* L.f. oil into biodiesel," *Energy Conversion and Management*, vol. 153, pp. 462–472, 2017.

[5] S. Van de Vyver, J. Geboers, P. A. Jacobs, and B. F. Sels, "Recent advances in the catalytic conversion of cellulose," *ChemCatChem*, vol. 3, no. 1, pp. 82–94, 2011.

[6] H. Zhang, H. Pan, and S. Yang, "Upgrading of cellulose to biofuels and chemicals with acidic nanocatalysts," *Current Nanoscience*, vol. 13, no. 5, pp. 513–527, 2017.

[7] M. Dusselier, P. Van Wouwe, A. Dewaele, E. Makshina, and B. F. Sels, "Lactic acid as a platform chemical in the biobased economy: the role of chemocatalysis," *Energy and Environmental Science*, vol. 6, no. 5, pp. 1415–1442, 2013.

[8] P. Maki-Arvela, I. L. Simakova, T. Salmi, and D. Y. Murzin, "Production of lactic acid/lactates from biomass and their catalytic transformations to commodities," *Chemical Reviews*, vol. 114, no. 3, pp. 1909–1971, 2013.

[9] H. Li, S. Yang, A. Riisager et al., "Zeolite and zeotype-catalysed transformations of biofuranic compounds," *Green Chemistry*, vol. 18, no. 21, pp. 5701–5735, 2016.

[10] R. O. de Souza, L. S. Miranda, and R. Luque, "Bio (chemo) technological strategies for biomass conversion into bioethanol and key carboxylic acids," *Green Chemistry*, vol. 16, no. 5, pp. 2386–2405, 2014.

[11] H. Li, A. Riisager, S. Saravanamurugan et al., "Carbon-increasing catalytic strategies for upgrading biomass into energy-intensive fuels and chemicals," *ACS Catalysis*, vol. 8, no. 1, pp. 148–187, 2017.

[12] H. Li, W. Zhao, A. Riisager et al., "A Pd-Catalyzed in situ domino process for mild and quantitative production of 2, 5-dimethylfuran directly from carbohydrates," *Green Chemistry*, vol. 19, no. 9, pp. 2101–2106, 2017.

[13] H. Li, Z. Fang, J. Luo, and S. Yang, "Direct conversion of biomass components to the biofuel methyl levulinate catalyzed by acid-base bifunctional zirconia-zeolites," *Applied Catalysis B: Environmental*, vol. 200, pp. 182–191, 2017.

[14] M. Brin, "The synthesis and metabolism of lactic acid isomers," *Annals of the New York Academy of Sciences*, vol. 119, no. 3, pp. 942–956, 1965.

[15] M. Brin, "Lactic acid–some definitions," *Annals of the New York Academy of Sciences*, vol. 119, no. 1, pp. 1084–1090, 1965.

[16] R. Datta and M. Henry, "Lactic acid: recent advances in products, processes and technologies-a review," *Journal of Chemical Technology and Biotechnology: International Research in Process, Environmental and Clean Technology*, vol. 81, no. 7, pp. 1119–1129, 2006.

[17] C. S. Pereira, V. M. Silva, and A. E. Rodrigues, "Ethyl lactate as a solvent: properties, applications and production

processes-a review," *Green Chemistry*, vol. 13, no. 10, pp. 2658–2671, 2011.

[18] S. Aparicio and R. Alcalde, "Insights into the ethyl lactate + water mixed solvent," *Journal of Physical Chemistry B*, vol. 113, no. 43, pp. 14257–14269, 2009.

[19] M. Ilmén, K. Koivuranta, L. Ruohonen, P. Suominen, and M. Penttilä, "Efficient production of L-lactic acid from xylose by *Pichia stipitis*," *Applied and Environmental Microbiology*, vol. 73, no. 1, pp. 117–123, 2007.

[20] C. R. Soccol, L. P. Vandenberghe, C. Rodrigues, A. B. P. Medeiros, C. Larroche, and A. Pandey, "Production of organic acids by solid-state fermentation," in *Current Developments in Solid-State Fermentation*, pp. 205–229, Springer, Berlin, Germany, 2008.

[21] M. Dusselier, M. Mascal, and B. F. Sels, "Top chemical opportunities from carbohydrate biomass: a chemist's view of the biorefinery," in *Selective Catalysis for Renewable Feedstocks and Chemicals*, pp. 1–40, Springer, Berlin, Germany, 2014.

[22] P. O. Carvalho, Q. B. Cass, S. A. Calafatti, F. J. Contesini, and R. Bizaco, "Review- alternatives for the separation of drug enantiomers: ibuprofen as a model compound," *Brazilian Journal of Chemical Engineering*, vol. 23, no. 3, pp. 291–300, 2006.

[23] E. Lee, M. B. Park, J. M. Kim, W. S. Kim, and I. H. Kim, "Simulated moving-bed for separation of mandelic acid racemic mixtures," *Korean Journal of Chemical Engineering*, vol. 27, no. 1, pp. 231–234, 2010.

[24] W. J. Pope, "Stereochemistry," *Annual Reports on the Progress of Chemistry*, vol. 2, pp. 168–184, 1905.

[25] P. Van Wouwe, M. Dusselier, A. Basiç, and B. F. Sels, "Bridging racemic lactate esters with stereoselective polylactic acid using commercial lipase catalysis," *Green Chemistry*, vol. 15, no. 10, p. 2817, 2013.

[26] H. Kishida, F. Jin, X. Yan, T. Moriya, and H. Enomoto, "Formation of lactic acid from glycolaldehyde by alkaline hydrothermal reaction," *Carbohydrate Research*, vol. 341, no. 15, pp. 2619–2623, 2006.

[27] X. Yan, F. Jin, K. Tohji, T. Moriya, and H. Enomoto, "Production of lactic acid from glucose by alkaline hydrothermal reaction," *Journal of Materials Science*, vol. 42, no. 24, pp. 9995–9999, 2007.

[28] Z. Shen, F. Jin, Y. Zhang et al., "Effect of alkaline catalysts on hydrothermal conversion of glycerin into lactic acid," *Industrial and Engineering Chemistry Research*, vol. 48, no. 19, pp. 8920–8925, 2009.

[29] X. Yan, F. Jin, K. Tohji, A. Kishita, and H. Enomoto, "Hydrothermal conversion of carbohydrate biomass to lactic acid," *AIChE Journal*, vol. 56, no. 10, pp. 2727–2733, 2010.

[30] F.-W. Wang, Z.-B. Huo, Y.-Q. Wang, and F.-M. Jin, "Hydrothermal conversion of cellulose into lactic acid with nickel catalyst," *Research on Chemical Intermediates*, vol. 37, no. 2–5, pp. 487–492, 2011.

[31] Y. Wang, F. Jin, M. Sasaki, F. Wang, Z. Jing, and M. Goto, "Selective conversion of glucose into lactic acid and acetic acid with copper oxide under hydrothermal conditions," *AIChE Journal*, vol. 59, no. 6, pp. 2096–2104, 2013.

[32] S. Zhang, F. Jin, J. Hu, and Z. Huo, "Improvement of lactic acid production from cellulose with the addition of Zn/Ni/C under alkaline hydrothermal conditions," *Bioresource Technology*, vol. 102, no. 2, pp. 1998–2003, 2011.

[33] Z. Huo, Y. Fang, D. Ren et al., "Selective conversion of glucose into lactic acid with transition metal ions in diluted aqueous NaOH solution," *ACS Sustainable Chemistry and Engineering*, vol. 2, no. 12, pp. 2765–2771, 2014.

[34] J. Duo, Z. Zhang, G. Yao, Z. Huo, and F. Jin, "Hydrothermal conversion of glucose into lactic acid with sodium silicate as a base catalyst," *Catalysis Today*, vol. 263, pp. 112–116, 2016.

[35] A. Onda, T. Ochi, K. Kajiyoshi, and K. Yanagisawa, "Lactic acid production from glucose over activated hydrotalcites as solid base catalysts in water," *Catalysis Communications*, vol. 9, no. 6, pp. 1050–1053, 2008.

[36] G. Epane, J. C. Laguerre, A. Wadouachi, and D. Marek, "Microwave-assisted conversion of D-glucose into lactic acid under solvent-free conditions," *Green Chemistry*, vol. 12, no. 3, pp. 502–506, 2010.

[37] E. M. Albuquerque, L. E. Borges, and M. A. Fraga, "Lactic acid production from hydroxyacetone on dual metal/base heterogeneous catalytic systems," *Green Chemistry*, vol. 17, no. 7, pp. 3889–3899, 2015.

[38] X. Wang, Y. Song, C. Huang, F. Liang, and B. Chen, "Lactic acid production from glucose over polymer catalysts in aqueous alkaline solution under mild conditions," *Green Chemistry*, vol. 16, no. 9, pp. 4234–4240, 2014.

[39] D. Esposito and M. Antonietti, "Chemical conversion of sugars to lactic acid by alkaline hydrothermal processes," *ChemSusChem*, vol. 6, no. 6, pp. 989–992, 2013.

[40] L. Li, L. Yan, F. Shen, M. Qiu, and X. Qi, "Mechanocatalytic production of lactic acid from glucose by ball milling," *Catalysts*, vol. 7, no. 6, p. 170, 2017.

[41] L. Li, F. Shen, R. L. Smith, and X. Qi, "Quantitative chemocatalytic production of lactic acid from glucose under anaerobic conditions at room temperature," *Green Chemistry*, vol. 19, no. 1, pp. 76–81, 2017.

[42] C. Sánchez, I. Egüés, A. García, R. Llano-Ponte, and J. Labidi, "Lactic acid production by alkaline hydrothermal treatment of corn cobs," *Chemical Engineering Journal*, vol. 181, pp. 655–660, 2012.

[43] C. Sánchez, L. Serrano, R. Llano-Ponte, and J. Labidi, "Bread residues conversion into lactic acid by alkaline hydrothermal treatments," *Chemical Engineering Journal*, vol. 250, pp. 326–330, 2014.

[44] R. Younas, S. Zhang, L. Zhang et al., "Lactic acid production from rice straw in alkaline hydrothermal conditions in presence of NiO nanoplates," *Catalysis Today*, vol. 274, pp. 40–48, 2016.

[45] W. Jeon, C. Ban, G. Park, H. C. Woo, and D. H. Kim, "Hydrothermal conversion of macroalgae-derived alginate to lactic acid catalyzed by metal oxides," *Catalysis Science and Technology*, vol. 6, no. 4, pp. 1146–1156, 2016.

[46] F. M. Kerton, Y. Liu, K. W. Omari, and K. Hawboldt, "Green chemistry and the ocean-based biorefinery," *Green Chemistry*, vol. 15, no. 4, pp. 860–871, 2013.

[47] R. P. John, G. Anisha, K. M. Nampoothiri, and A. Pandey, "Micro and macroalgal biomass: a renewable source for bioethanol," *Bioresource Technology*, vol. 102, no. 1, pp. 186–193, 2011.

[48] R. M. West, E. L. Kunkes, D. A. Simonetti, and J. A. Dumesic, "Catalytic conversion of biomass-derived carbohydrates to fuels and chemicals by formation and upgrading of monofunctional hydrocarbon intermediates," *Catalysis Today*, vol. 147, no. 2, pp. 115–125, 2009.

[49] S. Lux and M. Siebenhofer, "Catalytic conversion of dihydroxyacetone to lactic acid with Brønsted acids and multivalent metal ions," *Chemical and Biochemical Engineering Quarterly*, vol. 29, no. 4, pp. 575–585, 2016.

[50] C. B. Rasrendra, B. A. Fachri, I. G. B. Makertihartha, S. Adisasmito, and H. J. Heeres, "Catalytic conversion of dihydroxyacetone to lactic acid using metal salts in water," *ChemSusChem*, vol. 4, no. 6, pp. 768–777, 2011.

[51] E. Taarning, S. Saravanamurugan, M. Spangsberg Holm, J. Xiong, R. M. West, and C. H. Christensen, "Zeolite-catalyzed isomerization of triose sugars," *ChemSusChem*, vol. 2, no. 7, pp. 625–627, 2009.

[52] Y. Koito, K. Nakajima, M. Kitano, and M. Hara, "Efficient conversion of pyruvic aldehyde into lactic acid by lewis acid catalyst in water," *Chemistry Letters*, vol. 42, no. 8, pp. 873–875, 2013.

[53] M. J. Antal Jr., W. S. Mok, and G. N. Richards, "Mechanism of formation of 5-(hydroxymethyl)-2-furaldehyde from D-fructose and sucrose," *Carbohydrate Research*, vol. 199, no. 1, pp. 91–109, 1990.

[54] Y. Hayashi and Y. Sasaki, "Tin-catalyzed conversion of trioses to alkyl lactates in alcohol solution," *Chemical Communications*, vol. 21, pp. 2716–2718, 2005.

[55] M. Bicker, S. Endres, L. Ott, and H. Vogel, "Catalytical conversion of carbohydrates in subcritical water: a new chemical process for lactic acid production," *Journal of Molecular Catalysis A: Chemical*, vol. 239, no. 1-2, pp. 151–157, 2005.

[56] C. Rasrendra, I. Makertihartha, S. Adisasmito, and H. Heeres, "Green chemicals from d-glucose: systematic studies on catalytic effects of inorganic salts on the chemoselectivity and yield in aqueous solutions," *Topics in Catalysis*, vol. 53, no. 15–18, pp. 1241–1247, 2010.

[57] R. M. West, M. S. Holm, S. Saravanamurugan et al., "Zeolite H-USY for the production of lactic acid and methyl lactate from C3-sugars," *Journal of Catalysis*, vol. 269, no. 1, pp. 122–130, 2010.

[58] E. Jolimaitre, D. Delcroix, N. Essayem, C. Pinel, and M. Besson, "Dihydroxyacetone conversion into lactic acid in an aqueous medium in the presence of metal salts: influence of the ionic thermodynamic equilibrium on the reaction performance," *Catalysis Science and Technology*, vol. 8, no. 5, pp. 1349–1356, 2018.

[59] V. Choudhary, S. H. Mushrif, C. Ho et al., "Insights into the interplay of Lewis and Brønsted acid catalysts in glucose and fructose conversion to 5-(hydroxymethyl) furfural and levulinic acid in aqueous media," *Journal of the American Chemical Society*, vol. 135, no. 10, pp. 3997–4006, 2013.

[60] H. Li, T. Yang, A. Riisager, S. Saravanamurugan, and S. Yang, "Chemoselective synthesis of dithioacetals from bio-aldehydes with zeolites under ambient and solvent-free conditions," *ChemCatChem*, vol. 9, no. 6, pp. 1097–1104, 2017.

[61] P. Y. Dapsens, C. Mondelli, and J. Pérez-Ramírez, "Highly selective Lewis acid sites in desilicated MFI zeolites for dihydroxyacetone isomerization to lactic acid," *ChemSusChem*, vol. 6, no. 5, pp. 831–839, 2013.

[62] A. Feliczak-Guzik, M. Sprynskyy, I. Nowak, and B. Buszewski, "Catalytic isomerization of dihydroxyacetone to lactic acid and alkyl lactates over hierarchical zeolites containing tin," *Catalysts*, vol. 8, no. 1, p. 31, 2018.

[63] X. Wang, F. Liang, C. Huang, Y. Li, and B. Chen, "Highly active tin (IV) phosphate phase transfer catalysts for the production of lactic acid from triose sugars," *Catalysis Science and Technology*, vol. 5, no. 9, pp. 4410–4421, 2015.

[64] K. Nakajima, J. Hirata, M. Kim et al., "Facile formation of lactic acid from a triose sugar in water over niobium oxide with a deformed orthorhombic phase," *ACS Catalysis*, vol. 8, no. 1, pp. 283–290, 2017.

[65] D. Cao, W. Cai, W. Tao, S. Zhang, D. Wang, and D. Huang, "Lactic acid production from glucose over a novel Nb_2O_5 nanorod catalyst," *Catalysis Letters*, vol. 147, no. 4, pp. 926–933, 2017.

[66] J. B. dos Santos, N. J. A. de Albuquerque, C. L. d. P. e Silva, M. R. Meneghetti, and S. M. P. Meneghetti, "Fructose conversion in the presence of Sn (IV) catalysts exhibiting high selectivity to lactic acid," *RSC Advances*, vol. 5, no. 110, pp. 90952–90959, 2015.

[67] W. Dong, Z. Shen, B. Peng et al., "Selective chemical conversion of sugars in aqueous solutions without alkali to lactic acid over a Zn-Sn-Beta Lewis acid-base catalyst," *Scientific Reports*, vol. 6, no. 1, p. 26713, 2016.

[68] M. Xia, W. Dong, M. Gu, C. Chang, Z. Shen, and Y. Zhang, "Synergetic effects of bimetals in modified beta zeolite for lactic acid synthesis from biomass-derived carbohydrates," *RSC Advances*, vol. 8, no. 16, pp. 8965–8975, 2018.

[69] S. Huang, K.-L. Yang, X.-F. Liu, H. Pan, H. Zhang, and S. Yang, "MIL-100 (Fe)-catalyzed efficient conversion of hexoses to lactic acid," *RSC Advances*, vol. 7, no. 10, pp. 5621–5627, 2017.

[70] D. Liu, K. H. Kim, J. Sun, B. A. Simmons, and S. Singh, "Cascade production of lactic acid from universal types of sugars catalyzed by lanthanum triflate," *ChemSusChem*, vol. 11, no. 3, pp. 598–604, 2018.

[71] F. Chambon, F. Rataboul, C. Pinel, A. Cabiac, E. Guillon, and N. Essayem, "Cellulose hydrothermal conversion promoted by heterogeneous Brønsted and Lewis acids: remarkable efficiency of solid Lewis acids to produce lactic acid," *Applied Catalysis B: Environmental*, vol. 105, no. 1-2, pp. 171–181, 2011.

[72] Y. Swesi, C. Nguyen, T. T. Ha Vu et al., "Direct solid lewis acid catalyzed wood liquefaction into lactic acid: kinetic evidences that wood pretreatment might not be a prerequisite," *ChemCatChem*, vol. 9, no. 12, pp. 2377–2382, 2017.

[73] L. Yang, J. Su, S. Carl, J. G. Lynam, X. Yang, and H. Lin, "Catalytic conversion of hemicellulosic biomass to lactic acid in pH neutral aqueous phase media," *Applied Catalysis B: Environmental*, vol. 162, pp. 149–157, 2015.

[74] P. Wattanapaphawong, P. Reubroycharoen, and A. Yamaguchi, "Conversion of cellulose into lactic acid using zirconium oxide catalysts," *RSC Advances*, vol. 7, no. 30, pp. 18561–18568, 2017.

[75] P. Wattanapaphawong, O. Sato, K. Sato, N. Mimura, P. Reubroycharoen, and A. Yamaguchi, "Conversion of cellulose to lactic acid by using ZrO_2–Al_2O_3 catalysts," *Catalysts*, vol. 7, no. 7, p. 221, 2017.

[76] F.-F. Wang, C.-L. Liu, and W.-S. Dong, "Highly efficient production of lactic acid from cellulose using lanthanide triflate catalysts," *Green Chemistry*, vol. 15, no. 8, pp. 2091–2095, 2013.

[77] X. Lei, F.-F. Wang, C.-L. Liu, R.-Z. Yang, and W.-S. Dong, "One-pot catalytic conversion of carbohydrate biomass to lactic acid using an $ErCl_3$ catalyst," *Applied Catalysis A: General*, vol. 482, pp. 78–83, 2014.

[78] F.-F. Wang, J. Liu, H. Li, C.-L. Liu, R.-Z. Yang, and W.-S. Dong, "Conversion of cellulose to lactic acid catalyzed by erbium-exchanged montmorillonite K10," *Green Chemistry*, vol. 17, no. 4, pp. 2455–2463, 2015.

[79] F.-F. Wang, H.-Z. Wu, H.-F. Ren, C.-L. Liu, C.-L. Xu, and W.-S. Dong, "Er/β-zeolite-catalyzed one-pot conversion of cellulose to lactic acid," *Journal of Porous Materials*, vol. 24, no. 3, pp. 697–706, 2017.

[80] Y. Wang, W. Deng, B. Wang et al., "Chemical synthesis of lactic acid from cellulose catalysed by lead(II) ions in water," *Nature Communications*, vol. 4, no. 1, p. 2141, 2013.

[81] Z. Tang, W. Deng, Y. Wang et al., "Transformation of cellulose and its derived carbohydrates into formic and lactic acids catalyzed by vanadyl cations," *ChemSusChem*, vol. 7, no. 6, pp. 1557–1567, 2014.

[82] W. Deng, P. Wang, B. Wang et al., "Transformation of cellulose and related carbohydrates into lactic acid with bifunctional Al(III)–Sn(II) catalysts," *Green Chemistry*, vol. 20, no. 3, pp. 735–744, 2018.

[83] S. M. Coman, M. Verziu, A. Tirsoaga et al., "NbF_5–AlF_3 catalysts: design, synthesis, and application in lactic acid synthesis from cellulose," *ACS Catalysis*, vol. 5, no. 5, pp. 3013–3026, 2015.

[84] M. Verziu, M. Serano, B. Jurca et al., "Catalytic features of Nb-based nanoscopic inorganic fluorides for an efficient one-pot conversion of cellulose to lactic acid," *Catalysis Today*, vol. 306, pp. 102–110, 2018.

[85] X. Yang, L. Yang, W. Fan, and H. Lin, "Effect of redox properties of $LaCoO_3$ perovskite catalyst on production of lactic acid from cellulosic biomass," *Catalysis Today*, vol. 269, pp. 56–64, 2016.

[86] K. M. Taylor-Pashow, J. Della Rocca, Z. Xie, S. Tran, and W. Lin, "Postsynthetic modifications of iron-carboxylate nanoscale metal–organic frameworks for imaging and drug delivery," *Journal of the American Chemical Society*, vol. 131, no. 40, pp. 14261–14263, 2009.

[87] S. Qiu, M. Xue, and G. Zhu, "Metal–organic framework membranes: from synthesis to separation application," *Chemical Society Reviews*, vol. 43, no. 16, pp. 6116–6140, 2014.

[88] A. Corma, H. García, and F. Llabrés i Xamena, "Engineering metal organic frameworks for heterogeneous catalysis," *Chemical Reviews*, vol. 110, no. 8, pp. 4606–4655, 2010.

[89] C. Li, X. Zhao, A. Wang, G. W. Huber, and T. Zhang, "Catalytic transformation of lignin for the production of chemicals and fuels," *Chemical Reviews*, vol. 115, no. 21, pp. 11559–11624, 2015.

[90] Z. M. Bundhoo, "Microwave-assisted conversion of biomass and waste materials to biofuels," *Renewable and Sustainable Energy Reviews*, vol. 82, pp. 1149–1177, 2018.

[91] Z.-Y. Ma, C. Yang, W. Wei, W.-H. Li, and Y.-H. Sun, "Surface properties and CO adsorption on zirconia polymorphs," *Journal of Molecular Catalysis A: Chemical*, vol. 227, no. 1-2, pp. 119–124, 2005.

[92] D. Bianchi, T. Chafik, M. Khalfallah, and S. J. Teichner, "Intermediate species on zirconia supported methanol aerogel catalysts: II. Adsorption of carbon monoxide on pure zirconia and on zirconia containing zinc oxide," *Applied Catalysis A: General*, vol. 105, no. 2, pp. 223–249, 1993.

[93] T. Yamaguchi, Y. Nakano, and K. Tanabe, "Infrared study of surface hydroxyl groups on zirconium oxide," *Bulletin of the Chemical Society of Japan*, vol. 51, no. 9, pp. 2482–2487, 1978.

[94] P. G. Jessop, "Searching for green solvents," *Green Chemistry*, vol. 13, no. 6, pp. 1391–1398, 2011.

[95] C. S. Pereira, S. P. Pinho, V. M. Silva, and A. E. Rodrigues, "Thermodynamic equilibrium and reaction kinetics for the esterification of lactic acid with ethanol catalyzed by acid ion-exchange resin," *Industrial and Engineering Chemistry Research*, vol. 47, no. 5, pp. 1453–1463, 2008.

[96] P. P. Pescarmona, K. P. Janssen, C. Delaet et al., "Zeolite-catalysed conversion of C3 sugars to alkyl lactates," *Green Chemistry*, vol. 12, no. 6, pp. 1083–1089, 2010.

[97] L. Li, C. Stroobants, K. Lin, P. A. Jacobs, B. F. Sels, and P. P. Pescarmona, "Selective conversion of trioses to lactates over Lewis acid heterogeneous catalysts," *Green Chemistry*, vol. 13, no. 5, pp. 1175–1181, 2011.

[98] Q. Guo, F. Fan, E. A. Pidko et al., "Highly active and recyclable Sn-MWW zeolite catalyst for sugar conversion to methyl lactate and lactic acid," *ChemSusChem*, vol. 6, no. 8, pp. 1352–1356, 2013.

[99] P. Y. Dapsens, M. J. Menart, C. Mondelli, and J. Pérez-Ramírez, "Production of bio-derived ethyl lactate on GaUSY zeolites prepared by post-synthetic galliation," *Green Chemistry*, vol. 16, no. 2, pp. 589–593, 2014.

[100] A. Feliczak-Guzik, M. Sprynskyy, I. Nowak, M. Jaroniec, and B. Buszewski, "Application of novel hierarchical niobium-containing zeolites for synthesis of alkyl lactate and lactic acid," *Journal of Colloid and Interface Science*, vol. 516, pp. 379–383, 2018.

[101] J. Wang, Y. Masui, and M. Onaka, "Conversion of triose sugars with alcohols to alkyl lactates catalyzed by Brønsted acid tin ion-exchanged montmorillonite," *Applied Catalysis B: Environmental*, vol. 107, no. 1-2, pp. 135–139, 2011.

[102] N. Godard, A. Vivian, L. Fusaro, L. Cannavicci, C. Aprile, and D. P. Debecker, "High-yield synthesis of ethyl lactate with mesoporous tin silicate catalysts prepared by an aerosol-assisted sol-gel process," *ChemCatChem*, vol. 9, no. 12, pp. 2211–2218, 2017.

[103] E. Pighin, V. Díez, and J. Di Cosimo, "Synthesis of ethyl lactate from triose sugars on Sn/Al_2O_3 catalysts," *Applied Catalysis A: General*, vol. 517, pp. 151–160, 2016.

[104] E. Pighin, V. Díez, and J. Di Cosimo, "Kinetic study of the ethyl lactate synthesis from triose sugars on Sn/Al_2O_3 catalysts," *Catalysis Today*, vol. 289, pp. 29–37, 2017.

[105] E. A. Pighin, J. I. Di Cosimo, and V. K. Diez, "Kinetic and mechanistic study of triose sugar conversion on Lewis and Brønsted acid solids," *Molecular Catalysis*, vol. 458, pp. 189–197, 2017.

[106] L. Zhou, L. Wu, H. Li et al., "A facile and efficient method to improve the selectivity of methyl lactate in the chemocatalytic conversion of glucose catalyzed by homogeneous Lewis acid," *Journal of Molecular Catalysis A: Chemical*, vol. 388-389, pp. 74–80, 2014.

[107] K. Nemoto, Y. Hirano, K.-i. Hirata et al., "Cooperative In–Sn catalyst system for efficient methyl lactate synthesis from biomass-derived sugars," *Applied Catalysis B: Environmental*, vol. 183, pp. 8–17, 2016.

[108] J. Wang, G. Yao, and F. Jin, "One-pot catalytic conversion of carbohydrates into alkyl lactates with Lewis acids in alcohols," *Molecular Catalysis*, vol. 435, pp. 82–90, 2017.

[109] M. S. Holm, S. Saravanamurugan, and E. Taarning, "Conversion of sugars to lactic acid derivatives using heterogeneous zeotype catalysts," *Science*, vol. 328, no. 5978, pp. 602–605, 2010.

[110] M. S. Holm, Y. J. Pagán-Torres, S. Saravanamurugan, A. Riisager, J. A. Dumesic, and E. Taarning, "Sn-Beta catalysed conversion of hemicellulosic sugars," *Green Chemistry*, vol. 14, no. 3, pp. 702–706, 2012.

[111] B. Murillo, A. Sánchez, V. Sebastián et al., "Conversion of glucose to lactic acid derivatives with mesoporous Sn-MCM-41 and microporous titanosilicates," *Journal of Chemical Technology and Biotechnology*, vol. 89, no. 9, pp. 1344–1350, 2014.

[112] S. Tolborg, I. Sádaba, C. M. Osmundsen, P. Fristrup, M. S. Holm, and E. Taarning, "Tin-containing silicates: alkali salts improve methyl lactate yield from sugars," *ChemSusChem*, vol. 8, no. 4, pp. 613–617, 2015.

[113] L. Yang, X. Yang, E. Tian, V. Vattipalli, W. Fan, and H. Lin, "Mechanistic insights into the production of methyl lactate by catalytic conversion of carbohydrates on mesoporous Zr-SBA-15," *Journal of Catalysis*, vol. 333, pp. 207–216, 2016.

[114] X. Yang, J. Bian, J. Huang et al., "Fluoride-free and low concentration template synthesis of hierarchical Sn-Beta zeolites: efficient catalysts for conversion of glucose to alkyl lactate," *Green Chemistry*, vol. 19, no. 3, pp. 692–701, 2017.

[115] J. Pang, M. Zheng, X. Li et al., "Catalytic conversion of carbohydrates to methyl lactate using isolated tin sites in SBA-15," *ChemistrySelect*, vol. 2, no. 1, pp. 309–314, 2017.

[116] J. Zhang, L. Wang, G. Wang et al., "Hierarchical Sn-Beta zeolite catalyst for the conversion of sugars to alkyl lactates," *ACS Sustainable Chemistry and Engineering*, vol. 5, no. 4, pp. 3123–3131, 2017.

[117] X. Yang, Y. Liu, X. Li et al., "Synthesis of Sn-containing nanosized beta zeolite as efficient catalyst for transformation of glucose to methyl lactate," *ACS Sustainable Chemistry and Engineering*, vol. 6, no. 7, pp. 8256–8265, 2018.

[118] F. de Clippel, M. Dusselier, R. Van Rompaey et al., "Fast and selective sugar conversion to alkyl lactate and lactic acid with bifunctional carbon–silica catalysts," *Journal of the American Chemical Society*, vol. 134, no. 24, pp. 10089–10101, 2012.

[119] B. Murillo, B. Zornoza, O. de la Iglesia, C. Téllez, and J. Coronas, "Chemocatalysis of sugars to produce lactic acid derivatives on zeolitic imidazolate frameworks," *Journal of Catalysis*, vol. 334, pp. 60–67, 2016.

[120] S. Yamaguchi, M. Yabushita, M. Kim et al., "Catalytic conversion of biomass-derived carbohydrates to methyl lactate by acid-base bifunctional γ-Al_2O_3," *ACS Sustainable Chemistry and Engineering*, vol. 6, no. 7, pp. 8113–8117, 2018.

[121] F. H. Lv, R. Bi, Y. H. Liu, W. S. Li, and X. P. Zhou, "The synthesis of methyl lactate and other methyl oxygenates from cellulose," *Catalysis Communications*, vol. 49, pp. 78–81, 2014.

[122] L. Yang, X. Yang, E. Tian, and H. Lin, "Direct conversion of cellulose into ethyl lactate in supercritical ethanol–water solutions," *ChemSusChem*, vol. 9, no. 1, pp. 36–41, 2016.

[123] D. Verma, R. Insyani, Y.-W. Suh, S. M. Kim, S. K. Kim, and J. Kim, "Direct conversion of cellulose to high-yield methyl lactate over Ga-doped Zn/H-nanozeolite Y catalysts in supercritical methanol," *Green Chemistry*, vol. 19, no. 8, pp. 1969–1982, 2017.

[124] T.-L. Ho, "Hard soft acids bases (HSAB) principle and organic chemistry," *Chemical Reviews*, vol. 75, no. 1, pp. 1–20, 1975.

[125] I. Tosi, A. Riisager, E. Taarning, P. R. Jensen, and S. Meier, "Kinetic analysis of hexose conversion to methyl lactate by Sn-Beta: effects of substrate masking and of water," *Catalysis Science and Technology*, vol. 8, no. 8, pp. 2137–2145, 2018.

[126] W. Deng, Y. Wang, S. Zhang et al., "Catalytic amino acid production from biomass-derived intermediates," *Proceedings of the National Academy of Sciences of the United States of America*, vol. 115, no. 20, pp. 5093–5098, 2018.

[127] W. Deng, Y. Wang, and N. Yan, "Production of organic acids from biomass resources," *Current Opinion in Green and Sustainable Chemistry*, vol. 2, pp. 54–58, 2016.